

UNCLASSIFIED

AD NUMBER

AD450199

LIMITATION CHANGES

TO:

Approved for public release; distribution is unlimited.

FROM:

Distribution authorized to U.S. Gov't. agencies and their contractors;
Administrative/Operational Use; SEP 1964. Other requests shall be referred to Air Force Systems Command, Wright-Patterson AFB, OH 45433.

AUTHORITY

AFML ltr 19 Jul 1971

THIS PAGE IS UNCLASSIFIED

UNCLASSIFIED

AD 4 5 0 1 9 9

DEFENSE DOCUMENTATION CENTER

FOR

SCIENTIFIC AND TECHNICAL INFORMATION

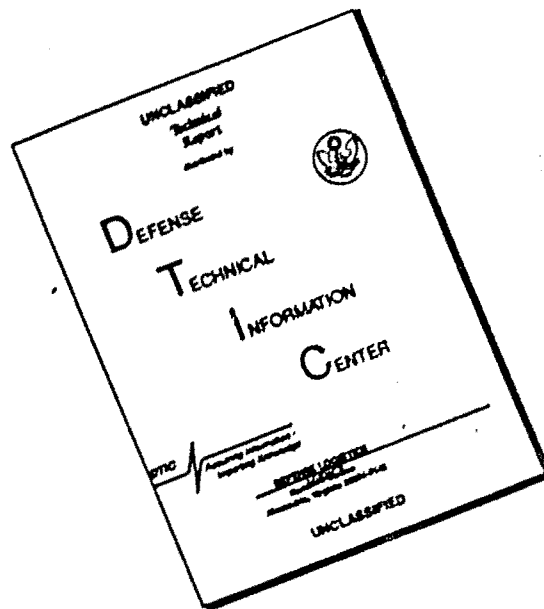
CAMERON STATION ALEXANDRIA, VIRGINIA



UNCLASSIFIED

NOTICE: When government or other drawings, specifications or other data are used for any purpose other than in connection with a definitely related government procurement operation, the U. S. Government thereby incurs no responsibility, nor any obligation whatsoever; and the fact that the Government may have formulated, furnished, or in any way supplied the said drawings, specifications, or other data is not to be regarded by implication or otherwise as in any manner licensing the holder or any other person or corporation, or conveying any rights or permission to manufacture, use or sell any patented invention that may in any way be related thereto.

DISCLAIMER NOTICE



THIS DOCUMENT IS BEST QUALITY AVAILABLE. THE COPY FURNISHED TO DTIC CONTAINED A SIGNIFICANT NUMBER OF PAGES WHICH DO NOT REPRODUCE LEGIBLY.

**BLANK PAGES
IN THIS
DOCUMENT
WERE NOT
FILMED**

450199

ML-TDR-64-313

450199

**FINAL REPORT ON
ELECTROLYTIC MACHINING DEVELOPMENT**

TECHNICAL DOCUMENTARY REPORT NO. ML-TDR-64-313

September 1964

**Fabrication Branch
Manufacturing Technology Laboratory
Research and Technology Division
Air Force Systems Command
United States Air Force
Wright-Patterson Air Force Base, Ohio**

Project No. MM7-648b



**(Prepared under Contract No. AF33(657)-8794 by the General Electric Company,
Large Jet Engine Department, Cincinnati, Ohio, Joseph Bayer, Marcus A. Cummings,
Allen U. Jollis, Authors)**

CATALOGED BY UJUC
AS AD No. _____

NOTICES

When Government drawings, specifications, or other data are used for any purpose other than in connection with a definitely related Government procurement operation, the United States Government thereby incurs no responsibility nor any obligation whatsoever; and the fact that the Government may have formulated, furnished, or in any way supplied the said drawings, specifications, or other data, is not to be regarded by implication or otherwise as in any manner licensing the holder or any other person or corporation, or conveying any rights or permission to manufacture, use, or sell any patented invention that may in any way be related thereto.

DDC release to OTS not authorized until June 1965.

Qualified requesters may obtain copies of this report from the Defense Documentation Center (DDC), (formerly ASTIA), Cameron Station, Bldg. 5, 5010 Duke Street, Alexandria, Virginia, 22314.

Copies of this report should not be returned to the Research and Technology Division, Wright-Patterson Air Force Base, Ohio, unless return is required by security considerations, contractual obligations, or notice on a specific document.

FOREWORD

This Final Technical Engineering Report covers all work performed under contract AF33(657)-8794 from 4 September 1962 to 3 June 1964.

This contract with the General Electric Company, Cincinnati, Ohio, 45215, was initiated under Project #7-648b, "Electrolytic Machining Development". It was administered under the direction of Mr. W. M. Webster, MATF, AF Materials Laboratory, Research and Technology Division, Air Force Systems Command, United States Air Force, Wright-Patterson Air Force Base, Ohio.

Mr. Guy Bellows, Manufacturing Engineering Research Laboratory, Large Jet Engine Department (LJED), General Electric Company, was the project manager. Joseph Bayer and Allen U. Jollis, Technical Engineers, LJED, and Marcus A. Cummings, Mathematical Applications Specialist, Advanced Engine Technology Department (AETD), were the project engineers and authors. Dr. J. W. Grenier and T. Lajcik, AETD, conducted a separate study of electrolytic cell reactions and contributed the detailed information in Section 6, Chapter III. Others who cooperated in the research and in the preparation of this report were: John L. Bemserderfer, LJED, design of experiments and statistical analysis; Miss Shyrl E. Emhoff, AETD, technical writer; Roy V. Holt, AETD, computer programming; W. W. Mitchell, AETD, electrolytic cell circuit design; John F. Wolfinger, LJED, electronic servo design. The assigned laboratory assistants were William L. Eisberg, Carl E. Hill and Barnell Van Hook.

The report has been assigned the General Electric number TIS R64FPD175.

The primary objective of the Air Force Manufacturing Methods program is to increase producibility and to improve the quality and efficiency of fabrication of aircraft, missiles, and their components. This report is published so that interested persons may participate in the progress of the program as it develops.

Your comments are solicited on the potential use of the information contained in this report as it applies to your present or future production programs. Suggestions concerning additional manufacturing methods development required on this or other subjects will be appreciated.

ABSTRACT

An investigation of electrolytic or electrochemical machining - a metal removal method - is described and the advantages over other machining methods are reported. Special emphasis was given to: investigating effects of process variables, including electrolytes, on metal removal rate and surface finish; investigating high current density electrolytic cell phenomena; defining process mathematical relationships; demonstrating a mathematical model on a digital computer for process simulation and design of cutting tools. An optimizing servocontrol and the production of exemplary parts are described. Guidelines for the preparation of equipment and process specifications are included.

The significant operating parameters and response variables which affect the process performance were identified for two combinations of work materials and electrolytes. Methods for determining parameters required in using the mathematical models were established. One mathematical model was programmed for a digital computer and cutting gaps occurring during machining of a selected contour were computed and compared to actual machining results.

The behavior of critical electrolytic cell parameters was studied at high current densities. A method was demonstrated for determining the true electropotential between electrodes under simulated electrolytic machining conditions.

Demonstrations showed that the electrolytic machining process requires the simultaneous control of the electrolyte properties, its fluid flow characteristics, the applied electropotential, and the motion of the electrode cutting tool; and, the surface finish of electrolytically machined parts depends upon the electrolyte properties, its fluid flow characteristics, and metal removal rate.

This technical documentary report has been reviewed and is approved.

FOR THE DIRECTOR:

Melvin E. Fields

MELVIN E. FIELDS, Colonel, USAF
Chief, Manufacturing Technology Division
Air Force Materials Laboratory

TABLE OF CONTENTS

	Page
LIST OF ILLUSTRATIONS	viii
LIST OF TABLES	xiii
CHAPTER I - INTRODUCTION	1
CHAPTER II - CONCLUSIONS	5
CHAPTER III - TECHNICAL DISCUSSION	7
1 THE ELECTROLYTIC MACHINING PROCESS	7
2 PROCESS VARIABLES	8
2.1 Significance Tests	9
2.2 Study of Response Variables	13
2.2.1 Estimate of Overpotential ΔE	13
2.2.2 Estimate of Metal Removal Factor K	14
2.2.3 Estimate of Specific Resistance ρ	14
2.3 Other Factors to be Considered	14
2.3.1 Ripple	14
2.3.2 Sludge	17
2.3.3 Other Temperature Considerations	17
3 MATHEMATICAL ANALYSIS	17
3.1 Steady State	20
3.1.1 Electrode Design for Steady State Machining	21
3.2 Transient Conditions	27
3.2.1 Excess Machining Stock Calculations	30
3.2.2 Electrode Design for Transient Shapes	31
4 VERIFICATION OF A MATHEMATICAL MODEL	32
4.1 The Computer Program	34
4.2 Discussion of Results	40
5 THE ROLE OF THE ELECTROLYTE	51
5.1 The Electrolyte - Part of the Chemical Reaction	51
5.1.1 Reaction at the Anode	51
5.1.2 Reaction at the Cathode	52
5.1.3 Reactions in the Bulk of the Electrolyte	52

TABLE OF CONTENTS (Cont'd.)

	Page
5.2 Effect of Electrolyte Fluid Properties	52
5.2.1 Promoting Stability of Metal Removal	53
5.2.2 Conveying the Reaction Products	53
5.2.3 Conveyor of Heat	54
5.2.4 Effect of Static Pressure Head	54
5.3 Electrolyte - Part of the Electrical Circuit	54
6 ELECTROLYTIC CELL INVESTIGATION	58
6.1 Electrochemical theories	58
6.2 Experimental Methods	61
6.3 Static Cell Investigations	63
6.3.1 Test Series Ni/NaCl	66
6.3.2 Test Series Fe/NaNO ₃	69
6.3.3 Test Series Cr/NaCl	70
6.3.4 Test Series Fe/H ₂ SO ₄	74
6.3.5 Analysis of Surface Films and Finish	74
6.4 Dynamic Cell Investigations	76
6.4.1 Test Series R41/NaCl	80
6.4.2 Test Series Ni/NaCl	81
6.5 Discussion and Conclusions	83
7 SURFACE FINISH	84
7.1 Data Analysis	85
7.1.1 Associated Data Analysis Problems	86
7.2 Surface Roughness Investigation	86
7.2.1 Test Series AJ-G	87
7.2.2 Test Series JB-8	99
7.2.3 Conclusions	99
7.3 Subsurface Defects	101
8 PROCESS CONTROL AND REGULATION	101
8.1 Process Control	103
8.1.1 Adaptive Control	104
8.2 Feed Servo Investigation	104
9 ELECTRODE MATERIAL EVALUATION	108
CHAPTER IV - EXEMPLARY PARTS	111

TABLE OF CONTENTS (Cont'd.)

	Page
1 TREPANNING - EXEMPLARY PARTS 1 THROUGH 3	111
2 BLANKING - EXEMPLARY PARTS 4 THROUGH 7	116
3 CAVITY MACHINING - EXEMPLARY PART 8	129
4 CONTOUR MACHINING - EXEMPLARY PARTS 9 AND 10	141
CHAPTER V - PROCESS SPECIFICATION AND SELECTION GUIDE	147
1 PROCESS SPECIFICATION GUIDE	147
2 PROCESS SELECTION GUIDE	149
CHAPTER VI - EQUIPMENT SPECIFICATION GUIDE	153
CHAPTER VII - REFERENCES	161
CHAPTER VIII - APPENDIXES	163
I DEVELOPMENT APPROACHES	165
I. 1 Study of Operating Parameters by Curve Fitting Method	166
I. 2 The \bar{r} Approach	166
I. 3 Analysis of Electrolytic Cell Forces	167
I. 4 Temperature Effect on Cutting Gap	169
I. 5 Electrolyte Flow Observations	169
II DEVELOPMENT TESTS	171
II. 1 Operating Parameter Studies	172
II. 1. 1 Test Series JB-1	172
II. 1. 2 Test Series JB-2	172
II. 1. 3 Test Series JB-3	177
II. 1. 4 Test Series JB-4	177
II. 1. 5 Test Series JB-5 and JB-5A	180
II. 1. 6 Test Series JB-8	180
II. 1. 7 Test Series JB-9	183
II. 2 Temperature Studies	185
II. 2. 1 Test Series JB-6	185
II. 2. 2 Test Series JB-7	187
II. 3 Ripple Study	193
II. 4 Sludge Study	196

TABLE OF CONTENTS (Cont'd.)

	Page
II. 5 Surface Finish Studies	198
II. 5. 1 Test Series AJ-B	198
II. 5. 2 Test Series AJ-F	206
II. 5. 3 Test Series AJ-G	208
II. 5. 4 Test Series AJ-H	208
II. 5. 5 Test Series JB-4 (Surface Roughness Analysis)	210
II. 5. 6 Test Series JB-4 (Surface Defect Analysis)	210
II. 5. 7 Test Series JB-8 (Surface Roughness Analysis)	210
II. 5. 8 Test Series JB-9 (Surface Roughness Analysis)	212
II. 6 Contour Machining Tests	212
II. 7 Electrode Material Investigation	214
II. 8 Electrolyte Flow Studies	220
II. 9 Servocontrol Study	222
II. 10 Electrolytic Cell Investigation	227
II. 10. 1 Pulse Generator and Interrupter	227
II. 10. 2 Electrolytic Cells	230
II. 10. 3 Experimental Procedure	235
II. 10. 4 Test Data	236
III FORTRAN INSTRUCTIONS	249
IV TEST EQUIPMENT	265
IV. 1 Machine #1	266

DISTRIBUTION LIST

LIST OF ILLUSTRATIONS

	Page
Figure 1. Electrolytic Machining	7
Figure 2. Elements of an Electrolytic Machining Facility	8
Figure 3. Significant Factors Determining Applied Voltage	11
Figure 4. Significant Factors Determining Applied Voltage	12
Figure 5. Current vs Voltage Plots for Estimates of Overvoltage (ΔE)	15
Figure 6. Current Density vs Feed Rate Plots for Estimates of K	16
Figure 7. Viscosity of NaCl Versus Sludge Content from Electrolyte Used to Cut René 41	18
Figure 8. Sludge Content in NaCl Electrolyte vs Temperature at Various Electrolyte Concentrations	18
Figure 9. Effect of Single Cathode Mesh Rectangle on Anode Surface	22
Figure 10. Effect of Two Cathode Mesh Rectangles on Anode Surface	23
Figure 11. Transient Surface	27
Figure 12. Preform Machining	31
Figure 13. Flat Surface Machining	32
Figure 14. Electrode Tool Contour Machining Test	33
Figure 15. Quadrilateral ABCD	35
Figure 16. Gap Comparison Test #C1, .0028"	41
Figure 17. Gap Comparison Test #C3, .0018"	42
Figure 18. Gap Comparison Test #C4, .0025"	43
Figure 19. Gap Comparison Test #C5, .0009"	44
Figure 20. Gap Comparison Test #C6, .0016"	45
Figure 21. Gap Comparison Test #D1, .0038"	46
Figure 22. Gap Comparison Test #D2, .0012"	47
Figure 23. Gap Comparison Test #D3, .0012"	48
Figure 24. Average Overcut Index β vs. Cutting Gaps for Tests C1 through C6 and D1 through D3	49
Figure 25. Comparison of Average Overcut Index with the Actual Index for Test C3 .	50

LIST OF ILLUSTRATIONS (Cont'd.)

	Page
Figure 26. Specific Resistant vs NaCl Concentration at 72° F	56
Figure 27. Specific Resistance vs Concentration NaNO_3 at Various Temperatures	57
Figure 28. Current Conductance through an Electrolyte	59
Figure 29. Electrolytic Cell Regions	61
Figure 30. Decay Characteristic of Cell Potential	62
Figure 31. Luggin Capillary	63
Figure 32. Test Facilities for Electrolytic Cell Studies	64
Figure 33. Block Diagram of Test Facilities	65
Figure 34. Total ΔE vs Current Density for Various Temperatures Test Series Fe/ NaNO_3	70
Figure 35. n-Factor vs Current Density for Various Electrode Separations Test Series Fe/ NaNO_3	71
Figure 36. n-Factor vs Electrode Separation at 550 Ampere per Square Inch, Test Series Fe/ NaNO_3	71
Figure 37. Total ΔE vs Electrode Separation at Various Temperatures Test Series Cr/NaCl	72
Figure 38. Total ΔE vs Temperature at Various Electrode Separations Test Series Cr/NaCl	73
Figure 39. n-Factor vs Concentration at Various Current Densities Test Series Cr/NaCl	73
Figure 40. n-Factor vs Current Density at 2.0 Pounds of NaCl per Gallon Test Series Cr/NaCl	74
Figure 41. Electron Micrograph of a Nickel Anode after Electrolysis with 1.29 lb NaCl/gal, 868 amp/in ² , 138° F and 6.5 mil Gap Mag. 6000X .	75
Figure 42. Electron Micrograph of an Iron Anode after Electrolysis with 4.59 lb NaNO_3 /gal, 550 amp/in ² , 111° F and 17.0 mil Gap Mag. 6000X.	77
Figure 43. Electron Micrograph of a Chromium Anode after Electrolysis with 2.71 lb NaCl/gal, 868 amp/in ² , 139° F and 27.0 mil Gap Mag. 40,000X	78
Figure 44. Total ΔE vs Current Density for Various Anode Material/Electrolyte Combinations in Anodic Reaction Cell under Dynamic Electrolyte Conditions	79

LIST OF ILLUSTRATIONS (Cont'd.)

	Page
Figure 45. Total ΔE vs Current Density, Test Series René 41/NaCl	81
Figure 46. μ Factor vs Current Density at Various Electrolyte Inlet Pressures Test Series René 41/NaCl	82
Figure 47. Total ΔE vs Current Density at Various Electrolyte Flow Rates Test Series Ni/NaCl	82
Figure 48. μ Factor vs Current Density at Various Electrolyte Inlet Pressures Test Series Ni/NaCl	83
Figure 49. Design of Surface Finish Test, Test Series AJ-G	88
Figure 50. Significant Factors Contributing to Variations of Surface Roughness Test Series AJ-G1	89
Figure 51. Significant Factors Contributing to Variations of Surface Roughness Test Series AJ-G11	90
Figure 52. Significant Factors Contributing to Variations of Surface Roughness Test Series AJ-G111	91
Figure 53. Series AJ-G Surface Finish Specimens	92
Figure 54. Segment of Specimen G-12 and "Talisurf" Recording	93
Figure 55. Segment of Specimen G-14 and "Talisurf" Recording	94
Figure 56. Segment of Specimen G-18 and "Talisurf" Recording	95
Figure 57. Segment of Specimen G-5 and "Talisurf" Recording	96
Figure 58. Segments of Specimens G-2, 24 and 22	97
Figure 59. Effect of Tested Factors on Surface Lay	98
Figure 60. Factors Contributing to Variations of Surface Roughness Test Series JB-8	100
Figure 61. Subsurface Defects	102
Figure 62. Comparison of Gap Current, Constant vs Regulated Electrode Feed ...	103
Figure 63. Comparison of Recovery Times After Cutting Gap Change, Constant vs Regulated Electrode Feed	106
Figure 64. Response of Automatic Control to Erratic Process Changes (ECM Voltage - 12 Volt Constant)	107
Figure 65. Exemplary Parts 1 and 3	112
Figure 66. Exemplary Part 2, Mat'l: Titanium 8-1-1	113

LIST OF ILLUSTRATIONS (Cont'd.)

	Page
Figure 67. Cross Section Through Exemplary Part 2	118
Figure 68. Cross Section Through Exemplary Part 3 Intergranular Attack 0.002" Deep	119
Figure 69. Schematic Sketch of Tooling for Exemplary Parts 1 through 3	120
Figure 70. Tooling for Exemplary Parts 1 through 3	121
Figure 71. Electrode for Exemplary Parts 1 through 3	122
Figure 72. Exemplary Parts 4 and 5	124
Figure 73. Exemplary Parts 6 and 7	125
Figure 74. Cross Section Through Machined Edge of Exemplary Part 4	126
Figure 75. Tooling for Exemplary Part 4-7	127
Figure 76. Schematic Sketch of Tooling for Exemplary Parts 4-7	128
Figure 77. Cross Sections Through Machined Edge of Exemplary Part 5	133
Figure 78. Exemplary Part 8, Mat'l: René 41	135
Figure 79. Assembly of Tooling for Exemplary Part 6 in Machine #1	138
Figure 80. Schematic Sketch of Tooling for Exemplary Part 8 (Section A-A)	139
Figure 81. Tooling for Exemplary Part 8	140
Figure 82. Exemplary Parts 9 and 10	142
Figure 83. Schematic Sketch of Tooling for Exemplary Parts 9 and 10	145
Figure 84. Tooling for Exemplary Parts 9 and 10 Details of Electrode Ass'y and Work Holder	146
Figure 85. Facility Layout - Operating Parameter Studies	173
Figure 86. Test Facility - Operating Parameter Studies	175
Figure 87. Schematic Sketch of Tooling for Test Series JB-2 and JB-3	176
Figure 88. Schematic Sketch of Tooling for Test Series JB-4-5-8-9	179
Figure 89. $\frac{\bar{r}}{\rho}$ vs Gap Test Series JB-4	181
Figure 90. Significant Factors Determining Applied Voltage Test Series JB-8	184
Figure 91. Schematic Sketch of Tooling for Temperature Studies	188

LIST OF ILLUSTRATIONS (Cont'd.)

	Page
Figure 92. Gap vs Temperature Profile Test Series JB-6	189
Figure 93. Gap vs Temperature Profile Test Series JB-6	190
Figure 94. Gap vs Temperature Profile Test Series JB-6	191
Figure 95. Gap vs Temperature Profile Test Series JB-6	192
Figure 96. Gap vs Temperature Profile Test Series JB-7	194
Figure 97. Percent Ripple vs DC Voltage	195
Figure 98. Wave Form of DC Voltage "WAGNER" Power Pack	196
Figure 99. Significant Factors Contributing to Variations of Electrolyte Properties	199
Figure 100. Facility Layout; ECM Machine #2	201
Figure 101. Schematic Sketch of Tooling for AJ Series Surface Finish Tests	203
Figure 102. Tooling for AJ Series Surface Finish Tests	204
Figure 103. Factors Contributing To Variations of Surface Roughness Test Series AJ-F	207
Figure 104. Factors Contributing to Surface Roughness, Test Series JB-4	211
Figure 105. Factors Contributing To Surface Roughness, Test Series JB-9	213
Figure 106. Tooling for Servo Study	223
Figure 107. Schematic Diagram Gap Control Circuit	224
Figure 108. Block Diagram Gap Control Circuit	225
Figure 109. Armature Voltage Signals Gap Control Unit	226
Figure 110. Schematic Diagram of Lower Supply and Drive Circuit	228
Figure 111. Schematic Diagram of Control Logic Circuit	229
Figure 112. Static Electrolytic Cell	231
Figure 113. Schematic Sketch of Static Electrolytic Cell	232
Figure 114. Anodic Reaction Dynamic Cell and Electrolyte Supply Facility	233
Figure 115. Schematic Sketch of Anodic Reaction Dynamic Cell	234
Figure 116. ECM Machine #1	267
Figure 117. Facility Layout ECM Machine #1	268

LIST OF TABLES

	Page
Table 1. Significant Factors Affecting Current	10
Table 2. Operating Parameters, Contour Machining Tests	33
Table 3. Computer Input Description of Cathode Surface A_c	37
Table 4. Computer Output	38
Table 5. Computer Output, Cont'd.	39
Table 6. Anode ΔE Measurements Test Series Ni/NaCl - 1	67
Table 7. Calculated Cathode ΔE 's Test Series Ni/NaCl - 1	68
Table 8. Total ΔE Measurements Test Series Ni/NaCl - 2	68
Table 9. List of Electrode Materials	108
Table 10. Electrode Material Evaluation	109
Table 11. Operating Parameters, Exemplary Parts 1 Through 3	114
Table 12. Part Dimensions, Exemplary Parts 1 Through 3	115
Table 13. Surface Finish Measurements Exemplary Parts 1 Through 3	117
Table 14. Operating Parameters, Exemplary Parts 4 & 5	130
Table 15. Operating Parameters and Depth of Cut, Exemplary Parts 6 & 7	131
Table 16. Part Dimensions, Exemplary Part 4	132
Table 17. Operating Parameters, Exemplary Part 8	136
Table 18. Part Dimensions, Exemplary Part 8	137
Table 19. Operating Parameters, Exemplary Parts 9 & 10	143
Table 20. Legend For Facility Input Operating Parameter Studies Figures 85 & 86	174
Table 21. Estimates of ΔE , Test Series JB-5 and JB-5A	182
Table 22. Estimate of ΔE , Test Series JB-9	186
Table 23. Analysis of Ripple Effect	197
Table 24. Legend for Facility Layout Machine #2, Figure 100	202
Table 25. Computed Results, Tests #C1 and C3	215
Table 26. Computed Results, Tests #C4 and C5	216

LIST OF TABLES (Cont'd.)

	Page
Table 27. Computed Results, Test #C6	217
Table 28. Computed Results, Test #D2 and D3	218
Table 29. Total ΔE Measurements, Test Series Fe/ NaNO_3 Static Cell	237
Table 30. Anode ΔE Measurements, Test Series Fe/ NaNO_3 Static Cell	238
Table 31. Calculated Cathode ΔE 's, Test Series Fe/ NaNO_3 Static Cell	239
Table 32. Total ΔE Measurements, Test Series Cr/ NaCl Static Cell	240
Table 33. Anode ΔE Measurements, Test Series Cr/ NaCl Static Cell	241
Table 34. Calculated Cathode ΔE 's, Test Series Cr/ NaCl Static Cell	242
Table 35. Total ΔE Measurements, Test Series Fe/ H_2SO_4 Static Cell	243
Table 36. Total ΔE Measurements, Anodic Reaction Cell Test Series Ni/ NaCl	244
Table 37. Total ΔE Measurements, Anodic Reaction Cell Test Series Fe/ NaNO_3	245
Table 38. Total ΔE Measurements, Anodic Reaction Cell Test Series Cr/ NaCl	246
Table 39. Total ΔE Measurements, E. C. M. Cell, Test Series R41/ NaCl	247
Table 40. Total ΔE Measurements, E. C. M. Cell, Test Series Ni/ NaCl	248
Table 41. Legend For Facility Layout Machine #1, Figure 117	269

CHAPTER I

INTRODUCTION

1. BACKGROUND

Electrolytic machining, also called electrochemical machining (ECM), is a process which removes material from an electrically conductive workpiece by electrolytic action.

The workpiece and a cutting tool (electrode) are connected to a DC power supply - the workpiece is the anode connected to the positive pole, the electrode is the cathode connected to the negative pole.

An electrically conductive solution (electrolyte) is pumped through the gap between the workpiece and the electrode. Whenever there is current flow, electrolytic action takes place and metal is dissolved into the electrolyte from the workpiece.

In electrolytic machining, the electrode usually advances toward the workpiece, and the electrolytic action is regulated so that work surfaces are generated to desired shapes and tolerances.

This process offers many advantages over other metal removal and shaping methods:

- (a) The rate of electrolytic metal removal is independent of material hardness.
- (b) The process does not induce stresses in the workpiece.
- (c) It can generate irregular shapes on workpiece surfaces which are often inaccessible to other metal removal or shaping tools.
- (d) Complex shapes and contours can be machined with simple machine tool motions.
- (e) Electrolytic machining is a burr-free machining method and there is no tool wear.
- (f) Metal removal is accomplished at temperatures which preclude the occurrence of thermal damage to most work materials.

Electrolytic machining has already proven to be a valuable tool in industry, but its use often is restricted because of a lack of understanding of process variables and their interactions. Therefore, to achieve a better understanding of the electrolytic machining process, it is necessary to identify the critical process variables and to relate them to the environmental factors.

From this understanding, specific conclusions can be drawn about the practical aspects of the process, such as cutting rates, surface finish characteristics, dimensional accuracy, equipment, tool design, the economical advantages of the process, and inherent limitations.

This report includes the findings, substantiating facts, and data of an intensive process investigation. It incorporates all information previously published in two interim progress reports.

Manuscript released by authors October, 1964 for publication as an RTD Technical Documentary Report.

2. OBJECTIVES

The objectives of the contract were as follows:

- (a) Identifying all critical process variables and their interrelationships, and defining their effect on process performance by mathematical or empirical relationships.
- (b) Specifically studying the effect of electrolyte velocity and dissolution products (sludge) on gap resistance; electrolyte (point) temperature in the cutting gap; ripple or degree of rectification of DC power supplies and its effect on electrolytic machining; supplementary forms of energy such as ultrasonic vibration, and their effects on process performance.
- (c) Establishing a procedure for specifying compatible electrolyte-work material combinations.
- (d) Developing a computer programming routine whereby tool configurations are defined in conformance with element correlations, part geometry, and process parameters.
- (e) Investigating and rating candidate electrode tool materials.
- (f) Deriving a nomograph and a single chart for determining excess stock needed to generate desired configurations and tolerances in workpieces.
- (g) Demonstrating process capabilities on not less than four parts, with specific emphasis on one or more areas of advancement that enables the process to accomplish material removal more advantageously than competitive methods, and by measuring process performance in terms of penetration rates, surface finish, sub-surface defects, and dimensional reproducibility.
- (h) Preparing instructions for the preparation of process physical and operational specifications.

These objectives defined the planned approach to the process development task at the outset of the investigation. As the work progressed, and we gained a better understanding of the process phenomena, several areas of investigation were de-emphasized while others were extended beyond the scope of initial program objectives. In particular, we found that using a digital computer not only yielded a useful technique for designing contoured electrode tools, but that the computer is an indispensable tool for the mathematical description and simulation of the electrolytic machining process. Greater effort, therefore, was expended in the area of computer programming and simulation than had been anticipated.

Similarly, surface finish originally was considered significant only as a measure of process performance. In the course of our investigation we found that surface finish in electrolytic machining reflected other process performance criteria, and a considerable amount of effort was expended searching for empirical relationships between process operating variables and surface finish.

During the second half of the project the program objectives were extended to include a study of electrode reactions in high current density electrolytic cells so as to gain a better understanding of the electropotentials encountered in electrolytic machining.

3. PLAN OF THE REPORT

Following this introduction, a summary of our conclusions gives an over-all picture of our process investigation. Then, in Chapter III, we go into the details of the electrolytic machining process, the mathematical models used to express the relationship among the variables and their verification by tests, the role of the electrolyte, electrolytic cell reactions, surface finish characteristics, process control regulation, and electrode material evaluation. In Chapter IV, we explain the production of exemplary parts using four different electrolytic machining techniques to demonstrate some of the attributes and advantages of the electrolytic machining process over competitive metal removal and fabricating methods. Chapters V and VI include the guidelines for the preparation of the process applications and equipment specification. Development approaches which were not followed to a conclusion and detailed descriptions of all our tests are included in the Appendix with additional related material.

CHAPTER II

CONCLUSIONS

The following conclusions were drawn from the results of this project:

- (a) Approximating mathematical models of the electrolytic machining process are the best analytical tools now available for process simulation and for the design of electrode-cutting tools and workpiece excess machining stock. They consist of a series of nonlinear, simultaneous equations which are solved on a digital computer.

The models can be applied to specific electrolytic machining situations only after the value of a number of defined variables has been determined for given work materials and electrolytes.

- (b) The mathematical models include an overcut index which relates the direct effect of the current field between electrodes to its stray effect. It can be used to predict the geometric relationship between electrodes in electrolytic processes.

The overcut index is computed as the mathematical models are solved for specific electrolytic machining situations.

- (c) The computer programming should be extended to check and refine the models which cover transient electrolytic machining of all shapes and machining modes.
- (d) Nomographs or single charts for determining excess machining stock are not practical engineering aids at the present time since they cannot predict anticipated cutting area and gap relationships.
- (e) The electrolytic machining process requires the simultaneous control of many process variables which depend upon the electrolyte properties, its fluid flow characteristics, applied electropotential and, where applicable, on the motion of the electrode-cutting tool.

For each new electrolytic machining situation the flow pattern of the electrolyte fluid cannot always be predicted. This can impair, among other things, the ability to design precise tool geometries.

In a controlled electrolytic machining process, the metal removal rate is dependent only upon electrical current density.

- (f) The nature and values of the overpotential encountered in electrolytic machining cannot be predicted from the relationships which govern low current density electrolytic processes.

The factors which were found to influence its behavior during high current density electrolysis varied with the material and electrolyte.

The results of this investigation show a dependence of the overpotential on the method of electrolyte agitation (flow) and on current density. Under flowing electrolyte conditions, the dependence of the overvoltage on current density becomes increasingly smaller at levels above 200 amps/in².

- (g) The surface finishes in electrolytic machining depend upon electrolyte properties, its fluid flow characteristics, and metal removal rate.

Suitable relationships among operating parameters and surface finish measures are defined only for specific electrolytic machining situations.

The investigation of factors affecting surface finish should be extended to develop a logic for the selection of optimum combinations of operating parameters.

- (h) Stray currents in areas adjacent to the work surfaces may cause undesirable overcuts and selective etching. Selective etching may result in intergranular attack, pitting, or other subsurface defects.
- (i) The reported advantages of the electrolytic machining process can be achieved. Precise machine mechanisms and controls in combination with rigid machine structures are often required.
- (j) There is no universal electrolyte for machining all conductive work materials. An inexpensive, saline solution with stable operating characteristics, however, can be used as an electrolyte for a large variety of materials and applications.
- (k) An optimizing servocontrol can be designed to adjust cutting feeds so as to maximize metal removal rates, safeguard against process malfunctions, and assure producing acceptable workpieces.
- (l) Information on successfully selected operating parameters should be accumulated, analyzed, and published as handbook data. This information should include a listing of electrolytes for the materials used by the aerospace industry.

CHAPTER III

TECHNICAL DISCUSSION

1. THE ELECTROLYTIC MACHINING PROCESS

In the electrolytic machining process, the electrode tool and the workpiece are connected to a DC power supply, and the electrolyte is forced through the cutting gap. See Figure 1.

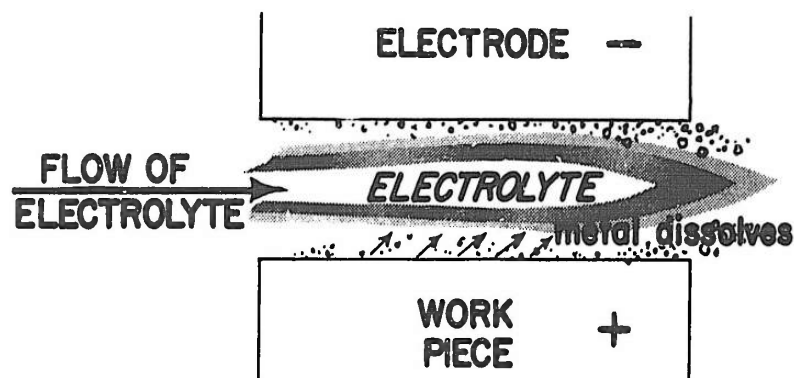


Figure 1. Electrolytic Machining

A typical electrolytic machining facility consists of four interrelated subsystems: the electrical power supply, the electrolyte supply system, the machine tool, and the electrode tool and workpiece fixture, Figure 2.

Shown in Figure 2 are: the electrical circuit consisting of connecting leads, the electrolyte, tooling, and workpiece; the electrolyte fluid loop consisting of a storage tank, a pump, filtration equipment, temperature regulating and control equipment, and the necessary piping. The machine tool may have one of several electro-mechanical or electro-hydraulic feed mechanisms, affording either manual control, automatic control by feedback circuits, or both.

Operating parameters and response variables affect the electrolytic machining process. For our discussion, we define operating parameters as those to which the operator may assign selected values. The response variables are those which depend on operating parameters and inherent properties of the workpiece and the tooling.

In setting up and conducting an electrolytic machining operation for a specific application, the following operating parameters are selected:

- (a) The chemical composition of the electrolyte supply, its concentration, its temperature, and the amount of dissolution products.
- (b) The electrolyte pressure head at the inlet and outlet.
- (c) The applied electropotential.

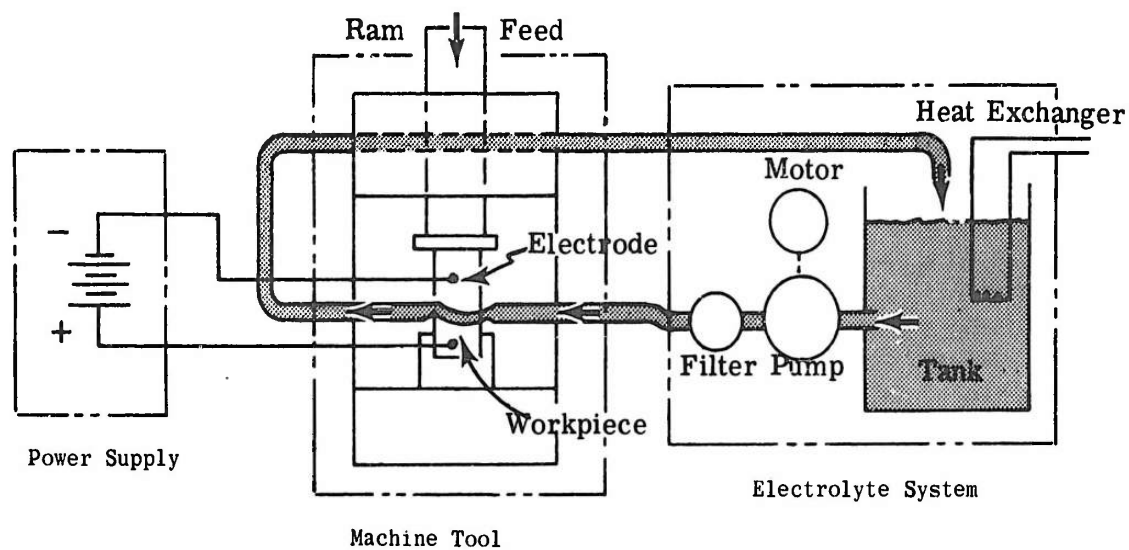


Figure 2. Elements of an Electrolytic Machining Facility

- (d) The rate of relative motion of workpiece to the electrode tool, usually the feed rate of the electrode.
- (e) The machining time.

The effects of these operating parameters on cutting rate, dimensional reproducibility, and surface finish must be known if desired results are to be accomplished.

2. PROCESS VARIABLES

The first objective of this program was to identify experimentally the significant process variables, to establish their interrelations, and to define their effect on process performance within the ranges applicable to electrolytic machining. The experimental investigation was done on a test apparatus described in detail in Appendix II. The apparatus used a planar anode and cathode whose surfaces were parallel and equal in area.

The tests were conducted under steady state conditions. The operating parameters were held constant and at levels so that the response variables, such as cutting gap, electrolyte velocity and current, would not vary during our tests.

This was accomplished by adjusting and maintaining the applied voltage so that a predetermined distance between the anode and cathode remained constant while the anode workpiece was advanced towards the stationary cathode tool. Under these conditions, metal was removed at the same rate the anode advanced towards the cathode.

Three separate electrolyte-alloy systems were studied:

- (a) The super-alloy (nickel base) René 41 and NaCl (sodium chloride) electrolyte of varying concentrations.

- (b) A tool steel and an electrolyte consisting of 0.22 lb/gal NaNO_2 (sodium nitrite) and of 1 lb/gal NaHCO_2 (sodium formate) electrolyte.
- (c) The super-alloy (iron base) A-286 and 5 lb/gal NaNO_3 (sodium nitrate) electrolyte.

Feed rate, electrolyte concentration, electrolyte temperature, electrolyte pressure drop, size of cutting gap, and gap pressure were investigated and their effects on current and applied voltage were determined.

2.1 Significance Tests

The significance of operating parameters was statistically determined and evaluated.

We found in our tests that from 98.9 to 99.9% of the variations in metal removal rate (measured as feed rate in these tests) were attributable to current, Table 1.

The required voltage was shown to be determined by the set values of feed rate, temperature, cutting gap and electrolyte concentration.

We investigated the significance of these factors in seven test series. See Appendix II.1. We will discuss the results from four representative test series.

Figures 3 and 4, which include the three electrolyte-alloy systems, summarize the test results. Each figure indicates the system tested, details the ranges used, and reports the percent variation in applied voltage attributed to significant candidate parameters and their statistical interactions.

The following factors and their interactions accounted for 98.9 to 100.0% of the observed variation in applied voltage:

- (a) Feed rate.
- (b) Electrolyte temperature.
- (c) Electrolyte concentration.
- (d) Cutting gap.

Feed rate significantly affected applied voltage in all tests. Whenever tested, the temperature significantly affected the applied voltage.

The cutting gap significantly affected the applied voltage in all tests done on the René 41-NaCl and A-286- NaNO_3 systems. The effect of gap on applied voltage was significant but small for the narrow gaps tested on the tool steel- NaNO_2 / NaHCO_2 system.

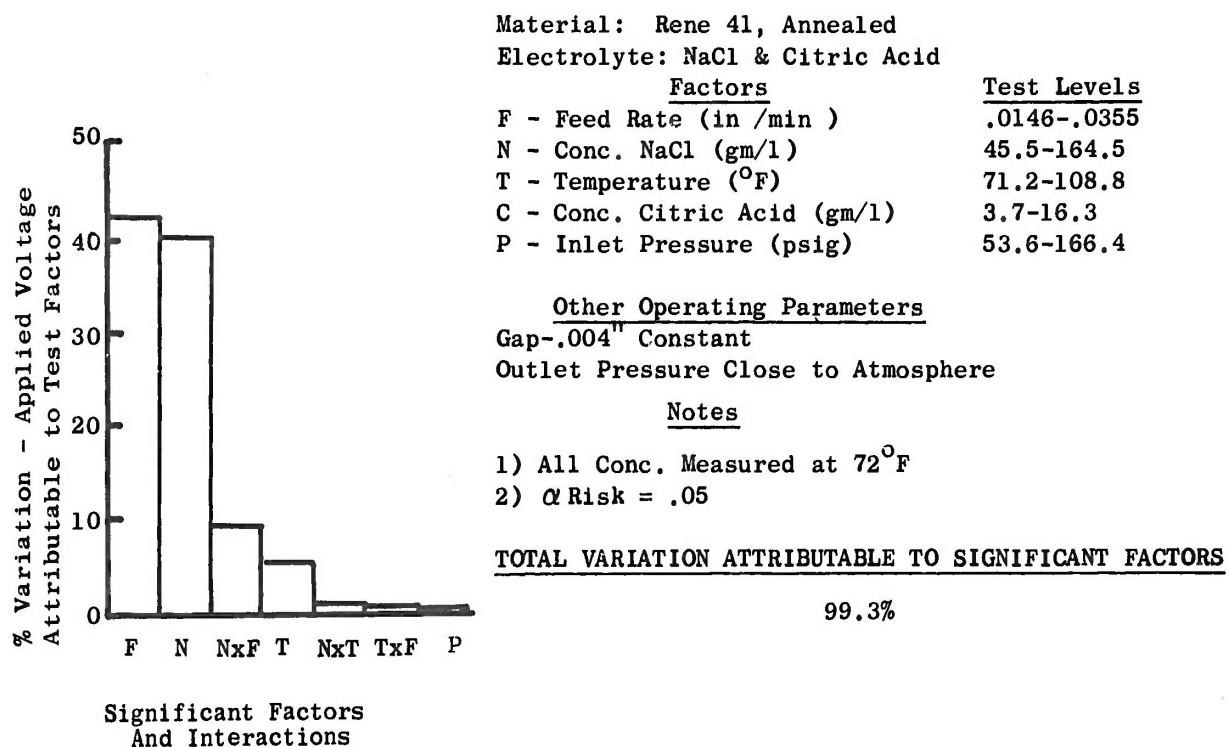
The electrolyte concentration was varied only for the René 41-NaCl alloy-electrolyte system. When NaCl concentrations were changed from 45.5 gm/l to 164.5 gm/l contents, the effect of concentration on applied voltage was significant, Figure 3(a). When the 164.5 gm/l solution was increased in concentration to 236.4 gm/l, the effect on voltage was significant but relatively small (1/2%), Figure 4(b).

The effect of pressure drop on applied voltage was tested in three test series. When the pressure drop affected the voltage significantly, its effect was small, Figures 3(a). and 4(b).

TABLE 1
SIGNIFICANT FACTORS AFFECTING CURRENT

Test Series No.	Electrolyte Alloy System Tested	Feed Rate F	Gap G	Temperature T	Pressure Drop P	PERCENTAGE VARIATION OF CURRENT DUE TO FACTOR	
						Interaction FxT	Interaction FxP
JB-1	René 41-NaCl	99.76	(2)	(1)	(1)	(1)	(1)
JB-2	René 41-NaCl	99.56	(1)	0.11	(1)	0.26	(1)
JB-3	Tool Steel NaNO ₂ /NaHCO ₂	99.27	0.19	0.08	0.19	(1)	0.14
JB-5	René 41-NaCl	99.68	(1)	(2)	(2)	(2)	(2)
JB-8 ₁	A286 NaNO ₃	98.91	0.74	0.23	(2)	(1)	(1)
JB-8 ₂	A286 NaNO ₃	99.50	0.26	0.08	(2)	(1)	(1)
JB-9	A286 NaNO ₃	99.49	0.23	0.09	(1)	(1)	(1)

NOTES: (1) Found to be insignificant at an α risk of .05.
(2) Not varied in this test.



(a) Test Series JB-1

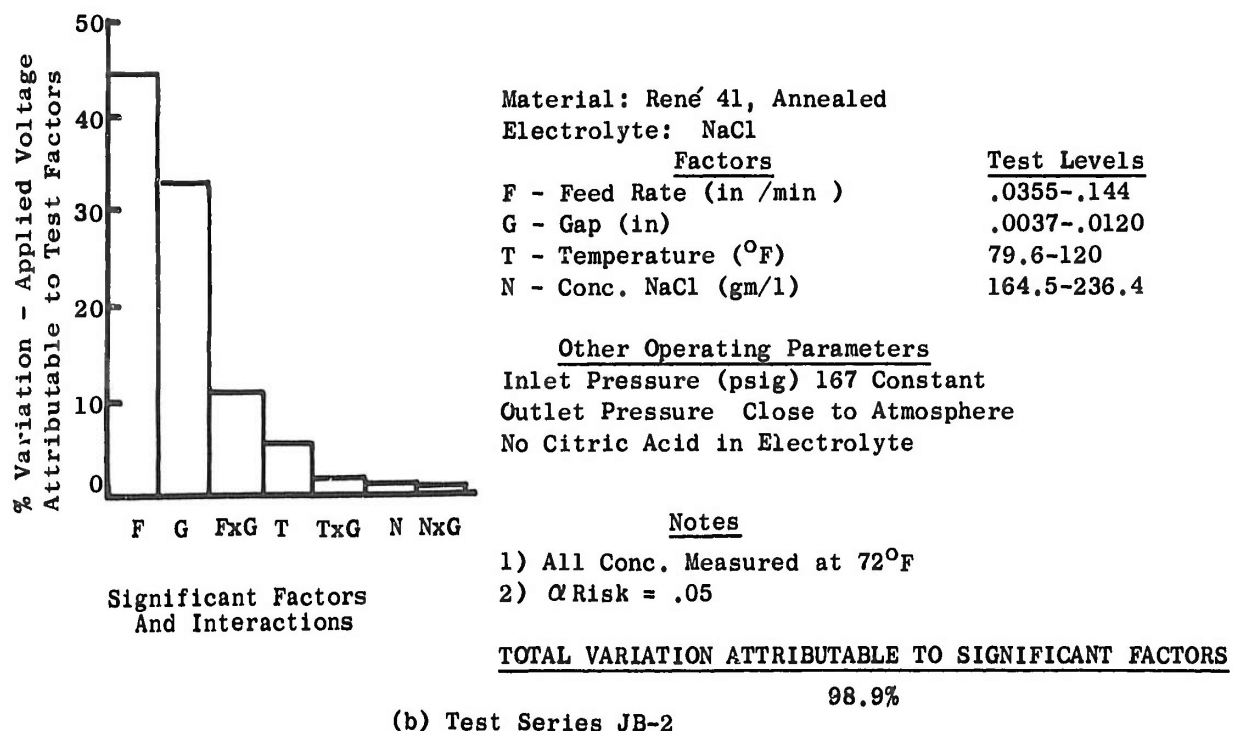
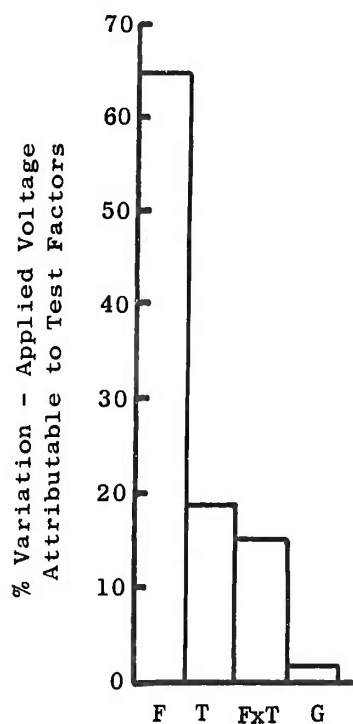


Figure 3. Significant Factors Determining Applied Voltage



Significant Factors
And Interactions

Material: 1025 Tool Steel, Annealed
Electrolyte: NaNO_2 - NaHCO_2

Factors	Test Levels
F - Feed Rate (in /min)	.0132-.0780
T - Temperature ($^{\circ}\text{F}$)	80-120
G - Gap (in)	.002-.005
P - Inlet Pressure (psig)	100-140

Other Operating Parameters

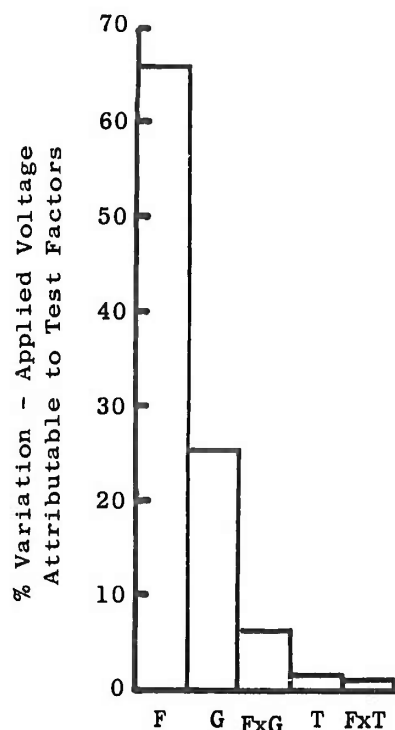
Conc. NaNO_2 - 26.4 gm/l - Constant
Conc. NaHCO_2 - 120 gm/l - Constant
Outlet Pressure Close to Atmospheric

Notes

- 1) All Concentrations at 72°F
- 2) α Risk = .05

TOTAL VARIATION ATTRIBUTABLE TO SIGNIFICANT FACTORS
99.9%

(a) Test Series JB-3



Significant Factors
And Interactions

Material: A286 - Annealed
Electrolyte: NaNO_3

Factors	Test Levels
F - Feed Rate (in /min)	.02-.06
G - Gap (in)	.012-.025
T - Temperature ($^{\circ}\text{F}$)	85-100
ΔP - Pressure Drop (psi)	20-60
P - Average Gap Pressure (psig)	40-100

Other Operating Parameters

Conc. NaNO_3 - 600 gm/l - Constant

Notes

- 1) All Concentrations at 72°F
- 2) α Risk = .05

TOTAL VARIATION ATTRIBUTABLE TO SIGNIFICANT FACTORS
100.0%

(b) Test Series JB-9

Figure 4. Significant Factors Determining Applied Voltage

It should be noted that while the effect of electrolyte pressure drop on applied voltage was of little significance for the ranges tested, we show in Section 7, Chapter III, that pressure drop and its resultant velocity plays an important role in electrolytic machining. For our tests, however, electrolyte velocity levels were selected that would result in stable machining conditions.

Those statistical interactions which were shown to be significant consisted of a combination of factors which were shown to be significant in themselves.

2.2 Study of Response Variables

In Section 3, Chapter III, we will demonstrate that the cutting gap (L_{11}) between the cathode and anode during electrolytic machining can be calculated when specific values are assigned in the equation:

$$L_{11} = \frac{E - \hat{\Delta E}}{F_i \rho \beta_i} K, \quad (8)$$

where

F_i - applied feed rate in in/min

E - applied electropotential in volts

$\hat{\Delta E}$ - estimated overpotential in volts

ρ - specific resistance of the electrolyte in ohm-in

K - constant for the metal being machined in $\text{in}^3/\text{amp-min}$

β_i - overcut index

We impose values for F and E on the system, we determine $\hat{\Delta E}$, ρ , and K from empirical data, and calculate β_i . Now, we will show a method for estimating the variables $\hat{\Delta E}$, K and ρ , and how imposed process conditions affect their value.

2.2.1 Estimate of Overpotential ($\hat{\Delta E}$)

The $\hat{\Delta E}$ in Equation (8) was derived from Ohm's Law as applied to electrolytic processes which relates the applied voltage (E) to the product of the current (I) and the resistance (R) as follows:

$$E - \Delta E = IR \quad (1)$$

ΔE in Equation (1), represents the threshold voltage which must be applied before electrolysis can proceed. The $\hat{\Delta E}$ in Equation (8) represents an estimate of the ΔE in Equation (1). It can be determined from experimental data by plotting the imposed voltage (E) against the current flow (I). When this was done for the data from test series JB-5 and 9, straight lines were drawn for the various cutting gap values, Figure 5. We interpreted these plots by referring to Equation (1) in the form

$$E = \hat{\Delta E} + IR \quad (1a)$$

When E was plotted against I and the best straight line fits were determined, common values of ΔE were obtained. The slope of each curve represented each resistance (R) associated with a given cutting gap. The ΔE 's are valid only for the ranges used in our tests.

Our analysis showed that the variation in ΔE is significantly smaller than the variation due to lack of fit of the straight line in the two test series. See Appendix II. 1. Therefore, it is reasonable to assume that ΔE can be considered constant for the alloy-electrolyte systems tested. In JB-5, the ΔE proved independent of gap, and feed rate (current density). In JB-9, the ΔE proved independent of gap, electrolyte pressures and velocity, temperature, and feed rate.

2.2.2 Estimate of Metal Removal Factor (K)

Metal removal or deposition which results when electricity is passed in electrolytic processes can be approximated by calculations based on Faraday's laws. These calculations, however, require a knowledge of the valence changes occurring during electrolysis, and the calculated values do not reflect the current efficiency obtainable in practical electrolytic processes.

In our mathematical analyses, Section 3, Chapter III, we therefore used an empirical factor K which relates actual volume metal removal to the electricity passed in practical electrolytic machining. We determined K by plotting feed rate against current density from data generated under the test conditions described at the beginning of this section. Thus, when the data from the test series JB-2, 4, 5 for René 41, NaCl systems and JB-8 and 9 for A-286- NaNO_3 system were plotted, straight lines were drawn, Figure 6. The slope of each curve represented an estimate of K for the alloy-electrolyte combination investigated.

The K for any specific alloy-electrolyte system was found to be constant at the current densities used in these tests. However, individual calculations indicated that K tended to change at current densities below 100 amp/in². Nevertheless, our tests indicated that K can be considered constant for the current density ranges used in practical electrolytic machining applications.

We further showed in our tests that the K for a given alloy-electrolyte composition is independent of the operating parameters, including electrolyte concentrations, and it, therefore, can be considered invariant for a given alloy-electrolyte system.

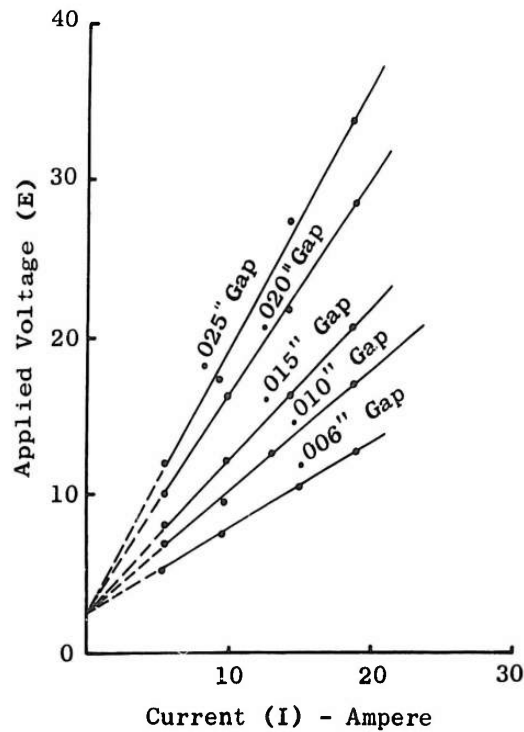
2.2.3 Estimate of Specific Resistance ρ

The specific resistance (ρ) for an electrolyte varies with a given chemical composition, concentration, and temperature. The specific resistance values (ρ) are determined with a standard conductivity cell. Methods of estimating will be discussed in Section 5, Chapter III.

2.3 Other Factors to be Considered in Electrolytic Machining

2.3.1 Ripple

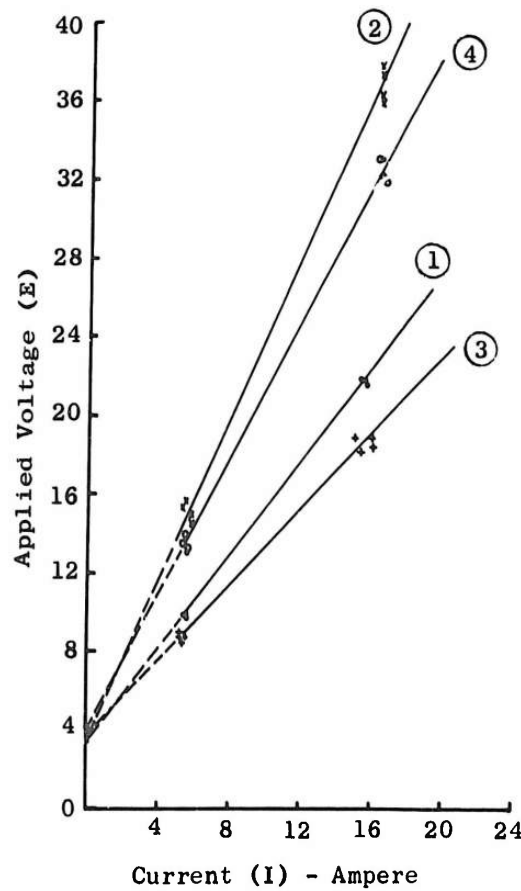
The ripple (voltage fluctuation) of the DC power supply often is suspected of affecting the process performance of electrolytic machining. Comparative data from



Material: Rene 41
Electrolyte: NaCl at 2.75 lb/gal
Temperature: 85°F

Estimated Value of $\hat{\Delta E} = 2.6$ volts

(a) Test Series JB-5



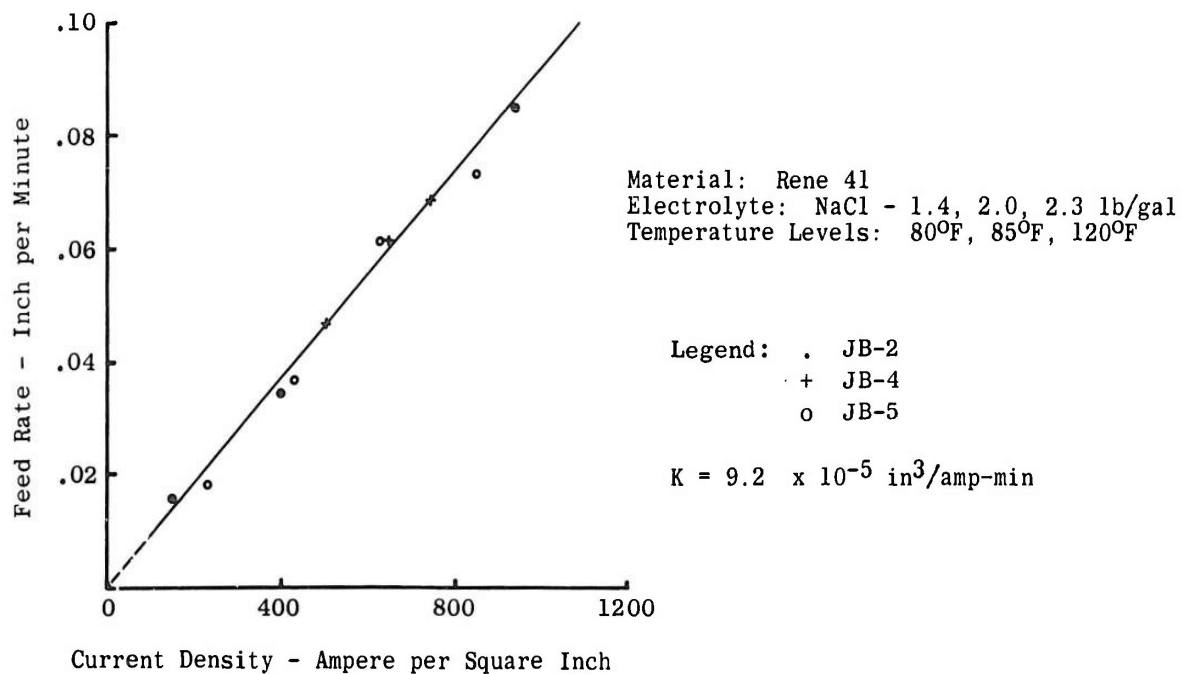
Material: A286
Electrolyte: NaNO₃ at 5.0 lb/gal

Test	Gap	Temp.
1	.012"	85°F
2	.025"	85°F
3	.012"	100°F
4	.025"	100°F

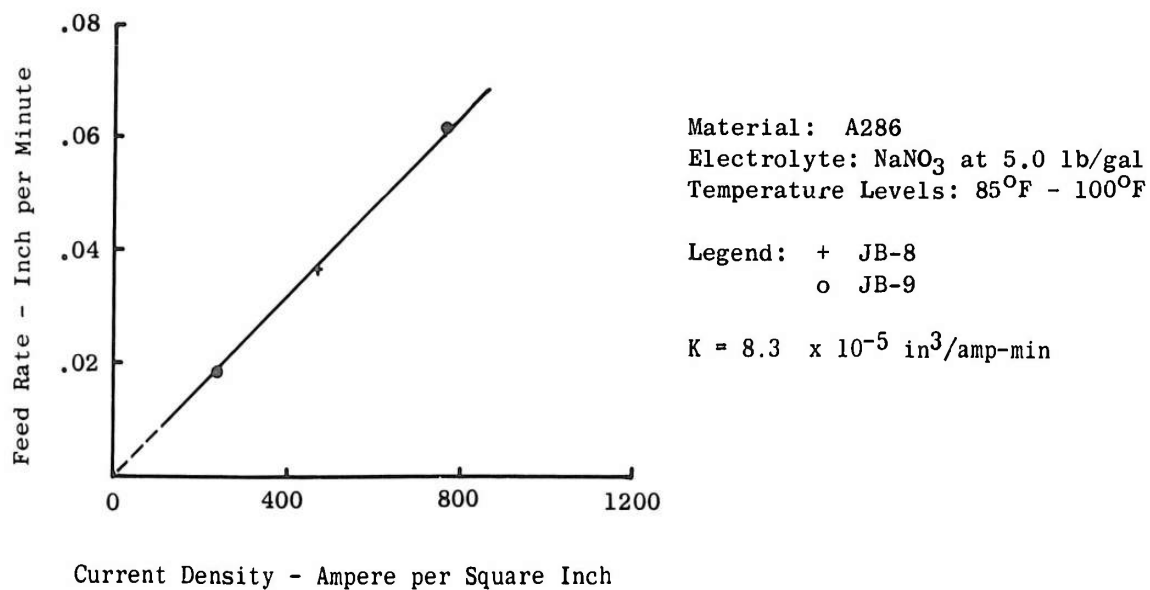
Estimated Value of $\hat{\Delta E} = 3.7$ volts

(b) Test Series JB-9

Figure 5. Current vs Voltage Plots for Estimates of Overvoltage ($\hat{\Delta E}$)



(a) Test Series JB-2, 4, 5



(b) Test Series JB-8 and 9

Figure 6. Current Density vs Feed Rate Plots for Estimates of K

Rene' 41-NaCl tests are available; one set of values was run using a power pack with high ripple (as much as 40% in one range of the test), and another set was run using a power pack of low ripple (did not exceed 4% over any part of the range). These tests showed that ripple did not affect the metal removal rate. Moreover, we found that ripple had no apparent effect on those response variables which depend upon voltage and current. See Appendix II. 3.

2.3.2 Sludge

During electrolytic machining, a precipitate called "sludge" can form as a product of electrochemical reactions.

In a series of tests on NaCl electrolyte (see Appendix II. 4), we noted that:

- (a) Sludge content had little effect on the specific gravity of the electrolytes.
- (b) Sludge does not significantly affect the conductivity of the electrolyte within the practical ranges of electrolytic machining.
- (c) The sludge content affects the viscosity of the electrolyte markedly. Figure 7 illustrates the effect of sludge on viscosity. In this case, the viscosity rises slowly to a sludge content of approximately 50% of the electrolyte volume; above 50% the viscosity increases at a rapidly accelerated rate. The sludge was measured in a test tube after it had been spun for 60 seconds in a laboratory centrifuge.
- (d) An increase in temperature reduces the sludge content, Figure 8.

2.3.3 Other Temperature Considerations

In our tests, temperature is shown to have a significant effect on:

- (a) The applied voltage.
- (b) The conductivity of the electrolyte.
- (c) The viscosity of the solution.
- (d) Surface finish; this will be discussed in Section 7, Chapter III.

The inlet temperature can be controlled externally. Thus, by necessity, the electrolyte temperature which concerns us, and which is the parameter we have used, is the temperature at the inlet of the tool. However, during electrolytic machining, heat is generated by the passage of current in the tool, the workpiece, and the electrolyte. We found in our tests that the heat generated, among other things, changed the temperature of the electrolyte in the cutting gap. With each change in electrolyte temperature, there is a corresponding change in those properties which it affects; for example, the specific resistance and the viscosity of the electrolyte, gap, and surface finish. See Appendix II. 2.

3. MATHEMATICAL ANALYSIS

A mathematical model is a convenient way to express the relationships among variables in any system under investigation. When electrical processes are considered, we think of the mathematical model of Ohm's law, if it is necessary to relate voltage, current and resistance, or perhaps Faraday's law to investigate metal deposition rates. These models are general in scope with specific definitions given to each parameter used. In many

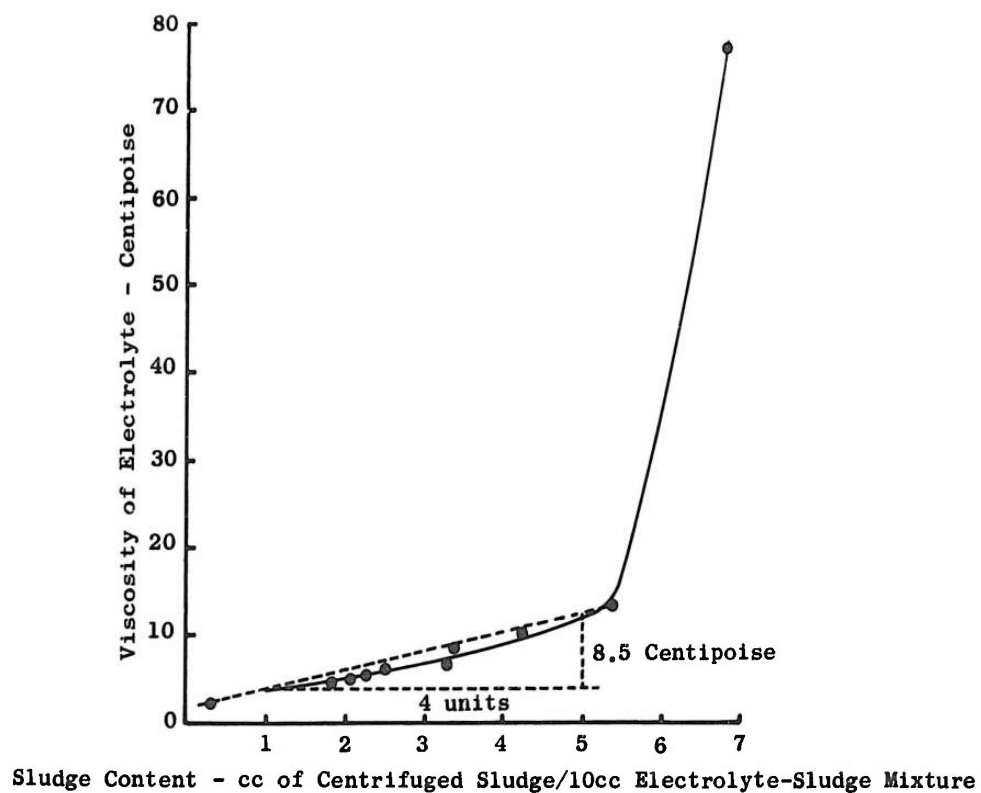


Figure 7. Viscosity of NaCl Versus Sludge Content from Electrolyte Used to Cut René 41

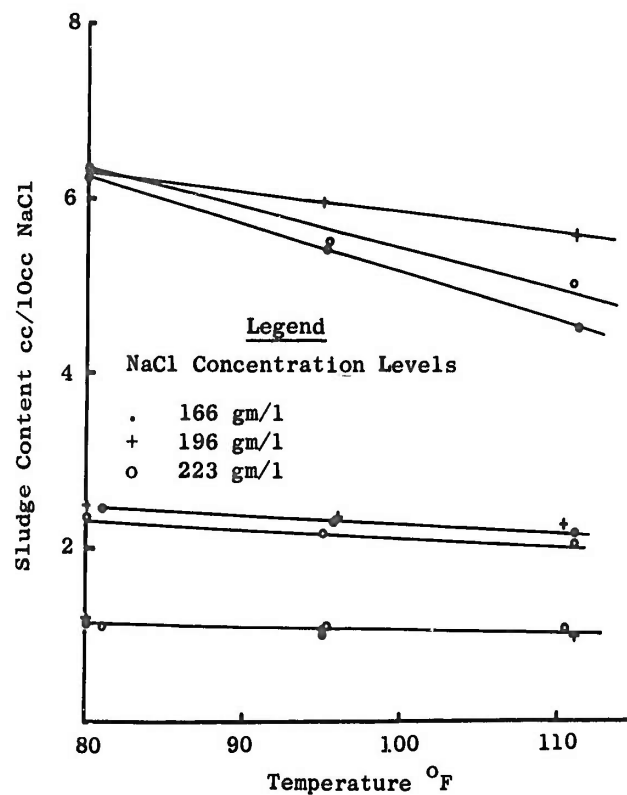


Figure 8. Sludge Content in NaCl Electrolyte vs Temperature at Various Electrolyte Concentrations

cases it is necessary to interpret these basic laws such that we can use them to express various special purpose phenomena, which are not specifically covered in the original definition of the model. One special case pertains to our immediate problem of using Ohm's and Faraday's laws to develop a meaningful relationship among the operating parameters and response variables which occur in electrolytic machining.

The cutting gaps between the electrode tool and the work surface are of particular interest in electrolytic machining. When we know the cutting gaps, we can design electrodes for desired workpiece shapes. This information is also necessary for calculating minimum machining time and the amount of machining stock required to achieve a given shape within a tolerance.

Starting with the basic definitions, we have developed mathematical models which permit us to relate more effectively some of the important process variables of electrochemical machining. Now, we shall develop the reasoning and logic which led to the development of the models in the form in which they will be used.

Beginning with Ohm's law as applied to electrochemistry,

$$\begin{aligned} E - \Delta E &= IR \\ \text{for } E - \Delta E &> 0 \end{aligned} \tag{1}$$

where

E is the applied electropotential in volt

ΔE is overpotential in volt

I is the current in amp

R is the resistance in ohms.

For our mathematical models we estimated the ΔE for given operating conditions from empirical data, Section 2, Chapter III, and use the symbol $\hat{\Delta E}$.

The resistance can be stated as

$$R = \frac{\rho L}{A_{cr}} \tag{2}$$

where, for R given in ohms,

L is the length of a conductor in inches

A_{cr} is the cross-section area of a conductor in in^2

ρ is the specific resistance of the electrolyte on ohm-in

From Faraday's laws we can relate volume metal removal to the electrocity passed during electrolysis as follows:

$$M_r d = \frac{Itw}{fz} \quad (3)$$

or

$$M_r = K_f It \quad (3a)$$

where

$$K_f = \frac{w}{zfd}$$

and

M_r is volume of metal removal or deposition

d is the material density

I is current

t is time

f is the Faraday constant

w is atomic weight

z is valence change during electrolysis

3.1 Steady State

Now let us examine the case where all operating parameters are held constant as time changes. That is to say, for a specific set of conditions and a given tool, an anode profile is obtained in a finite time (t_0) and the profile does not change with further machining under these fixed conditions. This we shall refer to as the steady state condition. This condition is accomplished when volume of metal removed (M_r) is equal to the volume displacement of the cathode.

The volume of metal removed can be related to the thickness of metal removed in the direction of feed (L_{oa}) and the surface area of the anode (A_a) from which metal is removed. That is to say,

$$M_r = L_{oa} A_a \quad (3b)$$

From our definition of steady state, we also have

$$L_{oa} A_a = L_{oc} A_c \quad (3c)$$

where L_{oc} is the distance of cathode travel and A_c is the surface area of the cathode. With the cathode displacement is associated a feed rate (F) which causes its displacement. Therefore, we may write that

$$F = L_{oc}/t \quad (3d)$$

To relate metal removal (M_r) to terms associated with the cathode for the defined case of steady state conditions we use Equations (3a), (3c) and (3d). However, instead of the constant K_f in Equation (3a) we use the metal removal factor K which we determined experimentally, Section 2, Chapter III.

We can therefore state that

$$KIt = L_{oc} A_c \quad (3e)$$

and

$$I = \frac{L_{oc}}{t} \cdot \frac{A_c}{K} \quad (3f)$$

$$\text{or} \quad I = \frac{FA_c}{K} \quad (3g)$$

where

I is the current in amp

K is the metal removal factor in $\text{in}^3/\text{amp-min}$

F is the applied feed in in/min

A_c is the surface area of the cathode in in^2 .

Substituting Equations (2) and (3g) into Equation (1), we have

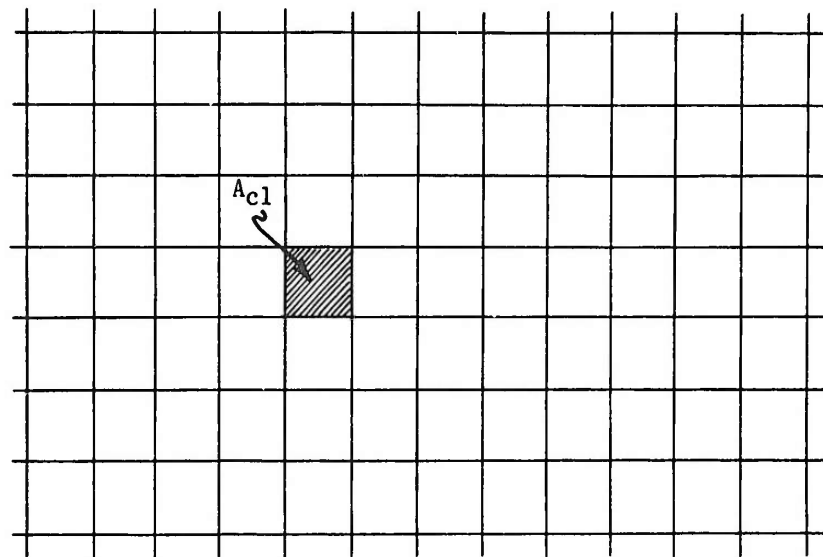
$$E - \Delta E = \frac{FA_c}{K} \cdot \frac{\rho L}{A_{cr}} \quad (4)$$

3. 1. 1 Electrode Design for Steady State Machining

We will now use the defined steady state case to investigate the design of an electrode tool which machines a required shape from a workpiece.

In order to develop this model we need to extend Equation (4) so that given an anode surface (A_a), described by a mesh of points, and given a set of operating parameters, we can use the model to determine the cathode surface (A_c) which produces A_a under the given conditions.

Assume that our required shape (A_a) is specified together with a set of operating parameters defining the conditions under which A_a can be successfully generated by electrolytic machining. The calculated distances (L_{11}) from each point on A_a measured along the normals to A_c will determine a tool (A_c), which has a mesh network similar to A_a . Assume that such a surface (A_c) has been found, and let A_{c1} represent a single mesh rectangle on A_c . See Figure 9. We can compute the distances (L_{1j}) from



View B-B

Mesh Network on A_c

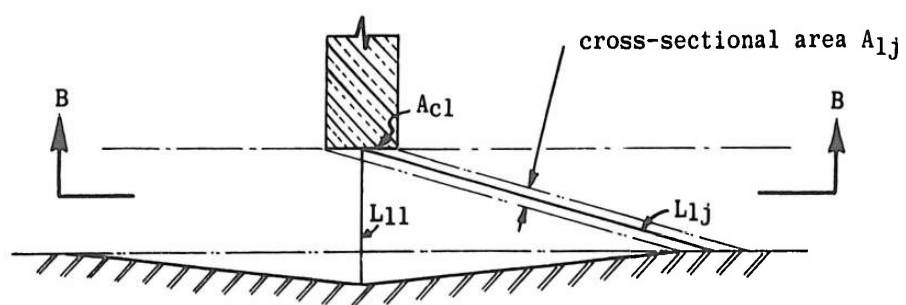


Figure 9. Effect of Single Cathode Mesh Rectangle on Anode Surface

the center of the mesh rectangle (A_{c1}) to the centers (j) of each mesh rectangle on A_a . To relate to the nomenclature given with Equation (2), we identify the distances (L_{1j}) as lengths of conductors, with a common base (A_{c1}), but with differing cross-section areas (A_{1j}). These A_{1j} 's are the projections of the mesh areas of A_a with respect to A_{c1} . If then, A_{c1} is the cathode surface affecting A_a , the total effect of A_{c1} is computed by summing all effects. Substituting the sum in Equation (4), we have

$$\sum_{j=1}^m \frac{A_{1j}}{L_{1j}} = \frac{FA_{c1}}{\frac{E - \Delta E}{\rho} K} \quad (5)$$

where m is the number of mesh rectangles on A_a .

There also is the case to consider where, with the selected operating parameters, there is some L_{1j} , and consequently a corresponding resistance, (R); the R is large enough to retard metal removal to an insignificant level. Let us call the L_{1j} a limiting distance. If the anode workpiece is a pure metal with a specific ΔE , no significant metal removal should occur at distances from A_{c1} which exceed the limiting L_{1j} . For a multiconstituent alloy, our ΔE may be considered to be the composite of the ΔE 's of the different alloying elements. Metal removal first slows down on the elements with larger ΔE 's, while other elements with smaller ΔE values continue to dissolve at faster rates. In the case of multiconstituents alloys, therefore, there should be an area on A_a where selective metal removal occurs — a phenomenon referred to as selective etching or selective attack.

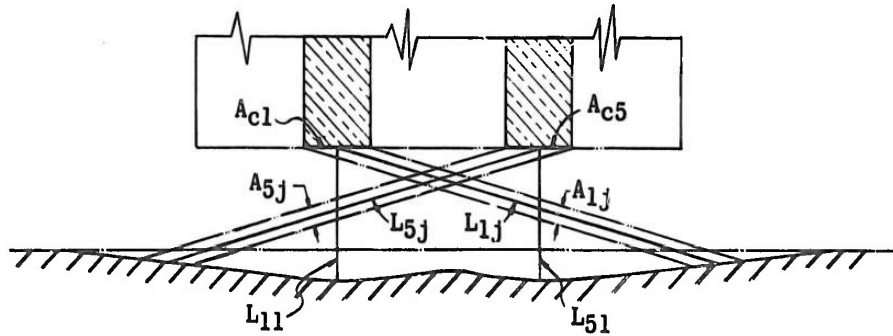


Figure 10. Effect of Two Cathode Mesh Rectangles on Anode Surface

Referring now to Figure 10 which illustrates the effect of two mesh rectangles on an anode surface (A_a), by reasoning similar to that which led to Equation (5), the effect of each mesh rectangle on A_c on the surface A_a is:

$$\begin{aligned}
\sum_{j=1}^m \frac{A_{1j}}{L_{1j}} &= \frac{F_1 A_{c1}}{\frac{E - \Delta E}{\rho} K} \\
\sum_{j=1}^m \frac{A_{2j}}{L_{2j}} &= \frac{F_2 A_{c2}}{\frac{E - \Delta E}{\rho} K} \\
&\vdots \\
\sum_{j=1}^m \frac{A_{nj}}{L_{nj}} &= \frac{F_n A_{cn}}{\frac{E - \Delta E}{\rho} K}
\end{aligned} \tag{6}$$

or we can use the more compact form

$$\sum_{j=1}^m \frac{A_{ij}}{L_{ij}} = \frac{F_i A_{ci}}{\frac{E - \Delta E}{\rho} K} \tag{6a}$$

where $i = 1, 2, \dots, n$, and n is the number of mesh rectangles on A_c . We use F_i to represent applied feed rate with respect to the mesh rectangle (A_{ci}).

Since F is defined as the applied feed in the direction of the ram travel, we must consider orientation of the mesh rectangles on the surface (A_c) with respect to F and compute F_i accordingly. This is discussed in detail in Section 4, Chapter III.

Equation (6a) can be rewritten as

$$\frac{A_{i1}}{L_{i1}} + \sum_{j=2}^m \frac{A_{ij}}{L_{ij}} = \frac{F_i A_{ci}}{\frac{E - \Delta E}{\rho} K} \tag{6b}$$

where $\frac{A_{i1}}{L_{i1}}$ is the effect of A_{c1} on the mesh rectangles on A_a , which are the shortest distances (L_{i1}) from A_{c1} . Equation (6b) is simplified:

$$\frac{A_{i1}}{L_{i1}} = \frac{F_i A_{ci}}{\frac{E - \Delta E}{\beta_1 \rho} K} \tag{6c}$$

where

$$\beta_i = \left\{ 1 - \frac{\sum_{j=2}^m \frac{A_{ij}}{L_{ij}}}{\sum_{j=1}^m \frac{A_{ij}}{L_{ij}}} \right\} \quad (7)$$

The β_i which we call "overcut index" relates current flow across the shortest gap distances (L_{i1}) to the currents flowing along all other paths (L_{ij}).

When the mesh on A_a and A_c is adjusted so that the mesh areas A_{i1} are equal to the mesh areas A_{ci} , Equation (6c) is reduced to the form

$$L_{i1} = \frac{E - \hat{\Delta E}}{F_i \rho \beta_i} K \quad (8)$$

Equation (8) brings into focus the problem of determining the functional dependence of any of the variables on each other and on the process environment. In our process we impose and control the feed rate (F_i) and the voltage (E), and they are therefore independent of the other variables.

The overcut index (β_i) in Equation (7) is dependent only on cutting gaps and areas. This was verified by experiments described in Section 4, Chapter III, in which we investigated the β_i for a range of gaps under varying process conditions and for two anode material/electrolyte combinations.

Our analyses of the effects of varying process conditions on our estimated factors $\hat{\Delta E}$ and K discussed in Section 2, Chapter III, did not disclose their functional dependence on the tested variables in the operating ranges used in practical electrolytic machining.

If, however, it were shown that our estimating methods do not apply to all engineering materials or electrolytic machining conditions, the variables we now use in our models can be substituted by expressions which describe their functional dependence on the critical process variables. Such expressions for variables $\hat{\Delta E}$ and K are discussed in Section 6, Chapter III, and we show in Section 5, Chapter III, expressions for the variable ρ . For this analysis, however, we will assume that $\hat{\Delta E}$ and K are invariant, and that ρ can be held constant by process control.

Equations (6b) and (8) are two mathematical models which may be used in designing a tool for an electrolytic machining problem. Equation (8) apparently is simpler and could be used if β_i were known. We would calculate gaps at a number of points on the anode surface and obtain a cathode tool. However, we have not found a simple calculating method for the β_i 's, and we resorted to solving Equation (6b) on a digital computer and

the following approach has been successful. In Equation (6b), $\sum_{j=2}^m \frac{A_{ij}}{L_{ij}}$ is considered as

a "stray" effect which is a small percentage of the total effect. To ensure that this is

considered, in the initial computer calculation, Equation (6b) is stated as

$$\frac{A_{i1}}{L_{i1}} + \omega \sum_{j=2}^m \frac{A_{ij}}{L_{ij}} = \frac{F_i A_{ci}}{\frac{E - \Delta E}{\rho} K} \quad (6d)$$

where

$$0 \leq \omega \leq \omega_0 \ll 1$$

The values ΔE , ρ , and K were obtained from empirical data. The required surface (A_a) is given as a set of points (x, y, z); a first guess at A_c is obtained on the computer by constructing a surface (A_c) which is the mirror image of A_a , or a constant distance (L) away from A_a . Since this L is only a guess at the actual gap, we assume that our L_{ij} 's are all in error by an amount ΔL_{ij} . Thus, we write Equation (6d) in the form

$$\frac{A_{i1}}{L_{i1} + \Delta L_{i1}} = \frac{F_i A_{ci}}{\frac{E - \Delta E}{\rho} K} - \omega \sum_{j=2}^m \frac{A_{ij}}{L_{ij}} \quad (6e)$$

$$\Delta L_{i1} = \frac{A_{i1}}{\frac{F_i A_{ci}}{\frac{E - \Delta E}{\rho} K} - \omega \sum_{j=2}^m \frac{A_{ij}}{L_{ij}}} - L_{i1} \quad (6f)$$

Next, we substitute the computed L_{ij} values from the first guess into the right hand side of Equation (6f); this gives us the first guess at the values L_{i1} . Our new L_{i1} values are computed by setting

$$L_{i1}^{\text{new}} = L_{i1}^{\text{old}} + \Delta L_{i1} \quad (6g)$$

Essentially this gives a second guess at A_c . This process of iteration continues until the convergence or tolerance criterion

$$\text{Max}_{(i)} |\Delta L_{i1}| \leq \epsilon_1 \quad (9)$$

is met,

where ϵ_1 is a small percentage of the computed gaps L_{i1} .

We would have thus described A_c , the distances (L_{ij}) and specific values of the overcut index (β_i).

Gaps obtained in this manner were compared with gaps obtained from actual test runs for two different electrolyte-material combinations with different process parameters. These results are discussed in Section 4, Chapter III, and the FORTRAN instructions for the computer program are included in Appendix III.

3.2 Transient Conditions

Even when the tool shape is known, other questions about the machining process have to be answered. For instance, how much stock is removed from a given raw stock anode, and what is the minimum time necessary to obtain the desired workpiece contour? This information can be obtained from models with which one can investigate the process under transient conditions. The models should make available the contour of the raw stock anode at any time during the machining.

To develop transient models, we assume that our tool surface (A_c) and raw stock anode surface (A_s) are given. Since applied feed rate (F_i) is defined as rate of change of the tool or workpiece position, Equation (3c), we want to determine the appearance of the surface (A_s) after machining for time (t_n), Figure 11. As in the steady state case, we use a mesh network over A_c and a corresponding one over A_s , and the two surfaces are separated by starting gaps (L_{ij}^*). Thus, all L_{ij}^* values are known before the system starts operating.

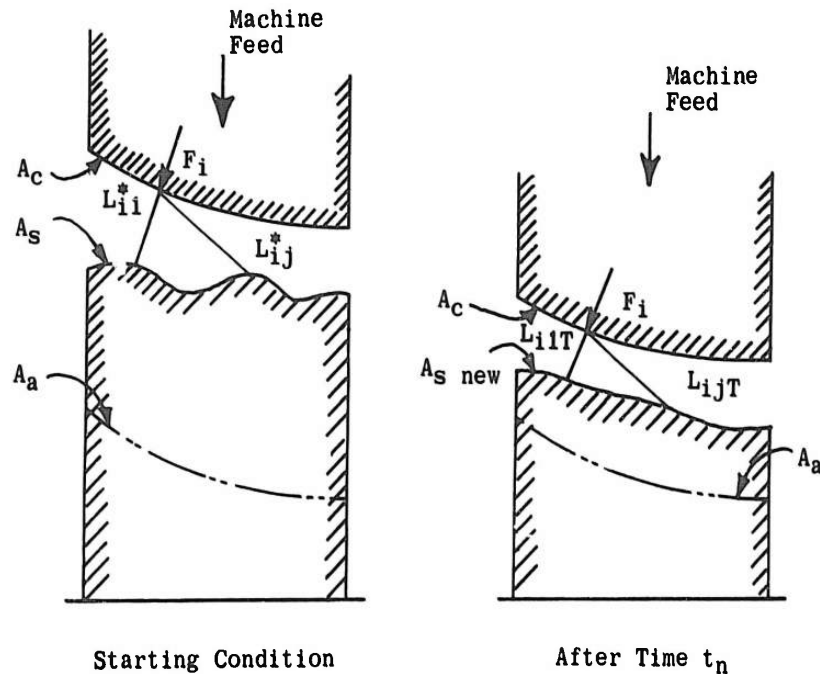


Figure 11. Transient Surface

For a specified time (t_n), the cathode surface travels a distance which is equal to the feed rate (F_i) multiplied by the time (t_n).

The transient model can be handled similarly to Equation (6f). The ΔL_{i1} values or $F_i t_n$ are known as soon as feed rate and time are specified, and the gaps are to be found. The maximum t_n at any time step is chosen so that the maximum $F_i t_n$ is always less than the corresponding value of L_{ijT} . We therefore have

$$L_{jiT} = \frac{A_{i1}}{\frac{F_i A_{c1}}{E - \Delta E} K - \omega \sum_{j=2}^m \frac{A_{ij}}{L_{ijT}}} - F_i t_n \quad (10)$$

The guess at L_{ijT} would be substituted into the right hand side of Equation (10) and L_{i1T} values computed, giving the next guess at A_s .

The process of iteration is continued until a new surface (A_s) is described for a given time step (t_n). The convergence criterion for this case is

$$\left| L_{i1T} - \left[\frac{A_{i1}}{\frac{F_i A_{c1}}{E - \Delta E} K - \omega \sum_{j=2}^m \frac{A_{ij}}{L_{ijT}}} - F_i t_n \right] \right| \leq \epsilon_2 \quad (11)$$

where ϵ_2 is a small percentage of the gaps (L_{ijT}).

The model, Equation (10), can be used to simulate transient process conditions under constant and variable electrode feeds (F_i).

A more general model can be set up which is independent of the applied (external) feed rate. From Equation (3a) and (4), by using the metal removal factor K we have

$$L_{ijT} = \frac{A_{ij}}{K} \quad (12)$$

Substituting Equation (12) into Equation (10), then

$$L_{ijT} = \frac{A_{ij}}{K} \quad (13)$$

where L is the thickness of metal removed and L as the gap and considering first the case where no external

$$L_{oa} = L - L^* \quad (13a)$$

and substituting for L_o in Equation (13), we have

$$E - \Delta E = \frac{L (L - L^*) \rho A_a}{K A_{cr} t} \quad (13b)$$

Considering that the gaps vary between the two electrodes, we write

$$\sum_{j=1}^m \frac{A_{ij}}{L_{ijT} (L_{ijT} - L^*_{ij})} = \frac{\rho A_{ai}}{(E - \Delta E) K t} \quad (14)$$

The L^*_{ij} 's are determined at the start of the process; the L_{ijT} 's are the total transient gaps.

As we did with the previous models, for computational purposes we write

$$L_{ijT} (L_{ijT} - L^*_{ij}) = \frac{A_{i1}}{\frac{A_{ai} \rho}{(E - \Delta E) K t} - \omega \sum_{j=2}^m \frac{A_{ij}}{L_{ijT} (L_{ijT} - L^*_{ij})}} \quad (14a)$$

Using the quadratic formula, then

$$L_{i1T} = \frac{L^*_{i1}}{2} + \frac{1}{2} \left(L^*_{i1} + \frac{4 A_{i1}}{\frac{A_{ai} \rho}{(E - \Delta E) K t} - \epsilon \sum_{j=2}^m \frac{A_{ij}}{L_{ijT} (L_{ijT} - L^*_{ij})}} \right)^{1/2} \quad (14b)$$

where the plus sign is chosen for consistency with Equation (13a).

The convergence of Equation (14b) can be handled the same as Equation (10).

We defined internal feed rate as the rate of change of the cutting gap (L_{i1T}) with respect to time. We can now determine the internal feed rate for any time t_n to t_m with the expression

$$F_{iT(int)} = \frac{L_{i1Tm} - L_{i1Tn}}{t_m - t_n} \quad (14c)$$

Equation (14b) is a general model with which we can simulate many special machining cases including the cases treated thus far.

Although developed for dwell cutting which does not use an applied feed, the model Equation (14b) can be readily programmed to include external electrode feeds. In this case we would calculate the gap changes for each interval (t_n) and adjust the cathode position after each calculation. Hence, we can either impose a predetermined applied feed, or we can determine that applied feed program which will achieve a final shape in the shortest machining time.

This model can also be used for the programming of adaptive control methods. For example, by putting restraints on the L_{i1T} 's and monitoring the input parameters we can maximize cathode feed and workpiece removal rates.

Although the models, Equations (10) and (14b) have not been tested, we will discuss briefly the approaches to solving the problems of calculating excess machining stock and designing electrodes for transient shapes.

3.2.1 Excess Machining Stock Calculations

A nominal workpiece surface (A_a) was used as a basis for our electrode design. The electrode surfaces were defined by the distances L_{i1} from a nominal anode surface A_a . When we now assign a tolerance band (ϵ_3), around the nominal surface (A_a), the calculations with a transient model, Equation (10) or (14b), are continued for a sufficient number of time steps (t_n) until the computed surface (A_s) deviates from the nominal surface (A_a) by an amount no greater than ϵ_3 .

This requirement is satisfied when

$$|L_{i1T} - L_{i1}| \leq \epsilon_3 \quad (15)$$

Now excess stock and minimum time (t_{min}) to obtain A_a within ϵ_3 are calculated. The minimum time is computed by summing the t_n , and excess stock equals the feed rate multiplied by the total minimum time

$$t_{min} = \sum_n t_n \quad (16)$$

$$X_{si} = F_i t_{min} \quad (17)$$

where X_{si} is amount of excess stock in the direction of feed.

In practical applications, we are also concerned with the tolerance of the raw stock. The greater the deviation of the raw stock surface (A_s) from the desired final part shape, the more excess machining stock is required, and an economic balance may often exist between the cost of producing a raw stock tolerance and the cost of excess stock.

We will review two excess stock conditions; one, where a "preform" surface (A_s) varies from A_a by a tolerance $\Theta > \epsilon_3$, the other where the final shape is machined from a flat raw stock surface.

In both cases, we must select starting gaps (L_{i1}^*) so that the maximum stock condition on surface (A_s) is a minimum distance (G_s) from the cathode surface (A_c).

When we consider the preform case, Figure 12, we use the maximum stock conditions ($A_{s \text{ max}}$) for the selection of a minimum starting gap (G_s), and we use the minimum stock as the starting condition ($A_{s \text{ min}}$) for our calculations.

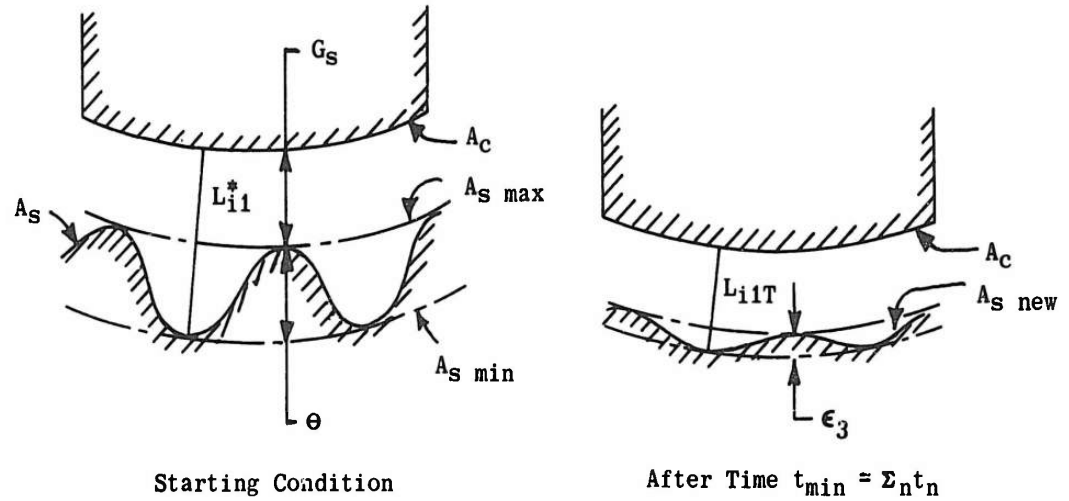


Figure 12. Preform Machining

The case where a shape is to be machined into a flat raw stock surface is illustrated in Figure 13. Minimum gaps (G_s) and the conditions for L_{i1}^* at the beginning of the calculations are described. As in the previous case, the calculations are continued for a sufficient number of time steps (t_n) until all points on the surface (A_s) fall within the tolerance band (ϵ_3).

3.2.2 Electrode Design for Transient Shapes

There may be the case where a raw stock shape is given and the amount of excess stock is restricted so that steady state machining conditions cannot be achieved. In this case, we can apply the mathematical description of transient machining, Equation (10), for the design of the electrode surface (A_c) if we compute the L_{i1}^* with respect to the required nominal shape (A_a) for a given amount of excess stock, and if we restrict the cutting time (t_n) as follows:

$$t_{\text{max}} = \frac{X_{si}}{F_i} \quad (18)$$

where

$$X_{si} = X_{s\text{imin}} + \epsilon_3$$

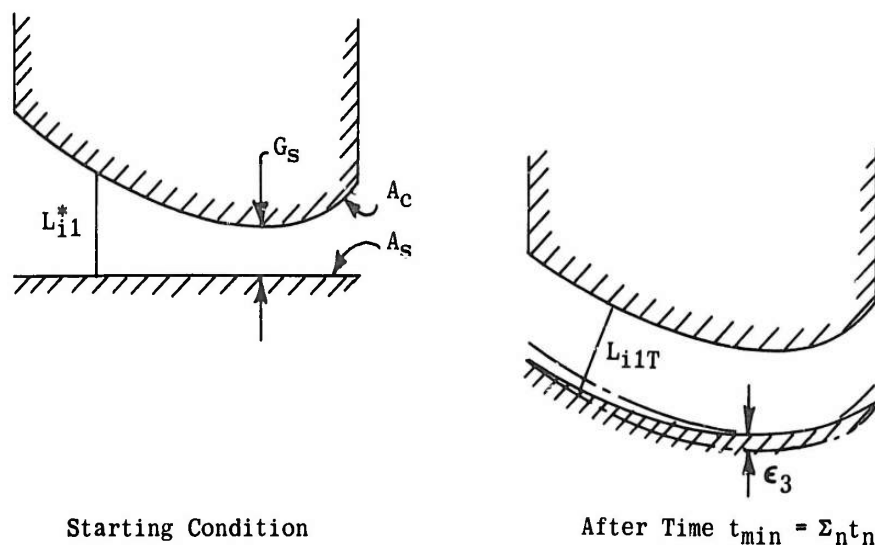


Figure 13. Flat Surface Machining

There may be cases where a given raw stock shape cannot be machined to a final shape within given tolerances with selected operating parameters. In that case, we may assign different operating parameters and repeat our computations to investigate whether the desired final shape can be achieved under any electrolytic machining condition.

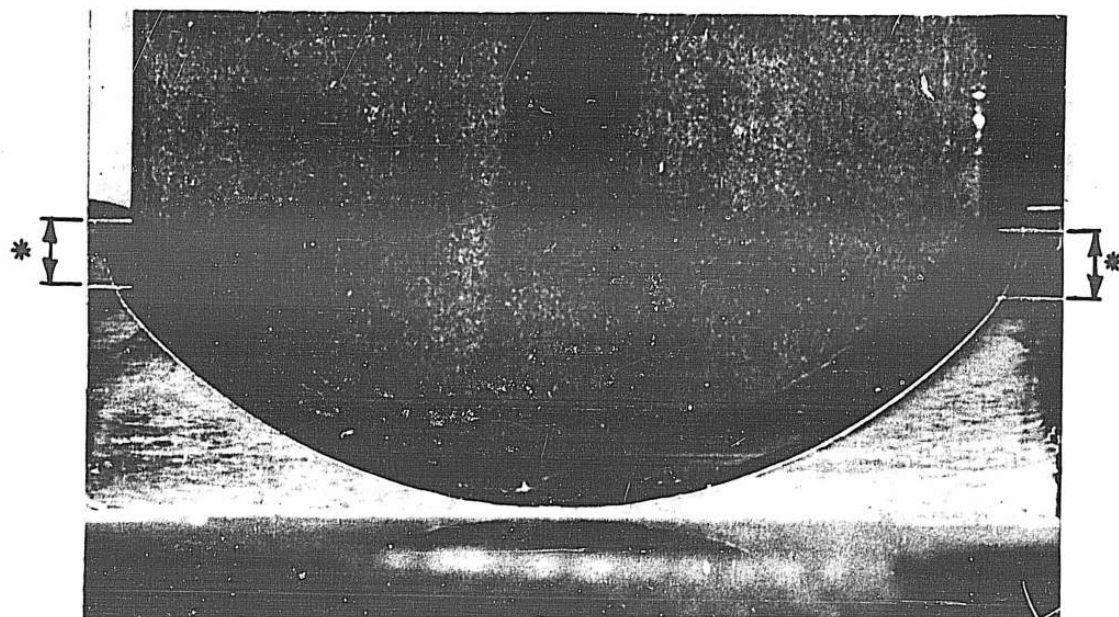
4. VERIFICATION OF A MATHEMATICAL MODEL

Various mathematical models were described in Section 3, Chapter III, for specific electrolytic machining conditions. We tested one of these models by comparing actual machining and computed results. The model which we selected describes steady state machining, Equation (6d). This was programmed for the IBM 7094 digital computer.

The steady state model is useful for the design of electrode tools. In our tests, we fixed the shape of the electrode tool and computed resultant cutting gaps for various combinations of operating parameters. The shape of our electrode tool was the segment of a cylinder with a radius of 1.0000", a chord of 1.509", and a width of 0.920", Figure 14.

The test tooling, which is further described in Section 4, Chapter IV, has a device for the measurement of the cutting gap. Although gap dimensions were computed for the entire cutting area, we had to confine the gap comparison to that cylindrical section line which intersects the gap measurement pin. The measuring procedure is described in Appendix II. 6. 1.

We machined the nickel-base alloy René 41 with NaCl electrolyte and the iron-base alloy A-286 with NaNO_3 electrolyte. Moreover, we used five combinations of operating parameters for the René 41 material and three combinations for the A-286 material. See Table 2. We machined three workpieces with each combination of operating parameters, and we used an average of the three gap measurements in our comparison with the calculated gaps.



* Vertical cathode surfaces were not considered in computer calculations.

Figure 14. Electrode Tool Contour Machining Test

TABLE 2
OPERATING PARAMETERS, CONTOUR MACHINING TESTS

OPERATING PARAMETERS	Rene 41 Matl Test No.					A286 Matl Test No.		
	C1	C3	C4	C5	C6	D1	D2	D3
Electrolyte composition	NaCl	NaCl	NaCl	NaCl	NaCl	NaNO ₃	NaNO ₃	NaNO ₃
Electrolyte concentration(lb/gal)	2.1	2.1	2.1	2.1	2.1	5.0	5.0	5.0
Electrolyte temperature, tank(°F)	94	94	94	94	94	100	100	100
Electrolyte temperature rise**(°F)	6.5	11.0	2.0	6.0	6.0	4.0	11.0	15.0
Applied feed (in/min)	.040	.060	.020	.040	.060	.020	.040	.060
Applied voltage (volt)	11.0	14.5	6.0	8.0	11.0	14.0	12.0	16.0
Cutting time (min)	4.75	3.15	9.5	4.75	3.15	25.0	12.5	8.33
Average current* (amp)	663	957	333	619	917	426	736	1,087
Electrolyte pressure, inlet* (psig)	240	240	200	240	275	240	240	240
Electrolyte pressure, outlet*(psig)	20	20	40	20	20	20	20	20
Electrolyte flow* (gal/min)	4.4	4.5	2.4	2.7	3.4	8.9	3.6	3.6

* Average values at end of machining cycle.
 ** Average values measured in exit channel of machining fixture. (See Fig. 83.)

4.1 The Computer Program

We developed the computer program for the steady state machining case and for the selected electrode shape by:

- (a) Describing the electrode tool (cathode) as a set of points.
- (b) Constructing normals and computing direction cosines.
- (c) Constructing a workpiece (anode) surface.
- (d) Computing feed rates (F_i), areas (A_{ij}), and distances (L_{ij}).
- (e) Computing changes in gaps by iteration.
- (f) Correcting the shape of the anode surface.
- (g) Satisfying the convergence criterion.

A detailed discussion of this procedure follows:

Let a cathode surface A_c be oriented to any (X, Y, Z) coordinate system such that the Z axis corresponds to the direction of the feed rate at the center of the tool. Lines $X = \text{constant}$, $Y = \text{constant}$ are drawn on the surface (A_c) defining a mesh network. The points of intersection of these lines (X_{ci} , Y_{cj} , Z_{cij}) will describe the surface (A_c). The set of points (X_{ai} , Y_{aj} , Z_{aj}) on the workpiece are determined by giving a first guess of the gaps (L) and assuming a mirror image of the cathode. This is accomplished in the following manner:

We consider a plane described by any five neighboring points on the cathode, Figure 15.; e.g., the points

$$(X_{ci-1}, Y_{cj}, Z_{ci-1,j}); (X_{ci}, Y_{cj-1}, Z_{ci,j-1}); (X_{ci}, Y_{cj}, Z_{ci,j});$$

$$(X_{ci}, Y_{cj+1}, Z_{ci,j+1}); (X_{ci+1}, Y_{cj}, Z_{ci+1,j}).$$

If α , δ , γ are the direction cosines of the normal to this plane, then

$$X_{cl} = X_{ci} + \alpha L \quad (19)$$

$$Y_{cl} = Y_{cj} + \delta L \quad (20)$$

$$Z_{cl} = Z_{cij} + \gamma L \quad (21)$$

where L is the guess at the gap between the anode and the cathode, and

$$F_i = F \cos \gamma_i \quad (22)$$

is the applied feed in the direction of the normal.

To compute a projected anode area A_{ij} associated with an area A_{ci} on the cathode, we chose a corresponding ABCD on the anode

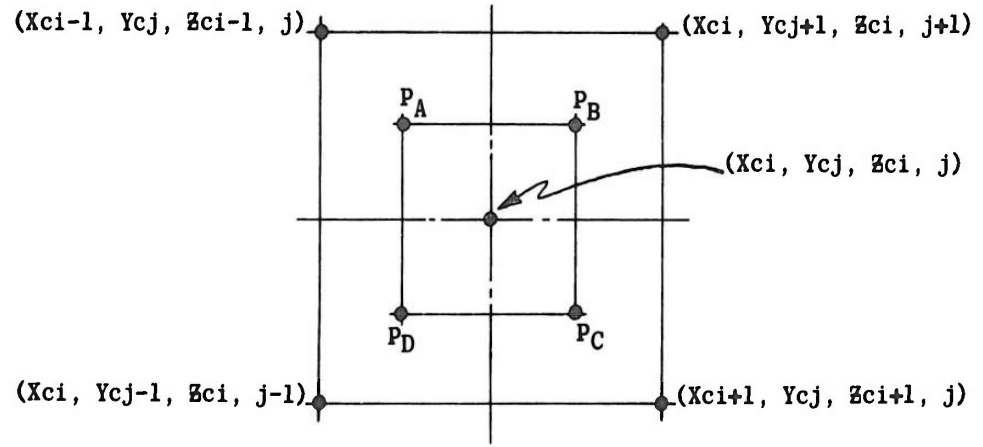


Figure 15. Quadrilateral ABCD

such that its corner points are:

$$P_A: \left\{ X_A = \frac{X_{ai_1} + X_{ai_3}}{2}; \quad Y_A = \frac{Y_{ai_1} + Y_{ai_3}}{2}; \quad Z_A = f(X_A, Y_A) \right\}$$

$$P_B: \left\{ X_B = \frac{X_{ai_2} + X_{ai_3}}{2}; \quad Y_B = \frac{Y_{ai_2} + Y_{ai_3}}{2}; \quad Z_B = f(X_B, Y_B) \right\}$$

$$P_C: \left\{ X_C = \frac{X_{ai_4} + X_{ai_3}}{2}; \quad Y_C = \frac{Y_{ai_4} + Y_{ai_3}}{2}; \quad Z_C = f(X_C, Y_C) \right\}$$

$$P_D: \left\{ X_D = \frac{X_{ai_4} + X_{ai_5}}{2}; \quad Y = \frac{Y_{ai_4} + Y_{ai_5}}{2}; \quad Z_D = f(X_D, Y_D) \right\}$$

where $f(x, y)$ is the equation of the least squares surface. If A is the area ABCD, then

$$A_{ij} = 2A_\gamma (\alpha \alpha_c + \delta \delta_c + \gamma \gamma_c) \quad (23)$$

is the projected area and α_c , δ_c , and γ_c are the direction cosines of the normal to the surface $f(x, y)$. The distances are computed as

$$L_{ij} = \left\{ (X_{cl} - X_{ai})^2 + (Y_{cl} - Y_{aj})^2 + (Z_{cl} - Z_{aij})^2 \right\}^{1/2} \quad (24)$$

Equations (6a), (6b) and (7) are computed during each iteration. The corrected anode surface is obtained by the set of equations

$$X_{cl \text{ new}} = X_{cl \text{ old}} + \alpha \Delta L_{i1} \quad (25)$$

$$Y_{cl \text{ new}} = Y_{cl \text{ old}} + \delta \Delta L_{i1} \quad (26)$$

$$Z_{cl \text{ new}} = Z_{cl \text{ old}} + \gamma \Delta L_{i1} \quad (27)$$

The iteration is continued until

$$\max \left| \Delta L_{i1} \right| \leq \epsilon_1 \quad (9a)$$

where ϵ_1 , a given small percentage of the gap, is used as a convergence criterion. In our case ϵ_1 was .0000001".

Tables 3, 4 and 5 show the computer input (description of cathode) and the output on the center x mesh line (number 6) after the first guess and after each iteration for test case D1.

In Table 3, the following input instructions are printed:

N is the number of X values
M is the number of Y values
N2 is the total number of iterations planned
NZ is the total number of Z
GAP is the initial starting gap
XP, YP, ZP are reference points for assimilated motion (not currently used)
IMAX is the current iteration
FO is the feed rate in in/min
K is the metal removal factor in in³/amp-min.

The input values for E , ΔE and ρ were not printed.

In Tables 4 and 5, column 1 is the x mesh line number, column 2 represents y point numbers, columns 3, 4, 5 are x, y, z coordinates respectively, column 6 is the computed change in gap (ΔL), column 7 is the value of L_{i1} , column 8 is the value of

$\sum_{j=2}^m \frac{A_{ij}}{L_{ij}}$, and column 9 is the computed value of the overcut index (β_1). The computed

coordinates for the anode are not a rectangular mesh. The solution of the system of equations was obtained in four iterations.

The FORTRAN instructions for this program are included in Appendix III.

COMPUTER INPUT DESCRIPTION OF CATHODE SURFACE Ac

N = 11 N = 24 N2 = 5 N2 = 15 GAP = 0.0190										
RP = 0. YP = 0. ZP = 23000.0000										
INAX = 0. F0 = 2.00000-02 K = 8.04000-05										
INPUT CATHODE										
X VALUES										
0.	0.0920	0.1840	0.2760	0.3680	0.4600	0.5520	0.6440	0.7360	0.8280	0.9200
Y VALUES										
-0.7833	-0.7273	-0.6714	-0.6154	-0.5595	-0.5035	-0.4476	-0.3916	-0.3357	-0.2797	-0.2238
0.1119	0.1678	0.2238	0.2797	0.3357	0.3916	0.4476	0.5035	0.5595	0.6154	0.6714
0.7273	0.7833	0.8393	0.8952	0.9511	1.0071	1.0630	1.1190	1.1749	1.2308	1.2868
Z VALUES										
1	2	3	4	5	6	7	8	9	10	11
1	0.3784	0.3127	0.2589	0.2110	0.1671	0.1232	0.0793	0.0354	0.0015	0.0000
1	0.1712	0.1361	0.1058	0.0799	0.0540	0.0281	0.0022	0.0000	0.0000	0.0000
1	0.0580	0.0399	0.0254	0.0142	0.0063	0.0016	0.0000	0.0000	0.0000	0.0000
1	0.0063	0.0016	0.0000	0.0000	0.0000	0.0000	0.0000	0.0000	0.0000	0.0000
1	0.0580	0.0399	0.0254	0.0142	0.0063	0.0016	0.0000	0.0000	0.0000	0.0000
1	0.1712	0.1361	0.1058	0.0799	0.0540	0.0281	0.0022	0.0000	0.0000	0.0000
1	0.3784	0.3127	0.2589	0.2110	0.1671	0.1232	0.0793	0.0354	0.0015	0.0000
1	0.3784	0.3127	0.2589	0.2110	0.1671	0.1232	0.0793	0.0354	0.0015	0.0000
2	0.3784	0.3127	0.2589	0.2110	0.1671	0.1232	0.0793	0.0354	0.0015	0.0000
2	0.0580	0.0399	0.0254	0.0142	0.0063	0.0016	0.0000	0.0000	0.0000	0.0000
2	0.0063	0.0016	0.0000	0.0000	0.0000	0.0000	0.0000	0.0000	0.0000	0.0000
2	0.0580	0.0399	0.0254	0.0142	0.0063	0.0016	0.0000	0.0000	0.0000	0.0000
2	0.1712	0.1361	0.1058	0.0799	0.0540	0.0281	0.0022	0.0000	0.0000	0.0000
2	0.3784	0.3127	0.2589	0.2110	0.1671	0.1232	0.0793	0.0354	0.0015	0.0000
3	0.3784	0.3127	0.2589	0.2110	0.1671	0.1232	0.0793	0.0354	0.0015	0.0000
3	0.1712	0.1361	0.1058	0.0799	0.0540	0.0281	0.0022	0.0000	0.0000	0.0000
3	0.0580	0.0399	0.0254	0.0142	0.0063	0.0016	0.0000	0.0000	0.0000	0.0000
3	0.0063	0.0016	0.0000	0.0000	0.0000	0.0000	0.0000	0.0000	0.0000	0.0000
3	0.0580	0.0399	0.0254	0.0142	0.0063	0.0016	0.0000	0.0000	0.0000	0.0000
3	0.1712	0.1361	0.1058	0.0799	0.0540	0.0281	0.0022	0.0000	0.0000	0.0000
3	0.3784	0.3127	0.2589	0.2110	0.1671	0.1232	0.0793	0.0354	0.0015	0.0000
4	0.3784	0.3127	0.2589	0.2110	0.1671	0.1232	0.0793	0.0354	0.0015	0.0000
4	0.1712	0.1361	0.1058	0.0799	0.0540	0.0281	0.0022	0.0000	0.0000	0.0000
4	0.0580	0.0399	0.0254	0.0142	0.0063	0.0016	0.0000	0.0000	0.0000	0.0000
4	0.0063	0.0016	0.0000	0.0000	0.0000	0.0000	0.0000	0.0000	0.0000	0.0000
4	0.0580	0.0399	0.0254	0.0142	0.0063	0.0016	0.0000	0.0000	0.0000	0.0000
4	0.1712	0.1361	0.1058	0.0799	0.0540	0.0281	0.0022	0.0000	0.0000	0.0000
4	0.3784	0.3127	0.2589	0.2110	0.1671	0.1232	0.0793	0.0354	0.0015	0.0000
5	0.3784	0.3127	0.2589	0.2110	0.1671	0.1232	0.0793	0.0354	0.0015	0.0000
5	0.1712	0.1361	0.1058	0.0799	0.0540	0.0281	0.0022	0.0000	0.0000	0.0000
5	0.0580	0.0399	0.0254	0.0142	0.0063	0.0016	0.0000	0.0000	0.0000	0.0000
5	0.0063	0.0016	0.0000	0.0000	0.0000	0.0000	0.0000	0.0000	0.0000	0.0000
5	0.0580	0.0399	0.0254	0.0142	0.0063	0.0016	0.0000	0.0000	0.0000	0.0000
5	0.1712	0.1361	0.1058	0.0799	0.0540	0.0281	0.0022	0.0000	0.0000	0.0000
5	0.3784	0.3127	0.2589	0.2110	0.1671	0.1232	0.0793	0.0354	0.0015	0.0000
6	0.3784	0.3127	0.2589	0.2110	0.1671	0.1232	0.0793	0.0354	0.0015	0.0000
6	0.1712	0.1361	0.1058	0.0799	0.0540	0.0281	0.0022	0.0000	0.0000	0.0000
6	0.0580	0.0399	0.0254	0.0142	0.0063	0.0016	0.0000	0.0000	0.0000	0.0000
6	0.0063	0.0016	0.0000	0.0000	0.0000	0.0000	0.0000	0.0000	0.0000	0.0000
6	0.0580	0.0399	0.0254	0.0142	0.0063	0.0016	0.0000	0.0000	0.0000	0.0000
6	0.1712	0.1361	0.1058	0.0799	0.0540	0.0281	0.0022	0.0000	0.0000	0.0000
6	0.3784	0.3127	0.2589	0.2110	0.1671	0.1232	0.0793	0.0354	0.0015	0.0000
7	0.3784	0.3127	0.2589	0.2110	0.1671	0.1232	0.0793	0.0354	0.0015	0.0000
7	0.1712	0.1361	0.1058	0.0799	0.0540	0.0281	0.0022	0.0000	0.0000	0.0000
7	0.0580	0.0399	0.0254	0.0142	0.0063	0.0016	0.0000	0.0000	0.0000	0.0000
7	0.0063	0.0016	0.0000	0.0000	0.0000	0.0000	0.0000	0.0000	0.0000	0.0000
7	0.0580	0.0399	0.0254	0.0142	0.0063	0.0016	0.0000	0.0000	0.0000	0.0000
7	0.1712	0.1361	0.1058	0.0799	0.0540	0.0281	0.0022	0.0000	0.0000	0.0000
7	0.3784	0.3127	0.2589	0.2110	0.1671	0.1232	0.0793	0.0354	0.0015	0.0000
8	0.3784	0.3127	0.2589	0.2110	0.1671	0.1232	0.0793	0.0354	0.0015	0.0000
8	0.1712	0.1361	0.1058	0.0799	0.0540	0.0281	0.0022	0.0000	0.0000	0.0000
8	0.0580	0.0399	0.0254	0.0142	0.0063	0.0016	0.0000	0.0000	0.0000	0.0000
8	0.0063	0.0016	0.0000	0.0000	0.0000	0.0000	0.0000	0.0000	0.0000	0.0000
8	0.0580	0.0399	0.0254	0.0142	0.0063	0.0016	0.0000	0.0000	0.0000	0.0000
8	0.1712	0.1361	0.1058	0.0799	0.0540	0.0281	0.0022	0.0000	0.0000	0.0000
8	0.3784	0.3127	0.2589	0.2110	0.1671	0.1232	0.0793	0.0354	0.0015	0.0000
9	0.3784	0.3127	0.2589	0.2110	0.1671	0.1232	0.0793	0.0354	0.0015	0.0000
9	0.1712	0.1361	0.1058	0.0799	0.0540	0.0281	0.0022	0.0000	0.0000	0.0000
9	0.0580	0.0399	0.0254	0.0142	0.0063	0.0016	0.0000	0.0000	0.0000	0.0000
9	0.0063	0.0016	0.0000	0.0000	0.0000	0.0000	0.0000	0.0000	0.0000	0.0000
9	0.0580	0.0399	0.0254	0.0142	0.0063	0.0016	0.0000	0.0000	0.0000	0.0000
9	0.1712	0.1361	0.1058	0.0799	0.0540	0.0281	0.0022	0.0000	0.0000	0.0000
9	0.3784	0.3127	0.2589	0.2110	0.1671	0.1232	0.0793	0.0354	0.0015	0.0000
10	0.3784	0.3127	0.2589	0.2110	0.1671	0.1232	0.0793	0.0354	0.0015	0.0000
10	0.1712	0.1361	0.1058	0.0799	0.0540	0.0281	0.0022	0.0000	0.0000	0.0000
10	0.0580	0.0399	0.0254	0.0142	0.0063	0.0016	0.0000	0.0000	0.0000	0.0000
10	0.0063	0.0016	0.0000	0.0000	0.0000	0.0000	0.0000	0.0000	0.0000	0.0000
10	0.0580	0.0399	0.0254	0.0142	0.0063	0.0016	0.0000	0.0000	0.0000	0.0000
10	0.1712	0.1361	0.1058	0.0799	0.0540	0.0281	0.0022	0.0000	0.0000	0.0000
10	0.3784	0.3127	0.2589	0.2110	0.1671	0.1232	0.0793	0.0354	0.0015	0.0000
11	0.3784	0.3127	0.2589	0.2110	0.1671	0.1232	0.0793	0.0354	0.0015	0.0000
11	0.1712	0.1361	0.1058	0.0799	0.0540	0.0281	0.0022	0.0000	0.0000	0.0000
11	0.0580	0.0399	0.0254	0.0142	0.0063	0.0016	0.0000	0.0000	0.0000	0.0000
11	0.0063	0.0016	0.0000	0.0000	0.0000	0.0000	0.0000	0.0000	0.0000	0.0000
11	0.0580	0.0399	0.0254	0.0142	0.0063	0.0016	0.0000	0.0000	0.0000	0.0000
11	0.1712	0.1361	0.1058	0.0799	0.0540	0.0281	0.0022	0.0000	0.0000	0.0000
11	0.3784	0.3127	0.2589	0.2110	0.1671	0.1232	0.0793	0.0354	0.0015	0.0000

TABLE 4
COMPUTER OUTPUT

First Guess on Anode
(Mirror Image of
Cathode Surface A_c)

Mesh Line	Coordinates		
	x	y	z
1	24	0.36800	0.51314
2	25	0.36800	0.57014
3	26	0.36800	0.62710
4	27	0.36800	0.68412
5	28	0.36800	0.74121
6	29	0.36800	0.79776
7	1	0.46000	0.75424
8	2	0.46000	0.71121
9	3	0.46000	0.66817
10	4	0.46000	0.62517
11	5	0.46000	0.58215
12	6	0.46000	0.53914
13	7	0.46000	0.49613
14	8	0.46000	0.45310
15	9	0.46000	0.41008
16	10	0.46000	0.36706
17	11	0.46000	0.32404
18	12	0.46000	0.28102
19	13	0.46000	0.23800
20	14	0.46000	0.19498
21	15	0.46000	0.15196
22	16	0.46000	0.10894
23	17	0.46000	0.06592
24	18	0.46000	0.02290
25	19	0.46000	0.00000
26	20	0.46000	0.00000
27	21	0.46000	0.00000
28	22	0.46000	0.00000
29	23	0.46000	0.00000
30	24	0.46000	0.00000
31	25	0.46000	0.00000
32	26	0.46000	0.00000
33	27	0.46000	0.00000
34	28	0.46000	0.00000
35	29	0.46000	0.00000
36	1	0.55200	0.51314
37	2	0.55200	0.57014
38	3	0.55200	0.62710
39	4	0.55200	0.68412
40	5	0.55200	0.74121
41	6	0.55200	0.79776
42	7	0.55200	0.75424
43	8	0.55200	0.71121
44	9	0.55200	0.66817
45	10	0.55200	0.62517
46	11	0.55200	0.58215
47	12	0.55200	0.53914
48	13	0.55200	0.49613
49	14	0.55200	0.45310
50	15	0.55200	0.41008
51	16	0.55200	0.36706
52	17	0.55200	0.32404
53	18	0.55200	0.28102
54	19	0.55200	0.23800
55	20	0.55200	0.19498
56	21	0.55200	0.15196
57	22	0.55200	0.10894
58	23	0.55200	0.06592
59	24	0.55200	0.02290
60	25	0.55200	0.00000

First Iteration

Mesh Line	Coordinates			ΔL	L_{11}	m Σ $j=2$	β_i
	x	y	z				
1	24	0.36800	0.51314	0.13010	3.13731-02	2.91860-02	3.01731-02
2	25	0.36800	0.57014	0.14503	1.29705-02	2.99762-02	3.19705-02
3	26	0.36800	0.62710	0.15954	1.44070-02	2.96612-02	2.94070-02
4	27	0.36800	0.68412	0.17369	3.45908-02	2.91632-02	2.95908-02
5	28	0.36800	0.74121	0.18800	2.00191-02	2.97477-02	3.90174-02
6	29	0.36800	0.79776	0.19290	2.02602-02	2.97088-02	3.92623-02
7	1	0.46000	0.75424	0.19388	2.02079-02	2.97276-02	3.92879-02
8	2	0.46000	0.71121	0.19488	2.00412-02	2.90727-02	2.90433-02
9	3	0.46000	0.66817	0.19588	1.66364-02	2.93408-02	2.96244-02
10	4	0.46000	0.62517	0.19688	1.44266-02	2.91517-02	2.94266-02
11	5	0.46000	0.58215	0.19788	1.26255-02	2.91535-02	2.91205-02
12	6	0.46000	0.53914	0.19888	1.11955-02	2.92477-02	2.91958-02
13	7	0.46000	0.49613	0.19988	1.00073-02	2.97091-02	2.90875-02
14	8	0.46000	0.45310	0.20088	0.81816-02	2.91824-02	2.91817-02
15	9	0.46000	0.41008	0.20188	0.66551-02	2.97534-02	2.94655-02
16	10	0.46000	0.36706	0.20288	0.54016-02	2.96148-02	2.96014-02
17	11	0.46000	0.32404	0.20388	0.44305-02	2.94397-02	2.97010-02
18	12	0.46000	0.28102	0.20488	0.36623-02	2.92919-02	2.93632-02
19	13	0.46000	0.23800	0.20588	0.30094-02	2.92152-02	2.90099-02
20	14	0.46000	0.19498	0.20688	0.24247-02	2.92224-02	2.97772-02
21	15	0.46000	0.15196	0.20788	0.19351-02	2.97330-02	2.97733-02
22	16	0.46000	0.10894	0.20888	0.14773-02	2.97220-02	2.97772-02
23	17	0.46000	0.06592	0.20988	0.10496-02	2.97138-02	2.96099-02
24	18	0.46000	0.02290	0.21088	0.06523-02	2.91323-02	2.91362-02
25	19	0.46000	0.00000	0.21188	0.02838-02	2.91503-02	2.94437-02
26	20	0.46000	0.00000	0.21288	0.00142-02	2.96014-02	2.96014-02
27	21	0.46000	0.00000	0.21388	0.00000	2.97522-02	2.97522-02
28	22	0.46000	0.00000	0.21488	0.00000	2.91817-02	2.91817-02
29	23	0.46000	0.00000	0.21588	0.00000	2.90875-02	2.90875-02
30	24	0.46000	0.00000	0.21688	0.00000	2.91824-02	2.91824-02
31	25	0.46000	0.00000	0.21788	0.00000	2.97091-02	2.97091-02
32	26	0.46000	0.00000	0.21888	0.00000	2.91824-02	2.91824-02
33	27	0.46000	0.00000	0.21988	0.00000	2.97091-02	2.97091-02
34	28	0.46000	0.00000	0.22088	0.00000	2.91824-02	2.91824-02
35	29	0.46000	0.00000	0.22188	0.00000	2.97091-02	2.97091-02
36	1	0.55200	0.51314	0.13010	2.02158-02	2.97017-02	2.97017-02
37	2	0.55200	0.57014	0.14503	2.00277-02	2.91023-02	2.91023-02
38	3	0.55200	0.62710	0.15954	1.66002-02	2.91869-02	2.96003-02
39	4	0.55200	0.68412	0.17369	1.45982-02	2.96773-02	2.93952-02
40	5	0.55200	0.74121	0.18800	1.29759-02	2.99765-02	3.15759-02

Second Iteration

1	24	0.36800	0.51373	0.11017	-7.69873-05	2.49695-02	3.00941-02	0.91140-02
2	25	0.36800	0.57172	0.14511	-6.37276-05	2.97604-02	3.14768-02	0.87994-01
3	26	0.36800	0.62800	0.15957	-7.17478-04	2.97021-02	2.92922-02	0.79118-01
4	27	0.36800	0.68412	0.17369	-1.21225-04	2.90414-02	2.94568-02	0.70118-01
5	28	0.36800	0.74121	0.18814	-1.07213-04	2.98197-02	3.00178-02	0.71226-01
6	29	0.36800	0.79776	0.19297	-1.18589-04	2.99261-02	2.91816-02	0.72089-01
7	1	0.46000	0.75424	0.19379	-1.71917-04	2.92162-02	2.91688-02	0.72089-01
8	2	0.46000	0.71121	0.19481	-1.98184-04	2.98007-02	2.98431-02	0.71486-01
9	3	0.46000	0.66817	0.19581	-1.42957-04	2.97008-02	2.94915-02	0.70571-01
10	4	0.46000	0.62517	0.19681	-1.15222-04	2.97984-02	2.91008-02	0.69571-01
11	5	0.46000	0.58215	0.19781	-0.94304-05	2.93973-02	2.93087-02	0.67724-01
12	6	0.46000	0.53914	0.19881	-0.79375-05	2.90629-02	2.91161-02	0.65040-01
13	7	0.46000	0.49613	0.19981	-0.68188-05	2.94537-02	2.90185-02	0.62507-01
14	8	0.46000	0.45310	0.20081	-0.59007-05	2.92201-02	2.91211-02	0.60929-01
15	9	0.46000	0.41008	0.20181	-0.54539-05	2.93940-02	2.96111-02	0.60929-01
16	10	0.46000	0.36706	0.20281	-0.47985-05	2.92088-02	2.95916-02	0.60929-01
17	11	0.46000	0.32404	0.20381	-0.43095-05	2.97951-02	2.94776-02	0.58584-01
18	12	0.46000	0.28102	0.20481	-0.37652-05	2.97684-02	2.90935-02	0.56019-01
19	13	0.46000	0.23800	0.20581	-0.30322-05	2.92625-02	2.95879-02	0.56019-01
20	14	0.46000	0.19498	0.20681	-0.20237-05	2.99600-02	2.97842-02	0.56019-01
21	15	0.46000	0.15196	0.20781	-0.10762-05	2.95315-02	2.96976-02	0.56019-01
22	16	0.46000	0.10894	0.20881	-0.10270-05	2.95989-02	2.97362-02	0.56019-01
23	17	0.46000	0.06592	0.20981	-0.05020-05	2.92801-02	2.97070-02	0.56019-01
24	18	0.46000	0.02290	0.21081	-0.37648-05	2.97766-02	2.90935-02	0.56019-01
25	19	0.46000	0.00000	0.21181	-0.43093-05	2.92906-02	2.94617-02	0.56019-01
26	20	0.46000	0.00000	0.21281	-0.37618-05	2.92994-02	2.90935-02	0.56019-01
27	21	0.46000	0.00000	0.21381	-0.43093-05	2.92994-02	2.90935-02	0.56019-01
28	22	0.46000	0.00000	0.21481	-0.43093-05	2.92994-02	2.90935-02	0.56019-01
29	23	0.46000	0.00000	0.21581	-0.43093-05	2.92994-02	2.90935-02	0.56019-01
30	24	0.46000	0.00000	0.21681	-0.43093-05	2.92994-02	2.90935-02	0.56019-01
31	25	0.46000	0.00000	0.21781	-0.43093-05	2.92994-02	2.90935-02	0.56019-01
32	26	0.46000	0.00000	0.21881	-0.43093-05	2.92994-02	2.90935-02	0.56019-01
33	27	0.46000	0.00000	0.21981	-0.43093-05	2.92994-02	2.90935-02	0.56019-01
34	28	0.46000	0.00000	0.22081	-0.43093-05	2.92994-02	2.90935-02	0.56019-01
35	29	0.46000	0.00000	0.22181	-0.43093-05	2.92994-02	2.90935-02	0.56019-01
36	1	0.55200	0.51314	0.11017	-7.69873-05	2.49695-02	3.00941-02	0.91140-02
37	2	0.55200	0.57172	0.14511	-6.37276-05	2.97604-02	3.14768-02	0.87994-01
38	3	0.55200	0.62800	0.15957	-7.17478-04	2.97021-02	2.92922-02	0.79118-01
39	4	0.55200	0.68412	0.17369	-1.21225-04	2.90414-02	2.94568-02	0.70118-01
40	5	0.55200	0.74121	0.18814	-1.07213-04	2.98197-02	3.00178-02	0.71226-01
41	6	0.55200	0.79776	0.19297	-1.18589-04	2.99261-02	2.91816-02	0.72089-01
42	7	0.55200	0.75424	0.19379	-1.71917-04	2.92162-02	2.91688-02	0.72089-01
43	8	0.55200	0.71121	0.19481	-1.98184-04	2.98007-02	2.98431-02	0.71486-01
44	9	0.55200	0.66817	0.19581	-1.42957-04	2.97008-02	2.94915-02	0.70571-01
45	10	0.55200	0.62517	0.19681	-1.15222-04	2.97984-02	2.91008-02	0.69571-01
46	11	0.55200	0.58215	0.19781	-0.94304-05	2.93973-02	2.93087-02	0.67724-01
47	12	0.55200	0.53914	0.19881	-0.79375-05	2.90629-02	2.91161-02	0.65040-01
48	13	0.55200	0.49613	0.19981	-0.68188-05	2.94537-02	2.90185-02	0.62507-01
49	14	0.55200	0.45310	0.20081	-0.59007-05	2.92201-02	2.91211-02	0.60929-01
50	15	0.55200	0.41008	0.20181	-0.54539-05	2.93940-02	2.96111-02	0.60929-01
51	16	0.55200	0.36706	0.20281	-0.47985-05	2.92088-02	2.95916-02	0.60929-01
52	17	0.55200	0.32404	0.20381	-0.43095-05	2.97951-02	2.94776-02	0.58584-01
53	18	0.55200	0.28102	0.20481	-0.37652-05	2.97684-02	2.90935-02	0.56019-01
54	19	0.55200	0.23800	0.20581	-0.30322-05	2.92625-02	2.95879-02	0.56019-01
55	20	0.55200	0.19498	0.20681	-0.20237-05	2.99600-02	2.97842-02	0.56019-01
56	21	0.55200	0.15196	0.20781	-0.10762-05	2.95315-02	2.96976-02	0.56019-01
57	22	0.55200	0.10894	0.20881	-0.10270-05	2.95989-02	2.97362-02	0.56019-01
58	23	0.55200	0.06592	0.20981	-0.05020-05	2.92801-02	2.97070-02	0.56019-01
59	24	0.55200	0.02290	0.21081	-0.37648-05	2.97766-02	2.90935-02	0.56019-01
60	25	0.55200	0.00000	0.21181	-0.43093-05	2.92906-02	2.94617-02	0.56019-01
61	26	0.55200	0.00000	0.21281	-0.37618-05	2.92994-02	2.90935-02	0.56019-01
62	27	0.55200	0.00000	0.21381	-0.43093-05	2.92994-02	2.90935-02	0.56019-01
63	28	0.55200	0.00000	0.21481	-0.43093-05	2.92994-02	2.90935-02	0.56019-01
64	29	0.55200	0.00000	0.21581	-0.43093-05	2.92994-02	2.90935-02	0.56019-01
65	30	0.55200	0.00000	0.21681	-0.43093-05	2.92994-02	2.90935-02	0.56019-01
66	31	0.55200	0.00000	0.21781	-0.43093-05	2.92994-02	2.90935-02	0.56019-01
67	32	0.55200	0.00000	0.21881	-0.43093-05	2.92994-02	2.90935-02	0.56019-01
68	33	0.55200	0.00000	0.21981	-0.43093-05	2.92994-02	2.90935-02	0.56019-01
69	34	0.55200	0.00000	0.22081	-0.43093-05	2.92994-02	2.90935-02	0.56019-01
70	35	0.55200	0.00000	0.22181	-0.43093-05	2.92994-02	2.90935-02	0.56019-01

TABLE 5
COMPUTER OUTPUT, CONT'D

Mesh Line	Coordinates			ΔL	L_{i1}	m Σ $j=2$	β_i
x y	x	y	z				
5 24	0.36800	0.51873	0.11017	6.38887-07	2.49715-02	3.00948-02	8.91121-01
5 25	0.36800	0.57713	0.14510	8.06060-07	2.57645-02	3.14776-02	8.87971-01
5 26	0.36800	0.63600	0.18563	1.07009-06	2.67023-02	3.32932-02	8.83886-01
5 27	0.36800	0.69514	0.23259	1.44634-06	2.80452-02	3.54582-02	8.79152-01
5 28	0.36800	0.75568	0.28614	2.33669-06	2.88319-02	3.68201-02	8.72274-01
5 29	0.36799	0.81309	0.35296	8.63336-07	3.99423-02	3.91424-02	9.12065-01
6 1	0.46000	-0.81311	0.35296	8.71718-07	4.02322-02	3.91696-02	9.11441-01
6 2	0.46000	-0.75569	0.28611	2.35392-06	2.97996-02	3.88454-02	8.71434-01
6 3	0.46000	-0.69517	0.23257	1.45845-06	2.79021-02	3.54929-02	8.78335-01
6 4	0.46000	-0.63600	0.18561	1.07428-06	2.68033-02	3.33105-02	8.83150-01
6 5	0.46000	-0.57716	0.14508	8.12579-07	2.58311-02	3.15090-02	8.87221-01
6 6	0.46000	-0.51874	0.11015	6.40983-07	2.50656-02	3.01168-02	8.90421-01
6 7	0.46000	-0.46063	0.07986	5.30155-07	2.44584-02	2.90191-02	8.93037-01
6 8	0.46000	-0.40269	0.05403	4.47268-07	2.39220-02	2.81215-02	8.95192-01
6 9	0.46000	-0.34492	0.03221	3.89293-07	2.35359-02	2.74115-02	8.96916-01
6 10	0.46000	-0.28728	0.01415	3.47383-07	2.32104-02	2.68520-02	8.98292-01
6 11	0.46000	-0.22972	-0.00038	3.15951-07	2.29575-02	2.64177-02	8.99373-01
6 12	0.46000	-0.17224	-0.01154	2.94065-07	2.27667-02	2.60928-02	9.00185-01
6 13	0.46000	-0.11480	-0.01943	2.79397-07	2.26338-02	2.58682-02	9.00747-01
6 14	0.46000	-0.05739	-0.02413	2.71015-07	2.25573-02	2.57365-02	9.01078-01
6 15	0.46000	-0.	-0.02569	2.68221-07	2.25327-02	2.56929-02	9.01190-01
6 16	0.46000	-0.05739	-0.02413	2.71015-07	2.25601-02	2.57365-02	9.01078-01
6 17	0.46000	0.11480	-0.01943	2.79397-07	2.26414-02	2.58682-02	9.00747-01
6 18	0.46000	0.17224	-0.01154	2.94298-07	2.27778-02	2.60928-02	9.00185-01
6 19	0.46000	0.22972	-0.00038	3.15951-07	2.29718-02	2.64177-02	8.99373-01
6 20	0.46000	0.28728	0.01415	3.47383-07	2.32309-02	2.68520-02	8.98292-01
6 21	0.46000	0.34492	0.03221	3.89293-07	2.35846-02	2.74115-02	8.96916-01
6 22	0.46000	0.40269	0.05403	4.47035-07	2.39612-02	2.81215-02	8.95192-01
6 23	0.46000	0.46063	0.07986	5.29690-07	2.44964-02	2.90191-02	8.93037-01
6 24	0.46000	0.51874	0.11015	6.41681-07	2.51358-02	3.01167-02	8.90421-01
6 25	0.46000	0.57716	0.14508	8.12113-07	2.59275-02	3.15090-02	8.87221-01
6 26	0.46000	0.63600	0.18561	1.07475-06	2.68808-02	3.33105-02	8.83150-01
6 27	0.46000	0.69517	0.23257	1.45799-06	2.82266-02	3.54929-02	8.78335-01
6 28	0.46000	0.75569	0.28611	2.35392-06	2.90304-02	3.68454-02	8.71434-01
6 29	0.46000	0.81311	0.35296	7.71718-07	4.02322-02	3.91696-02	9.11441-01
7 1	0.55200	-0.81304	0.35298	8.56817-07	3.98273-02	3.91027-02	9.12133-01
7 2	0.55200	-0.75569	0.28613	2.33669-06	2.98919-02	3.88325-02	8.72241-01
7 3	0.55200	-0.69514	0.23259	1.44867-06	2.77104-02	3.54596-02	8.79148-01
7 4	0.55200	-0.63598	0.18563	1.06916-06	2.66228-02	3.32846-02	8.83911-01
7 5	0.55200	-0.57714	0.14510	8.06060-07	2.56516-02	3.14829-02	8.87955-01

Third Iteration

5 16	0.36800	0.05739	-0.02411	-1.86265-09	2.24195-02	2.57189-02	9.01693-01
5 17	0.36800	0.11479	-0.01941	-1.86265-09	2.25001-02	2.58504-02	9.01365-01
5 18	0.36800	0.17223	-0.01152	-1.62981-09	2.26353-02	2.60747-02	9.00808-01
5 19	0.36800	0.22972	-0.00037	-1.62981-09	2.28277-02	2.63991-02	9.00001-01
5 20	0.36800	0.28727	0.01417	-1.39698-09	2.30850-02	2.68329-02	8.98931-01
5 21	0.36800	0.34491	0.03223	-1.39698-09	2.34160-02	2.73922-02	8.97566-01
5 22	0.36800	0.40268	0.05404	-2.56114-09	2.38337-02	2.81017-02	8.95853-01
5 23	0.36800	0.46063	0.07988	-4.88944-09	2.43381-02	2.89982-02	8.93717-01
5 24	0.36800	0.51873	0.11017	-4.88944-09	2.49713-02	3.00948-02	8.91121-01
5 25	0.36800	0.57713	0.14510	-5.12227-09	2.57676-02	3.14776-02	8.87971-01
5 26	0.36800	0.63600	0.18563	-8.38190-09	2.67019-02	3.32932-02	8.83886-01
5 27	0.36800	0.69514	0.23259	-9.77889-09	2.80456-02	3.54582-02	8.79152-01
5 28	0.36800	0.75568	0.28614	-2.37487-08	2.88312-02	3.68201-02	8.72274-01
5 29	0.36799	0.81309	0.35296	-7.43058-09	3.99097-02	3.91424-02	9.12065-01
6 1	0.46000	-0.81311	0.35296	-6.98492-09	4.02313-02	3.91696-02	9.11442-01
6 2	0.46000	-0.75569	0.28611	-2.70084-08	2.97897-02	3.88454-02	8.71434-01
6 3	0.46000	-0.69517	0.23257	-1.33668-08	2.78915-02	3.54929-02	8.78335-01
6 4	0.46000	-0.63600	0.18561	-5.58794-09	2.68040-02	3.33105-02	8.83150-01
6 5	0.46000	-0.57716	0.14508	-7.45058-09	2.58276-02	3.15090-02	8.87221-01
6 6	0.46000	-0.51874	0.11015	-4.42378-09	2.50656-02	3.01167-02	8.90421-01
6 7	0.46000	-0.46063	0.07986	-2.56114-09	2.44568-02	2.90191-02	8.93037-01
6 8	0.46000	-0.40269	0.05403	-3.72529-09	2.39213-02	2.81215-02	8.95192-01
6 9	0.46000	-0.34492	0.03221	-3.25963-09	2.35359-02	2.74115-02	8.96916-01
6 10	0.46000	-0.28728	0.01415	-2.32831-09	2.32104-02	2.68520-02	8.98292-01
6 11	0.46000	-0.22972	-0.00038	-2.32831-09	2.29575-02	2.64177-02	8.99373-01
6 12	0.46000	-0.17224	-0.01154	-1.39698-09	2.27667-02	2.60928-02	9.00185-01
6 13	0.46000	-0.11480	-0.01943	-1.86265-09	2.26338-02	2.58682-02	9.00747-01
6 14	0.46000	-0.05739	-0.02413	-1.62981-09	2.25573-02	2.57365-02	9.01078-01
6 15	0.46000	0.	-0.02569	-1.86265-09	2.25327-02	2.56929-02	9.01190-01
6 16	0.46000	0.05739	-0.02413	-1.39698-09	2.25601-02	2.57365-02	9.01078-01
6 17	0.46000	0.11480	-0.01943	-1.39698-09	2.26414-02	2.58682-02	9.00747-01
6 18	0.46000	0.17224	-0.01154	-2.32831-09	2.27778-02	2.60928-02	9.00185-01
6 19	0.46000	0.22972	-0.00038	-2.56114-09	2.29718-02	2.64177-02	8.99373-01
6 20	0.46000	0.28728	0.01415	-2.79397-09	2.32307-02	2.68520-02	8.98292-01
6 21	0.46000	0.34492	0.03221	-3.25963-09	2.35651-02	2.74115-02	8.96916-01
6 22	0.46000	0.40269	0.05403	-3.02680-09	2.39613-02	2.81215-02	8.95192-01
6 23	0.46000	0.46063	0.07986	-3.02680-09	2.44944-02	2.90191-02	8.93037-01
6 24	0.46000	0.51874	0.11015	-3.49244-09	2.51358-02	3.01167-02	8.90421-01
6 25	0.46000	0.57716	0.14508	-7.91624-09	2.59280-02	3.15090-02	8.87221-01
6 26	0.46000	0.63600	0.18561	-6.51926-09	2.68743-02	3.33105-02	8.83150-01
6 27	0.46000	0.69517	0.23257	-1.58325-08	2.82206-02	3.54929-02	8.78335-01
6 28	0.46000	0.75569	0.28611	-2.70084-08	2.90306-02	3.68454-02	8.71434-01
6 29	0.46000	0.81311	0.35296	-6.98492-09	4.02313-02	3.91696-02	9.11442-01
7 1	0.55200	-0.81304	0.35298	-5.12227-09	3.98898-02	3.91027-02	9.12133-01
7 2	0.55200	-0.75569	0.28613	-2.23517-08	2.95895-02	3.88324-02	8.72242-01
7 3	0.55200	-0.69514	0.23259	-1.39698-08	2.77114-02	3.54596-02	8.79149-01
7 4	0.55200	-0.63598	0.18563	-7.43058-09	2.66232-02	3.32846-02	8.83911-01
7 5	0.55200	-0.57714	0.14510	-5.58794-09	2.56577-02	3.14828-02	8.87956-01

Final Iteration

4.2 Discussion of Results

The actual and computed gaps along the selected section line are plotted in Figures 16. through 20. for the René 41/NaCl combinations and in Figures 21. through 23. for the A-286/NaNO₃ combinations. The actual gaps in the plots are an average of the individual gaps measured on each of three workpieces.

The discrepancies between actual and calculated gaps may be attributed to the following factors:

- (a) Measurement errors.
- (b) The effect of process variations on the dimensional repeatability of the workpiece.
- (c) The actual cathode shape extended approximately 1/8" into the vertical sides of the electrodes, Figure 14. These additional electrode surfaces were not taken into consideration when we calculated comparative gaps.
- (d) The calculated gaps are computed on the basis of empirical data which may have deviated from the actual machining conditions used in these tests. In particular, the values of ΔE and ρ used in the calculations were for constant electrolyte temperatures while the electrolyte temperature in the cutting gap increased during machining. See Table 2.
- (e) Steady state conditions were assumed in the computer model. The amount of machining stock and the cutting time during actual machining tests varied, Table 2.

The average of the computed overcut index values were plotted against the corresponding cutting gaps for our test cases, Figure 24., and the average overcut index compared with the computed values for test case C-3, Figure 25.

We found that the average overcut index was dependent upon the cutting gap, but independent of the specific values for

$$\frac{E - \Delta E}{\rho F_1} K$$

where

$$F_1 = F \cos \gamma_1 \quad (22)$$

The rise of the overcut index values at the corner points of the cathode is explained by the assumed case where the cutting currents at the corner of the electrode in the computer model were confined to the opposing anode surfaces. The currents at the electrode corners during actual machining tests were permitted to stray. This also contributed to the deviation of the actual from the computed gaps at the electrolyte inlet and outlet sides of the cutting gaps.

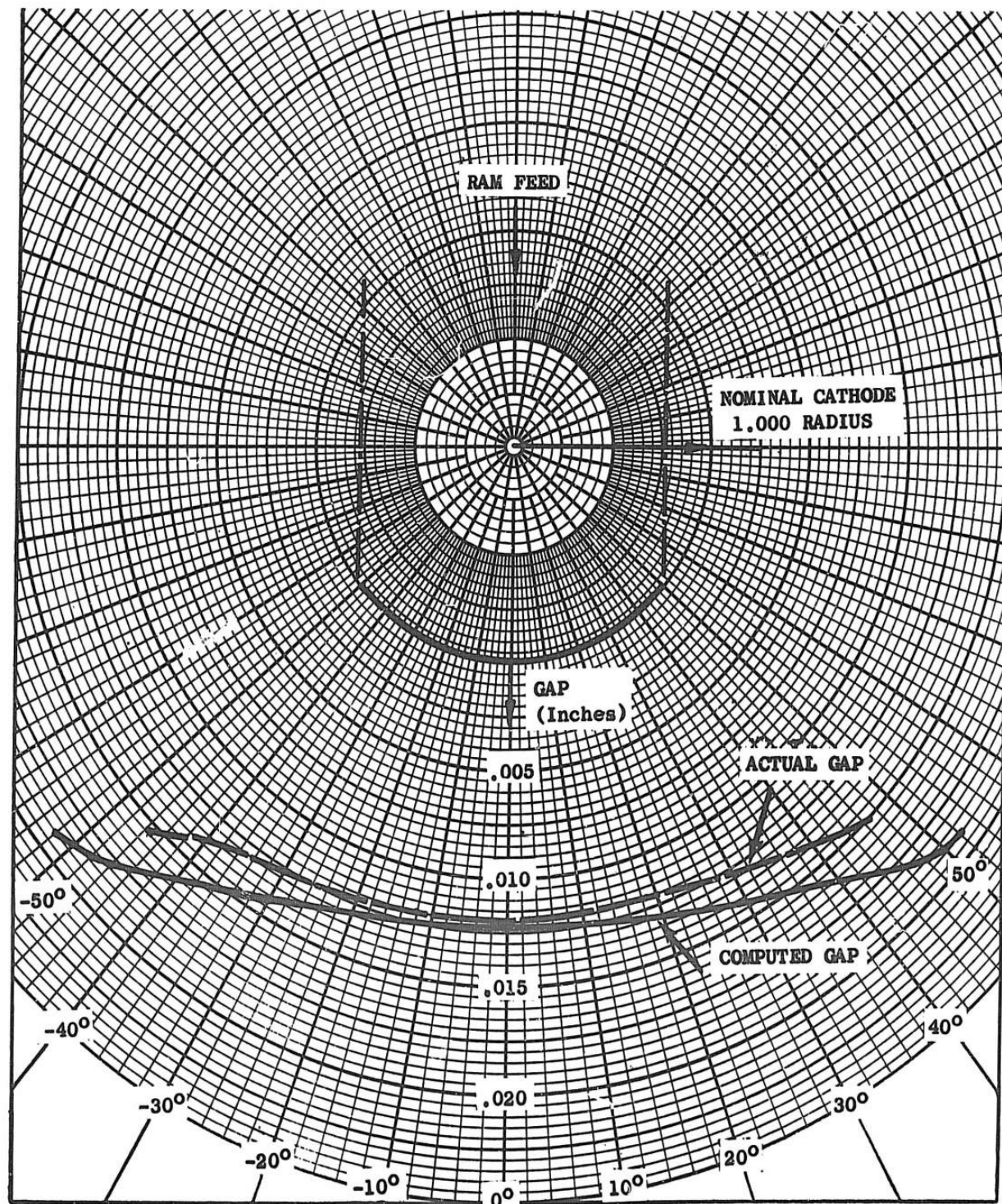


Figure 16. Gap Comparison Test #C1
Maximum Difference - .0028"

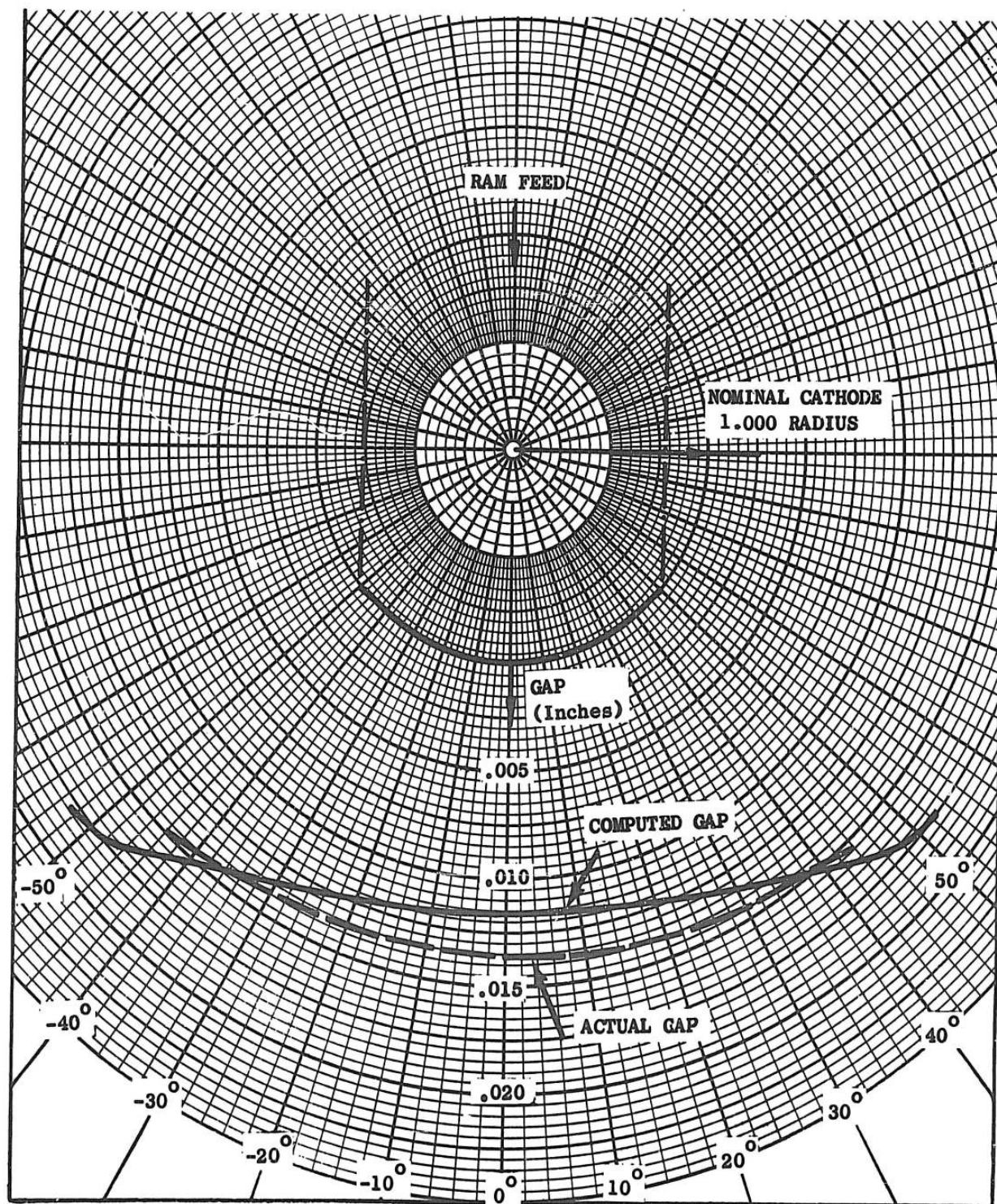


Figure 17. Gap Comparison Test #C3
Maximum Difference - .0018"

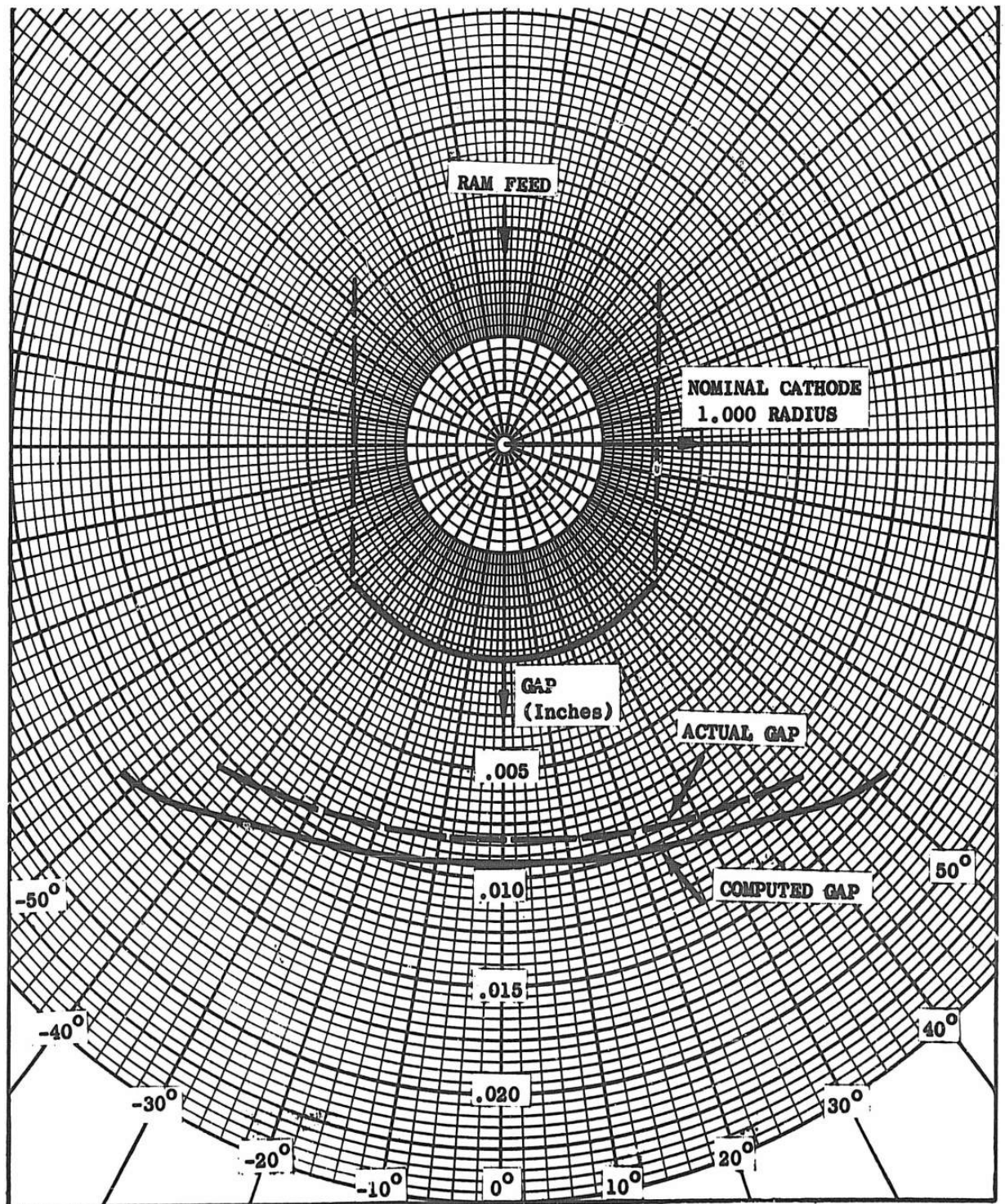


Figure 18. Gap Comparison Test #C4
Maximum Difference - .0025"

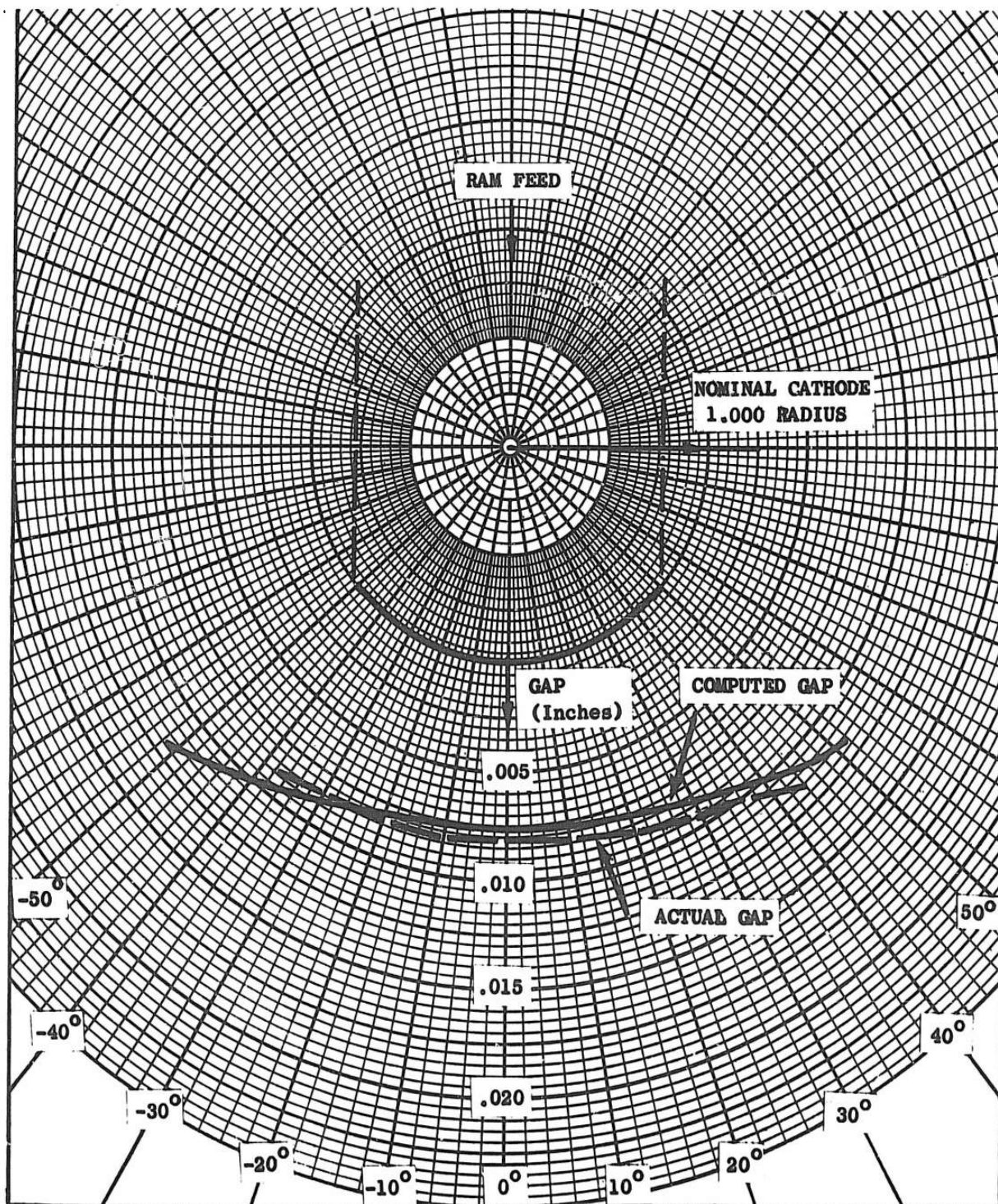


Figure 19. Gap Comparison Test #C5
Maximum Difference - .0009"

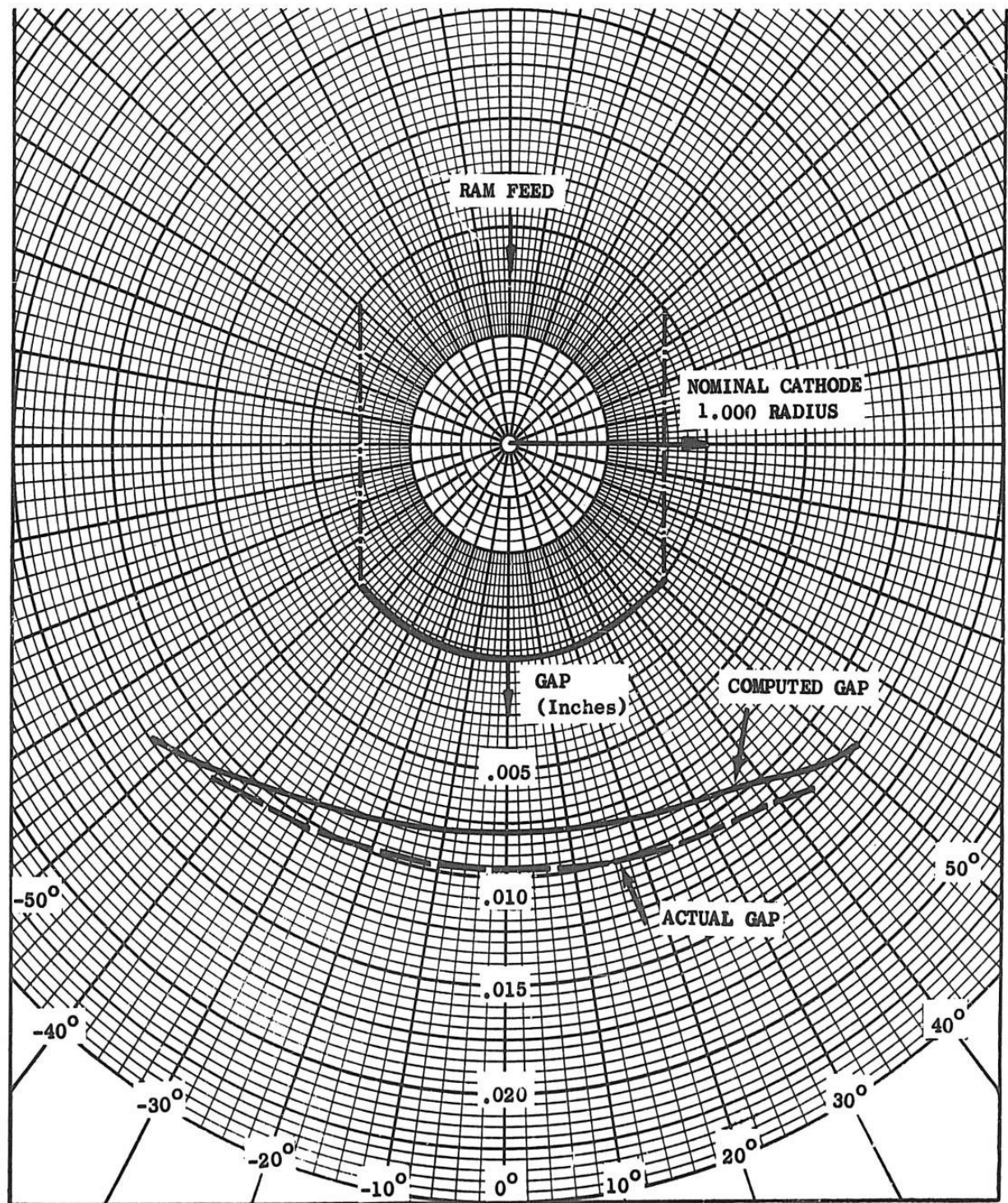


Figure 20. Gap Comparison Test #C6
Maximum Difference - .0016"

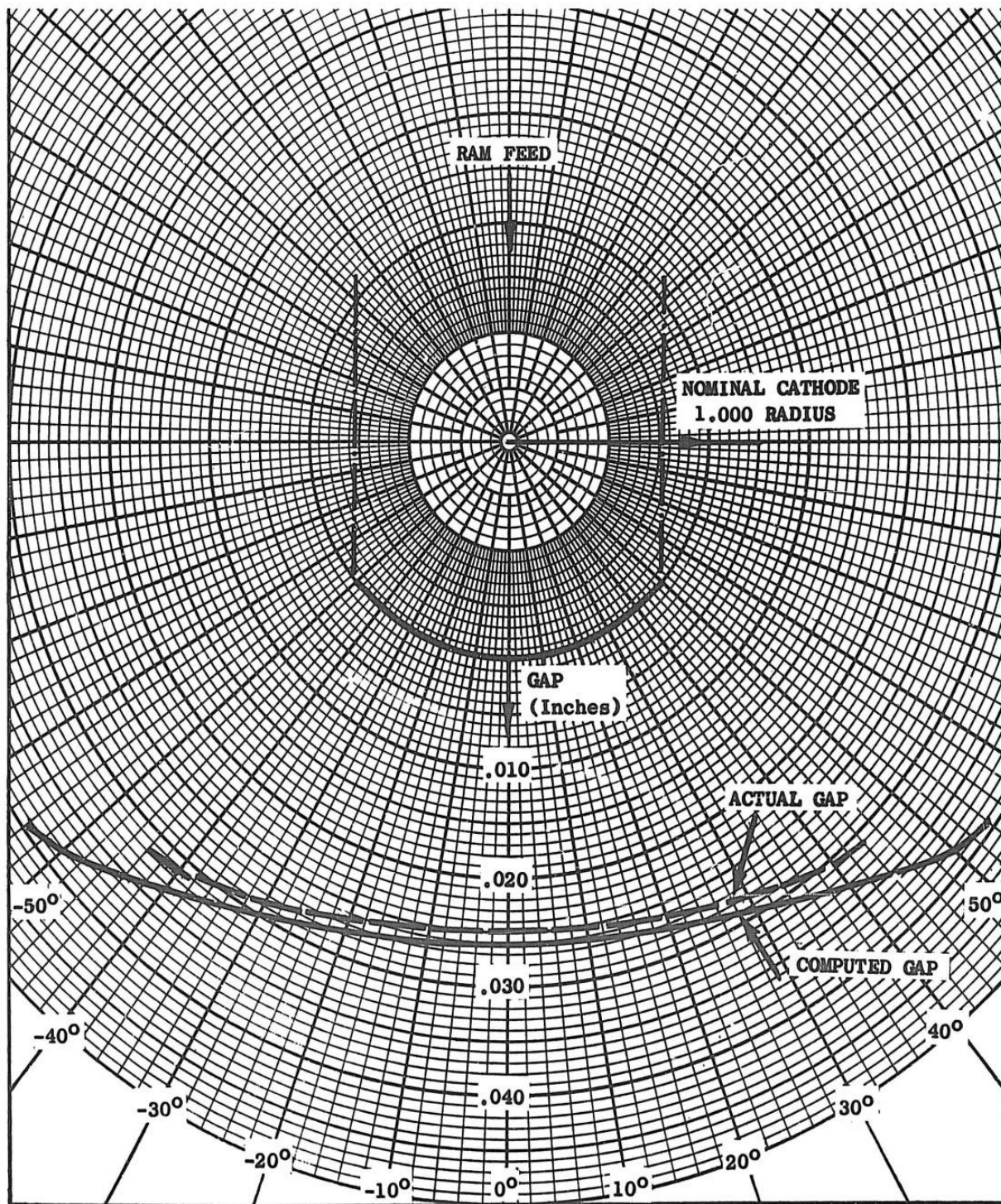


Figure 21. Gap Comparison Test #D1
Maximum Difference - .0038"

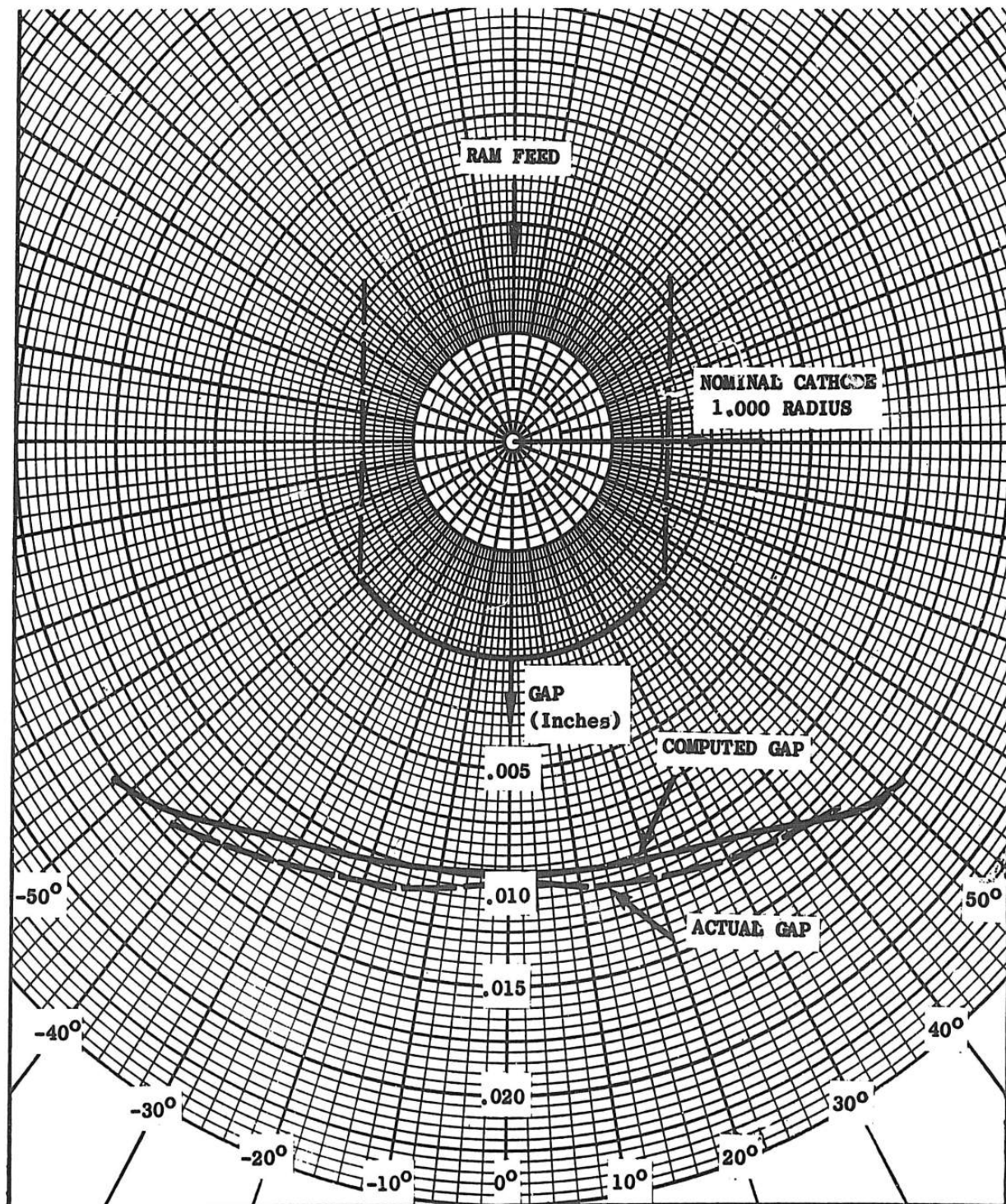


Figure 22. Gap Comparison Test #D2
Maximum Difference - .0012"

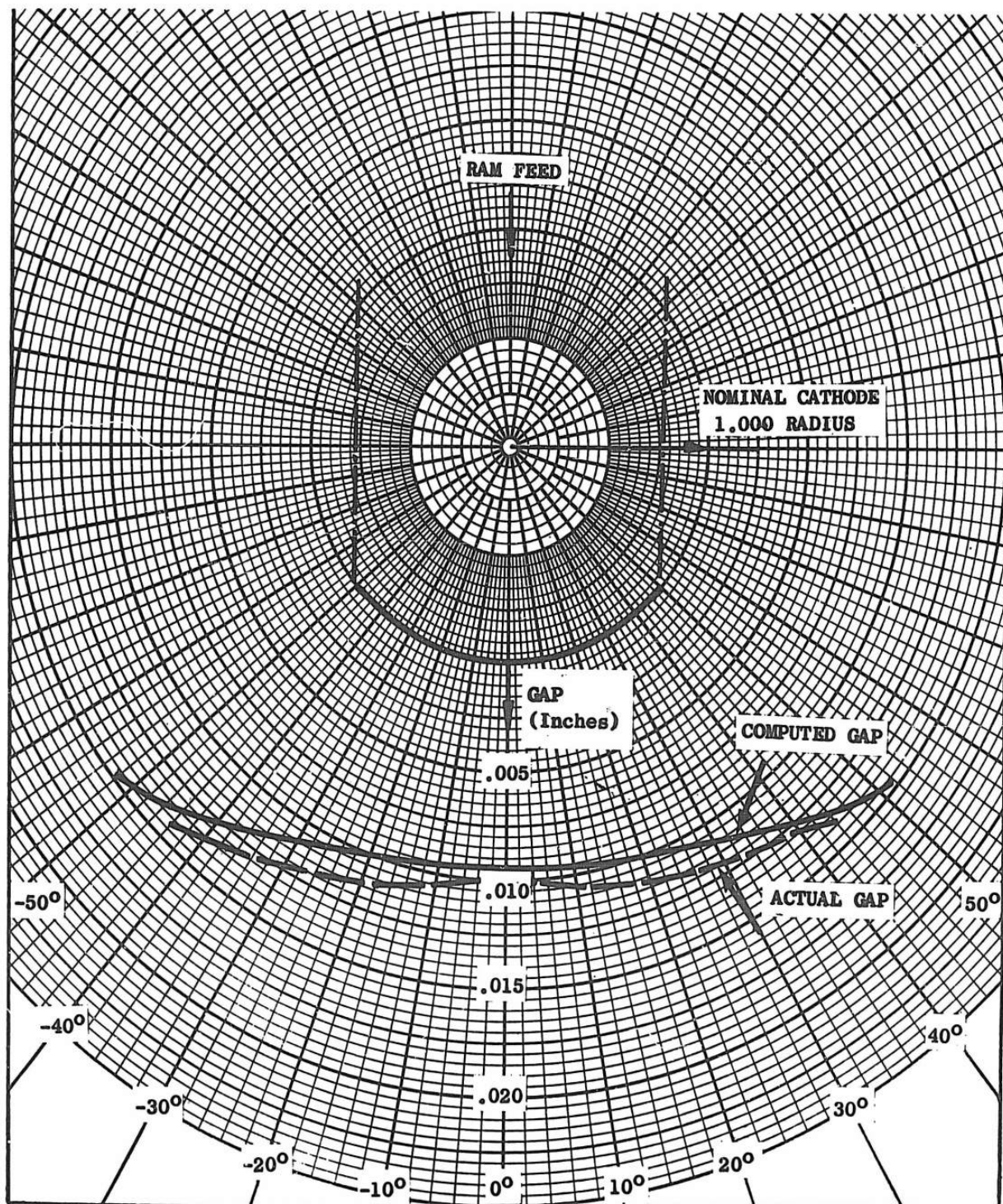
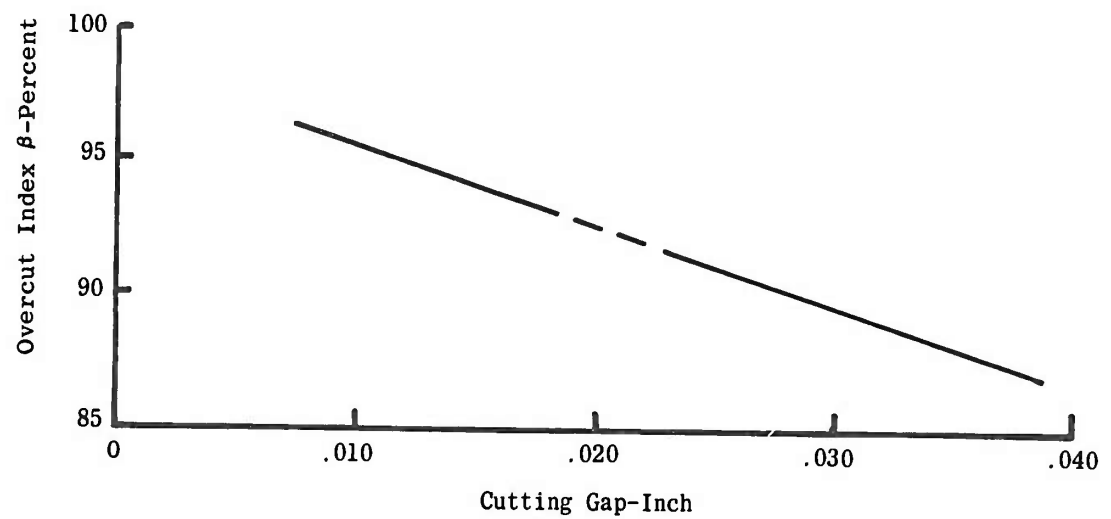


Figure 23. Gap Comparison Test #D3
Maximum Difference - .0012"



TEST NO.	RANGE OF GAPS	
C1	.0122" - .0182"	René 41/NaCl Electrolyte
C3	.0116" - .0172"	
C4	.0095" - .0140	
C5	.0076" - .0112"	
C6	.0080" - .0118"	
D1	.0257" - .0388"	A286/NaNO ₃ Electrolyte
D2	.0098" - .0125"	
D3	.0096" - .0123"	

Figure 24. Average Overcut Index β vs. Cutting Gaps for Tests C1 through C6 and D1 through D3

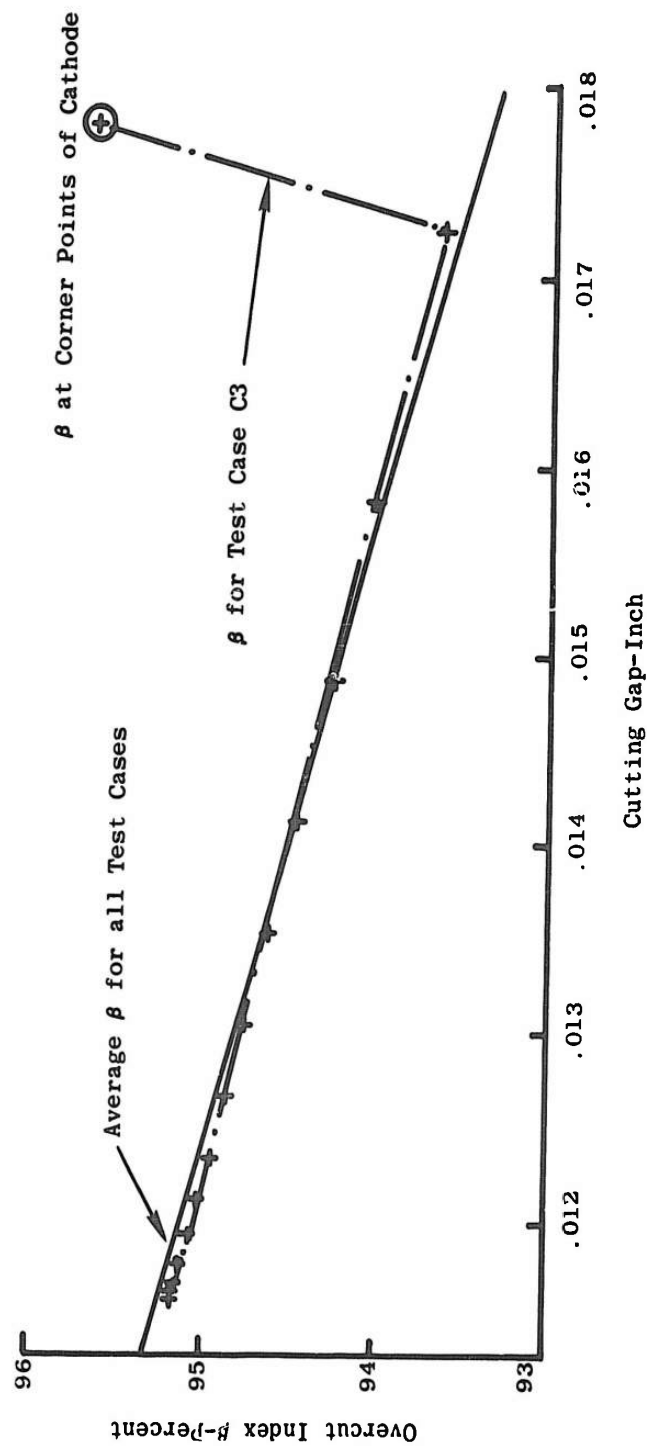


Figure 25. Comparison of Average Overcut Index with the Actual Index for Test C3

5. THE ROLE OF THE ELECTROLYTE

Our study of electrolytes was restricted to aqueous solutions of salts which emphasized the following three interrelated functions:

- (a) Chemical reaction involvement.
- (b) The effect of its fluid properties on the over-all process.
- (c) Action as a conductor between the anode and cathode.

5.1 The Electrolyte - Part of the Chemical Reaction

The electrolyte actively participates in the electrochemical reactions taking place during metal dissolution. These reactions are influenced by one of the following properties of electrolytes:

- (a) Acidic - the hydrogen ion (H^+) content is higher than the hydroxyl ion (OH^-) content.
- (b) Basic - the hydroxyl ion content is higher than the hydrogen ion content.
- (c) Neutral - the hydroxyl ion and the hydrogen ion are equal. Neutral solutions have a pH of 7. For our discussion, electrolytes with pH from 6 to 8 are considered neutral; below pH6, acidic; above pH8, basic.

We can differentiate the type of reactions expected from these electrolyte properties in the following cell regions:

- (a) The anode surface.
- (b) The cathode surface.
- (c) The bulk of the electrolyte.

We shall demonstrate in a simple form the type of reactions that are likely to occur during electrolytic machining.

5.1.1 Reaction at the Anode

Oxidation takes place at the anode.

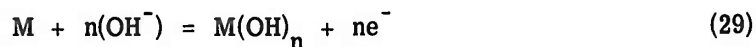
Generally, in acidic electrolytes, the metal dissolution reaction is:



where M is any metal in the alloy

M^{n+} is the metal ion at valence n and ne^- the electron loss.

Generally, in a basic solution:



where (OH^-) is the hydroxyl ion.

$M(OH)_n$ is the hydroxide of the metal.

In neutral electrolytes either of these reactions can occur.

Metal dissolution is the predominant effect at the anode; however, other chemical reactions, such as the production of oxygen and chlorine gases, are possible although they were not observed in our investigations. Metal dissolution does not proceed when adherent, nonporous, dielectric films form at the anode.

For example, sodium chloride cannot be used as an electrolyte for tungsten because the insoluble tungsten oxide forms. On the other hand, an electrolyte may contain a component which forms a soluble complex and prevents the occurrence of an insoluble film.

Usually, with a given electrolyte, a metal element oxidizes to a single valence state, but each constituent of an alloy workpiece may oxidize to one or more valence states. The valences of metal ions are influenced by the electrolyte composition, concentration, and temperature. For example, iron can oxidize to either the ferrous or ferric state with a chloride electrolyte:



5.1.2 Reaction at the Cathode

Reduction of a positive ion takes place at the cathode and, as a result, metal may plate out and hydrogen may evolve. When these results occur, the metal plating is the reverse of Equation (28), namely:



and hydrogen is evolved in an acidic electrolyte



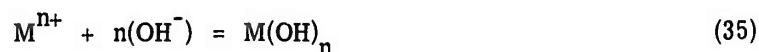
and in the neutral or basic electrolyte



In electrolytic machining with neutral electrolytes, an insignificant amount of metal is deposited at the cathode surface. However, in acid and basic electrolytes, measurable quantities of metal deposit on the cathode tool. As the plating builds up, it can disturb the flow and alter the shape of the tool. This may be prevented by intermittently reversing the polarity.

5.1.3 Reactions in the Bulk of the Electrolyte

Secondary reactions take place in the bulk of the electrolyte which may produce precipitates. In the case of a neutral electrolyte, the metal ions (M^{n+}) from the anode and the hydroxyl ions (OH^{-}) from the cathode react to form a metal hydroxide precipitate:



The precipitate constitutes the bulk of the sludge in the electrolytes.

5.2 Effect of Electrolyte Fluid Properties

The fluid properties of the electrolyte affect the process by:

- (a) Promoting the stabilization of the metal removal rate.
- (b) Conveying the reaction products from the cutting area.
- (c) Conveying the heat of reaction from the cutting area.
- (d) Providing a static pressure head.

5.2.1 Promoting Stability of Metal Removal

In a neutral electrolyte at current densities used in electrolytic machining, the reaction products at the electrodes, (M^{n+}) at the anode and (OH^-) at the cathode, build up concentrations rapidly which exceed those concentrations in the bulk of the electrolyte. At rapid electrolyte velocities in the gap, mixing occurs and the reaction products move rapidly into the bulk of the electrolyte where they form the metal hydroxide precipitate, Equation (35). This, in turn, causes a decrease in the concentrations of the ions in the neighborhood of the electrodes, and further reaction takes place. For a given metal removal rate, a minimum electrolyte velocity is required to stabilize the operating conditions at the electrodes and in the bulk of the electrolyte.

In acidic and basic electrolytes, the reaction products are not precipitated, and the ion concentration in the electrolyte continues to increase. Stabilization, therefore, does not occur.

5.2.1.1 pH, a Factor

It has been shown that in neutral electrolytes, the precipitation of metal hydroxide is desirable to stabilize the process. The same mechanism also maintains the pH at neutral.

If acidic or basic electrolytes are used, the pH changes and thus must be controlled.

5.2.1.2 Aging

We observed that when a fresh neutral NaCl electrolyte was first used in clean equipment, the metal removal rate was erratic and resulted in rough surface finishes. The metal removal rate stabilized when precipitates first appeared in the electrolyte. This phenomenon is not uncommon in processes depending upon chemical reactions. Aging of the chemical solutions is often required to promote stable reactions.

We found that if we added sludge to the fresh electrolyte and allowed the electrolyte to mix well, we avoided the erratic behavior.

5.2.2 Conveying the Reaction Products

We have discussed the conditions under which insoluble reaction products (sludge) can form. The increase of sludge content in the electrolyte flowing through the cutting area is proportional to the metal removal rate and inversely proportional to the mass flow of the electrolyte.

If the sludge is not flushed rapidly from the gap, it can:

- (a) Decrease the electrolyte velocity by increasing its viscosity.
- (b) Disrupt the flow by accumulating in the cutting gap.
- (c) Build up on the tool and workpiece surfaces.

When the flow is allowed to stagnate, a gelatinous layer can form at the electrodes. One circumstance under which it formed is reported under "Exemplary Parts", Section 1, Chapter IV.

In some cases of electrolytic machining, rapid electrolyte velocities cannot be achieved. When neutral electrolytes are used in combination with restricted velocities, the sludge can accumulate in and plug the electrolyte passage. In these cases, acidic or

basic electrolytes are used, or chelating agents are added to neutral electrolytes to prevent sludge formation.

5. 2. 2. 1 Sludge Removal

As the sludge is flushed from the cutting gap, it accumulates in the stored electrolyte and can re-enter the cutting gap. To prevent accumulation, the sludge is removed or its formation prevented by:

- (a) Discarding the sludge-contaminated electrolyte.
- (b) Clarifying.
- (c) Chelating.

The method most suitable for a given application depends on the particular production needs.

5. 2. 2. 2 Other Forms of Energy

The planned investigation of ultrasonic or other forms of energy as a supplement to fluid kinetic energy was put aside in order to concentrate on the basic process phenomena. Therefore, conclusions cannot be drawn on the merits of using ultrasonic energy.

However, the combination of the ultrasonic and the electrolytic machining processes have been studied by other investigators, ⁽¹⁶⁾ and another method known as electrolytically assisted grinding is an industrial process in which abrasive forces supplement the velocity of the electrolytes.

5. 2. 3 Conveyor of Heat

Heat generated during electrolytic machining increases the temperature in the cutting area. The fluid velocity is adjusted to stabilize the temperature in the cutting gap, to prevent the electrolyte from boiling, and to minimize thermal effects on the tooling and the workpiece.

5. 2. 4 Effect of Static Pressure Head

A positive pressure drop produced by the difference in pressure head at the inlet and outlet of the cutting gap provides the needed fluid velocities. Adjustments of outlet pressure (back pressure) are often used to regulate the static pressure in the cutting gap.

In our tests with three electrolyte compositions, where we investigated gap pressures from 14 psig to above 200 psig, no effects on process performance were noted which could be attributed to static pressure head itself.

5. 3 Electrolyte - Part of the Electrical Circuit

The electrolyte is the conductor in the electrical circuit between the anode and the cathode; its resistance affects the choice of gaps and feed rates within a given range of voltage from a power pack. The specific resistance (ρ) of the electrolyte is defined as the resistance of a unit cube of the electrolyte. The reciprocal of specific resistance is the specific conductivity (λ).

(16), See References

The resistance (or the conductivity) of the electrolyte depends upon:

- (a) Temperature
- (b) Composition and concentration of its constituents.
- (c) Aging.

The specific resistance for an electrolyte with a given chemical composition, concentration, and temperature is determined with a standard conductivity cell. In pure electrolytes, the specific resistance, and consequently the specific conductivity, varies only with temperature and concentration, Figures 26. and 27. The specific conductivity of a pure electrolyte can be determined from handbook data. In acidic and basic electrolytes, these estimates are of little value. Their composition was altered considerably during machining as was shown in our previous discussion.

In the case of many neutral electrolytes, the composition is not altered sufficiently to cause a significant variation in the specific resistance.

In the case of univalent salts, such as NaCl, λ can be estimated:

$$\lambda = a + b\sqrt{C} \quad (36)$$

where a and b are constants for a particular salt, and C is the concentration of the salt. For NaCl at 18°C, a good estimate would be:

$$\lambda_0 = .0.03 + .0144 \sqrt{C} \quad (36a)$$

The effect of temperature on the conductivity of simple salts can be estimated by:

$$\lambda = \lambda_0 [1 + d(T - T_0)] \quad (37)$$

where λ_0 is the conductivity at temperature $T_0 = 18^\circ\text{C}$, and λ is the conductivity at temperature T .

When λ is expressed in mho/cm, and T is in $^\circ\text{C}$, the parameter d for salts is generally between .020 and .025. In the case of sodium chloride, d is .024 or .0133 if T and T_0 are expressed in $^\circ\text{F}$.

As an acidic or basic electrolyte is used its conductivity changes and should be determined in a conductivity cell.

In the case of a neutral electrolyte its conductivity stabilizes as it ages. However, tests run by us ⁽¹⁾ indicated that when a fresh NaCl electrolyte was aged, its conductivity did not change significantly.

We recommend that if estimates are used to determine the conductivity of other neutral electrolytes, the effect of usage should be checked experimentally.

Tests completed and reported in Section 2, Chapter III, indicated that sludge content has an insignificant effect on the electrolyte conductivity.

(1), See References

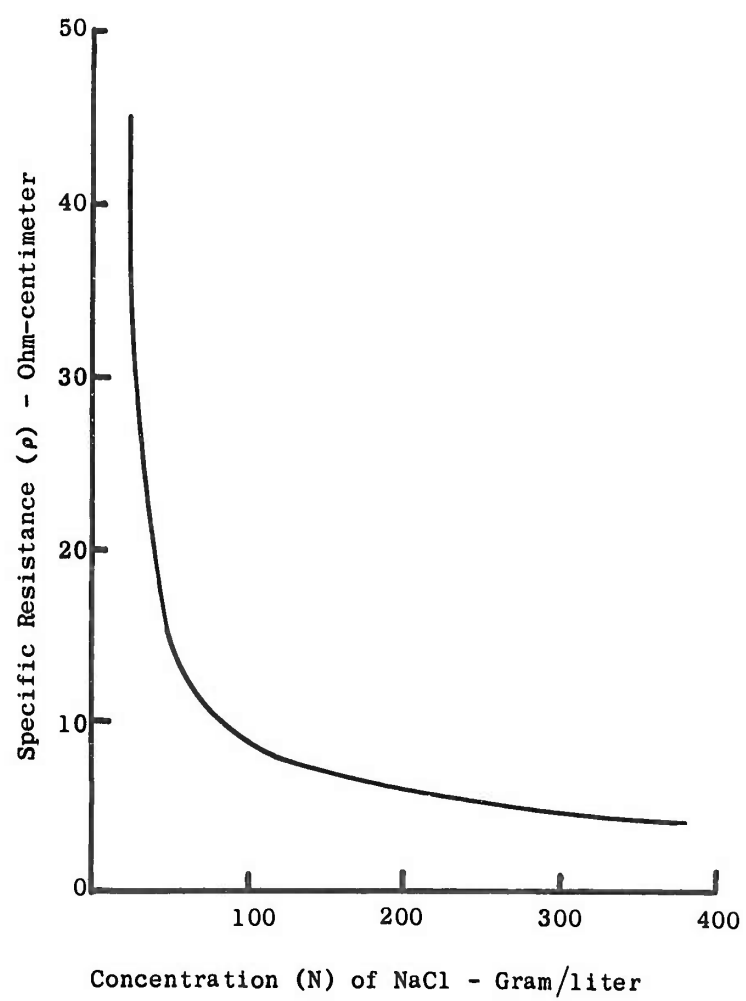


Figure 26. Specific Resistant vs NaCl Concentration at 72°F

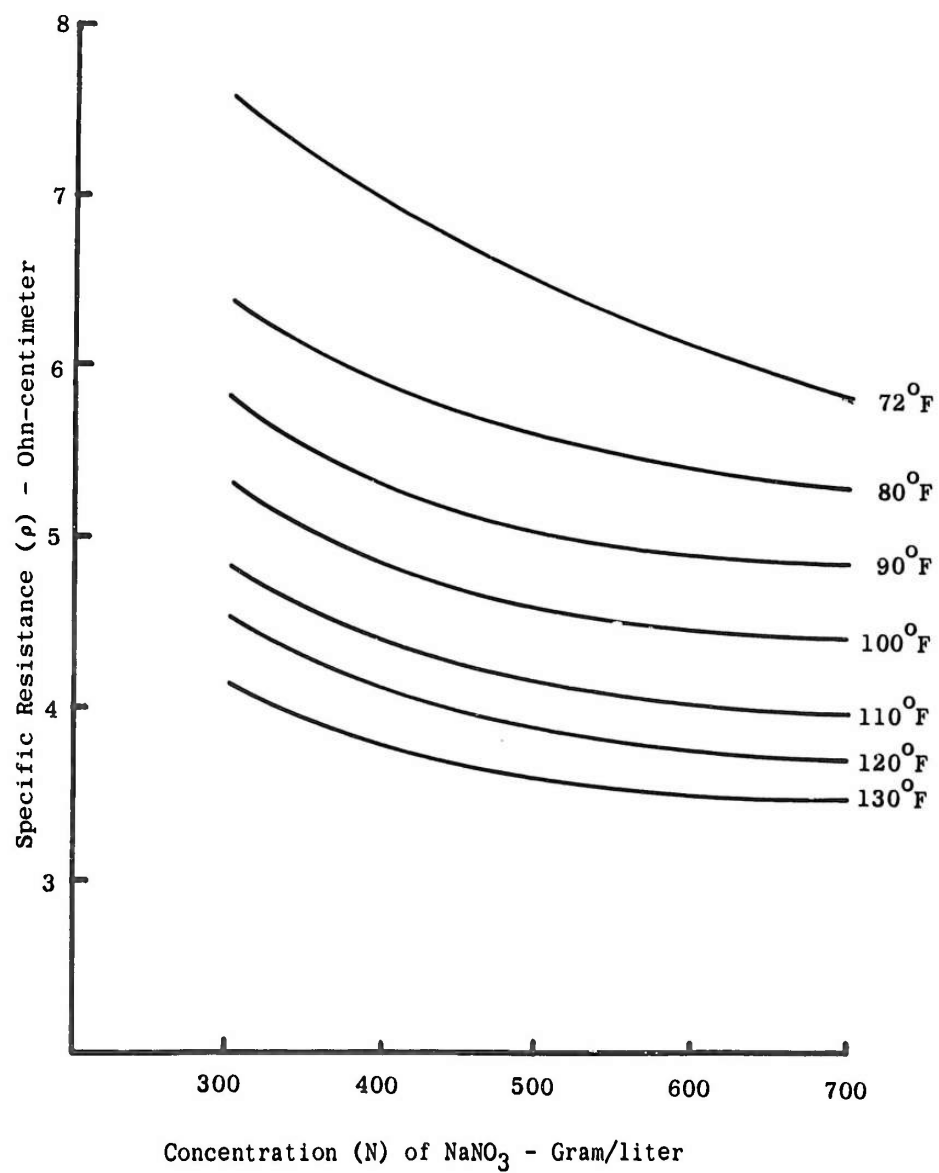


Figure 27. Specific Resistance vs Concentration NaNO_3 at Various Temperatures

6. ELECTROLYTIC CELL INVESTIGATION

During the second half of this project, a separate study was initiated to investigate electrode reactions in high current density electrolytic cells, and to compare the results to known electrochemical theories and prior conclusions.

In our mathematical analysis, Section 3, Chapter III, we developed mathematical models by interpreting fundamental laws so that they would express the phenomena encountered in electrolytic machining.

Our models use parameters which represent the potential of the current field in the cutting gap and the effect of the field on metal removal.

While much is known about the relationships governing these parameters for anodic reactions which occur at low current densities, little information was available about their behavior during high current density reactions. Moreover, the effect of the dynamic parameters of the electrolyte on high current density reactions was not known.

In order to apply and test our mathematical models, we used a metal removal factor K , and we treated the electropotential encountered in electrolytic machining as a continuum consisting of the applied voltage (E) and a variable ΔE . We developed an experimental method to determine their values, and we showed in Section 2, Chapter III, how these values are estimated.

Although we found these estimating methods very useful for the alloy/electrolyte combinations investigated, we recognized that they may not apply for all materials encountered in electrolytic machining. We concluded that additional research was required to understand anodic reaction phenomena at high current densities in the presence of flowing electrolytes.

Dr. J. W. Grenier and T. Lajcik conducted a separate electrolytic cell investigation and contributed the detailed information in this section.

The investigation was conducted in two phases: First, reactions under static electrolyte conditions were studied; second, the electrode reactions under dynamic electrolyte conditions were observed and analyzed.

6.1 Electrochemical Theories

Under ideal conditions the operation of a simple electrolytic cell obeys well-established laws. Negative ions migrate to the anode and positive ions to the cathode as a consequence of an electrical potential between anode and cathode. Electrons which enter the electrolyte on the cathode are removed at the anode either by oxidation of the negative ions or by oxidation of the anodic metals. If the weight of material reduced at the cathode or oxidized at the anode is proportional to the quantity of electricity passed, the process is said to obey Faraday's Law. If thermodynamic equilibrium is attained in a non-dynamic cell, the Nernst Law relating potential to electrolyte specie and concentration applies.

As stated in Section 2, Chapter III, Ohm's Law for electrolytic processes is:

$$E - \Delta E_{\text{total}} = IR \quad (1)$$

where

E is applied potential in volt

ΔE_{total} is an overpotential in volt

I is current in amp

R is resistance in ohm

In Figure 28 OA is the overpotential (ΔE), OC is a charging current before electrolysis, and BD is the linear IR term after electrolysis has been initiated.

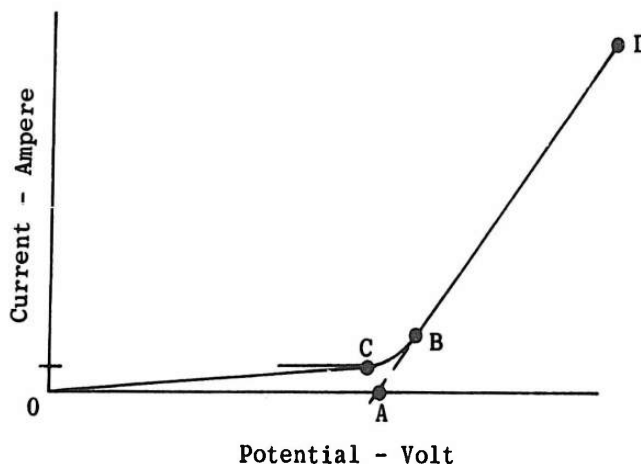


Figure 28. Current Conductance through an Electrolyte

The current OC produces a double layer of ions in the electrolyte making them the plates of a small capacitor. The resistance of the electrolyte to passage of current is dependent upon the properties of the electrolyte, particularly its specie, concentration, and temperature. The resistance occurring in the electrolyte can be described by its specific resistance (ρ). See Section 5.3, Chapter III.

Under ideal thermodynamic conditions, i. e., no passage of current, the thermodynamic value of the overpotential can be determined. Nernst⁽¹²⁾ showed that the potential at any electrode depended upon the type of chemical reaction and the properties of the electrolyte about the electrode.

$$E = E_0 - \frac{RT}{nF_y} \ln \frac{a_{\text{products}}}{a_{\text{reactants}}} \quad (38)$$

where E_0 is the critical potential at standard conditions, R, T, n and F_y have the usual thermodynamic connotations, and a_{products} and $a_{\text{reactants}}$ refer to the activities of the product and reactant of the chemical reaction taking place at the electrode.

(12) See References

Assuming ideal behavior of the product and reactant ions, the activity can be equated to molar concentrations.

With the passage of current, other effects take place and the critical potential no longer consists only of the thermodynamic quantity, E_o , corrected by the concentration term

$$\frac{RT}{nF_y} \ln \frac{a_{\text{products}}}{a_{\text{reactants}}}$$

but the voltage required to maintain electrolysis increases by a quantity η called the overvoltage. Although overvoltage has never been precisely ascertained, it has been associated with the kinetics of the electrode processes and frequently obeys Tafel's Law⁽¹⁴⁾ which defines the overvoltage as

$$\eta = a + b \ln I \quad (39)$$

where η is the overvoltage and I is the electrical current. The constants a and b known as the Tafel coefficients have been determined for a number of electrode-electrolyte systems^{(2), (7), (8), (10), (15), (17)}. The electrode effect occurs at both electrodes but is usually larger at the cathode if hydrogen gas is being evolved.

During electrolysis, ions of different electrical species are being added to or removed from the electrolyte, causing concentration gradients to occur. This condition makes the passage of electrical current by these ions more difficult by diminishing the force of the electrostatic field, and under certain conditions, additional voltage is required to maintain the passage of current. This effect (concentration polarization) can result in a limiting current, i. e., the current attains and maintains a definite value regardless of further increases in voltage.

Deviations from Faraday's Law have been observed for many metals⁽⁴⁾, even at low current densities where thermodynamic criteria are more nearly met. The Nernst equation is true only in thermodynamically reversible systems. Tafel's Law has been observed to hold well at low current densities, but it failed at current densities above 10 ampere/square inch⁽²⁾. The source of these deviations has been attributed to formation of surface films⁽⁹⁾, diffusion and transport phenomena⁽³⁾, chemical oxidation of the electrodes by the electrolyte and relative kinetic rates of electrode reactions⁽¹¹⁾. Many of these phenomena have been studied at low current density levels and various mathematical models have been postulated in the referenced literature.

For our investigation, we were concerned with five electrolytic cell regions and the reactions which occurred within them, Figure 29.

Zone A represents the voltage required for the reduction of an ion to a lower valence state. Zone B is the region in which concentration polarization would develop; this may be reduced by efficient agitation. Zone C represents the bulk electrolyte region; the voltage drop through this resistance is dependent upon the ion transport properties of the electrolyte. The anode concentration polarization Zone D is similar to B in character inasmuch as a concentration gradient is involved; however, the anode region concentration polarization arises from a build-up of anode dissolution products. Zone E represents the

(2), (3), (4), (7), (8), (9), (10), (11), (14), (15), (17): See References

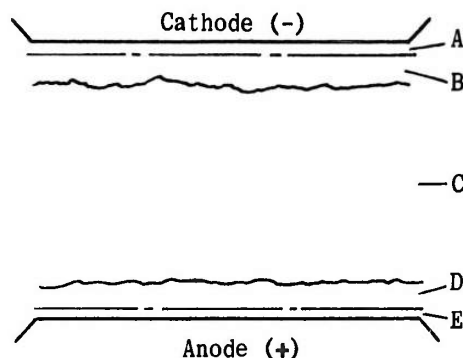


Figure 29. Electrolytic Cell Regions

voltage required for formation of the metal ions from the anodic workpiece.

Under dynamic electrolyte conditions, the concentration polarization effects in Zones B and D may be stabilized and incorporated with their respective electrode zones A and E. Cathode region A is the zone in which the reduction of hydrogen ions to hydrogen gas occurs and is a source of a cathode ΔE .

The intermediate region, C, containing the bulk of the electrolyte, conducts current between the cathode and anode regions and is discussed in Section 5.3, Chapter III. Under static electrolyte conditions at high current densities, the conductivity of the electrolyte may be influenced by limitations of ion mobility as energy input is consumed and heat is imparted to the solution.

The anode region, E, is the site of dissolution of the workpiece in electrolytic metal removal processes. The voltage drop at the anode may be attributable to the thermodynamic voltage, and to an anode ΔE produced by the formation of oxide films and electrolyte-metal ion reaction products.

Equation (1), therefore, can be written as

$$E - (\Delta E_{\text{anode}} + \Delta E_{\text{cathode}}) = IR \quad (1b)$$

where

ΔE_{anode} is the overpotential associated with anode reactions and perhaps polarization

$\Delta E_{\text{cathode}}$ is the overpotential associated with cathode reactions and perhaps polarization.

and

$$\Delta E_{\text{total}} = \Delta E_{\text{anode}} + \Delta E_{\text{cathode}} \quad (1c)$$

6.2 Experimental Methods

Ideally, electrode reactions should be studied under conditions approximating thermodynamic equilibrium. However, the utilization of high current densities produces

experimental conditions under which it is difficult to achieve a true thermal equilibrium. Nevertheless, we designed experiments in which we were able to determine the magnitude of the total ΔE and identify electrolytic cell parameters which effect its behavior. In the static cell tests, we also determined anode ΔE 's and we calculated cathode ΔE 's by deducting ΔE_{anode} from the measured ΔE_{total} .

In addition, we measured anode dissolution rates and we derived relative current efficiency criteria to demonstrate the effects of the electrolytic cell conditions on observed conditions of metal loss and applied current; and, from the static cell tests, we selected specimens for an analysis of surface films and finish.

To enable us to determine the ΔE 's we applied the electrical current in short pulses, and we measured the decay characteristics of the potential on an oscilloscope after each current pulse.

The current generator was designed specifically for this application. It is termed a galvanostatic control pulse generator because the pulse current is maintained constant while the voltage varies to obtain a preselected current level. This type of current generator is necessary to produce a steady current density under fluctuating resistance conditions. The termination of the pulse, a square wave, triggers the oscilloscope which projects the decay characteristic of the electropotential, Figure 30.

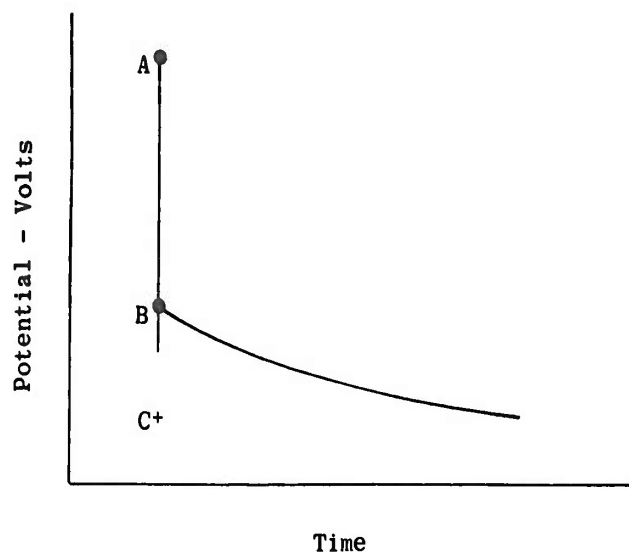


Figure 30. Decay Characteristic of Cell Potential

Point A is the applied potential required to maintain the preselected current. Upon termination of the pulse, the potential collapses in microseconds to point B where it decays exponentially to point C, the nullpoint. The potential drop AB represents an overvoltage ΔE . Where the potential across the anode and cathode was measured, drop AB represented the total ΔE . The anode ΔE was determined by measuring the potential between the anode and a Luggin capillary in conjunction with a salt bridge and a saturated calomel electrode, Figure 31.

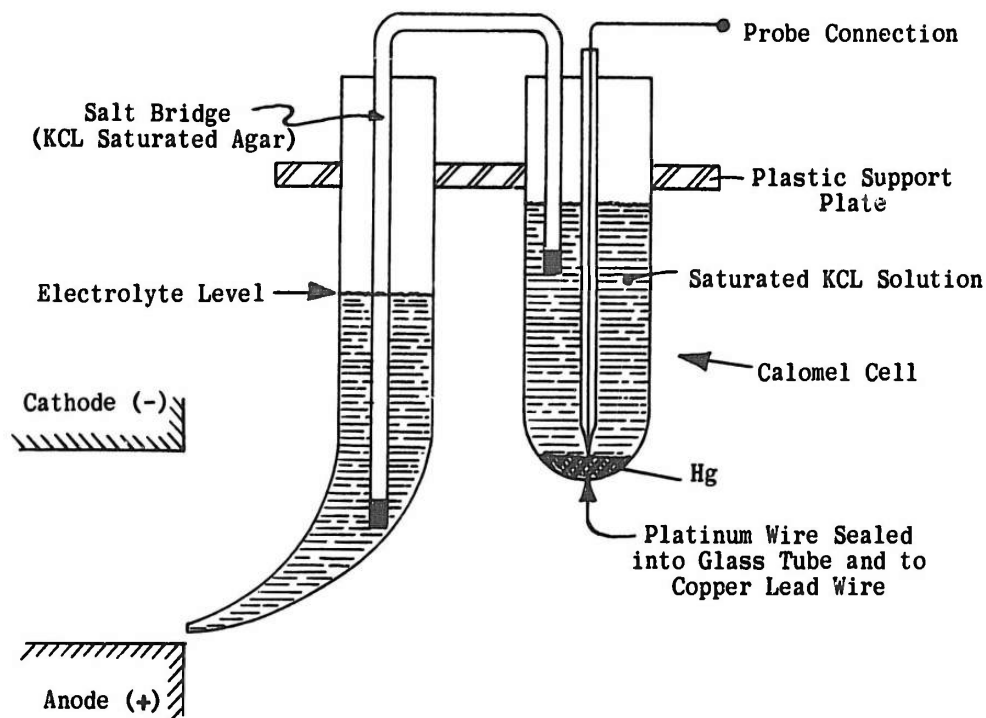


Figure 31. Luggin Capillary

The test facilities, Figures 32 and 33, consisted of the pulse generator, current interrupter, cells for establishing and maintaining the geometric conditions of the electrodes and an oscilloscope with fractional microsecond rise and fall time.

A detailed description of the test facilities and procedures is included in Appendix II. 10 and II. 1. 4. 3.

6.3 Static Cell Investigations

We tested three combinations of electrode material and electrolyte. In addition, we attempted to investigate the iron-sulfuric acid system, but this test series ($\text{Fe}/\text{H}_2\text{SO}_4$) was not concluded.

We used the statistical Box method for the design of our experiments, and we related current density, electrolyte temperature, electrolyte concentration, and electrode separation (gap) to the total ΔE .

When the electrode separation permitted the use of the Luggin capillary, we measured anode ΔE 's, and for the same test points we calculated cathode ΔE 's by deducting ΔE_{anode} from ΔE_{total} .

We continued our tests for 30 minutes and recorded our ΔE measurements in 5-minute intervals.

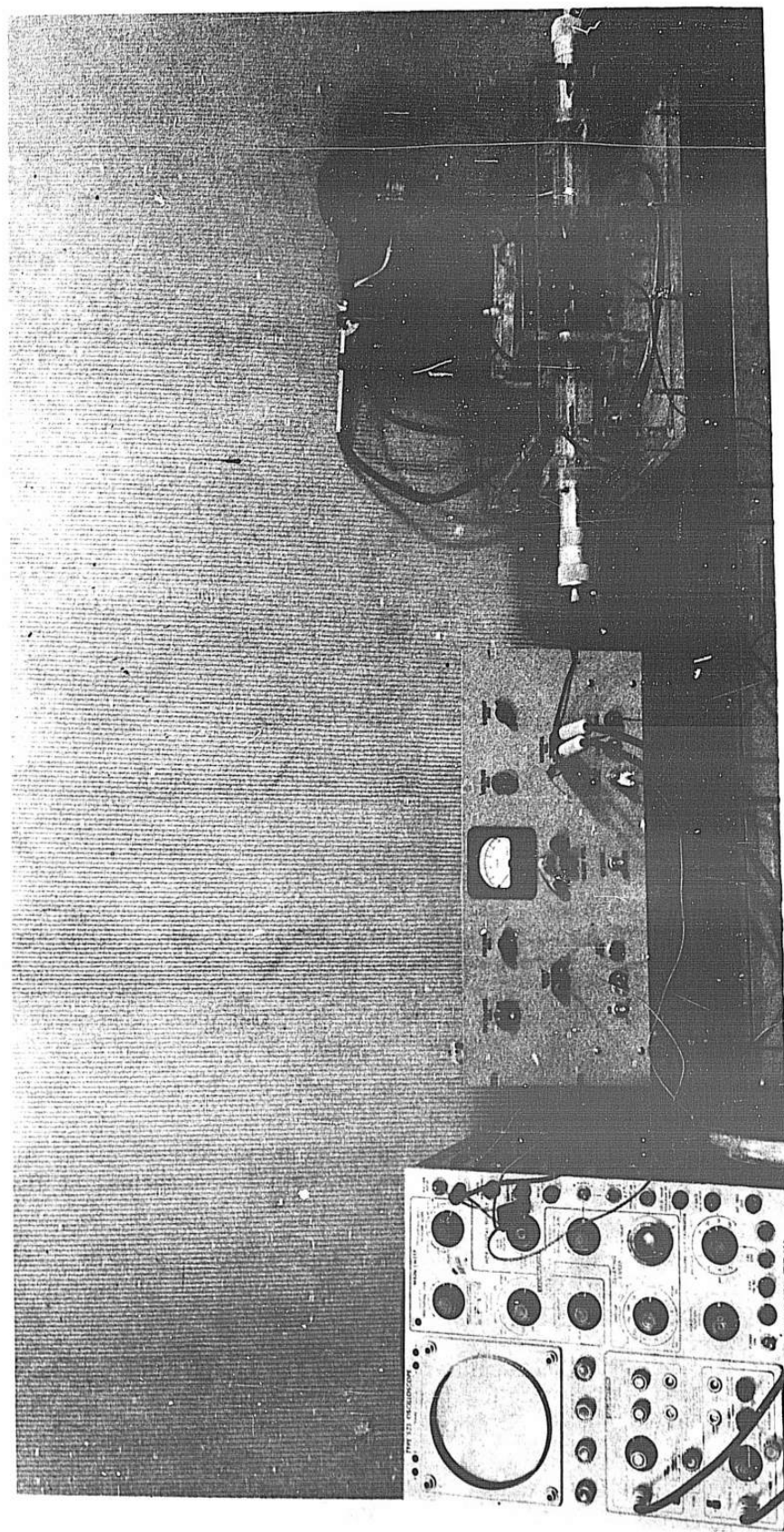


Figure 32. Test Facilities for Electrolytic Cell Studies

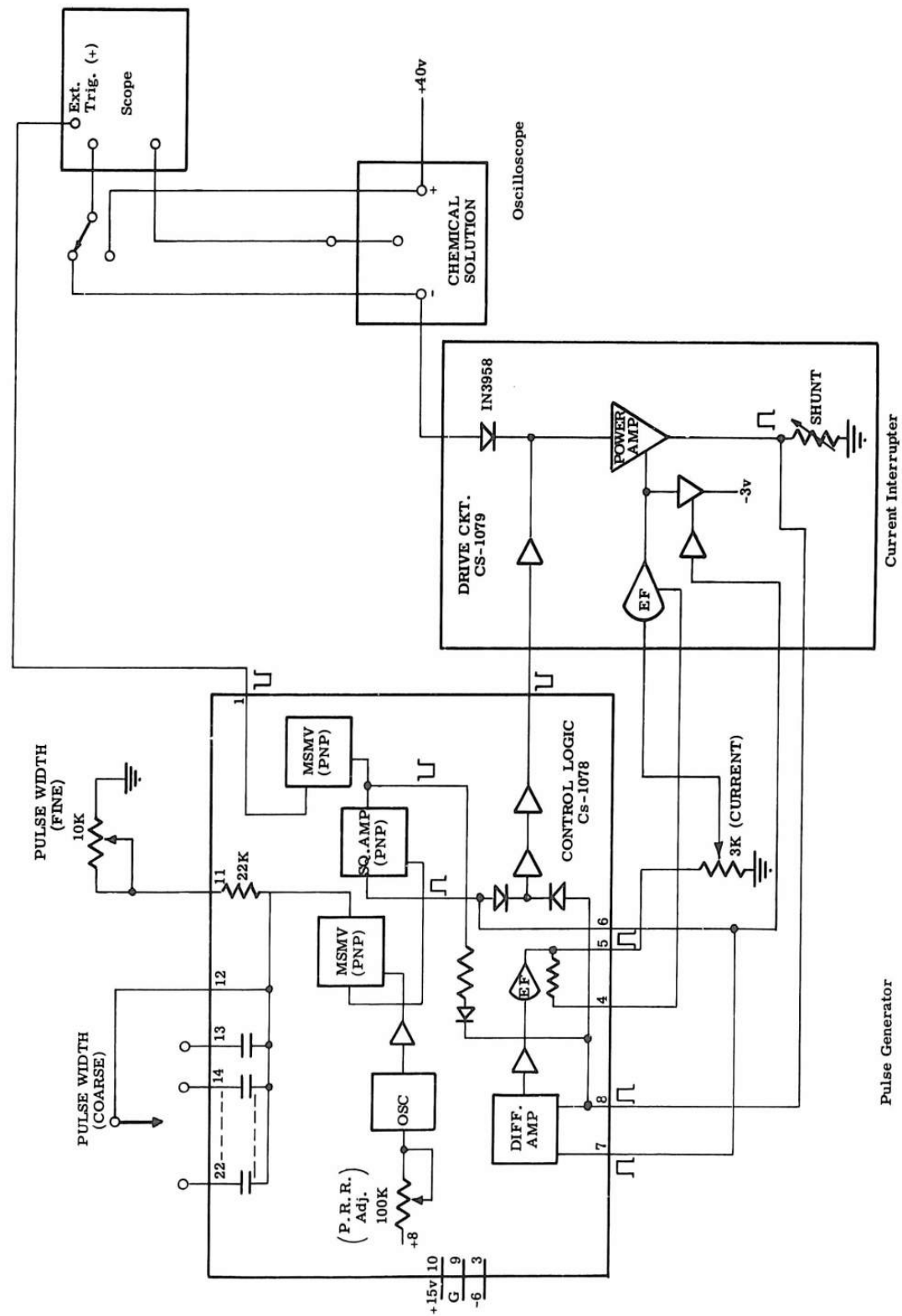


Figure 33. Block Diagram of Test Facilities

We interpreted our data by the standard methods used for Box experiments. In addition, we analyzed the two-level factorial portion of the experiments separately by the half-normal probability plot method⁽⁵⁾ to estimate our experimental errors and lack of curve fits.

We calculated equations to describe the effect of the statistically significant factors on the total ΔE , and we plotted some of the calculated relationships to indicate the direction of the effects and to approximate their relative magnitude. It must be pointed out, however, that the equations and plots are useful only for the ranges in which we collected our data, and no extrapolation is justifiable.

When we started our first test series with nickel electrodes and sodium chloride electrolyte, we measured the applied voltage E and the anode ΔE . The data analysis showed that the techniques employed in interpreting the oscilloscopic traces required refinements and that the measurements of the applied voltage were unreliable. Therefore, we repeated these tests and measured the total ΔE directly in this and all subsequent test series.

The magnitude of the calculated experimental errors from the static cell data analysis is believed to be due to hydrogen bubble formation which varied while electrolysis was in progress.

As a consequence, test factors or their statistical interactions, which were not disclosed as being significant in our analyses, may have contributed to the variations of the ΔE 's. Their effect, however, would be relatively small when compared to the effects which were shown to be significant.

In addition to determining the ΔE 's, we measured the weight loss of the anode specimens for two of our test series, and from Faraday's Law we calculated an "n-factor" by relating weight loss to effective current and cutting time as follows:

$$n = \frac{it}{F} \times \frac{\text{gm mol wt}}{\text{wt loss}} \quad (40)$$

where

n is a dimensionless number which represents a ratio of current efficiency and valence change occurring during electrolysis.

i is the effective current in amp

t is the effective cutting time in sec

F is the Faraday constant in coulombs

We checked the effects of the tested factors on the n factor by the same analysis method used for the ΔE_{total} relationships.

6.3.1 Test Series Ni/NaCl

In this test series we used nickel electrodes and a sodium chloride electrolyte, and we selected the following test levels:

(5): See References

Factor	Description	Levels				
		$-\alpha$	-1	0	+1	$+\alpha$
x_1	Current density I/A (amp/in ²)	100	232	550	868	1000
x_2	Temperature T (F°)	72.0	83.4	111.0	138.6	150.0
x_3	Concentration N (lb/gal)	1.00	1.29	2.00	2.71	3.00
x_4	Gap L (.001")	2.0	6.5	17.0	27.5	32.0

Tables 6 and 7 show the results of our first run in which we measured the total E and the anode ΔE . We calculated ΔE_{total} as the difference between total E and the IR drop across the electrolyte. Table 8 shows the results of our second run in which we incorporated experimental refinements and measured the total ΔE directly.

The statistical analysis of the data from our second run did not disclose a dependence of ΔE_{total} on any of the experimental variables.

The anode ΔE , Table 6, reflects the IR drop over an oxide film and an absorbed layer of hydrated metal hydroxide or metal ion layer. The steady increase of potential in the Ni-NaCl system corresponds with the buildup of an oxide and/or an absorbed layer.

The cathode ΔE , Table 7, had to be calculated from the data obtained in our first experimental run with its uncertainty of interpretation. The values reflect the error due to hydrogen bubble formation.

TABLE 6
ANODE ΔE MEASUREMENTS TEST SERIES Ni/NaCl - 1

Test Number	Current Density amp/in ²	Temperature °F	Concentration lb/gal	Gap (mils)	Anode ΔE (Volt) vs S. C. E.		
					0-1 Minutes	15 Minutes	30 Minutes
1	868	83	1.29	27.5	2	2	3
2	868	83	2.71	27.5	1	4	5
3	232	83	1.29	27.5	1.2	1.6	2.2
4	232	83	2.71	27.5	3	4	4
5	232	139	1.29	27.5	1.0	0	0
6	232	139	2.71	27.5	2	2.0	2.5

TABLE 7
CALCULATED CATHODE ΔE 's TEST SERIES Ni/NaCl - 1

Test Numbers	Current Density amp/in ²	Temperature °F	Concentration lb/gal	Gap (mils)	Cathode ΔE (Volts)		
					0-1 Minutes	15 Minutes	30 Minutes
1	868	83	1.29	27.5	23	19.5	18.0
2	868	83	2.71	27.5	8.0	1.0	1.0
3	232	83	1.29	27.5	11.6	11.9	11.3
4	232	83	2.71	27.5	17	8	9
5	232	139	1.29	27.5	10.4	7.7	8.5
6	232	139	2.71	27.2	14.2	8	8

TABLE 8
TOTAL ΔE MEASUREMENTS TEST SERIES Ni/NaCl - 2

Test Numbers	Current Density amp/in ²	Temperature °F	Concentration lb/gal	Gap (mils)	Total ΔE (Volts)		
					0 Minute	1 Minute	2 Minutes
1	868	139	2.71	27.5	10	10	10.5
2	868	139	2.71	6.5	9.5	8.5	10
3	868	139	1.29	27.5	10	11	11
4	868	139	1.29	6.5	10	10	11
5	868	83	2.71	27.5	11.5	11.5	11.5
6	868	83	2.71	6.5	9	9	9
7	868	83	1.29	27.5	12	12.5	12.5
8	868	83	1.29	6.5	12	12	12
9	232	139	2.71	27.5	19.8	20	20
10	232	139	2.71	6.5	15.3	19.5	18
11	232	139	1.29	27.5	16.5	15.9	16.4
12	232	139	1.29	6.5	13.3	11.7	11.7
13	232	83	2.71	27.5	20.8	15.8	15.7
14	232	83	2.71	6.5	10.9	13.5	13.5
15	232	83	1.29	27.5	20.3	20.2	20.5
16	232	83	1.29	6.5	13.8	14.7	15.4
17	1000	111	2.0	17	12	13	12
18	100	111	2.0	17	5	5	5
19	550	150	2.0	17	9.5	9.5	9.5
20	550	72	2.0	17	8	9	8
21	550	111	3.0	17	6	8	8
22	550	111	1.0	17	10.5	9.5	8.5
23	550	111	2.0	32	9	8	8
24	550	111	2.0	20	11	14.5	14.5
25	550	111	2.0	17	8	8	8
26	2000	111	2.0	17	16	19.5	19.5

6.3.2 Test Series Fe/NaNO₃

In this test series we used iron electrodes and a sodium nitrate electrolyte, and we tested factors x_1 , x_2 and x_4 at the same levels as in the Ni/NaCl test series.

Test factor x_3 , the electrolyte concentration, was varied as follows:

Level:	$-\alpha$	-1	0	+1	$+\alpha$
N :	3.34	3.71	4.59	5.47	5.84 (lb/gal)

The results of our tests are included in Appendix II. 10.4.1.

The best curve fit equations for total ΔE and the n-factor were calculated as

$$\Delta E_{\text{total}} = 10.76 - 0.91X_1 - 2.97(X_1 - b) - 2.07X_1X_2 \quad (41)$$

and

$$\begin{aligned} n = 7.00 - 5.22X_1 + 1.84X_4 + 6.71(X_4^2 - 6) - 4.39X_1X_2 + \\ 4.26X_1X_3 - 4.58X_1X_4 + 7.42X_2X_4 - 5.33X_1X_2X_4 \end{aligned} \quad (42)$$

where

$$X_1 = \frac{I/A - 550}{318} \text{ in amp/in}^2$$

$$X_2 = \frac{T - 111}{27.6} \text{ in } ^\circ\text{F}$$

$$X_3 = \frac{N - 4.59}{088} \text{ in lb/gal}$$

$$X_4 = \frac{L - 17.0}{10.5} \text{ in inches} \times 10^{-3}$$

$$b = 0.800$$

The experimental error for this test series was calculated as $\sigma_{\Delta E} = 2.25$ volts.

From Equation (41) we plotted total ΔE against current density for three temperatures, Figure 34.

Current density was the predominant effect on ΔE_{total} in this test series. The plots indicate that the total ΔE reaches a maximum at progressively lower current densities as the electrolyte temperature increases after which the ΔE_{total} decreases again. Temperature itself had no independent effect on ΔE_{total} in our curve fit equation.

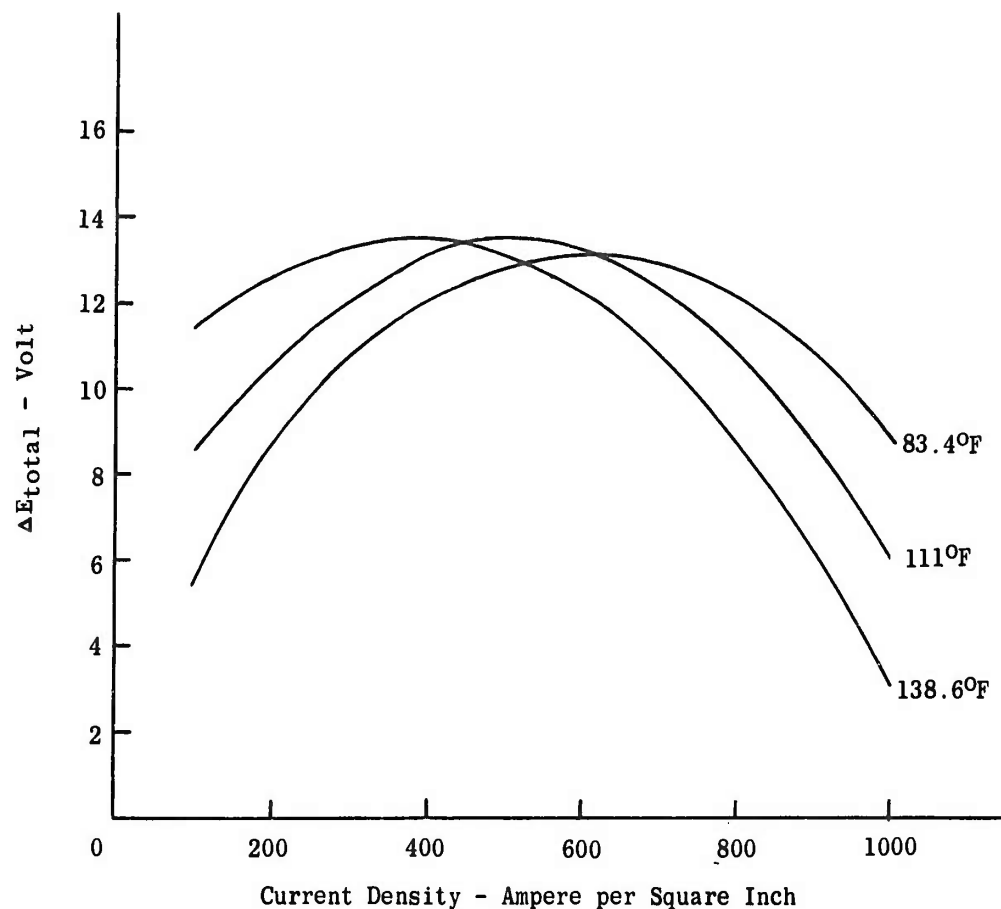


Figure 34. Total ΔE vs Current Density for Various Temperatures
Test Series Fe/ NaNO_3

From Equation (42) we plotted n-factor against current density, Figure 35, and against electrode separation, Figure 36.

The n-Factor shows a linear decrease with increasing current density at all electrode gaps investigated. The decrease is less apparent as the gap becomes larger, Figure 35. A smaller cutting efficiency, therefore, is indicated at the 6.5 mil gap level rather than at the larger gaps.

The small number of measurements precluded the use of a statistical evaluation of the anode ΔE . However, the anode ΔE appeared to be dependent upon the anode reaction products which occurred in the form of a black gelatinous residue during electrolysis.

6.3.3 Test Series Cr/ NaCl

In this test series we used chromium anodes, a chrome plated cathode and a sodium chloride electrolyte. We tested factors x_1 through x_4 at the same levels as in the Ni/ NaCl test series.

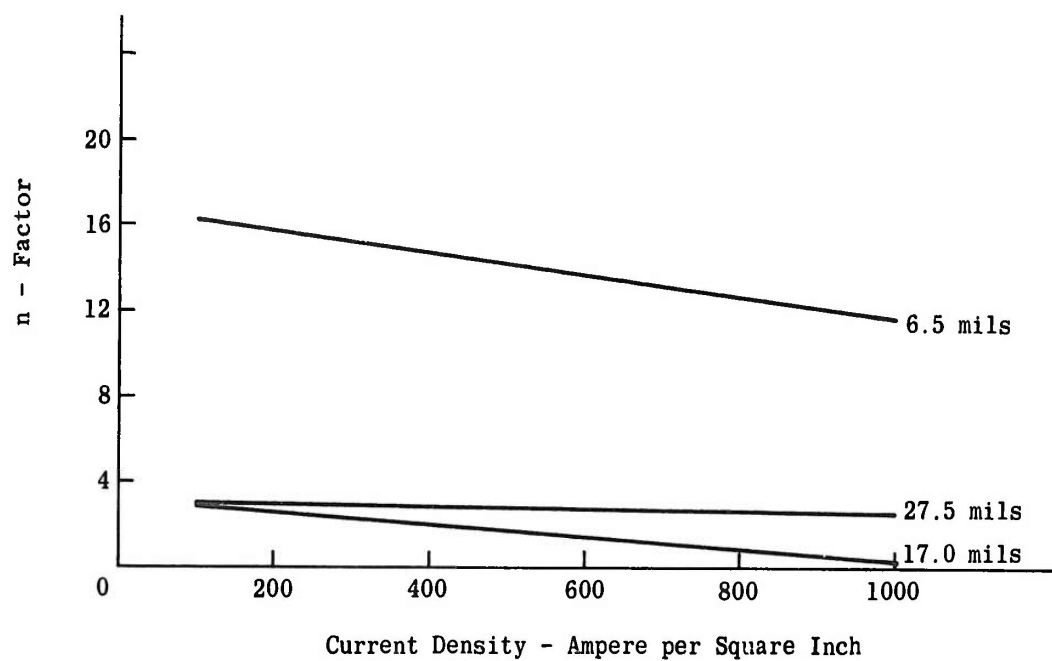


Figure 35. n-Factor vs Current Density for Various Electrode Separations
Test Series Fe/NaNO₃

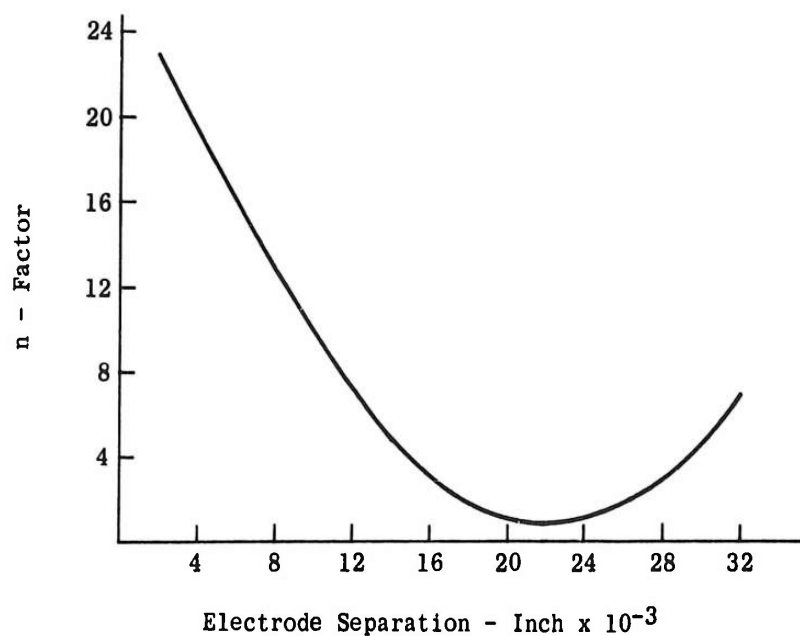


Figure 36. n-Factor vs Electrode Separation at 550 Ampere per Square Inch
Test Series Fe/NaNO₃

The results of our tests are included in Appendix II.10.4.1.

The best curve fit equations for total ΔE and the n-Factor were calculated as

$$\Delta E_{\text{total}} = 7.57 - 1.89X_2 + 0.99X_4 + 2.27(X_4^2 - b) \quad (43)$$

and

$$n = 5.91 + 1.62X_1 - 0.15X_3 + 0.56(X_3^2 - b) - 0.47X_1X_3 - 0.32X_2X_4 \quad (44)$$

where the values of X_1 , X_2 , X_4 and b are the same as in Equation (42), and

$$X_3 = \frac{N - 2.00}{.071} \text{ in lb/gal.}$$

The experimental error for this test series was calculated as $\sigma_{\Delta E} = 3.7$ Volts.

From Equation (43) we plotted total ΔE against gap for three temperatures, Figure 37, and against temperature for three gaps, Figure 38.

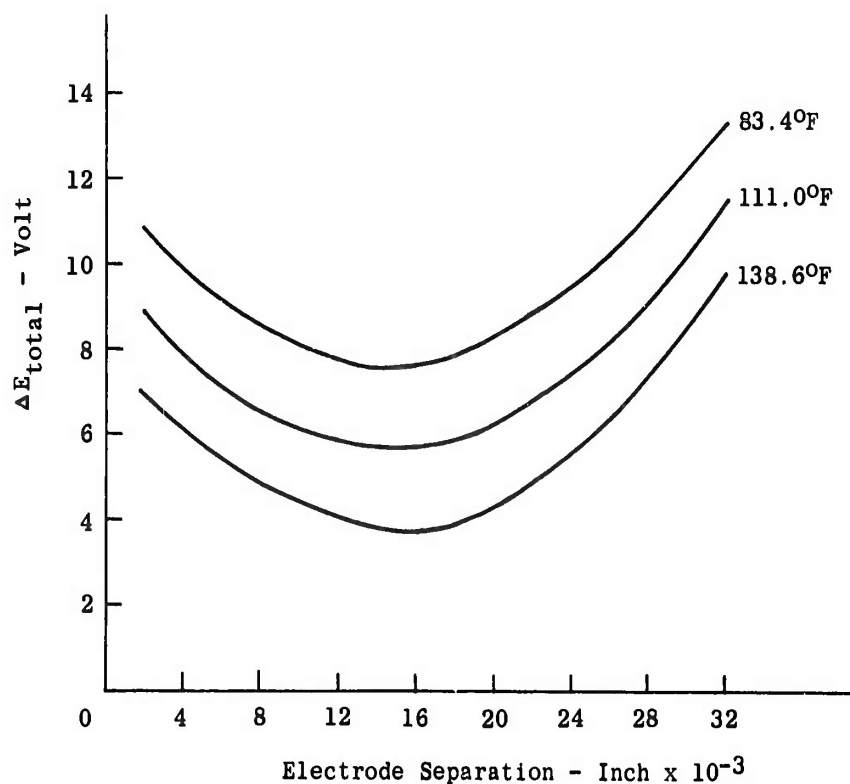


Figure 37. Total ΔE vs Electrode Separation at Various Temperatures
Test Series Cr/NaCl

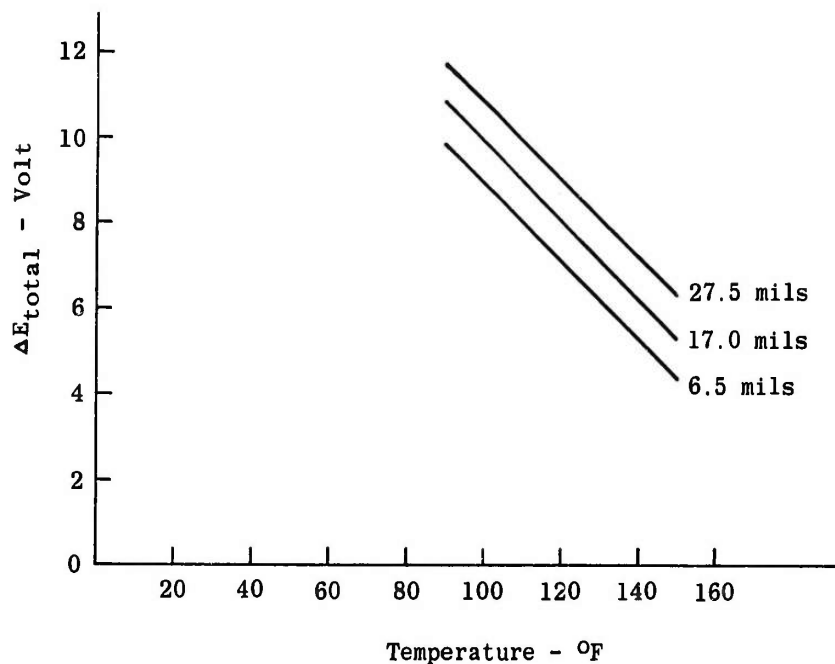


Figure 38. Total ΔE vs Temperature at Various Electrode Separations
Test Series Cr/NaCl

The total ΔE in this test series was strongly affected by electrolyte temperature and gap. This was the only case where electrode separation had a significant effect on total ΔE . Neither current density nor electrolyte concentration appeared to have influenced the variations of ΔE_{total} .

From Equation (44) we plotted n against concentration, Figure 39., and against current density, Figure 40.

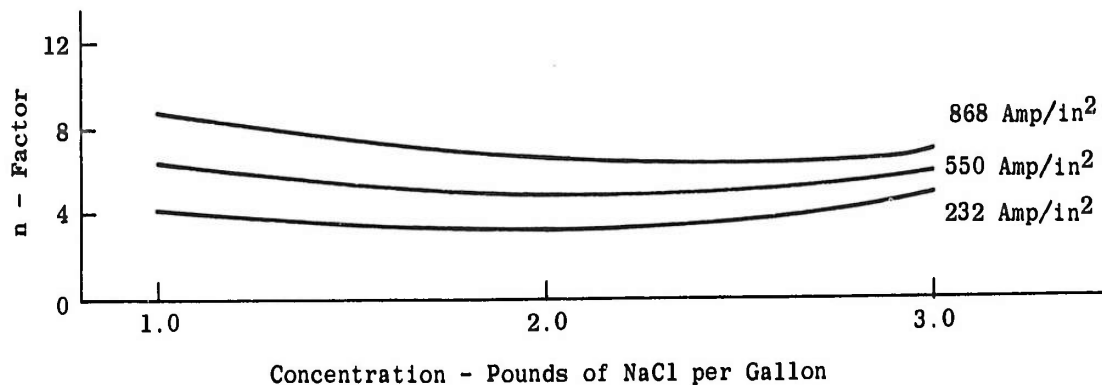


Figure 39. n-Factor vs Concentration at Various Current Densities
Test Series Cr/NaCl

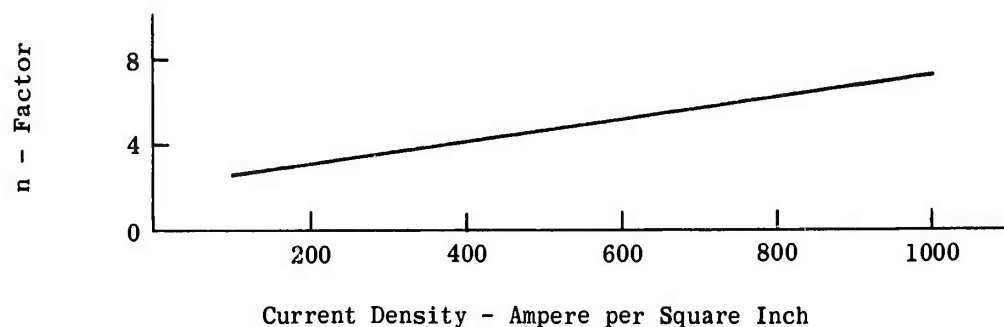


Figure 40. n-Factor vs Current Density at 2.0 Pounds of NaCl per Gallon
Test Series Cr/NaCl

The n-Factor showed a linear relationship with current density and a slight dependence on electrolyte concentration.

The anode ΔE appeared to depend only on current density while the calculated cathode ΔE remained relatively constant.

6.3.4 Test Series Fe/H₂SO₄

The test series was abandoned when it became apparent that the test conditions resulted in erratic ΔE measurements. The test runs which we conducted were not reproducible because of excessive chemical attack. The data are included for the record in Appendix II.10.4.1.

6.3.5 Analysis of Surface Films and Finish

We examined specimens from the static cell investigation with a low-power magnification microscope to determine the cutting characteristics, and using an electron microscope we analyzed the surface films.

- (a) On the nickel anodes we saw evidence of selective cutting at the lower current densities, with the heaviest removal occurring at the edges. The activity at the various grains, particularly with reference to their crystallographic orientation, resulted in surfaces which appeared metallographically etched. Occasionally single grains appeared to have resisted the electrolytic action and stood in relief as a promontory, particularly at the low current densities.

The surfaces which had been exposed to the low and high current density levels showed the presence of nickel oxide, NiO, while the surfaces cut at the medium current densities showed only sodium chloride, NaCl. The NiO produced broad, weak lines in powder diffraction studies indicating that the oxide consisted of poorly developed crystallites.

The electron microscopy analysis was difficult because of the thickness of the oxide layer. A large number of replicas were required before sufficient material was removed to produce a transfer which we could view. Figure 41. shows the type of oxide formed. The grain at the upper left corner has a heavy oxide buildup and

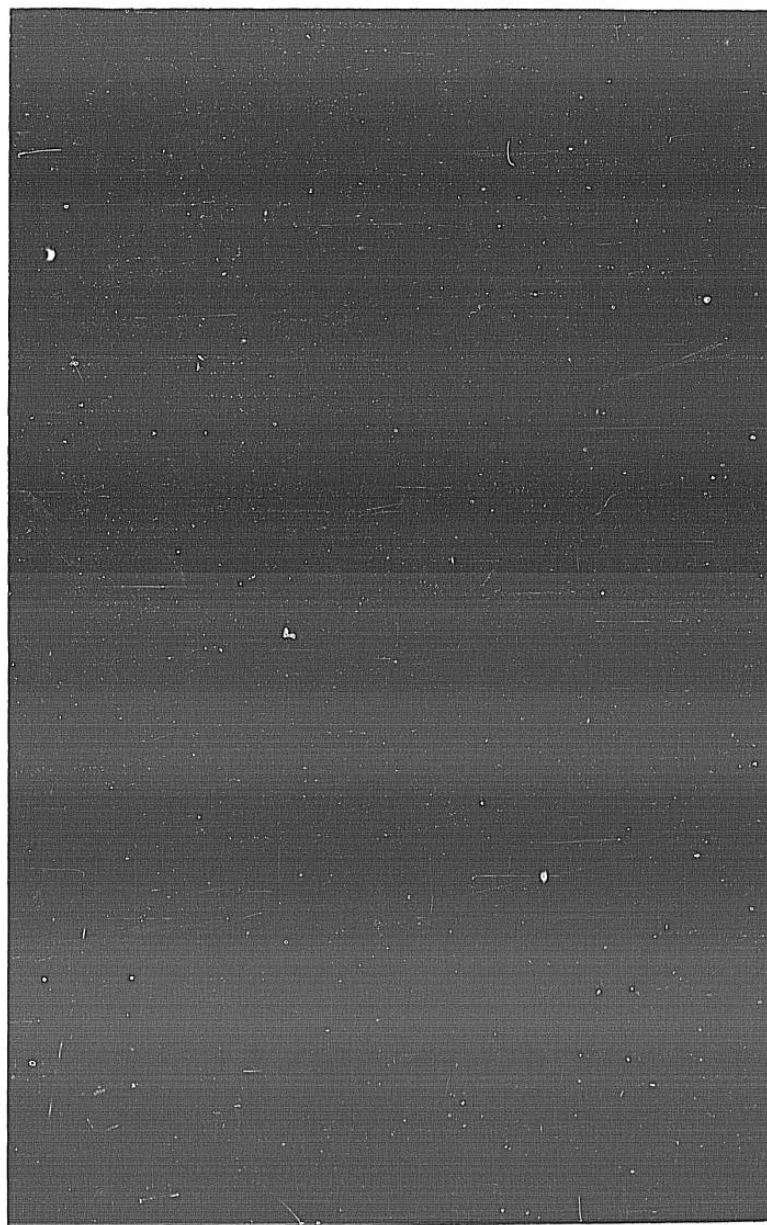


Figure 41. Electron Micrograph of a Nickel Anode after Electrolysis with 1.29 lb NaCl/
gal, 866 amp/in², 130° F and 6.5 mil Gap

Mag. 6000X

depicts the difference in chemical reactivity of crystal faces whereas the lower right corner grain is virtually untouched.

- (b) The iron anodes cut with sodium nitrate electrolyte appeared to have been less susceptible to selective etching than were the nickel anodes cut with sodium chloride. Only the edges of the iron specimens were attacked, but the over-all surface contours were maintained at all current density levels.

We observed that a large amount of black hydrated ferric oxide, $\text{Fe}_2\text{O}_3 \cdot x\text{H}_2\text{O}$, formed during electrolysis. The X-ray powder analysis of the surfaces of the iron anodes showed only the presence of Fe_2O_3 (magnetite) in a very fine particle of $\alpha\text{Fe}_2\text{O}_3$ (goethite) which we did not see on any of the other five samples examined.

The electron-microscopy showed only the presence of an amorphous structured oxide layer. Figure 42. shows the typical appearance of 6000X. The dark spots represent heavier particles which pulled out of the replica; these are equally amorphous in shape.

- (c) The appearance of the chromium anodes was smooth and bright and showed little rounding of the edges. We did not observe any preferential etching of grains at any temperature or at any current density. Preliminary examination of the chromium anode surface indicated X-ray analysis would not be fruitful. Examination of the surface by electron microscopy showed the absence of oxide. If oxide is present, it may be on the monomolecular level. Figure 43 shows a 40,000X magnification of the surface of the chromium. This particular anode was cut at a current-density of 868 amp/in² at a temperature of 139°F.

6.4 Dynamic Cell Investigation

For our dynamic cell investigations we used two test rigs which we labeled "Anodic Reaction Dynamic Cell" and "ECM Cell". The rigs are described in Appendix II. 10. 2. 2 and II. 1. 4. 3 respectively. We used the same current supply and recording facilities that we used in the static cell tests.

The experiments in the anodic reaction cell were limited to a preliminary study of the effects of electrolyte velocity on the total ΔE at various current densities for three anode material/electrolyte combinations. Although we did not use a statistical design of experiments, the data show a dependence of total ΔE on current density. See Figure 44. and Appendix II. 10. 4. 2.

The tests in the ECM cell, for which we used a three-factor Box experiment, yielded information applicable to the ECM process. We tested two anode material/electrolyte combinations to check the effect of current density, electrolyte flow rate, and electrolyte pressure on the total ΔE and on a relative cutting efficiency factor μ . No relative electrode feeds were used during these tests; instead, we allowed the electrode separations (gaps) to increase during electrolysis, and we measured the gap increase after the test had been completed. The electrolyte temperature and concentration were held constant.

We determined the μ factor by relating the measured depth of each cut to effective current and cutting time as follows:

$$\mu = \frac{\text{depth of cut (in } 10^{-1} \text{ mils)}}{i \times t} \quad (45)$$

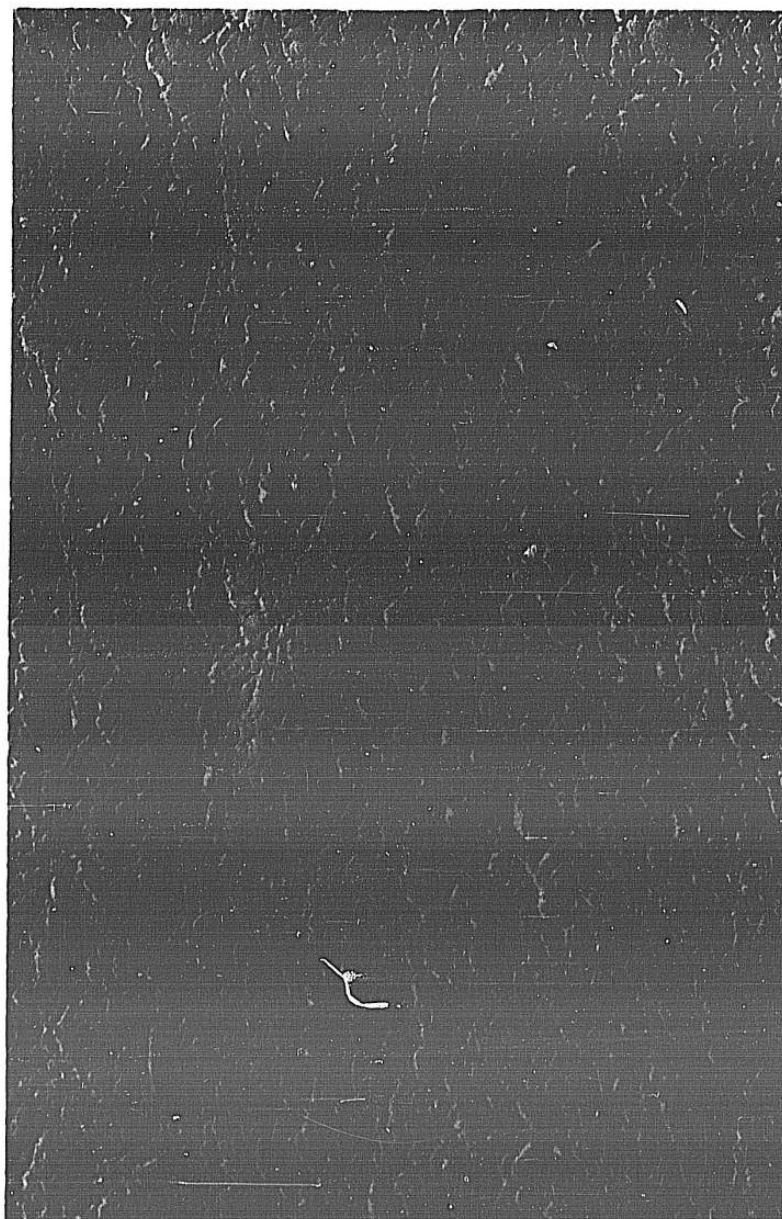


Figure 42. Electron Micrograph of an Iron Anode after Electrolysis with 4.59 lb NaNO_3 /gal, 550 amp/in², 111° F and 17.0 mil Gap.

Mag. 6000X

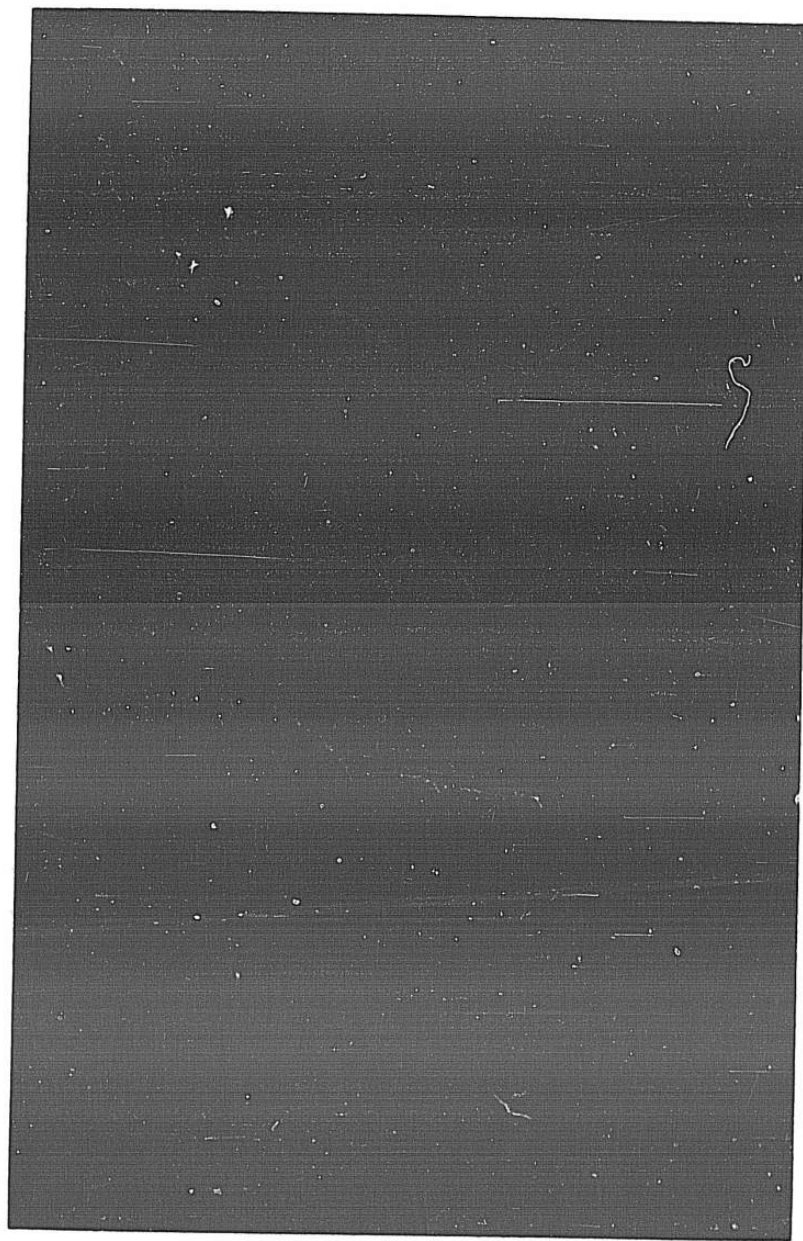


Figure 43. Electron Micrograph of a Chromium Anode after Electrolysis with
2.71 lb NaCl/gal, 868 amp/in², 139°F and 27.0 mil Gap

Mag. 40,000X

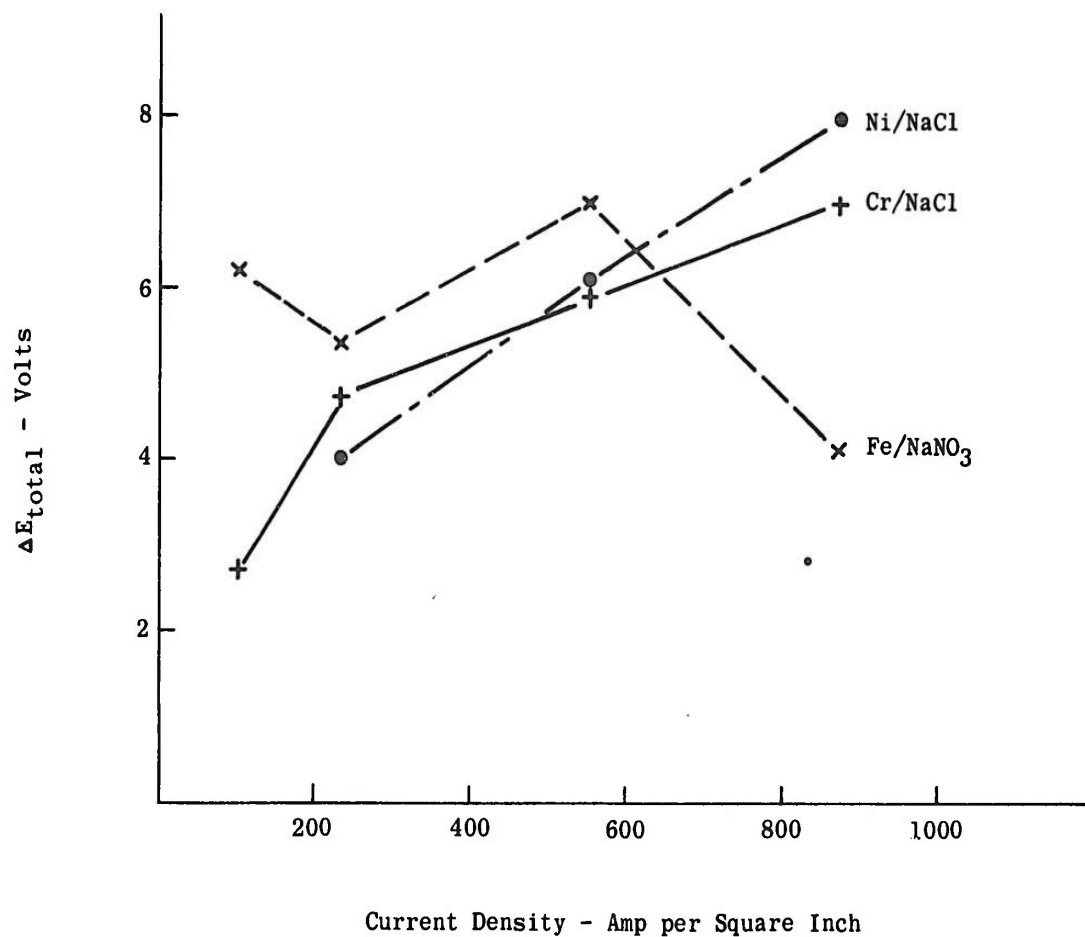


Figure 44. Total ΔE vs Current Density for Various Anode Material/Electrolyte Combinations in Anodic Reaction Cell under Dynamic Electrolyte Conditions

where

μ is a relative cutting efficiency in mils/amp-sec

i is the effective current in amp

t is the effective cutting time in sec.

μ is equal to the reciprocal of the n-factor used in the static cell studies if it is multiplied by

$$\frac{\text{gm mol wt}}{96,500 \times \text{area} \times \text{mat'l density}}$$

We continued our test for four minutes and we recorded our ΔE measurements in one minute intervals.

We interpreted our data by the same methods used for analysis of the static cell tests, and we used curve fit equations and graphical plots to demonstrate the effects of the statistically significant factors on the total ΔE and the μ factor.

The calculated experimental errors in the ΔE analyses from these tests were consistently small, ranging from a $\sigma_{\Delta E}$ of 0.23 volt to 0.15 volts.

6.4.1 Test Series R'41/NaCl

In this test series, we used electrodes made from the nickel-base alloy René 41 and a sodium chloride electrolyte with a concentration of 2.35 lb/gal at 90°F, and we selected the following test levels:

Factor	Description	Levels				
		$-\alpha$	-1	0	+1	$+\alpha$
x_1	Current density I/A (amp/in ²)	25	67	263	458	500
x_2	Flow rate M (cc/min)	500	722	1,750	2,778	3,000
x_3	Inlet pressure P (psig)	30	54	165	276	300

We used constant starting gaps of .010", and we controlled the electrolyte flow rate at the selected levels by adjusting the gap exit pressure.

The results of our tests are included in Appendix II. 10.4.3.

The best curve fit equations for the total ΔE and μ factor were calculated as

$$\Delta E_{\text{total}} = 2.75 + 0.97X_1 - 0.86(X_1^2 - b) \quad (46)$$

$$\mu = 5.87 + 3.96X_1 - 0.84X_3 - 1.8(X_3^2 - b) - 1.00X_1X_3 \quad (47)$$

where

$$X_1 = \frac{I/A - 263}{196} \text{ in amp/in}^2$$

$$X_2 = \frac{M - 1,750}{1,028} \text{ in cc/min}$$

$$X_3 = \frac{P - 165}{111} \text{ in psig}$$

$$b = 0.7303$$

A strong effect of current density on the total ΔE is apparent, particularly in the low current density area, Figure 45. It must be pointed out that test point at the $+\alpha$ level of factor x_1 (current density) approached the maximum capacity of the power supply, and the oscilloscope trace was unsteady and not well discernible. The recorded measurement of the ΔE for this test point may have unduly influenced the apparent downturn of the ΔE curve at the higher current density.

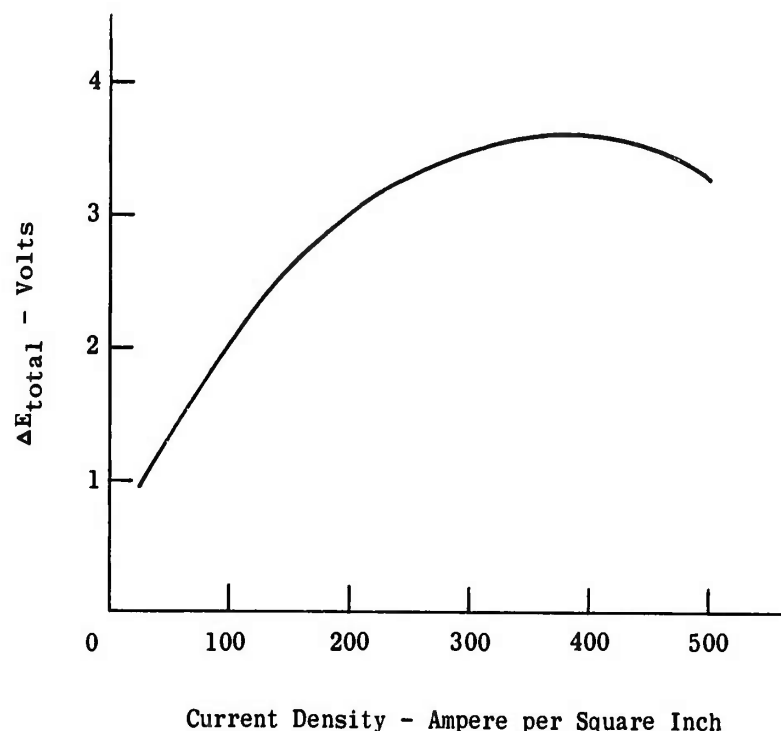


Figure 45. Total ΔE vs Current Density
Test Series René 41/NaCl

The μ factor in this test series depended upon current density, and to a lesser degree on the electrolyte inlet pressure, Figure 46.

6.4.2 Test Series Ni/NaCl

In this test series, we used nickel anodes, a René 41 cathode, and a sodium chloride electrolyte at the same concentration and temperature as for the René 41/NaCl tests, and we used the same factors, test levels and starting gaps.

The results of this test series are included in Appendix II. 10.4.3.

The best curve fit equations for the total ΔE and μ factor were calculated as

$$\Delta E_{\text{total}} = 3.35 + 0.99X_1 + 0.27X_2 - 0.63(X_1^2 - b) + 0.34X_2X_3 \quad (48)$$

and

$$\mu = 10.15 + 5.03X_1 - 0.56X_3 - 2.51(X_3^2 - b) \quad (49)$$

where the values of X_1 , X_2 , X_3 and b are the same as in Equations (46) and (47).

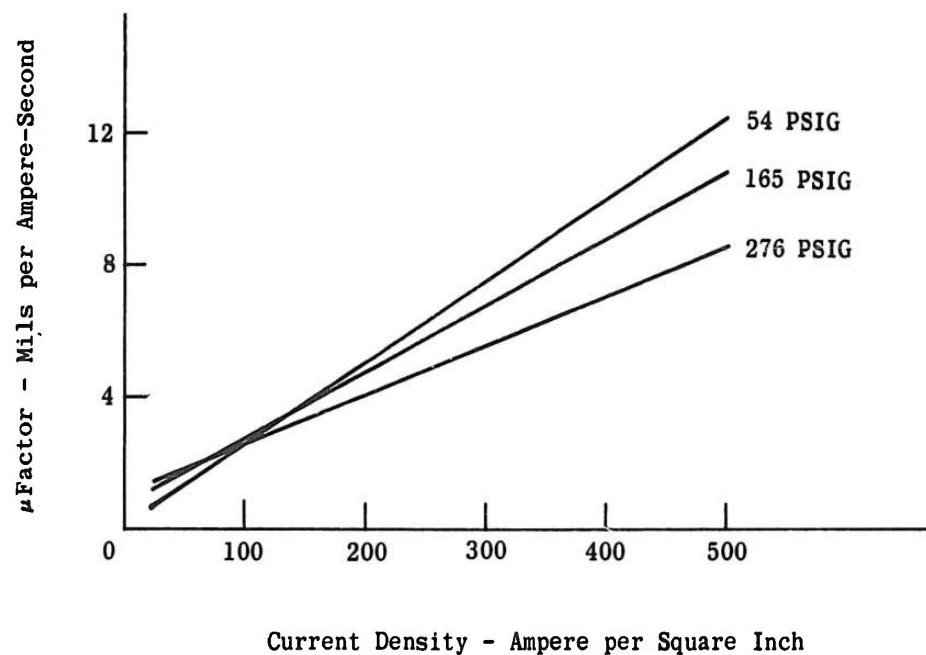


Figure 46. μ Factor vs Current Density at Various Electrolyte Inlet Pressures
Test Series René 41/NaCl

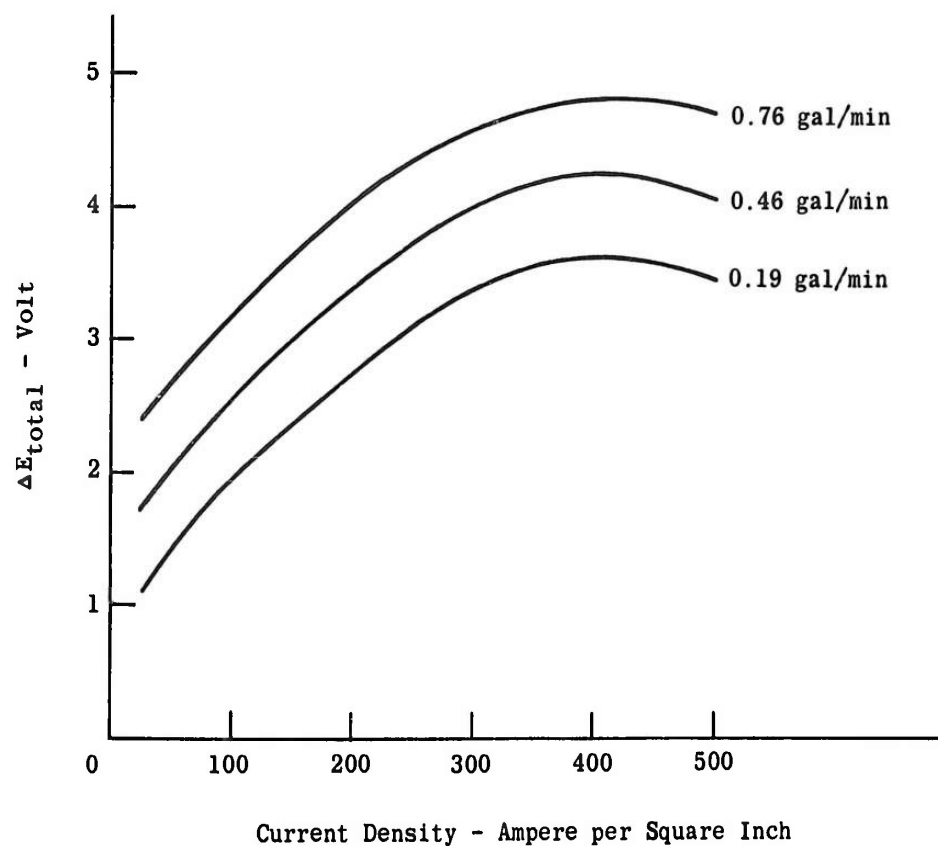


Figure 47. Total ΔE vs Current Density at Various Electrolyte Flow Rates
Test Series Ni/NaCl

Equation (48) shows the total ΔE to be significantly affected by current density, particularly at low current densities, and to a lesser degree by electrolyte flow rate and a flow rate/pressure interaction effect, Figure 47.

The μ factor, Equation (49), was dependent upon current density, and to a lesser degree on electrolyte inlet pressure, Figure 48.

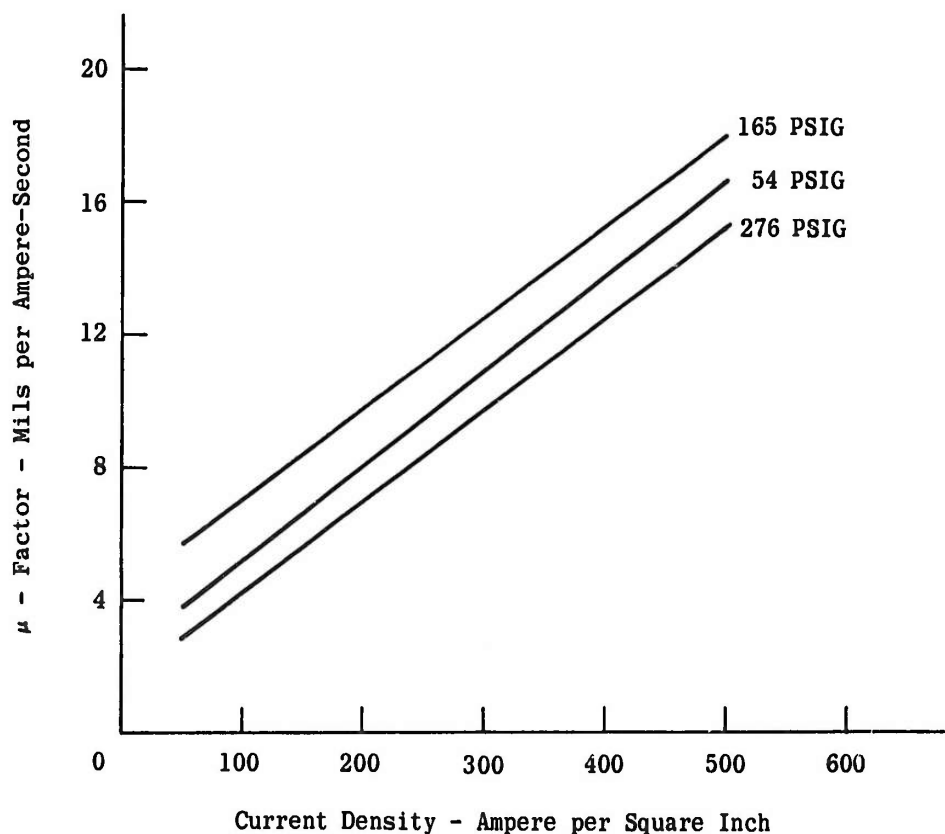


Figure 48. μ Factor vs Current Density at Various Electrolyte Inlet Pressures
Test Series Ni/NaCl

6.5 Discussion and Conclusions

- (a) The experimental facilities and procedures used for this investigation provide a useful method to determine ΔE values under simulated electrolytic machining conditions.
- (b) The results of this work show that the basic laws governing low current density anodic reactions do not apply to high current density electrolytic reactions.
- (c) The static cell investigation did not disclose a consistent pattern of ΔE effects. The factors influencing the total ΔE varied with the material/electrolyte combination.

The anodic behavior of nickel, chromium, and iron differed greatly and influenced the anodic ΔE .

The fluctuations observed in the anode ΔE 's are too small to account for the variability in total ΔE in the static cell measurements. The total ΔE variability, therefore, is believed to be the result of hydrogen bubble formation.

In the static cell tests, the magnitude of the cathodic ΔE included a concentration polarization term which depended upon the thickness of the absorbed layer. This supposition is based upon the observation that the total ΔE is much reduced in the dynamic cells.

- (d) In the dynamic cell studies the higher electrolyte velocities reduced the anodic surface film in which concentration polarization occurs.

The decrease of the total ΔE with flow velocity, in the case of iron electrolysis with a sodium nitrate electrolyte, can be attributed to the formation of a gelatinous anodic film which is more effectively removed at higher flow rates.

- (e) The results of the dynamic cell investigations point to a dependence of the ΔE 's on current density at the lower current density levels; this dependence decreases at densities above 200 amp/in².

The estimated ΔE used in our mathematical models, Section 3, Chapter III, approximates the actual ΔE at the current density levels used in practical electrolytic machining for the René 41/NaCl alloy-electrolyte combination.

However, these tentative conclusions should be confirmed by expanding the dynamic cell investigations to higher current density levels and to different engineering alloys. The ΔE investigation for dynamic electrolyte conditions should include an analysis of the effects which were found to influence the behavior of ΔE under static electrolyte conditions.

7. SURFACE FINISH

Specific surface finishes are an engineering requirement for any machined surface and are therefore used as a measure of production performance along with rates of metal removal.

With chip cutting methods, a wide range of surface finishes can be accomplished, and their quality depends primarily on the metal removal rate. The electrolytic machining method differs from these processes in that maximum roughness levels cannot be exceeded. Our tests have shown that excessive surface roughness is an indication that incompatible operating parameters were chosen or occurred inadvertently for specific environmental conditions. It is a well known fact, for example, that when the local electrolyte velocity decreases below a minimum level during machining, the metal removal rate is retarded, the surface finish deteriorates, and electrical shorts can occur.

To investigate the effects of operating parameters on surface finish we studied two alloy-electrolyte combinations and we searched for empirical relationships between process operating parameters and surface roughness.

We used surface roughness height and surface lay as analysis criteria.* We supplemented the measurements of surface roughness and lay by metallographic examination of "subsurface" defects.

We conducted surface finish studies designated as JB series in the test apparatus used for the investigation of process variables described in Section 2, Chapter III and in the Appendix II. 1.

For the studies designated AJ series, we used a test apparatus which machined a 1" by 1" pocket into a 1" by 1-1/2" work surface. We held the imposed operating parameters constant at the selected levels, and we continued each test until the response variables had stabilized. The details of the JB and AJ test series are described in Appendix II. 5.

We conducted our tests on the nickel-base alloy René 41 with NaCl electrolyte and on the iron-base alloy A-286 with NaNO_3 electrolyte, and we investigated the effect of the following variables:

- (a) Feed rate.
- (b) Cutting gap.
- (c) Electrolyte.
- (d) Electrolyte pressure.
- (e) Electrolyte temperature.
- (f) Electrolyte viscosity.

7.1 Data Analysis

After we established a specific region for our examinations, we designed our experiments so that they could be analyzed by the following techniques:

- (a) Graphical analysis.
- (b) Regression analysis.
- (c) Factor analysis.
- (d) Analysis of variance.
- (e) Dimensional analysis.

Among these methods, only dimensional analysis failed to provide useful data.

* Surface roughness refers to relatively finely spaced surface irregularities; their height and width are considered in roughness measurements; their direction establishes surface lay.

Irregularities which are of greater spacing than roughness are defined as waviness. Waviness was not considered in our investigation.

Roughness height is rated in microinches arithmetical average (AA) deviation from the mean line, or in microinches root mean square average (RMS) deviation from the mean line. Surface roughness was measured with stylus-tracer type instruments in our investigation. See Appendix II. 5. Unless otherwise stated a roughness-width cutoff of .030" was used.

The model equations we used in the analysis techniques were:

- (a) Linear.
- (b) Power polynomial.
- (c) Log-linear.
- (d) Log polynomial.

And, we adhered to the following significance levels:

- (a) Data were self-supporting when the statistical test showed significance at a 99% level or higher.
- (b) Data were significant for comparison or guidance in further testing and analysis when the statistical test showed significance at a 95% level or higher.
- (c) If the statistical test exceeded a significance level of 90%, but not 99%, the information was meaningful when data from other series supported it.

For statistical analysis methods, we followed those given in the standard texts, with one exception. In the case of the two-level factorial data, we used the procedure described by Cuthbert Daniel.⁽⁵⁾

7.1.1 Associated Data Analysis Problems

There were four associated categories in which we encountered data analysis problems:

- (a) Boundary conditions. We had to restrict the test region within narrow bands because outside the bands we experienced process malfunctions.
- (b) Complexity of phenomena. Several disciplines complicated the search for the model format: electricity, chemistry, metallurgy, and fluid mechanics.
- (c) Response surface discontinuities. A different magnitude of results developed from one test region to another when one statistical factor in our testing ceased to be influential and another factor superseded it.
- (d) Measurement. In addition to the lack of repeatability, physical problems in measuring test factors and responses occurred.

7.2 Surface Roughness Investigations

For the alloy-electrolyte combinations investigated, we found that the following operating variables and their statistical interactions can have a significant effect on surface roughness:

- (a) Feed rate.
- (b) Electrolyte velocity or mass flow related to cutting gap.
- (c) Electrolyte viscosity.

(5): See References

(d) Electrolyte temperature.

(e) Length of work surface along electrolyte passage.

We further found that the relative significance of these factors depends upon the test range, tooling, and other testing conditions.

Cutting gap when considered independently from electrolyte velocity was significant only in one of our tests in which we investigated the surface finish of the iron-base alloy A-286 machined with NaNO_3 electrolyte.

Static electrolyte pressure in the cutting gap was not significant in our tests which were conducted at pressures between 19 psig and 230 psig.

We conducted eight test series. We will now discuss two of these tests in detail.

7.2.1 Test Series AJ-G

In this test we examined the effect of feed rate and electrolyte flow for two electrolyte temperatures and two cutting gaps on the surface roughness of René 41 when machined with sodium chloride. The surface roughness was measured at the flow entrance and at the flow exit. We conducted an analysis of variance in three over-lapping test regions, which we designed so that the combination of the variable factors in each test region would result in radically different surface finishes without causing process malfunctions. Figure 49, Figures 50. through 52., which summarize the test results, show that the relative significance of the effects on surface roughness was different at the flow entrance than at the flow exit. Furthermore, the figures show that the relative significance of the effects on surface roughness was also determined by the test ranges.

Further examination of the test specimens generated in these tests demonstrated smooth surface finishes and two distinct patterns of surface lay. One surface lay pattern was oriented in the direction of electrolyte flow, the other in a direction perpendicular to the flow, Figure 53. and Figures 54. through 58. As the operating parameters were varied, and as the surface finishes deteriorated, we first observed the flow directional lay pattern. When the surface finish deteriorated further, we noticed the lay pattern which is perpendicular to the flow.

In samples from tests AJ-GI and AJ-GII, we measured the distance from the flow entrance to the line where the transition between the flow oriented surface lay and smooth surface finish occurred and we analyzed the factors which affected the position of the transition, Figure 59.

The best curve fit for the location of the transition point from the flow entrance is expressed by:

$$\text{TP} = .91 + 14.6A + .43B + 44.0C - .015D \quad (50)$$

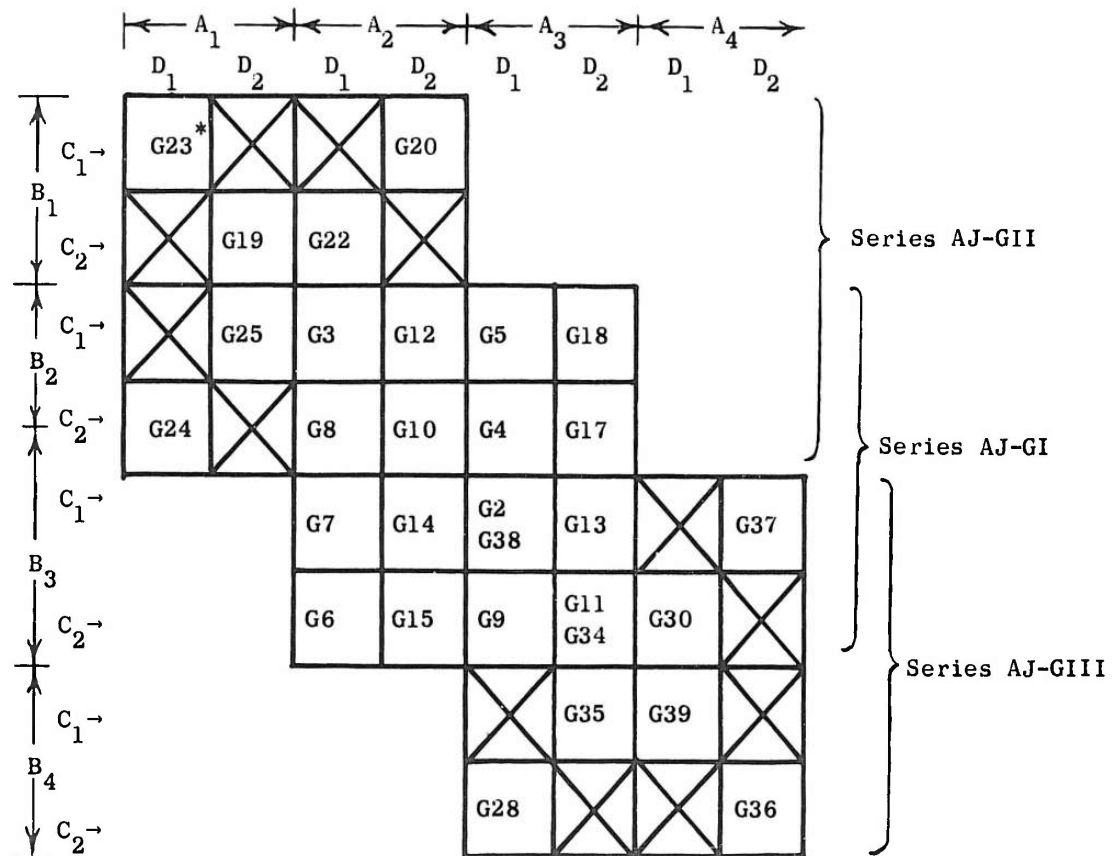
where TP is the transition point in inches from the flow entrance, and

$$A = \text{feed rate/mass flow in } \frac{1}{\text{in}^2}$$

$$B = \text{reciprocal of mass flow in } \text{mir}^3/\text{in}^3$$

$$C = \text{gap in inch}$$

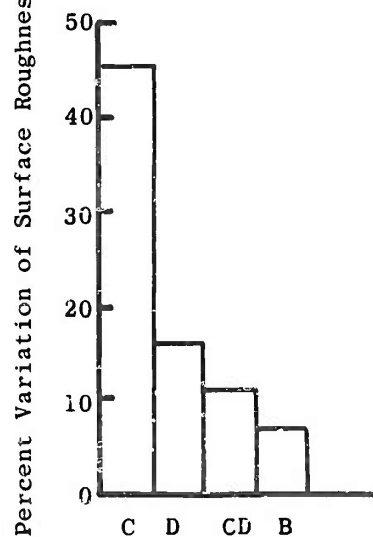
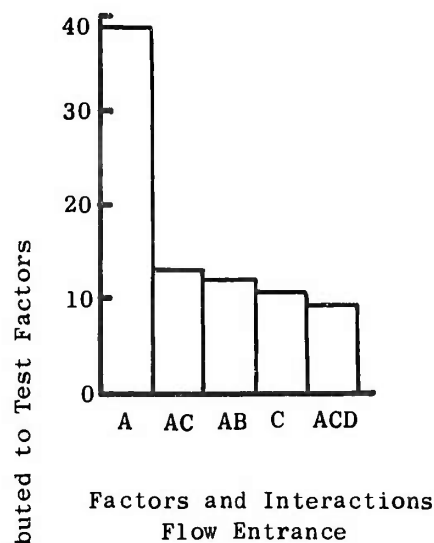
$$D = \text{temperature in } ^\circ\text{F}$$



* Specimen Number
 Series AJ-GI - 2^4 Factorial Analysis of Variance Test
 Series AJ-GII & III - $1/2 \times 2^4$ Factorial Analysis of Variance Tests

Factors		Levels			
		1	2	3	4
A	Feed Rate Mass Flow $\left(\frac{1}{\text{in } 2}\right)$	3.8×10^{-5}	5.8×10^{-5}	11.5×10^{-5}	23.1×10^{-5}
B	$\frac{1}{\text{Mass Flow}} \left(\frac{\text{min}}{\text{in } 3}\right)$	9.6×10^{-4}	14.4×10^{-4}	28.9×10^{-4}	57.7×10^{-4}
C	Cutting Gap (in)	.007	.018	-	-
D	Temperature ($^{\circ}\text{F}$)	84	105	-	-

Figure 49. Design of Surface Finish Test
 Test Series AJ-G



Material: René 41, mill annealed
Electrolyte: NaCl at 2.1 lb/gal

Factors

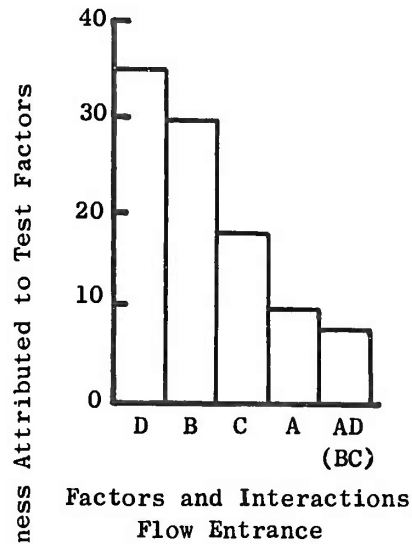
- A $\frac{\text{Feed rate}}{\text{Mass flow}} \left(\frac{1}{\text{in}^2} \right) 5.7 \times 10^{-5} - 11.5 \times 10^{-5}$
- B $\frac{1}{\text{Mass flow}} \left(\frac{\text{min}}{\text{in}^3} \right) 14.4 \times 10^{-4} - 28.9 \times 10^{-4}$
- C Cutting gap (in) .007-.018
- D Temperature ($^{\circ}\text{F}$) 84-105
- [F Feed rate (in /min) .020-.040-.080]
- [M Mass flow (gal/min) 1.5-3.0]

Other Operating Parameters

Average Pressure: 130 psig
Applied Voltage: 4.9-20.8V

Figure 50. Significant Factors Contributing to Variations of Surface Roughness
Test Series AJ-GI

Material: Rene' 41, mill annealed
Electrolyte: NaCl at 2.1 lb/gal



FACTORS

$$A - \frac{\text{Feed rate}}{\text{Mass flow}} \left(\frac{1}{\text{in}^2} \right) 3.8 \times 10^{-5} - 5.8 \times 10^{-5}$$

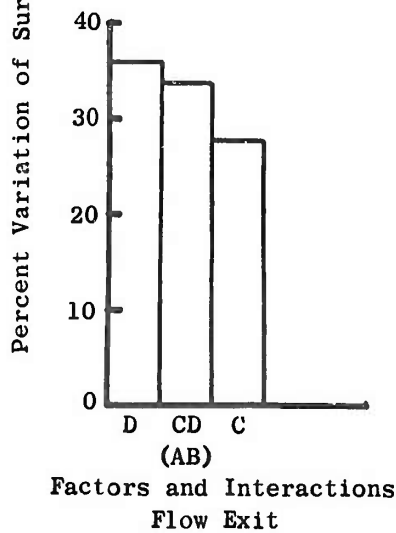
$$B - \frac{1}{\text{Mass flow}} \left(\frac{\text{min}}{\text{in}^3} \right) 9.6 \times 10^{-4} - 14.4 \times 10^{-4}$$

$$C - \text{Cutting gap (in)} .007 - .018$$

$$D - \text{Temperature (}^{\circ}\text{F)} .84^{\circ} - 105^{\circ}$$

$$[F - \text{Feed rate (in/min)} .026 - .040 - .060]$$

$$[M - \text{Mass flow (gal/min)} 3.0 - 4.5]$$

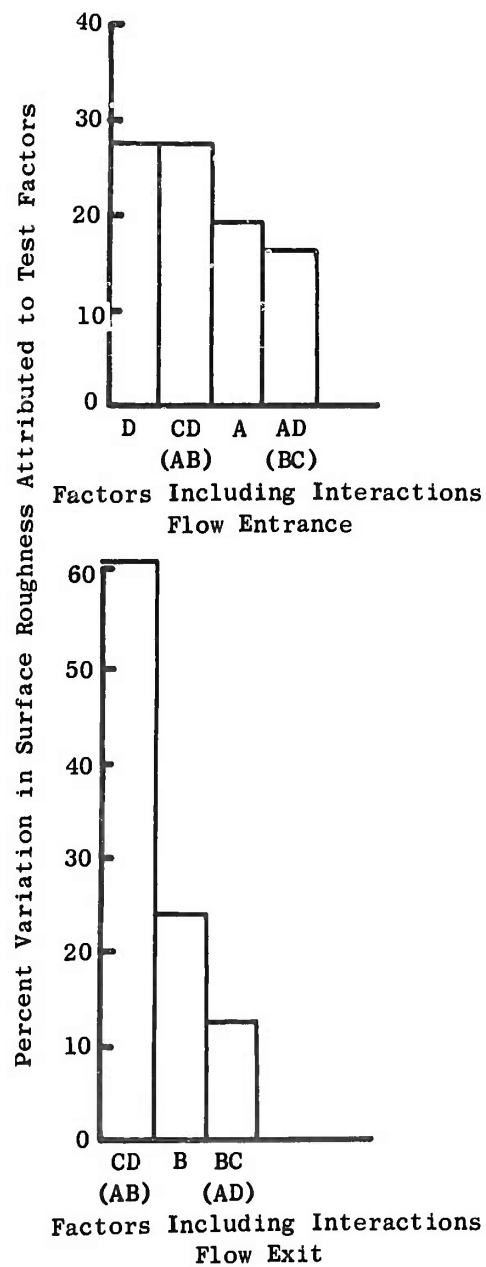


Other Operating Parameters

Average Pressure: 130 psig

Applied Voltage: 5.3-18.2V

Figure 51. Significant Factors Contributing to Variations of Surface Roughness
Test Series AJ-GII



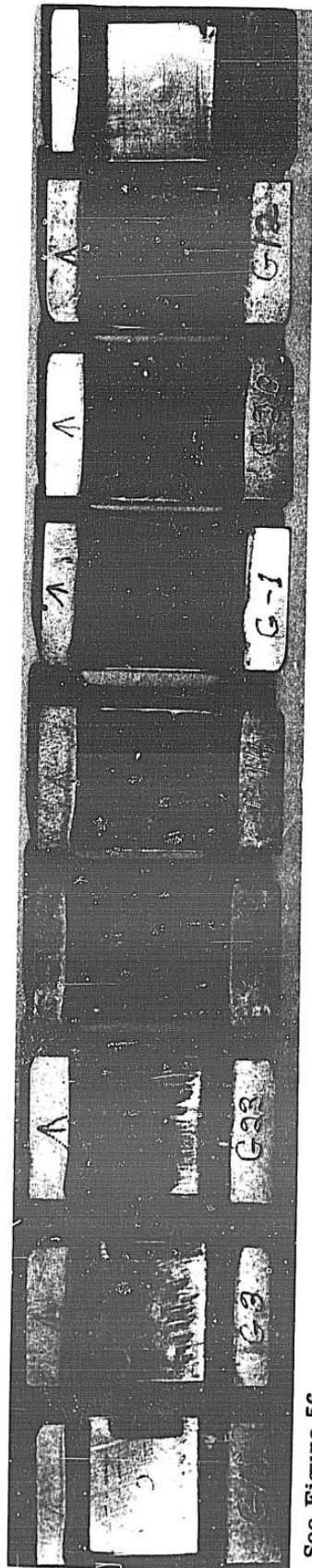
Material: René 41, mill annealed
Electrolyte: NaCl at 2.1 lb/gal

Factors	Test Levels
A $\frac{\text{Feed rate}}{\text{Mass flow}} \left(\frac{1}{\text{in}^2} \right)$	11.5×10^{-5} - 23.1×10^{-5}
B $\frac{1}{\text{Mass flow}} \left(\frac{\text{min}}{\text{in}^3} \right)$	28.9×10^{-4} - 57.7×10^{-4}
C Cutting gap (in)	.007-.018
D Temperature (°F)	84-105
F Feed rate (in /min)	.020-.040-.080
M Mass flow (gal/min)	.75-1.5

Other Operating Parameters

Average Pressure: 130 psig
Applied Voltage: 5.1-18.4V

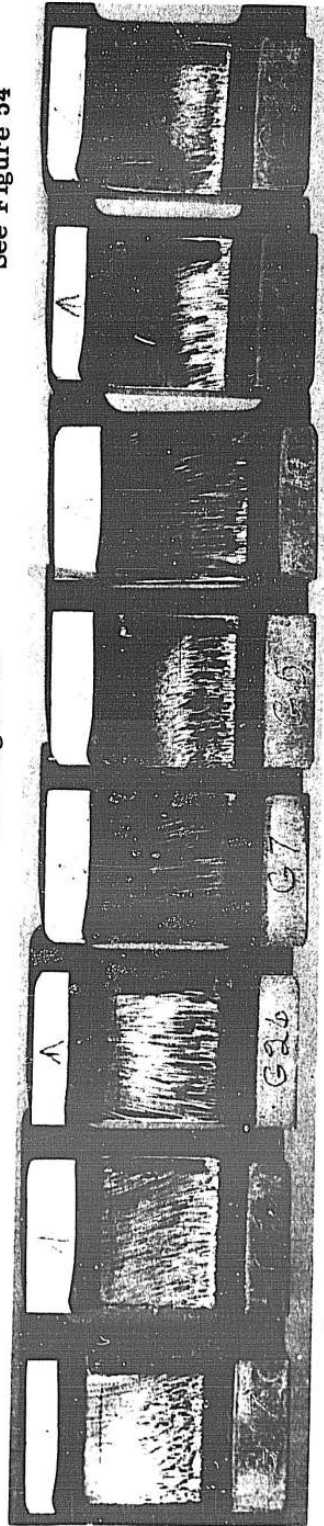
Figure 52. Significant Factors Contributing to Variations of Surface Roughness
Test Series AJ-GIII



See Figure 56

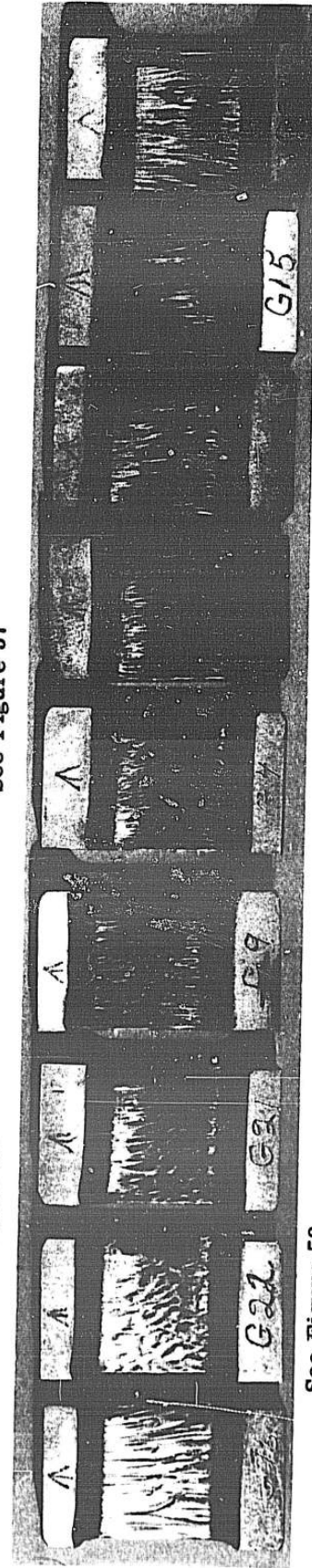
See Figure 55

See Figure 54



See Figure 58

See Figure 57



See Figure 58

See Figure 58

Figure 53. Series AJ-G Surface Finish Specimens

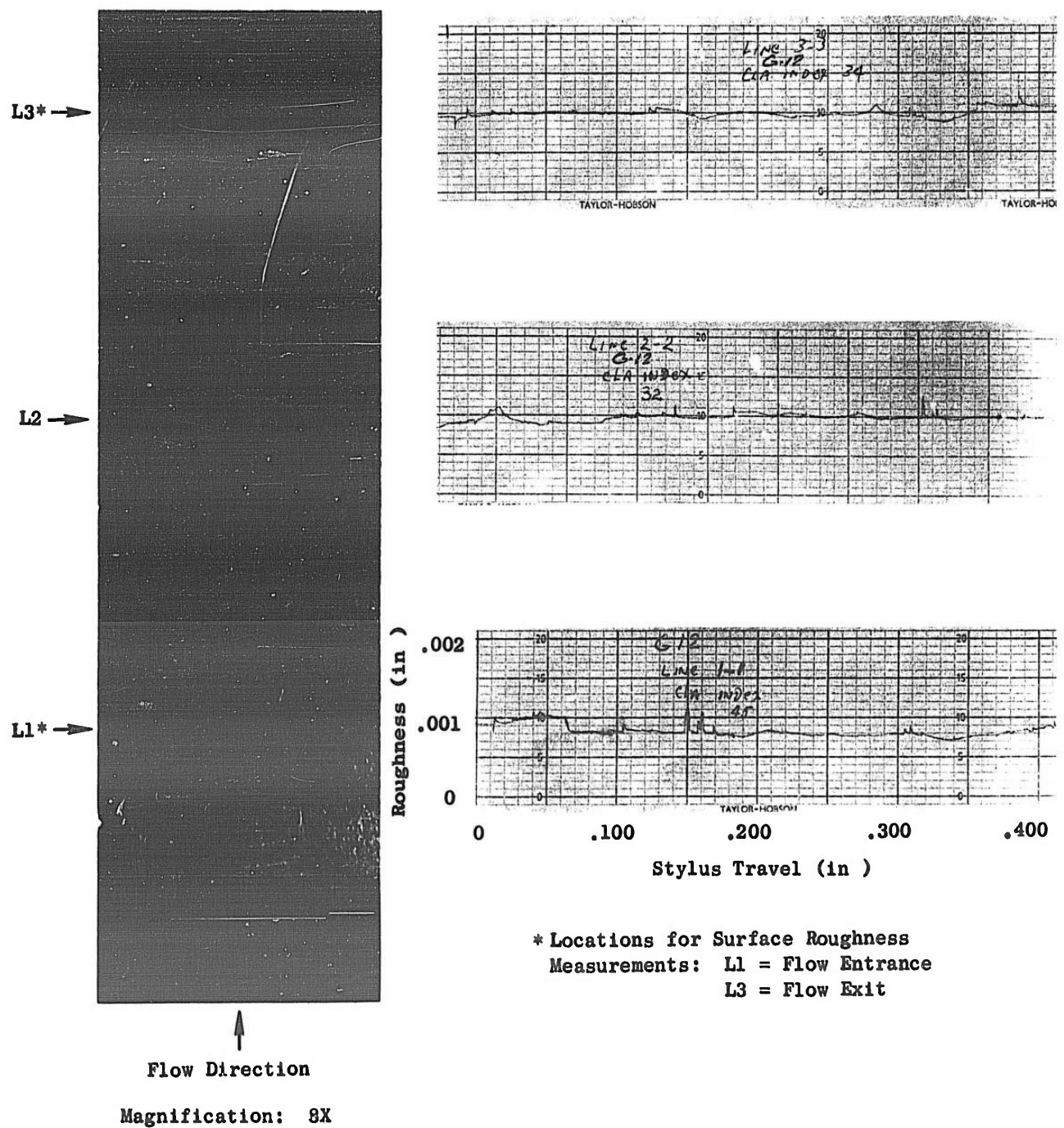


Figure 54. Segment of Specimen G-12 and "Talisurf" Recording

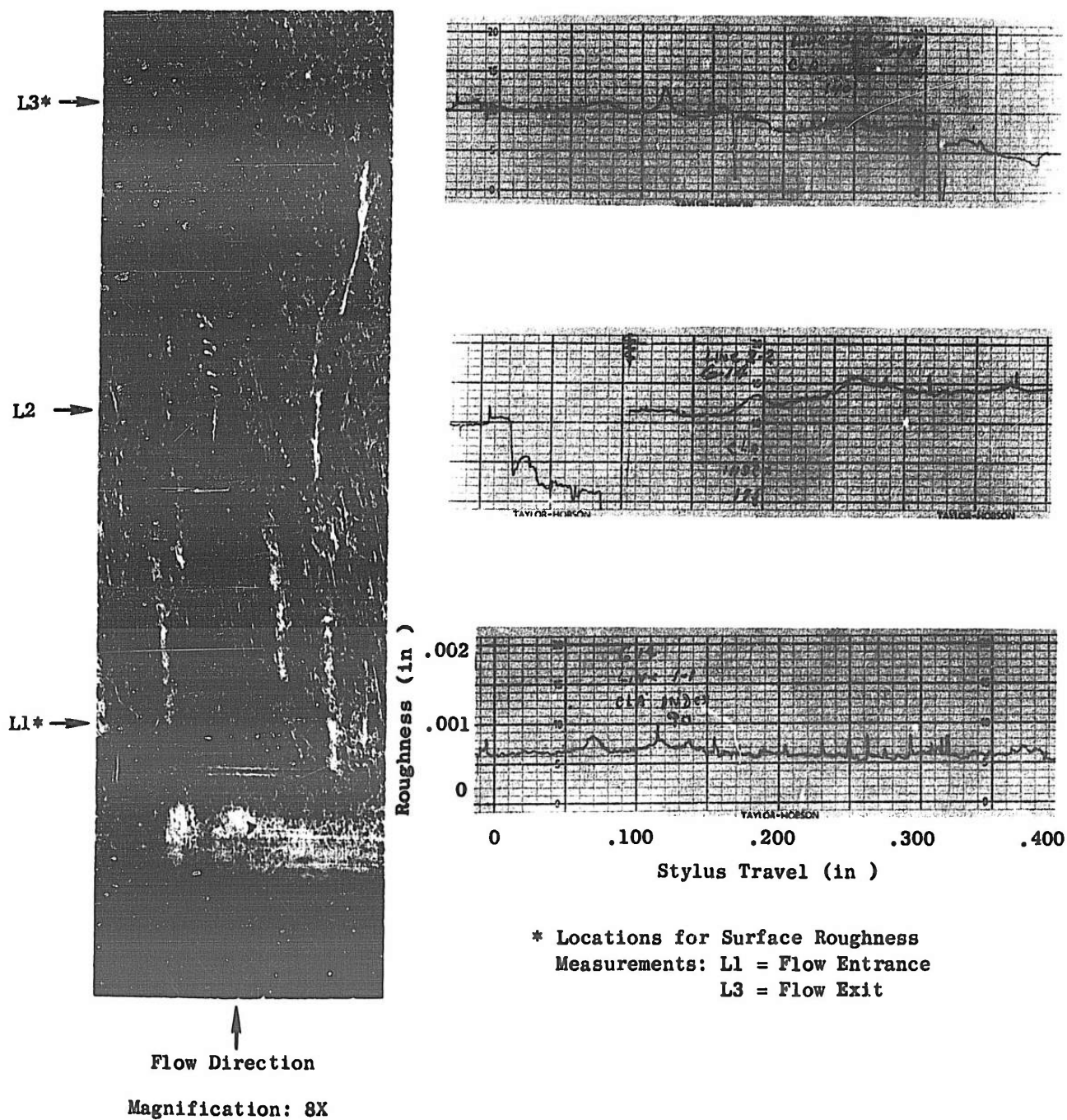
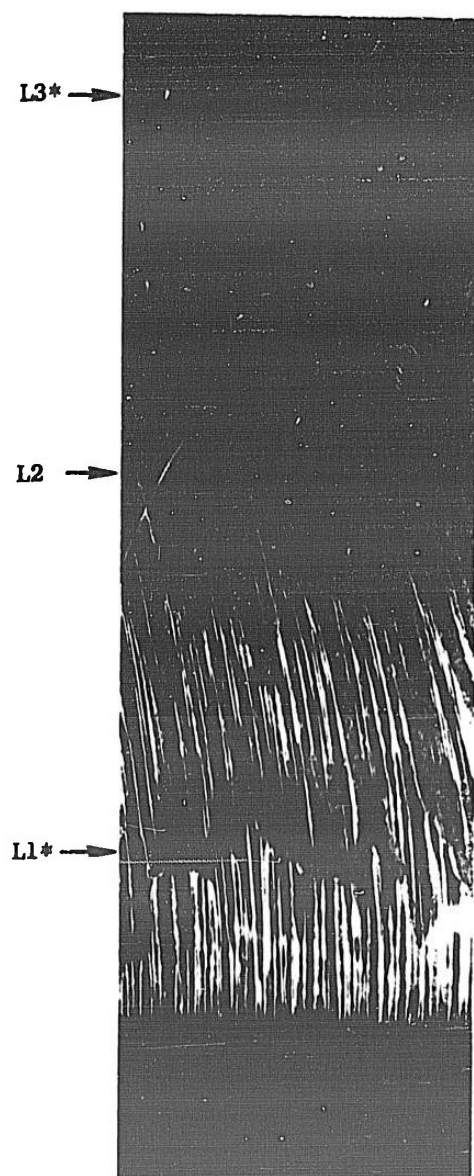
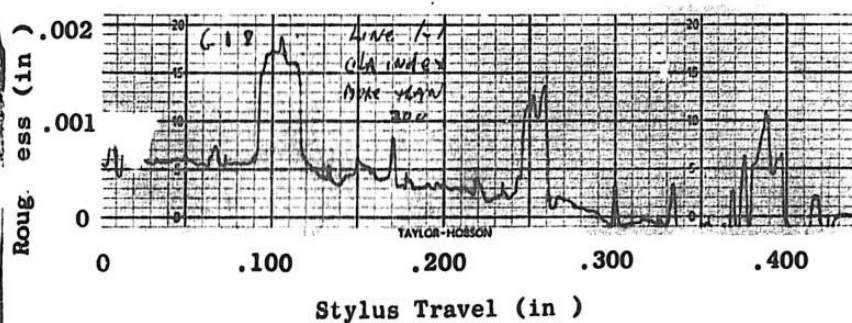
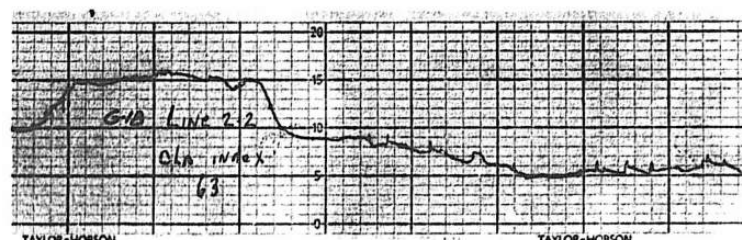
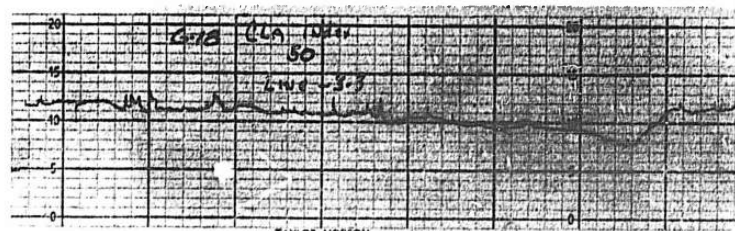


Figure 55. Segment of Specimen G-14 and "Talisurf" Recording

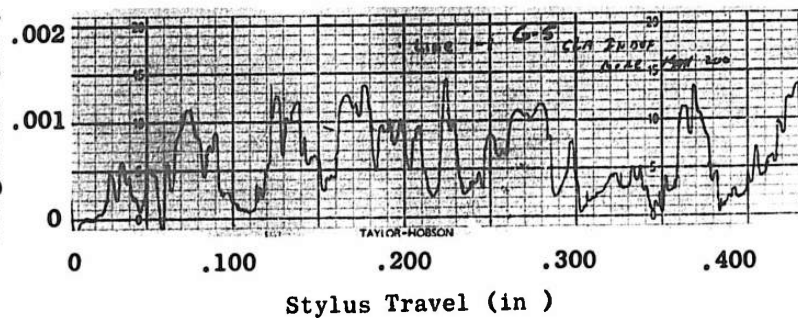
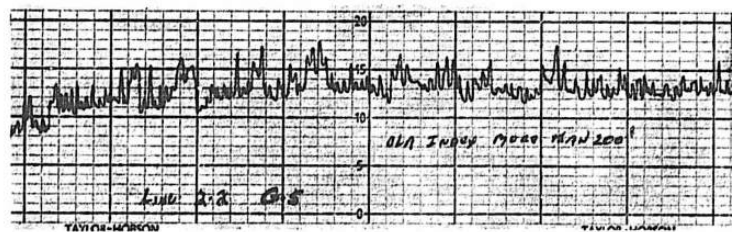
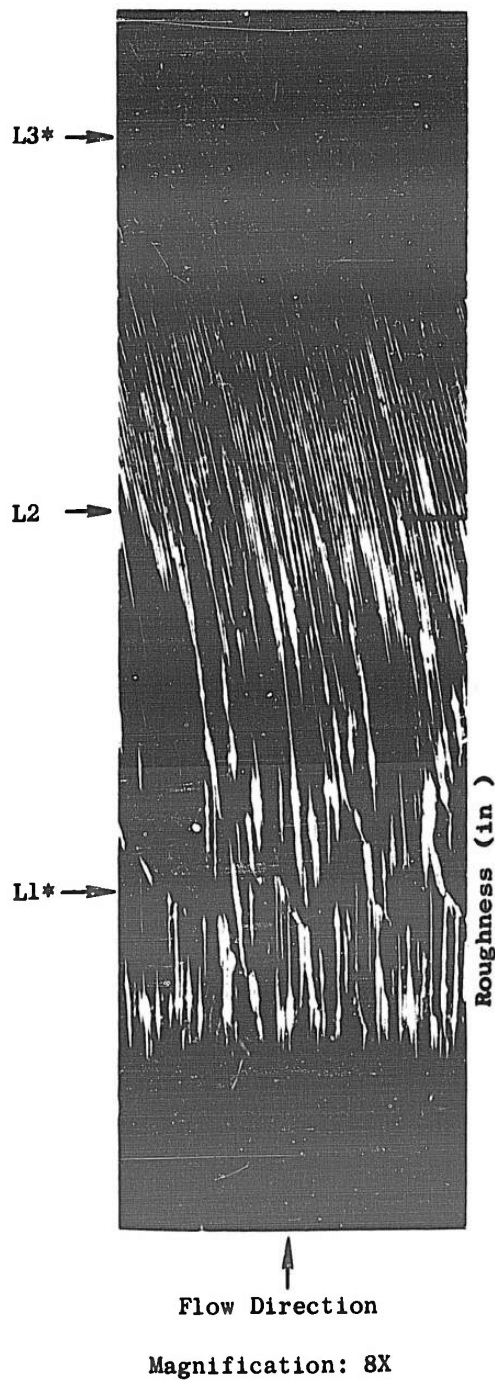


Magnification: 8X



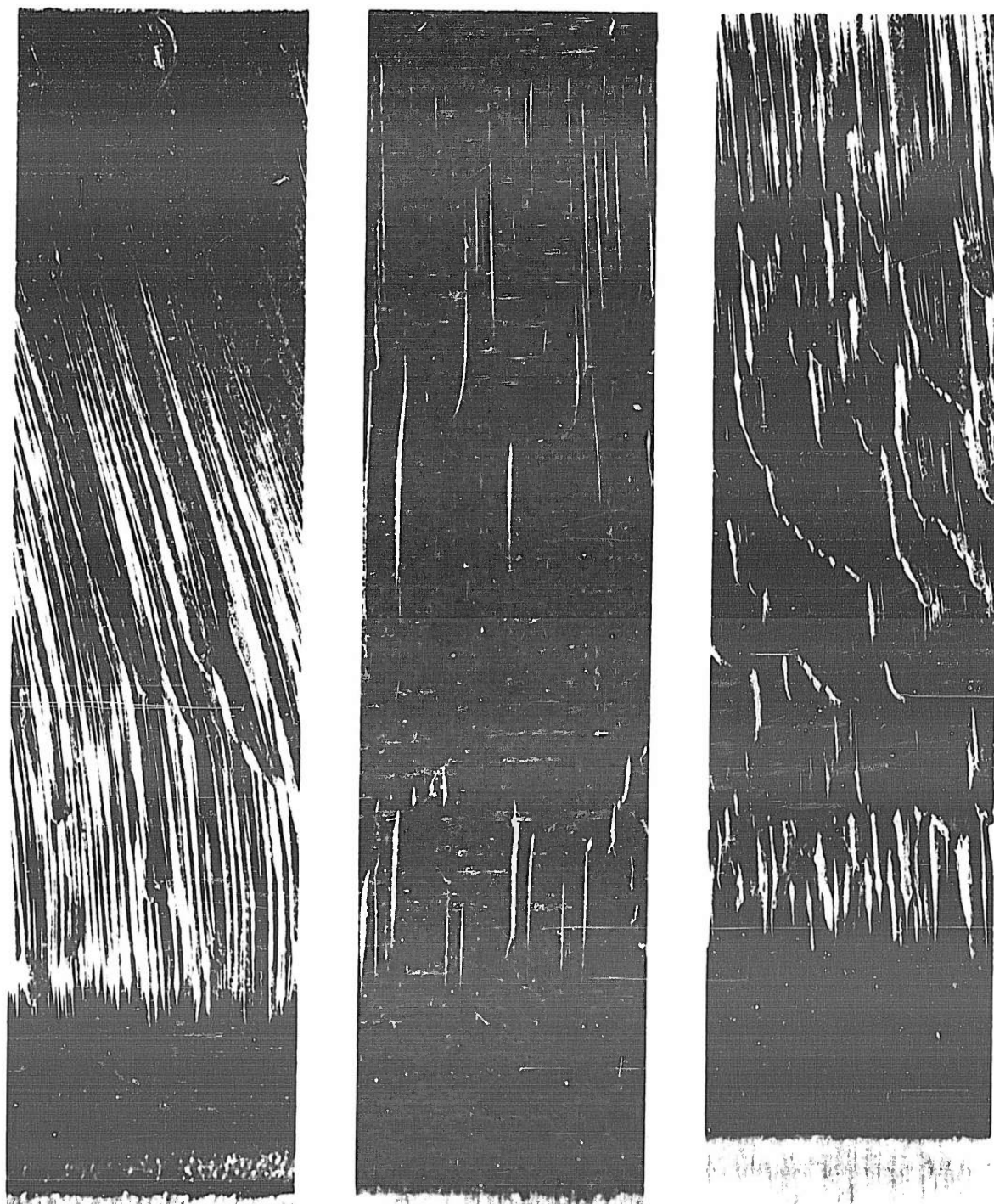
* Locations for Surface Roughness
Measurements: L1 = Flow Entrance
L3 = Flow Exit

Figure 56. Segment of Specimen G-18 and "Talisurf" Recording



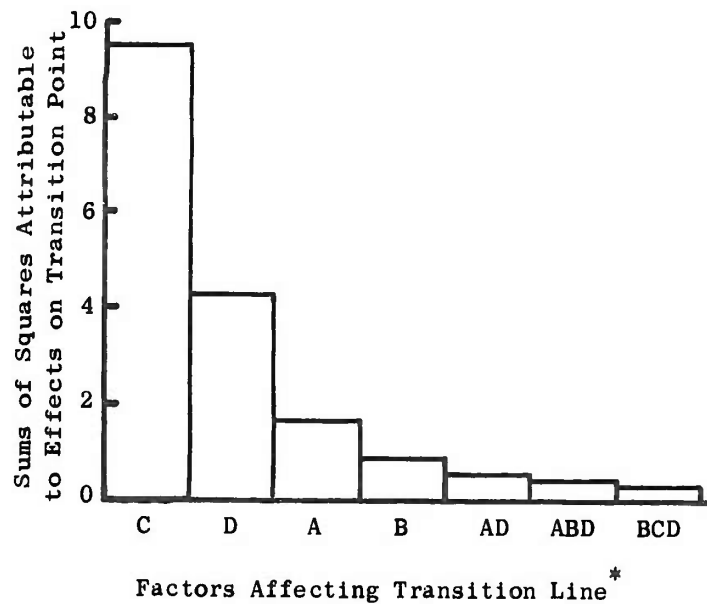
* Locations for Surface Roughness
Measurements: L1 = Flow Entrance
L3 = Flow Exit

Figure 57. Segment of Specimen G-5 and "Talisurf" Recording



Flow Direction
Magnification: 8X

Figure 58. Segments of Specimens G-2, 24 and 22



Material: René 41, mill annealed
Electrolyte: NaCl at 2.1 lb/gal

Factors		Test Levels
A - $\frac{\text{Feed Rate}}{\text{Mass Flow}}$	$\left(\frac{1}{\text{in}^2} \right)$	$3.8 \times 10^{-5} - 11.5 \times 10^{-5}$
B - $\frac{1}{\text{Mass Flow}}$	$\left(\frac{\text{min}}{\text{in}^3} \right)$	$9.6 \times 10^{-4} - 28.9 \times 10^{-4}$
C - Cutting Gap (in)		.007 - .018
D - Temperature ($^{\circ}\text{F}$)		84 - 105
[F - Feed rate (in /min)		.020 - .026 - .040 - .060 - .080]
[M - Mass flow (gpm)		1.5 - 3.0 - 4.5]
Average Pressure: 130 psig		
Applied Voltage: 4.9 - 20.8V		

* Transition Line - Dividing Line Between Flow Directional Lay and Smooth Surface Finish

Figure 59. Effect of Tested Factors on Surface Lay

The transition point in this test, therefore, moved toward zero and the surface finish improved with:

- (a) Decreasing gap.
- (b) Increasing temperature.
- (c) Increasing mass flow.
- (d) Decreasing feed.

7.2.2 Test Series JB-8

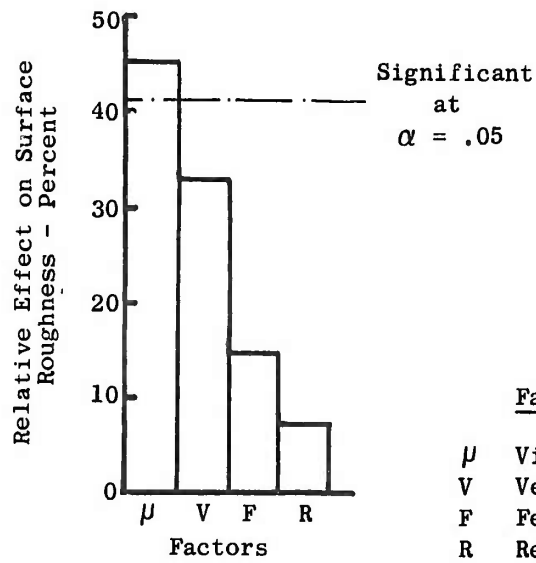
In these tests, we examined the effects of electrolyte velocity, viscosity, temperature, and feed rate on the surface roughness of A-286 alloy machined with 5 lb NaNO₃/gal.

We analyzed the data by regression analysis. See Figure 60. The analysis showed that the relative effects of the factors were different at two temperature levels (85° and 100°F), indicating that the temperature has a strong interacting effect. It also shows that at 85°F, only the viscosity had a significant effect; whereas, at 100°F, only the velocity had a significant effect.

7.2.3 Conclusions

From our tests, we concluded that when René 41 is machined with NaCl and A-286 is machined with NaNO₃:

- (a) Surface finish may be improved by changing any one of the operating parameters, as stated below, while holding the others constant:
 - (1) Increasing the electrolyte velocity.
 - (2) Increasing the electrolyte temperature.
 - (3) Decreasing the feed rate.
- (b) A prevailing surface finish may be maintained when operating parameters are varied and when a change of one of the operating parameters listed in (a) is accompanied by a compensating change of one or both of the other parameters. For example, the feed rate may be increased without adversely affecting surface finish if the electrolyte velocity or its temperature is increased.
- (c) Process malfunctions can be expected when the surface roughness exceeds a value of 200 microinches RMS.
- (d) A quantitative analysis of the relative effects of operating parameters on surface finish for a particular workpiece shape machined in a given tool may not be valid for a different workpiece shape or a different tool.
- (e) If the dissolution products (sludge) change the electrolyte viscosity they may adversely affect the resultant surface finish during electrolytic machining.
- (f) We did not find a functional relationship which consistently correlates the surface finish phenomena with externally controlled operating parameters.
- (g) Fractional experiments are not recommended for analyzing surface finish phenomena in electrolytic machining. Complete factorial designs can be useful.

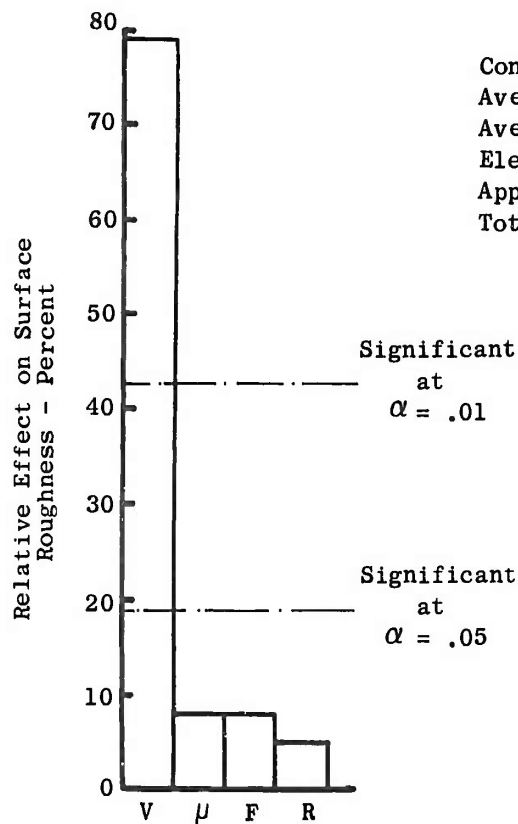


(a) At 85°F

Material: A286, mill annealed
Electrolyte: NaNO_3

Test Levels

Factors	Test Levels
μ Viscosity	1.41 to 1.95 Centipoises
V Velocity	4.96×10^4 to 16.56×10^4 in /min
F Feedrate	.020, -.040, .060 in /min
R Residual	Experimental error and all other factors



(b) At 100°F

Other Operating Parameters

Concentration: 5 lb/gal
Ave. Pressure Varied: 29 to 147 psig
Ave. Pressure Prop Varied: 56 to 294 psi
Electrolyte Flow Varied: 30 to 38 in³/min
Applied Voltage Varied: 6.1 to 24.1 volt
Total Current Varied: 5.2 to 16.4 amp

Figure 60. Factors Contributing to Variations of Surface Roughness, Test Series JB-8

Two-level experiments can be useful when the test region is limited—for extended test regions more levels should be used.

- (h) Multiple regression analysis is useful for selecting the best expression for explaining a response from a variety of potential causes. When interactions exist, note carefully the following procedures: include the interaction terms in the analysis, if possible; interpret the data only in the test region — extrapolation in our experiments proved to be erratic; improve precision and verify by testing the factors that were defined using multiple regression.
- (i) To control surface finish, we found that smooth surfaces without evidence of lay must first be achieved before the significant parameters affecting surface finish can be optimized. The testing to optimize must be performed for each electrolytic machining condition. The statistical methods for optimizing are covered in the literature⁽⁶⁾ as "Response Surface Methods".

7.3 Subsurface Defects

Surface defects of microscopic size are described as subsurface defects. Of particular interest in electrolytic machining are the defects caused by selective attack of alloy constituents in multiconstituent alloys.

In Section 3, Chapter III, we described the mechanism which contributes to selective attack; we concluded from past experiments that:

- (a) Selective etch occurs at low current densities (below 40 amp/in²) for René 41 cut with 2 lb NaCl/gal electrolyte.
- (b) Selective attack is localized around precipitates in the alloy.
- (c) Selective attack occurs as intergranular attack on precipitation-hardening, nickel-base alloys when the alloys are electrolytically machined in the age-hardened condition; that is, when the precipitates are concentrated in the grain boundaries.

These conclusions were substantiated in the case where the age-hardened nickel-base alloy M-252 was subjected to low current density. Severe attack occurred as reported in Section 1, Chapter IV. See Figure 61(a).

In our JB-4 test series of 106 specimens, we microscopically inspected the surfaces for subsurface defects. See Appendix II.5. These specimens were cut at various fluid pressures, gaps, feed rates and fluid velocities, and at current densities above 40 amp/in². No subsurface defects of over .0002" were reported for any of those specimens. There was evidence of superficial selective etch when precipitates were close to the surface. This is shown in Figure 61(b).

8. PROCESS CONTROL AND REGULATION

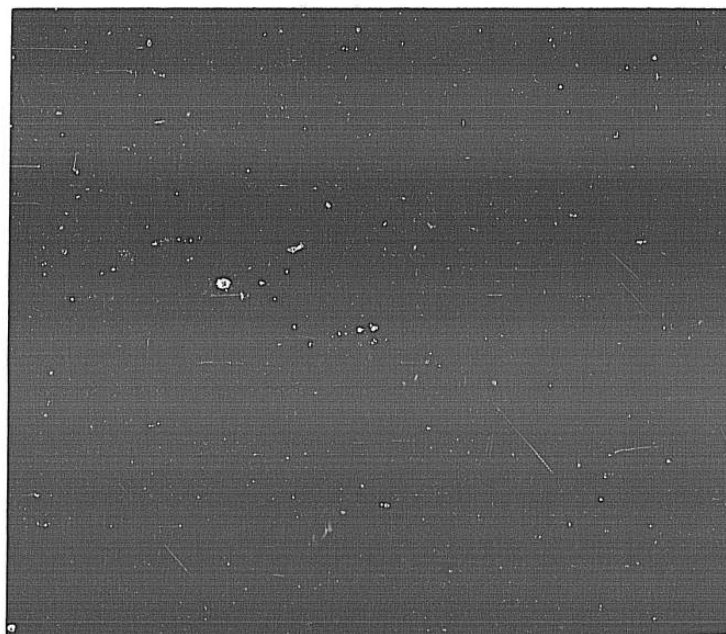
We have stated that production performance in electrolytic machining is measured by metal removal rate, surface finish characteristics, and dimensional repeatability.

When operating parameters have been selected for desired metal removal rates within stable operating limits, dimensional repeatability of consecutive like workpieces is achieved when the cutting gap size is repeated consistently, and when the machining cycle terminates at the same relative position to those datum points from which work surfaces are dimensionally defined.

(6): See References



(a) Cross Section of Exemplary Part #3
Material: M252, Age Hardened
Magnification 500X



(b) Cross Section of JB-4 Specimen #61
Material: Rene'41, Solution Treated
Magnification: 800X

Figure 61. Subsurface Defects

If the workpiece, or the electrode, or both, are held in a fixed position during the machining operation, the degree to which that position remains fixed, or the consistency of deflection if it occurs, are determining factors for the dimensional repeatability.

If the position of the workpiece, or the electrode, or both, are changed during the machining operation by feed mechanisms, the consistency with which the position change is repeated and terminated also is a determining factor for dimensional repeatability.

These factors are considered in the design of the electrolytic machining fixtures, machine structures, and feed mechanisms.

The third contributing factor to dimensional repeatability is the consistency in reproducing the cutting gap.

It was shown in Section 3, Chapter III, that the cutting gap at each point of the surface depends upon the operating variables in the expression:

$$L_{i1} = \frac{E - \Delta E}{\rho F i \beta i} K \quad (8)$$

The cutting gap, therefore, is uniformly reproduced when these factors, or the variables which significantly affect them, are consistently repeated. This is accomplished by process control or by sensing and correcting.

8.1 Process Control

In Section 3, Chapter III, we discussed the mathematical relationships valid for stable operating regions; and in Section 7, Chapter III, we showed that process stability depends upon electrolyte velocity, electrolyte temperature, feed rate, and cutting gap for the material/electrolyte systems investigated.

In Section 5, Chapter III, we emphasized that electrolyte concentration, electrolyte temperature, and where applicable, sludge content and electrolyte age affect the factors which determine the size of the cutting gap.

Process regulation is accomplished by imposing predetermined tolerance limits on the following externally controlled operation parameters:

- (a) Electrode potential.
- (b) Feed rate.
- (c) Electrolyte concentration, temperature, sludge content, and electrolyte age.
- (d) Inlet pressure.
- (e) Outlet pressure.

Not only does the cutting gap depend on the external conditions, but it depends on the current flow and the rate of chemical reactions in the cutting gap. In order to achieve process control and consistent cutting gaps, regulating external conditions must be supplemented by selecting process operating ranges which permit current flow and chemical reactions to stabilize so that the electrolyte temperature in the cutting gap remains constant during the machining cycle.

8.1.1 Adaptive Control

The cutting gap also could be reproduced if it were possible to measure its size at representative points during the machining operation, and if any one or more of the variables in Equation (8) were used to correct gap changes while the others are held within predetermined tolerance limits. While we do not know of any method by which the cutting gap can be measured directly during electrolytic machining, indirect measures of the average gap have been used for sensing and correcting.

In many cases, the electrolyte is confined to the cutting gap, and its flow rate under constant external conditions is an indirect measure of the average size of the cutting gap.

When current flow is confined to the cutting area, it also is an indirect measure of the average size of the cutting gap if external conditions are held constant. We investigated this electrolytic machining characteristic further in our program.

The currents were easily measured by shunts in the supply conduits, and the current flow was controlled within predetermined limits by adjusting the electrode feed rate.

8.2 Feed Servo Investigation

In our work we used the gap current as a signal to control the machine feed, and varied the feed to keep the gap current at a uniform level. We used a DC motor to actuate the feed mechanism, and we constructed an electronic circuit to translate the current signal into changes of the feed motor armature voltage. We also incorporated a current limiting relay into the circuit which disengages the servo mechanism upon erratic changes of the gap current.

Figures 62(a) and 62(b) compare the gap current under constant and regulated electrode feed. With the servo method, the gap current was held constant within 1.4% of the average current by regulating the electrode feed.

The cutting gaps were also manually changed to illustrate the capabilities of the system response to gap changes for controlled versus regulated feed. Figure 63.

Figure 64. shows the response of the current limiting relay, which was disengaged for the tests shown in Figure 63.

These tests demonstrated:

- (a) The regulating system can adjust the gap current to predetermined levels.
- (b) The current limiting relay can be used as a safety device to detect erratic current fluctuations which occur as a result of localized stoppage of metal removal or electrical shorts.

This servo principle may be applied to cutting currents, programmed to follow any path as for the generations of surfaces whose areas change during electrolytic machining, or for the purpose of deliberate feed rate changes.

A description of test and electronic circuit is included in Appendix II. 9.

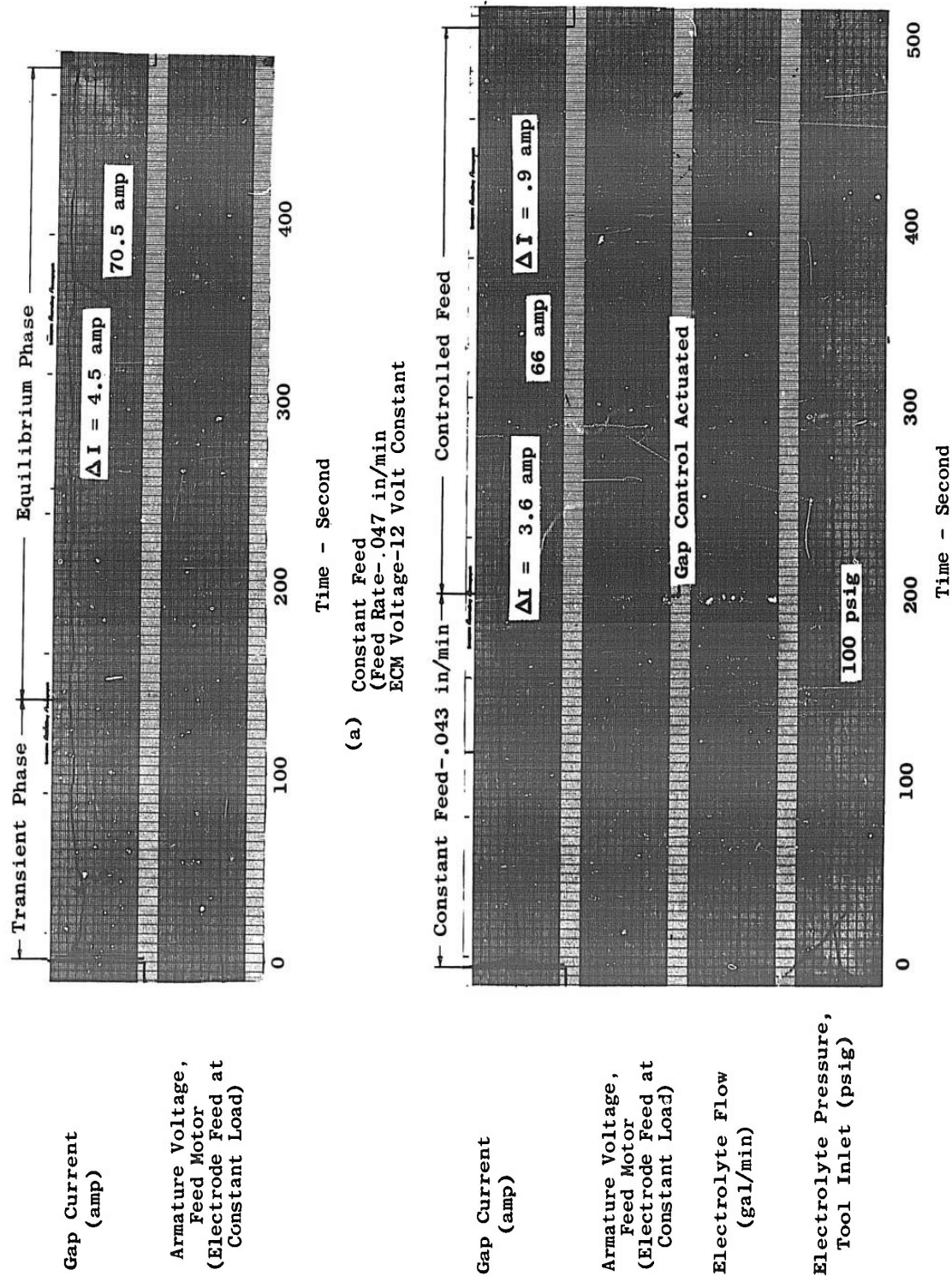


Figure 62. Comparison of Gap Current, Constant vs Regulated Electrode Feed

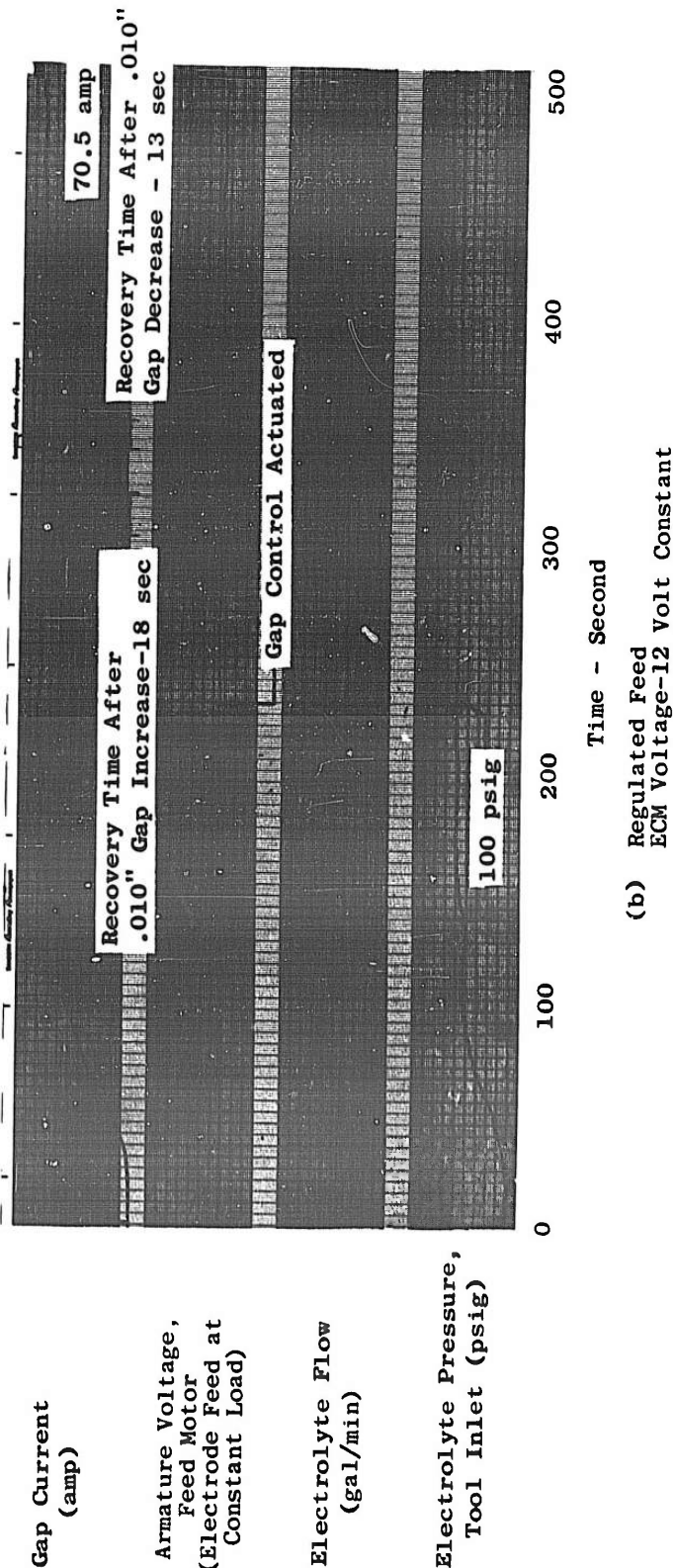
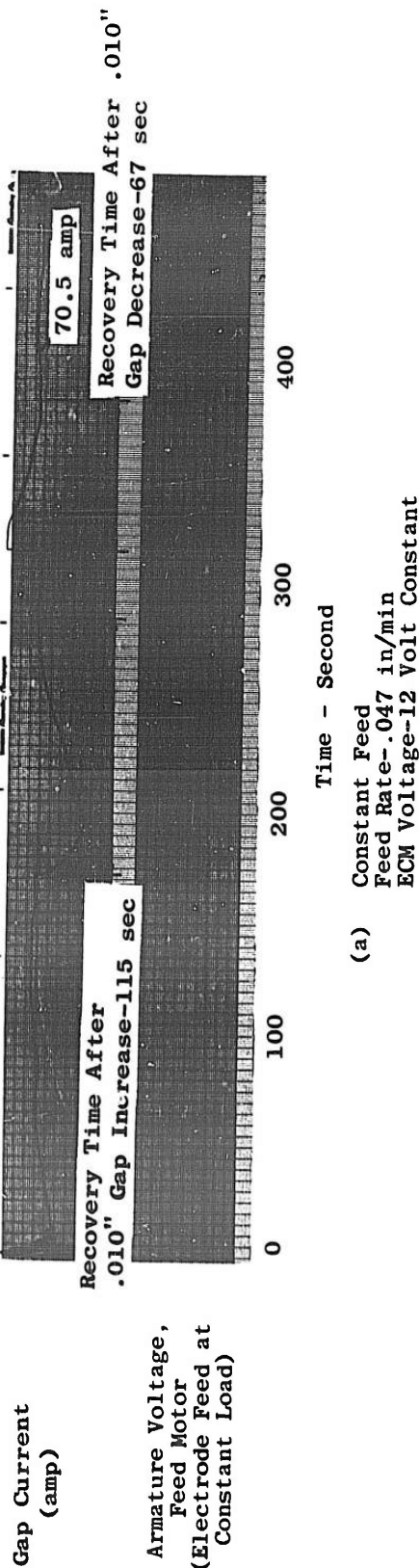


Figure 63. Comparison of Recovery Times After Cutting Gap Change, Constant vs Regulated Electrode Feed

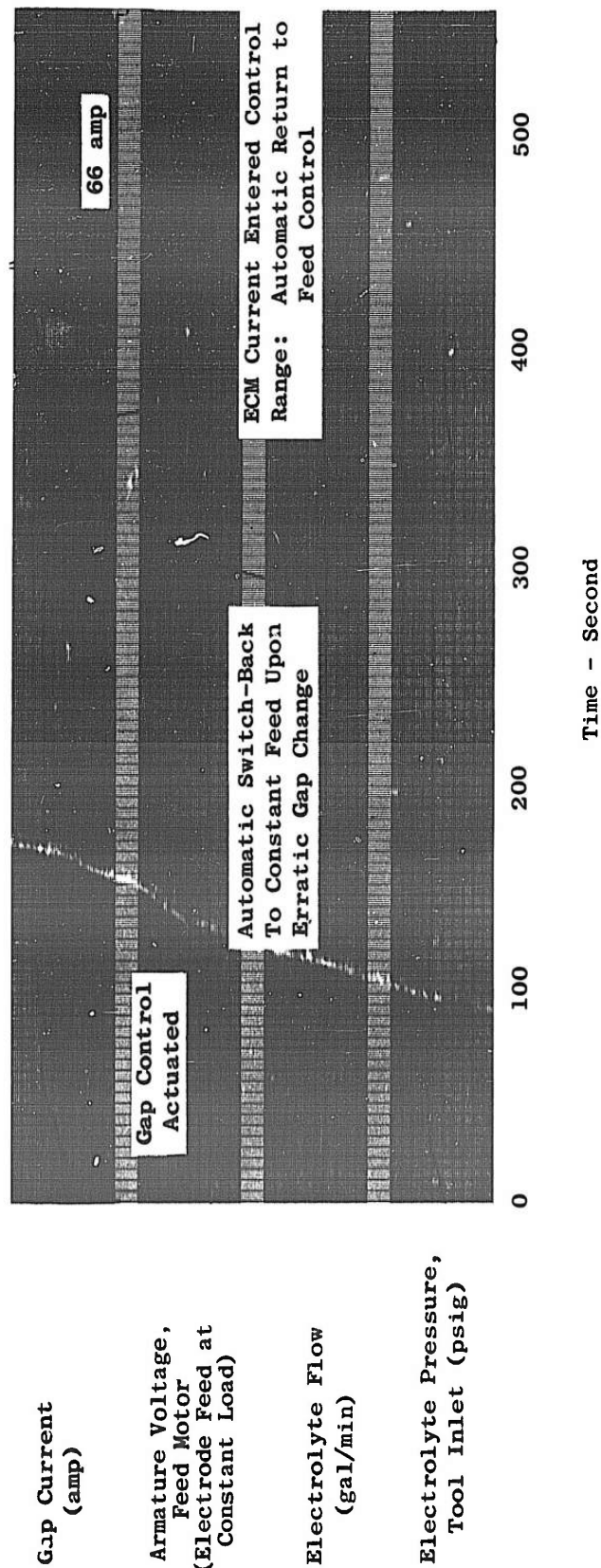


Figure 64. Response of Automatic Control to Erratic Process Changes (ECM Voltage - 12 Volt Constant)

9. ELECTRODE MATERIAL EVALUATION

We found that the performance of the electrolytic machining process generally is independent of hardness and other physical properties of the anode and the cathode materials.

We therefore confined our electrode material evaluation to those characteristics which determine the manufacturing and maintenance cost of electrode tools, and to the process functional properties, such as conductivity, corrosion resistance, and abrasion resistance.

We tested the spark resistance of the materials even though spark damage normally is not a problem in electrolytic machining. Such damage, however, can occur when the process malfunctions, and the material which exhibits the least damage from arcing requires the least work to repair.

We compiled information on the conductivity, corrosion resistance, machinability, and cost for fourteen candidate electrode materials. Moreover, we tested these materials to determine their resistance to abrasion.

A summary of the test results for these materials, together with the compiled information, is shown in Tables 9 and 10.

A description of the test procedure and the data for the abrasion and spark resistance studies are included in Appendix II. 7.

TABLE 9
LIST OF ELECTRODE MATERIALS

Matl No.	Description	ASTM or Specification No.
1	Electrical Tough Pitch Copper	ASTM B152
2	Free-Cutting Copper (1/2% Te)	ASTM B301
4	Aluminum Silicon Bronze	ASTM B21 Alloy A
5	Naval Brass	ASTM B21 Alloy C
7	Commercial Bronze	ASTM B134 Alloy 2
9	Titanium (99% pure)	ASTM B265, 58T, Grade 4
10	316 Stainless Steel	-
11	Elkonite 30W3 ⁽¹⁾	-
12	Gentrode ⁽²⁾	-
13	Manganese Copper	ASTM B136 Alloy A
14	Free-Cutting Copper (1% Pb)	-
15	Cartridge Brass	ASTM B19
16	Cupro-Nickel (10%)	MIL-L-15726A
17	Free-Cutting Brass	ASTM B16

(1) Mallory Metallurgical Co.

(2) General Electric Co.

TABLE 10
ELECTRODE MATERIAL EVALUATION

Mat'l (8) No.	Cost (2) \$/in ³	Conduc- tivity (3) % IACS	Corrosion Resistance .001"/Yr	Spark Resistance @15.3 Volt Gentrode Anode	(1) Spark Resistance @24.2 Volt M252 Anode	Machinability Index Free Cutting Brass = 100	Abrasion (9) Resistance Index
1	0.37	101	1.6 (4)	0	4	20	5
2	0.35	90	N.D. (7)	2	4	80	4
4	0.33	8	1.9 (4)	2	4	60	2
5	0.34	26	1.7 (4)	3	4	70	4
7	0.55	44	1.8 (4)	3	-	20	1
9	0.94	1	Nil	1	5	20	3
10	0.12	2.5	Ave 0.0 (5)	1	3	20	1
11	14.60	28	N.D. (7)	2	3	-- (6)	2
12	1.40	14	N.D. (7)	2	4	-- (6)	No Test - Very Poor
13	0.35	24	2.0 (4)	4	-	30	2
14	0.35	80	N.D. (7)	3	-	98	5
15	0.33	28	2.1 (4)	3	4	30	3
16	----	9	0.5 (4)	2	4	20	2
17	0.34	26	N.D. (7)	3	4	100	3

(1) Code for Spark Resistance: 0 = no damage, 1 = very slight tip damage, 2 = slight tip damage, 3 = moderate tip damage, 4 = extensive tip damage, 5 = severe tip damage.

(2) Based on quotations to General Electric - Evendale.

(3) Reported in Metals Handbook, Volume I, Eighth Edition.

(4) Reported in Metals Handbook, Volume I, Eighth Edition on page 986, Table 3 (Test A). Exposed to sea water at Kare Beach, North Carolina.

(5) Reported in Metals Handbook, Volume I, Eighth Edition on page 559, Table 4. Exposed to sea water at Kare Beach, North Carolina. One pit only in 944 days of exposure.

(6) Tends to chip. Must be machined with care.

(7) N.D. - No data available.

(8) See Table 6.

(9) Code for Abrasion Resistance: 1 = excellent, 2 = good, 3 = fair, 4 = poor, 5 = very poor.

CHAPTER IV

EXEMPLARY PARTS

Ten exemplary parts were produced by four different electrolytic machining techniques to demonstrate some of the attributes and advantages of the electrolytic machining process over competitive metal removal and fabricating methods.

The machining techniques were demonstrated on three nickel-base alloys, two stainless-steel alloys, one titanium alloy, and on powdered metal tungsten. Three different electrolyte compositions of varying concentrations were used for these tests.

We demonstrated the following advantages of electrolytic machining:

- (a) Metal removal rates are generally independent of material composition and hardness.
- (b) Brittle and crack sensitive materials can be machined to thin cross-sections.
- (c) Electrolytic machining leaves no edge burrs.
- (d) The process can generate irregular holes which are difficult or impossible to achieve by competitive methods.
- (e) Complex shapes and contours can be generated with simple machine tool feed motions.
- (f) The cutting tools for electrolytic machining do not wear or erode.

1. TREPANNING — EXEMPLARY PARTS 1 THROUGH 3

1.1 Purpose

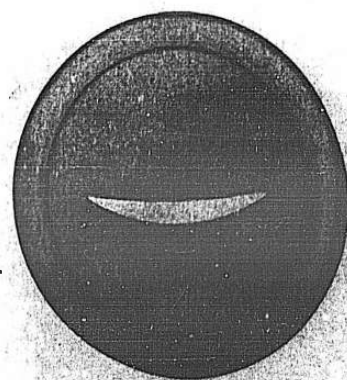
To demonstrate electrolytic trepanning as a machining method for thin shapes of uniform or tapered thicknesses.

1.2 Areas of Advancement

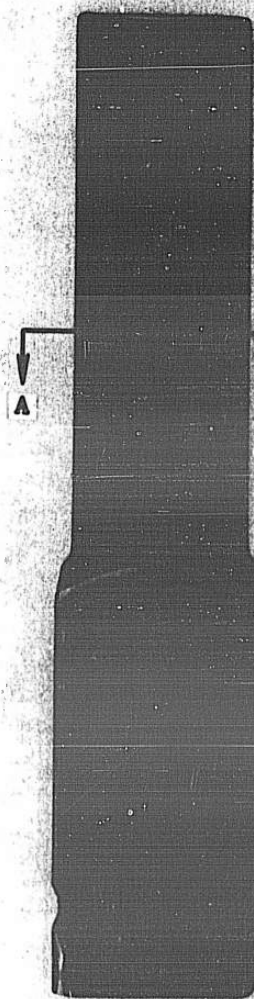
For given applications and materials, this method generates shapes of uniform thicknesses more advantageously than other processes. Compared to the extrusion processes, this method produces cross-sectional thicknesses within smaller dimensional tolerance on brittle materials.

1.3 Results

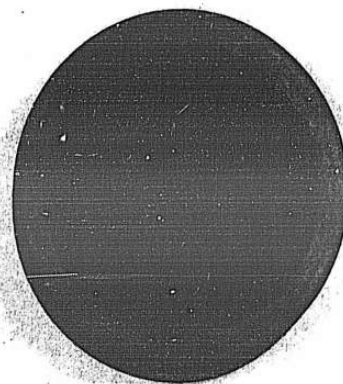
- (a) Shaped cross sections electrolytically machined along a 4" length from rectangular bars of 8-1-1 titanium alloy and M-252 nickel-base alloy, Figures 65. and 66.
- (b) Demonstrated a penetration rate (feed) of 0.200 in/min
- (c) The part dimensions are listed in Table 12
- (d) Surface finishes ranged from 120 to 280 microinches (AA) on the titanium alloy examples, and from 26 to 120 microinches (AA) on the nickel-base



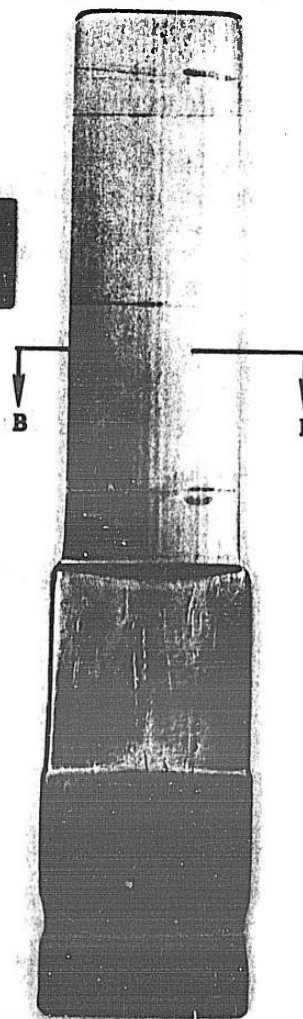
Sect A-A
(In Plastic Mount)



Exemplary Part 1
Mat'l: Titanium 8-1-1



Sect B-B
(In Plastic Mount)



Exemplary Part 3
Mat'l: M252

Figure 65. Exemplary Parts 1 and 3

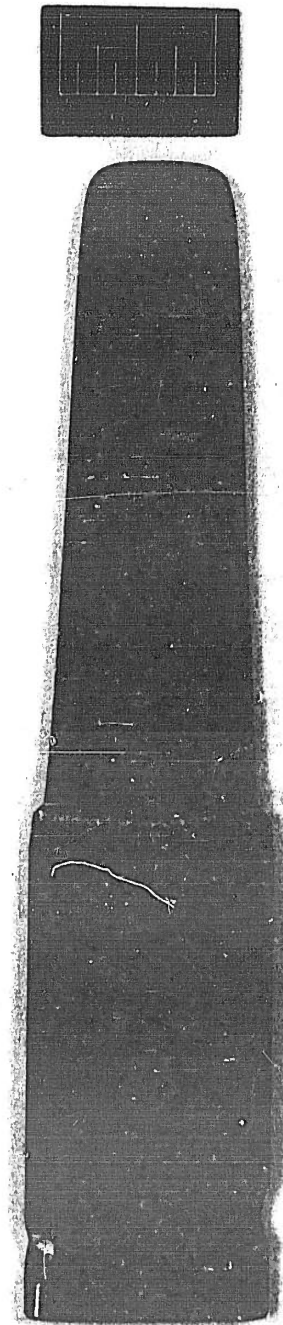
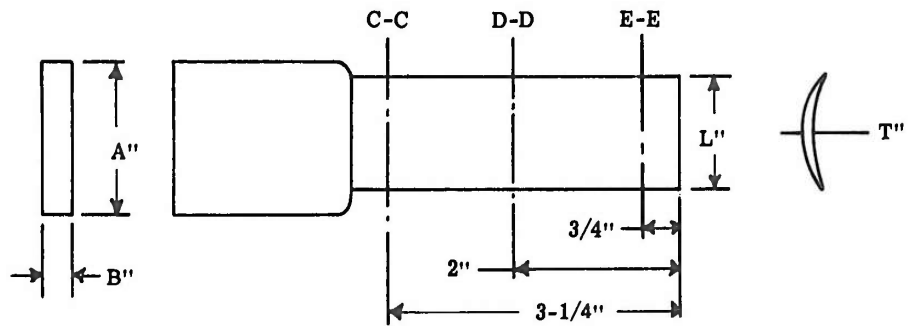


Figure 66. Exemplary Part 2
Mat'l: Titanium 8-1-1

TABLE 11
OPERATING PARAMETERS, EXEMPLARY PARTS 1 THROUGH 3

Operating Parameters	Exemplary Parts		
	1	2	3
	1 - 6	Ser. No. 7 & 8	M1 & M2
Electrolyte composition	NaCl	NaCl	NaCl
Electrolyte concentration (lb/gal)	0.8	0.8	2.05
Electrolyte temperature, tank (°F)	103	103	103
Feed rate (in/min)	.200	.200	.200
Applied voltage (volt)	20.0	20.0	20.0
Current, start (amp)	100	100	150
max (amp)	500	550	630
end (amp)	460	500	550
Electrolyte inlet pressure, start* (psig)	205	205	205
Electrolyte inlet pressure, end* (psig)	265	265	265
Electrolyte exit pressure, start* (psig)	50	50	50
Electrolyte exit pressure, end* (psig)	0	0	0
Ram stroke (in)	4.000	3.50 & 4.00	4.00 & 3.40
*The electrolyte pressures leveled off after initial 0.100" of travel at the values shown for end of stroke.			

TABLE 12
PART DIMENSIONS, EXEMPLARY PARTS 1 THROUGH 3



Exemplary Part	Ser. No.	Stock Dimensions		Finished Dimension L''			Finished Dimension T''		
		A''	B''	C-C	D-D	E-E	C-C	D-D	E-E
1 (Ti 8-1-1)	1	2-1/2"	1/4"	1.301	1.297	1.304	.143	.143	.143
	2			1.309	1.301	1.303	.142	.143	.143
	3			1.304	1.289	1.280	.143	.143	.143
	4			1.305	1.299	1.301	.143	.143	.144
	5			1.310	1.310	1.303	.143	.143	.141
	6			1.297	1.305	1.318	.143	.143	.143
2 (Ti 8-1-1)	7			1.257	1.125	1.020	.142	.132	.123
	8			1.265	1.126	1.013	.142	.133	.123
3 (M-252)	M1	2-1/2"	1/4"	1.253	1.247	1.248	.133	.136	.136
	M2			1.271	1.268	1.264	.133	.135	.135

alloy examples. See Table 13. The subsurface finish is shown in Figures 67. and 68.

1.4 Material Hardness

- (a) Exemplary Parts 1 and 2, (Titanium 8-1-1): 32-36 Rockwell C Scale
- (b) Exemplary Part 3 (M-252): 35-36 Rockwell C Scale

1.5 Tooling

The tooling is shown in Figures 69., 70. and 71. The workpiece (1) is fixed in the table mounted fixture base (2) and locator (3) with a low melting alloy matrix (4) of 58% Bi, 42% Sn. The matrix serves as a fixture, as an electrolyte seal, and as a current conductor. The electrode (5) is actuated by the vertical ram (6) of machine #1*. The electrolyte supply pressure is regulated at the pump; a hand-operated needle valve regulates the tool exit pressure.

As the ram mounted upper fixture assembly (7) advances toward the machine table (8), the machined workpiece is received by a plastic sleeve (9) and the electrode (5) and raw material guide (10) move toward the fixture base (2).

When the plastic sleeve (9) is removed and workpiece (1) is machined, the inside diameter of the upper fixture sleeve (7) serves as a secondary electrode which continues to machine the workpiece to a tapered shape along its length. This was demonstrated on Exemplary Part #2, see Figure 66.

1.6 Operating Parameters

See Table 11.

1.7 Comments

The shapes of Exemplary Parts 1 and 3 were generated by primary currents flowing between the workpiece and the electrode orifice. The roughness of the machined surfaces (Table 13 and Figures 67. and 68.) is believed to be the result of low density current.

The dimensional results shown in Table 12 indicate that the secondary currents participated in the shaping process only when the plastic sleeve (9) was removed.

In Exemplary Parts 1 and 3, films were observed on the machined surfaces. These films were wiped off after the parts had been removed from the fixture. We assumed that these films formed when the part entered the plastic sleeve and a zone of stagnant electrolyte. We further speculated that the dielectric properties of the films, rather than the shielding effect of the sleeve, prevented further metal removal after the shape had been generated in the electrode orifice (5).

2. BLANKING - EXEMPLARY PARTS 4 THROUGH 7

2.1 Purpose

To demonstrate electrolytic machining as a method for blanking sheet and foil materials; and embossing sheet, plate, and bar shapes by the use of stationary (fixed) electrodes.

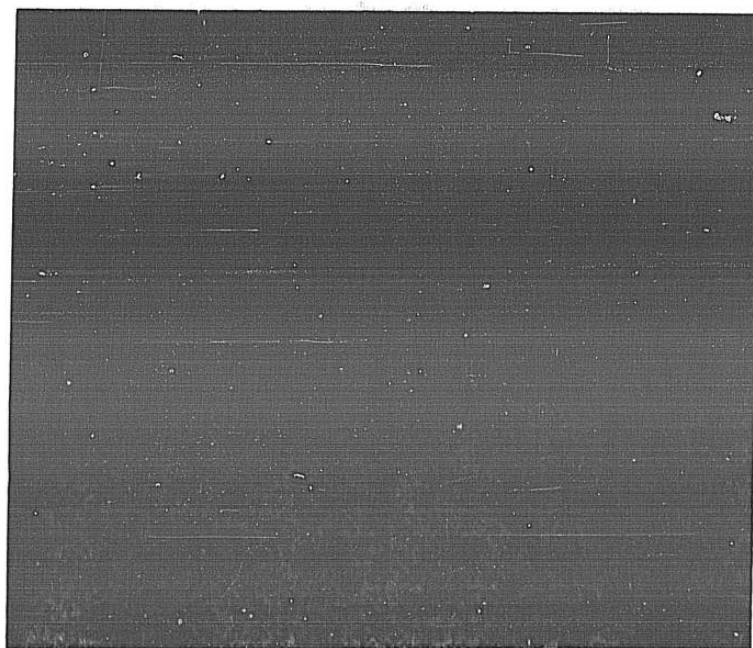
* See Appendix IV

TABLE 13
SURFACE FINISH MEASUREMENTS EXEMPLARY PARTS 1 THROUGH 3

Exemplary Part	Ser. No.	Location	Surface Roughness Micro-inches (AA)
1 (Ti 8-1-1)	4	Concave, tip section	220-280
		Concave, root section	220-240
		Concave, length	220-260
2 (Ti 8-1-1)	7	Concave, tip section	125-150
		Concave, root section	120-140
3 (M-252)	M1	Concave, tip section	60-100
		Concave, root section	35-75
	M2	Concave, tip section	100-120
		Concave, root section	26-32

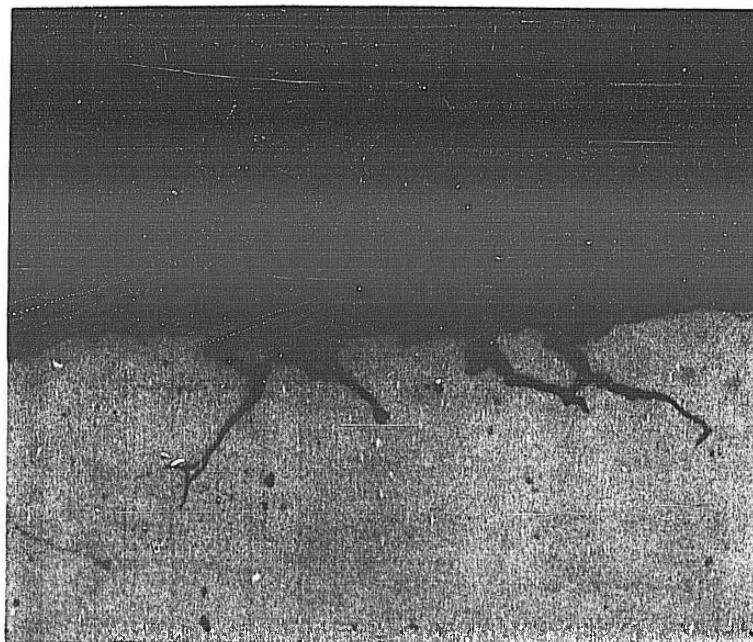


(a) Unetched; Magnification 250X

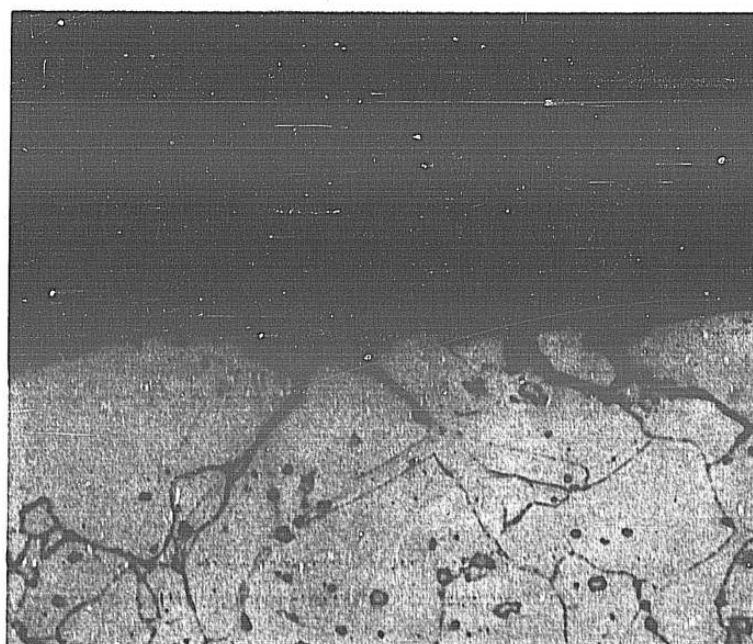


(b) Etchant HNO_3 and HCl ; Magnification 250X

Figure 67. Cross Section Through Exemplary Part 2



(a) Unetched: Magnification 500X



(b) Etchant; Schantz and HCl; Magnification 500X

Figure 68. Cross Section Through Exemplary Part 3 Intergranular Attack 0.002" Deep

1. Workpiece
2. Fixture Base
3. Locator
4. Matrix
5. Electrode
6. Machine Ram (Feed)
7. Upper Fixture Assy
8. Machine Table
9. Plastic Sleeve
10. Stock Guide
11. Lower Fixture Sleeve
12. Anode Bus

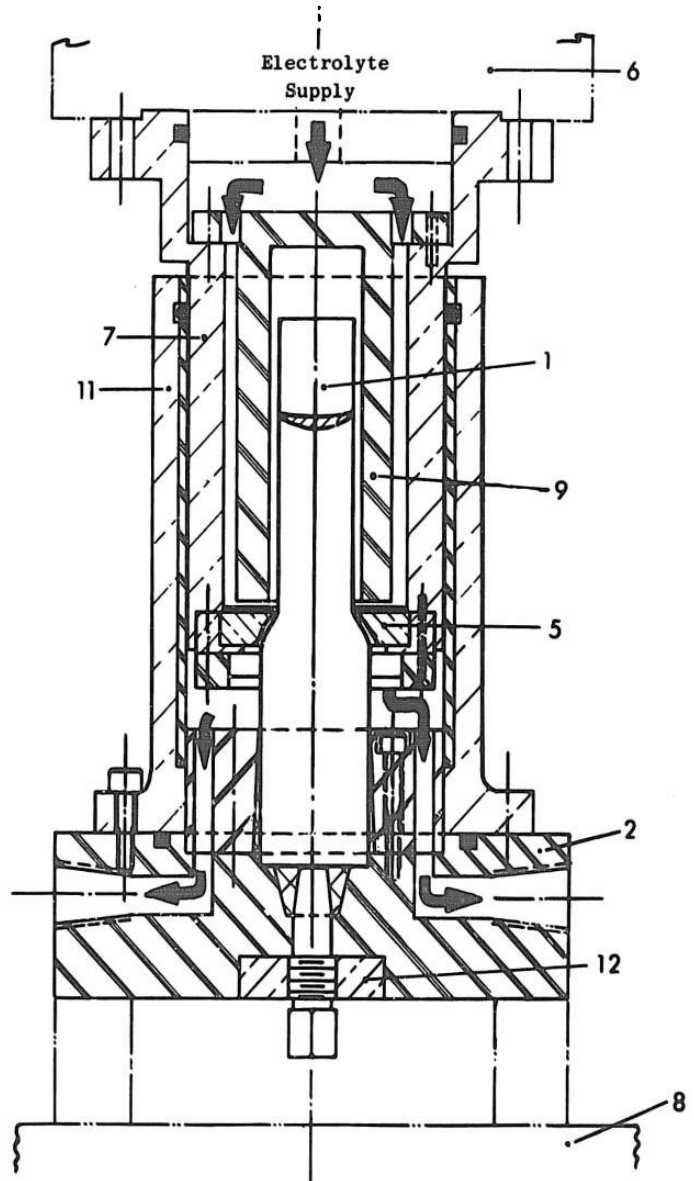
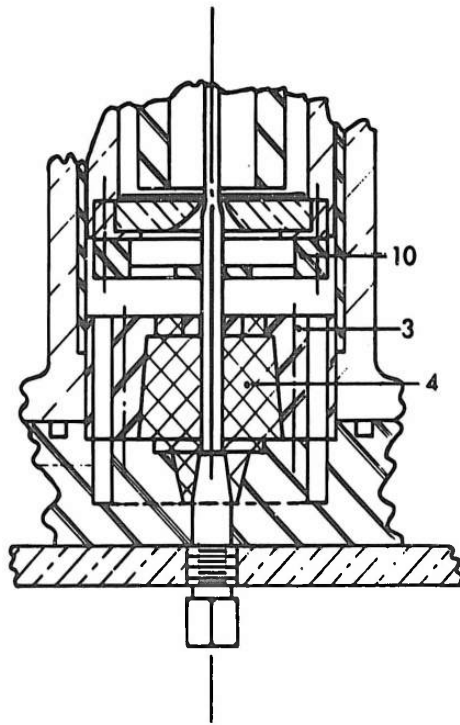
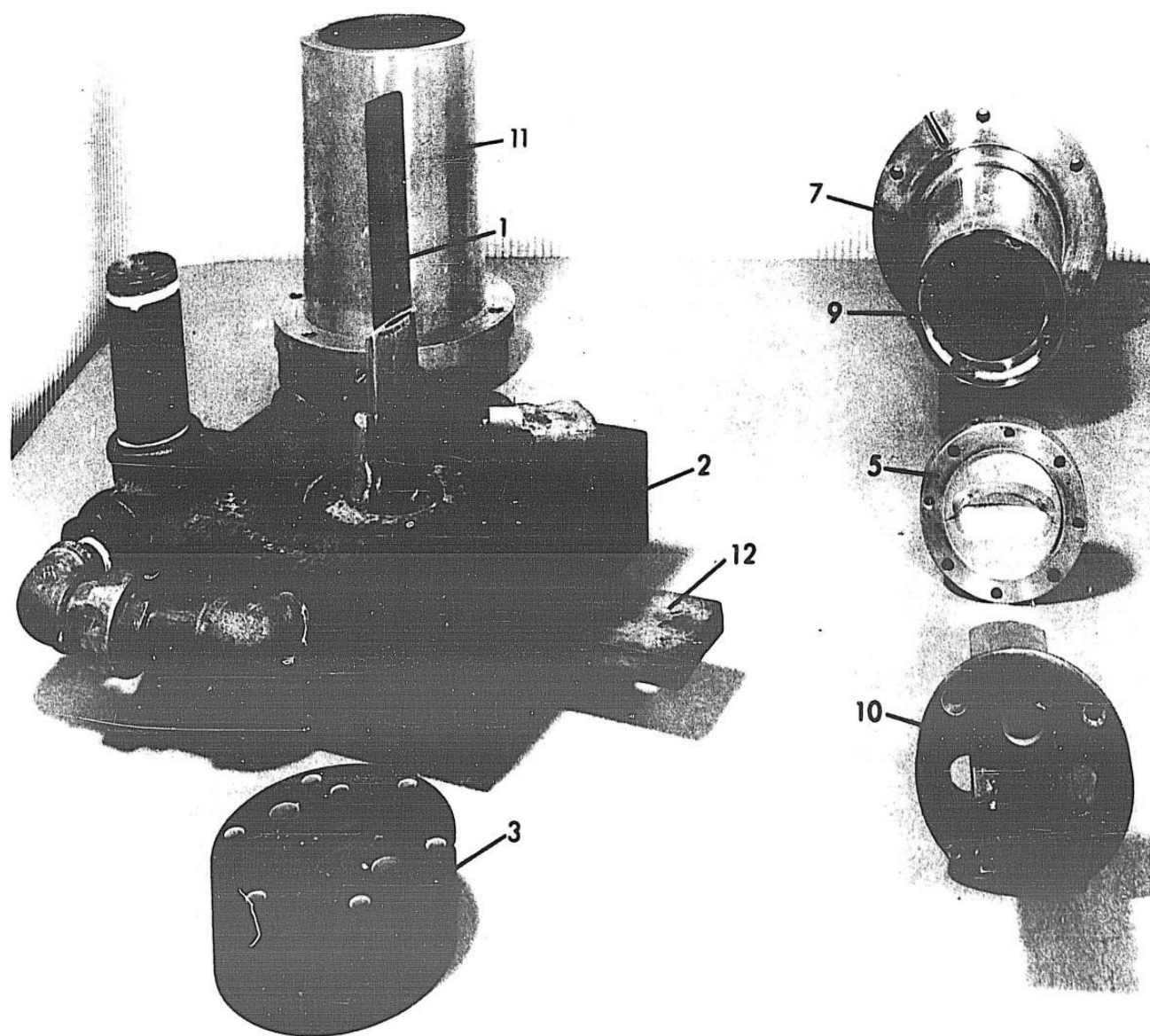


Figure 69. Schematic Sketch of Tooling for Exemplary Parts 1 through 3



- | | |
|-------------------------|--------------------------|
| 1. Workpiece | 9. Plastic Sleeve |
| 2. Fixture Base | 10. Stock Guide |
| 3. Locator | 11. Lower Fixture Sleeve |
| 5. Electrode | 12. Anode Bus |
| 7. Upper Fixture Sleeve | |

Figure 70. Tooling for Exemplary Parts 1 through 3

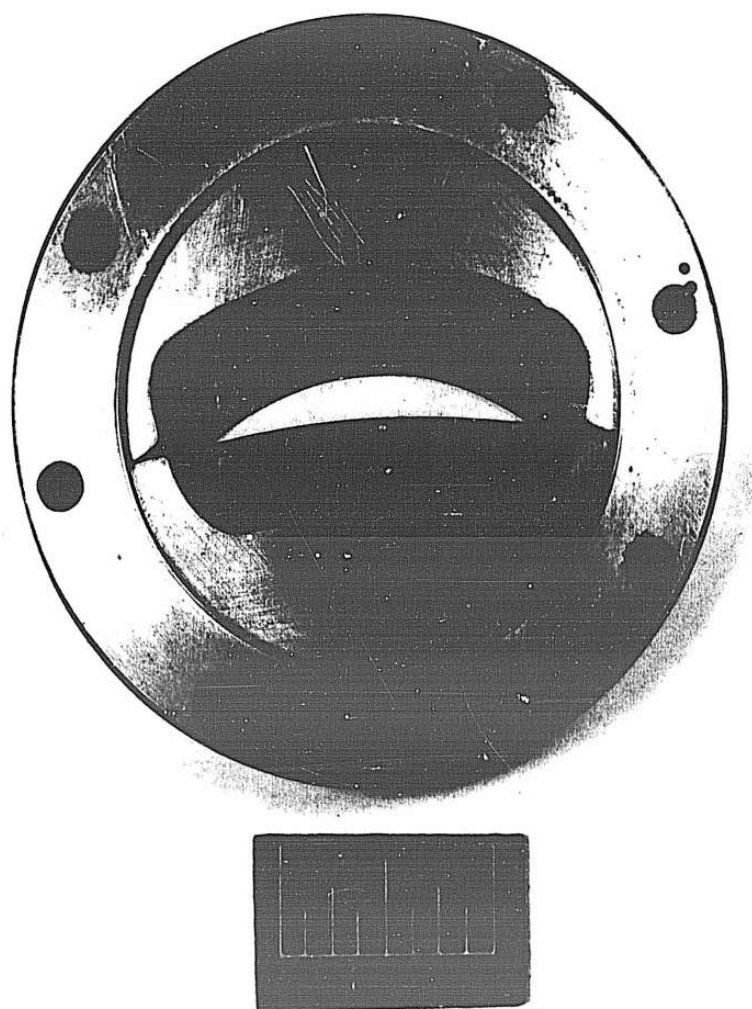


Figure 71. Electrode for Exemplary Parts 1 through 3

2.2 Areas of Advancement

For given applications and materials, this method accomplishes material removal more advantageously than other processes.

Compared to the punch press methods, the electrolytic blanking advantages are that it leaves no burrs, introduces no stresses into the workpiece, and requires no feed mechanism.

Compared to the chemical milling process, the advantages of the blanking and embossing methods are that simple chemical solutions are used and metal removal is achieved at faster rates.

2.3 Results

- (a) A pattern of three slots electrolytically generated in 0.030" Hastelloy X sheet material and in 0.008" tungsten foil. See Figure 72, Exemplary Parts 4 and 5.
- (b) A pattern of three grooves electrolytically embossed in René 41 nickel-base and in stainless steel plate materials. See Figure 73, Exemplary Parts 6 and 7.
- (c) The slot dimensions of Exemplary Part 4 are listed in Table 16. The depth dimensions of Exemplary Parts 6 and 7 are listed in Table 15.
- (d) The surface finishes of the embossed grooves range from 12 to 20 microinches (AA) on Exemplary Part 6 and from 2 to 6 microinches (AA) on Exemplary Part 7.

The subsurface finish of a machined edge Exemplary Part 4 is shown in Figure 74.

2.4 Material Hardness

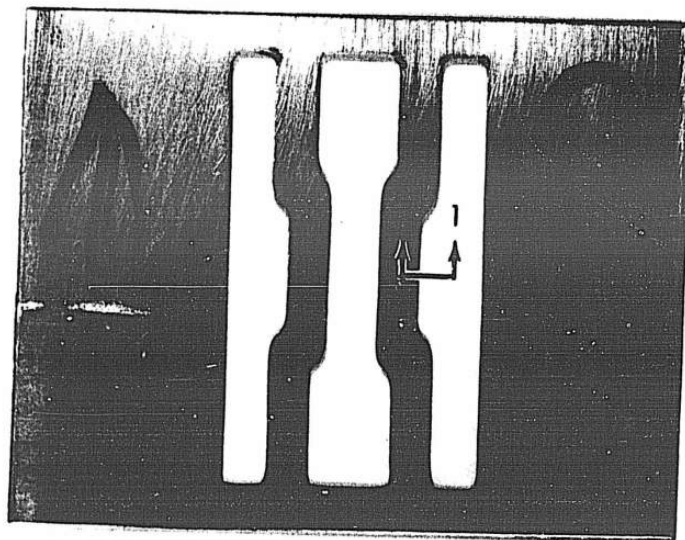
- (a) Exemplary Part 4 (Hastelloy X): 85-90 Rockwell B Scale.
- (b) Exemplary Part 5 (Commercially pure powdered metal tungsten): 41-42 Rockwell C Scale.
- (c) Exemplary Part 6 (René 41): 31-32 Rockwell C Scale.
- (d) Exemplary Part 7 (Carpenter Stainless #20): 34 Rockwell 30 N Scale.

2.5 Tooling

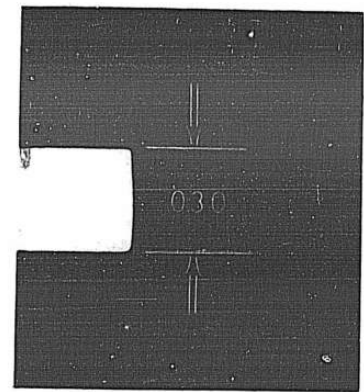
The tooling shown in Figures 75 and 76 consist of two electrodes (1) and (2) with their cutting surfaces recessed into plastic coated mounting surfaces. Guide pins (3) align the identical electrode cutting patterns in both electrodes.

The electrolyte is channeled through internal passages and slots across the cutting surfaces. The "O" ring seals (4) in the faces of the electrodes confine the electrolyte to the cutting area.

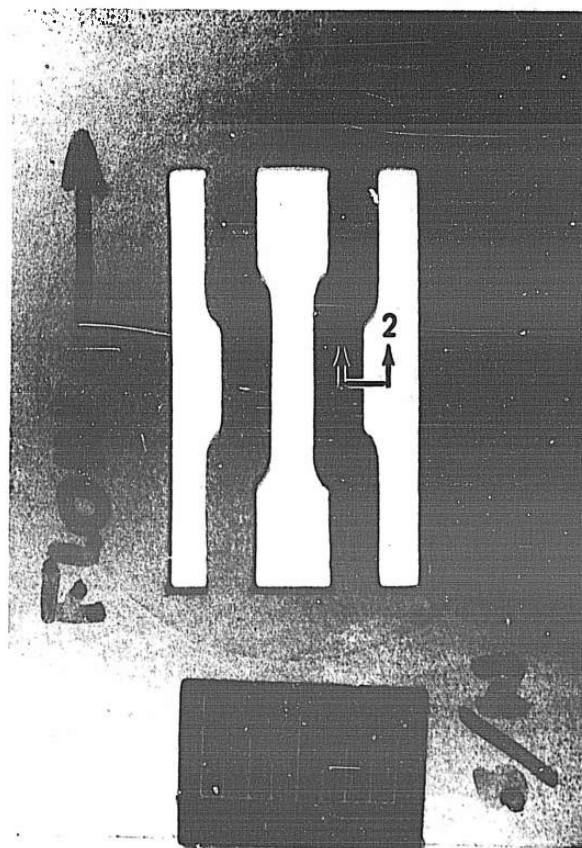
The cutting surfaces (6) are recessed into the electrode faces from 0.005" at the center to 0.008" at the electrolyte inlet and outlet ends.



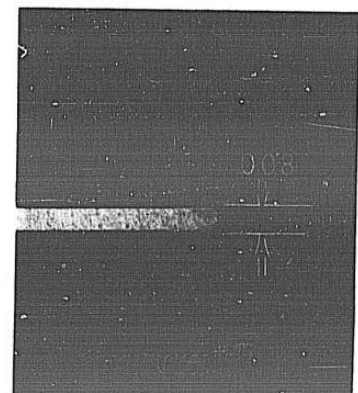
Exemplary Part 4, Hastelloy X



Section 1-1
16X

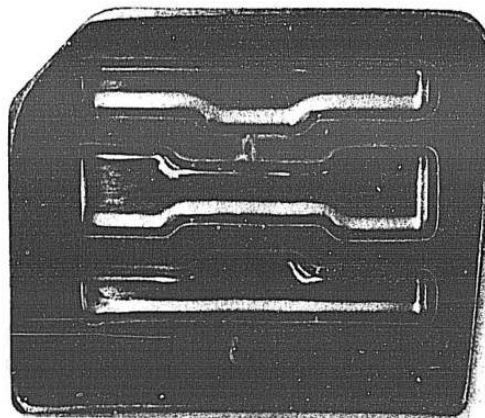


Exemplary Part 5, Powdered Metal Tungsten

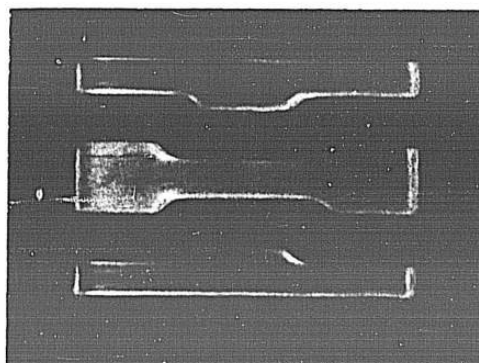
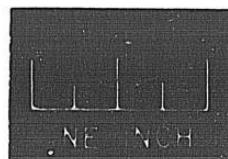


Section 2-2
16X

Figure 72. Exemplary Parts 4 and 5

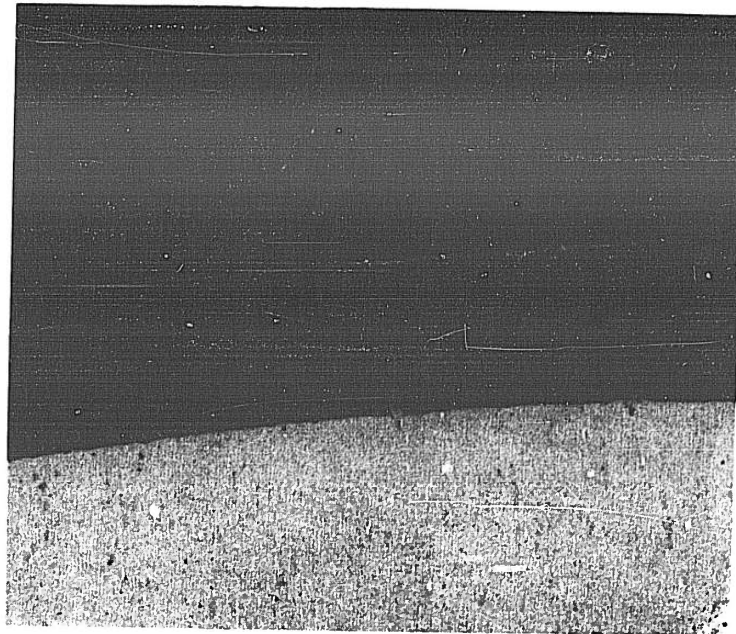


Exemplary Part 6 - Rene 41

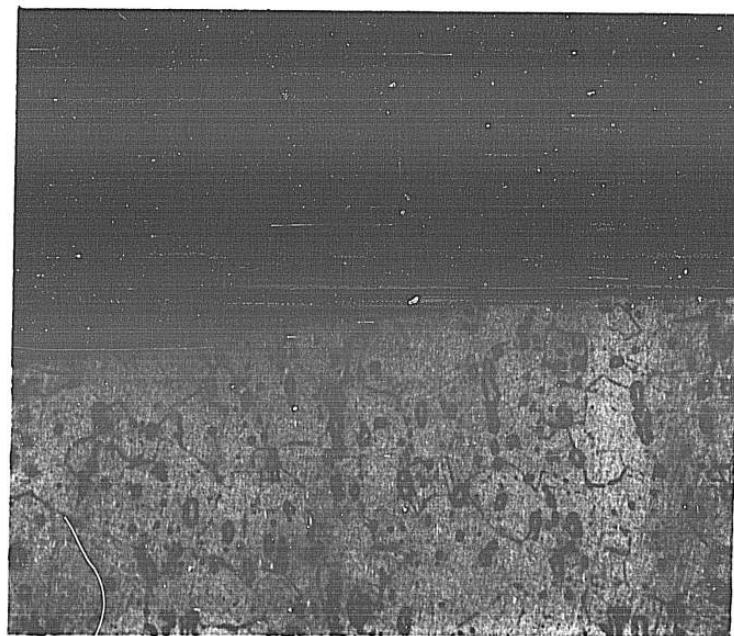


Exemplary Part 7 - Stainless Steel

Figure 73. Exemplary Parts 6 and 7

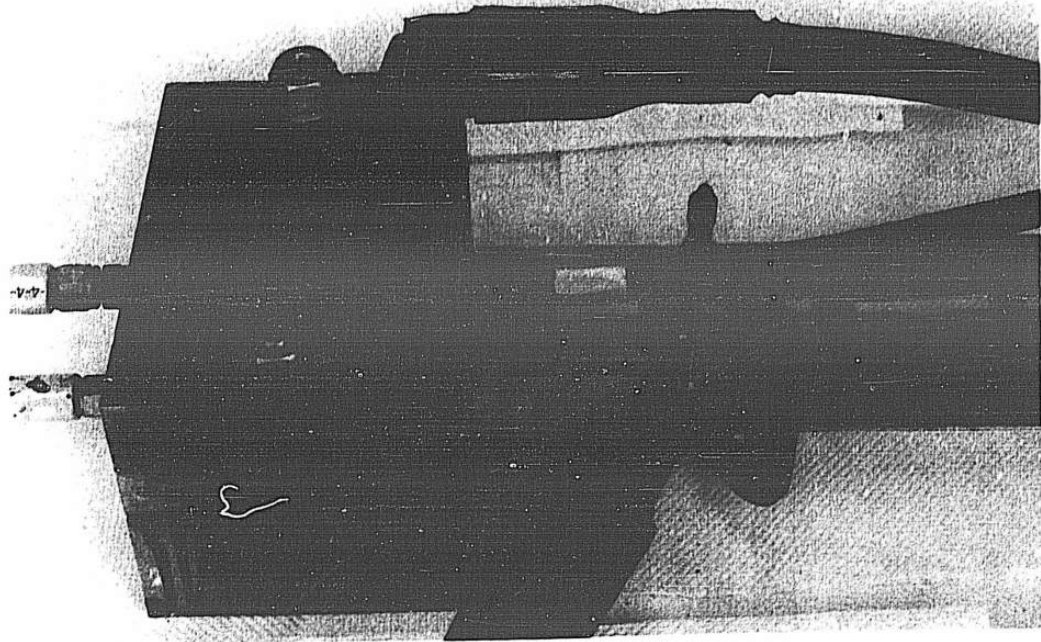


(a) No Etch; Magnification 250X

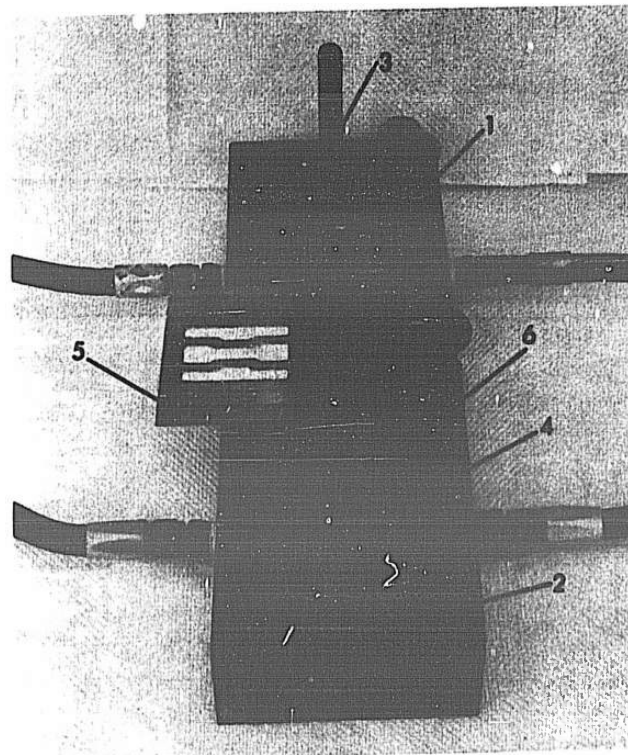


(b) Etchant; Schantz and HCl; Magnification 250X

Figure 74. Cross Section Through Machined Edge of Exemplary Part 4



(a) Tool Assembly



(b) Electrode Cutting Surfaces

- | | |
|------------------|--------------------|
| 1. Electrode | 4. O-Ring |
| 2. Electrode | 5. Workpiece |
| 3. Alignment Pin | 6. Cutting Surface |

Figure 75. Tooling for Exemplary Part 4-7

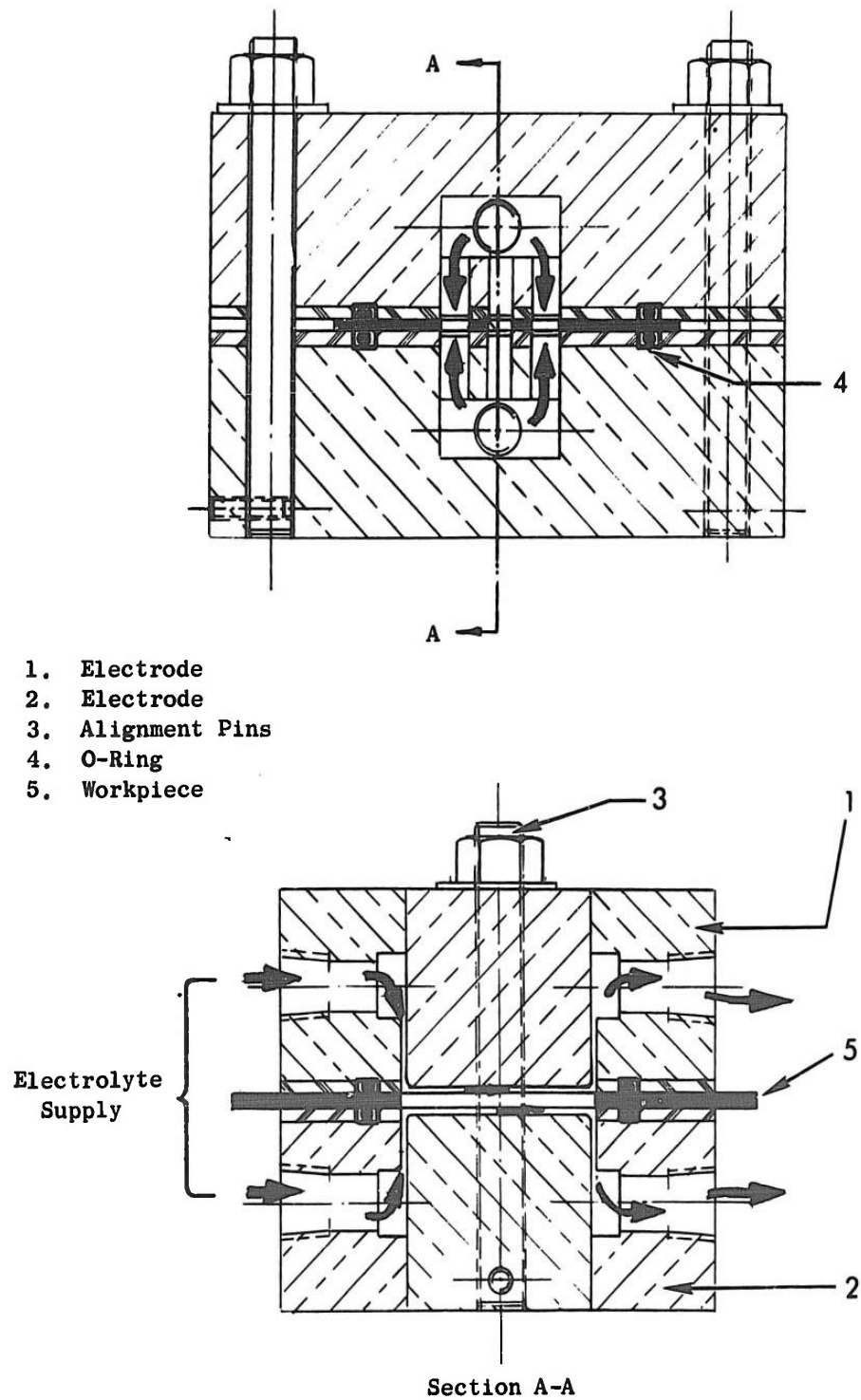


Figure 76. Schematic Sketch of Tooling for Exemplary Parts 4-7

When used as a blanking tool, the sheet or foil material (5) is clamped between the two electrodes, Figure 76. The cut-outs are generated by simultaneous metal removal from both sides of the workpiece surfaces.

When used as an embossing tool, only one electrode is clamped to the surface of the workpiece.

This tooling does not require an electrode feed mechanism.

2.6 Operating Parameters

See Tables 14 and 15.

2.7 Comments

- (a) We designed the tooling to generate cut-outs in sheet and foil materials by simultaneous metal removal from both sides of the workpiece thus generating square, burr-free edges. This was successfully accomplished when the electrode cutting edges were aligned and the cutting cycle was properly timed. See cross sectional view, Figure 72., Exemplary Parts 4 and 5. Where the electrode cutting surfaces were misaligned, burr-like edges resulted. See cross sectional view, Figure 77(a), Exemplary Part 5. Similar edge conditions result if the current is allowed to dwell for an excessive time period after the cut-out is completed. See cross sectional view, Figure 77(b), Exemplary Part 5.
- (b) When the applied voltage is held constant, the cutting current decreases, Tables 14 and 15, and the metal removal rate also decreases with cutting time. A constant voltage power supply therefore limits the depth of cut for a given electrolyte when the method is used for embossing; it limits the material thickness when the method is used for blanking. When the current density falls below a critical level, selective attack may occur on the work surface.
- (c) The starting gaps between the workpiece surface and the electrodes were built into the tooling by the depth the electrode cutting surfaces were recessed in the mounting faces. In some trials, the combination of small starting gaps and high voltages resulted in high starting currents. These currents, combined with small electrolyte flow rates at the beginning of the cut, caused excessive heat-up and damaged the plastic electrode coating which, in turn, resulted in irregular etch patterns on the workpiece. This can be prevented by increasing the starting gaps, increasing the electrolyte inlet pressure, or decreasing the starting voltage.

3. CAVITY MACHINING — EXEMPLARY PART 8

3.1 Purpose

To demonstrate electrolytic machining as a method for drilling deep holes and cavities.

3.2 Areas of Advancement

For given applications and materials, this method generates deep holes and cavities of regular or irregular shapes which cannot be accomplished by conventional processes.

TABLE 14
OPERATING PARAMETERS, EXEMPLARY PARTS 4 & 5

EXEMPLARY PART

OPERATING PARAMETERS	4			5	
	Ser No.			Ser. No.	
	3	5	11-25	30	32-35
Electrolyte composition	NaCl	NaCl	NaCl	NaOH	NaOH
Electrolyte concentration (lb/gal)	2.05	2.05	2.05	2.04	2.04
Electrolyte temperature, tank (°F)	75	75	75	-**	-**
Applied voltage* (volt)	14.0/11.0	10.0/10.0	8.0/8.0	5.0/5.0	6.0/6.0
Current* (amp)	1,040/50	**-/65	383/33	510/60	605/65
Cutting time (sec)	65	90	140	22	21
Dwell time (sec)	145	60	160	38	9
Electrolyte inlet pressure* (psig)	300/265	260/220	265/210	170/145	190/160
Electrolyte outlet pressure* (psig)	10/20	20/25	20/20	20/30	15/15
Electrolyte flow rate* (gal/min)	3.3/3.6	3.0/3.1	2.5/3.1	1.8/2.0	1.8/-**

*Listed values are at beginning and at end of cut.

**Not recorded

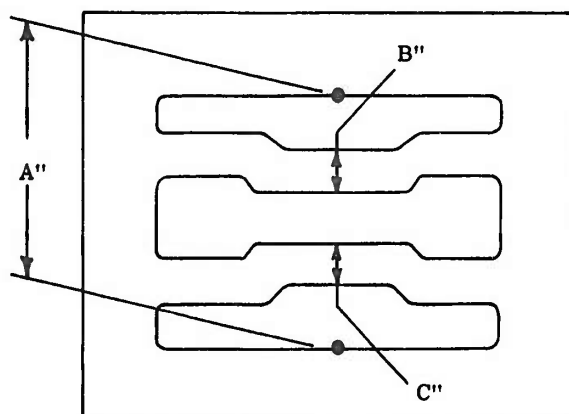
TABLE 15
OPERATING PARAMETERS AND DEPTH OF CUT, EXEMPLARY PARTS 6 & 7

EXEMPLARY PART

OPERATING PARAMETERS	6			7		
	Ser. No.			Ser. No.		
	1	2	3	3	4	8
Electrolyte composition	NaCl	NaCl	NaCl	NaCl	NaCl	NaCl
Electrolyte concentration (lb/gal)	2.1	2.1	2.1	0.67	0.67	0.67
Electrolyte temperature (°F)	73	73	73	84	84	99
Applied voltage* (volt)	10.0/10.0	10.0/10.0	10.0/10.0	6.0-2.5 min 9.0-2.0 min 18.0-bal.	6.0-1.0 min 18.0-bal.	6.0-1.0 min 18.0-bal.
Current* (amp)	280/93	280/93	280/93	115/128	81/123	75/135
Cutting time (min)	10.0	10.0	10.0	10.0	10.0	10.0
Depth of cut, electrolyte inlet (in)	.066	.063	.067	.057	.074	.073
Depth of cut, electrolyte outlet (in)	.071	.075	.071	.060	.078	.076
Electrolyte inlet pressure* (psig)	240/195	230/215	250/210	165/125	155/130	155/146
Electrolyte outlet pressure* (psig)	20/20	20/20	5/20	15/10	10/15	10/5
Electrolyte flow rate* (gal/min)	1.5/1.5	1.6/1.6	1.6/1.5	1.5/1.5	1.4/1.5	1.5/1.5

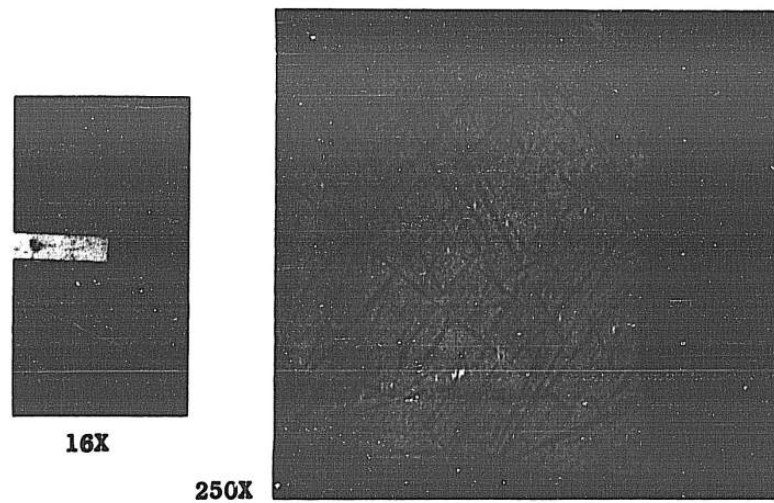
*At beginning and end of cut except as noted.

TABLE 16
PART DIMENSIONS, EXEMPLARY PART 4

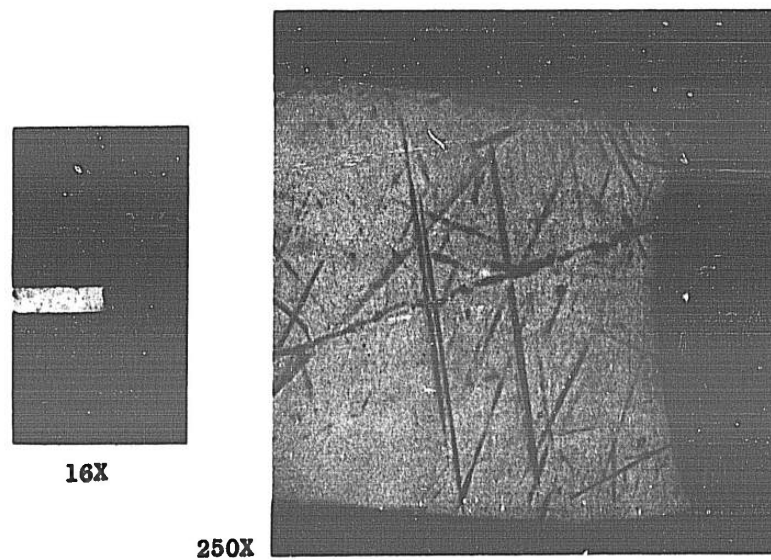


Plan View Of Workpiece

Ser. No.	Dimensions-inch		
	A	B	C
11	1.324	0.193	0.197
12	24	3	4
13	21	5	7
14	21	6	6
15	20	7	9
16	20	6	8
17	22	7	9
18	16	6	7
19	20	8	9
20	17	7	9
21	22	6	6
22	20	7	6
23	20	0.197	7
24	20	0.200	7
25	1.319	0.200	8
Average	1.3203	0.1965	0.1973
99% Spread	0.0125	0.0080	0.0075



(a) Effect of Electrode Misalignment



(b) Effect of Excessive Dwell Time

Figure 77. Cross Sections Through Machined Edge of Exemplary Part 5

Compared to broaching methods for irregular shapes and hard-to-machine materials, the electrolytic machining process is more advantageous in that it achieves metal removal at faster rates.

Compared to electro-discharge machining, electrolytic machining is advantageous in that it generates shaped cavities at faster metal removal rates without wearing or eroding the cutting tool.

3.3 Results

- (a) Rectangular holes electrolytically machined to a depth of 4-1/2" in the nickel-base alloy René 41. See Figure 78.
- (b) Demonstrated a penetration rate of .200 in/min.
- (c) The part dimensions are listed in Table 18.
- (d) The surface finishes on the cavity walls range from 15 to 30 microinches (AA).

3.4 Material Hardness

34-36 Rockwell C Scale

3.5 Tooling

The tooling is shown in Figures 79, 80 and 81. The part (1) is fixed in the table mounted work holder (2). The part is positioned by a disc (3) and supported by a stud (4). The cavity above the disc is filled with a low-melting alloy matrix (5) of 58% Bi and 42% Sn. The matrix serves as an electrolyte seal and as a current conductor.

The electrode (6) is actuated by the vertical ram (7) of machine #1.* The electrolyte supply pressure is regulated at the pump, a hand-operated needle valve regulates the tool exit pressure.

The electrolyte supply flows around the outside of the electrode, through the cutting gap, and returns through a passage in the electrode tool.

3.6 Operating Parameters

See Table 17.

* See Appendix IV

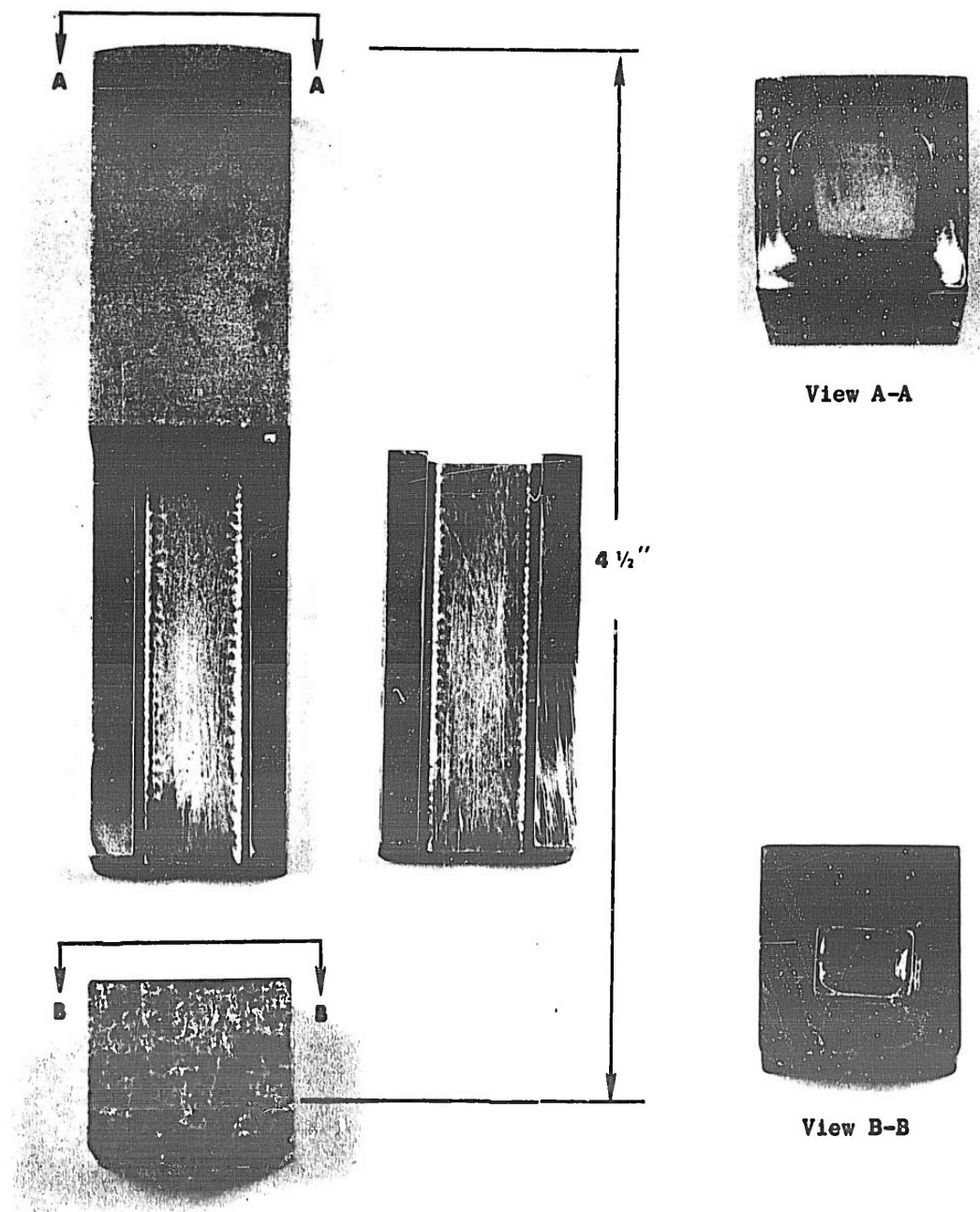
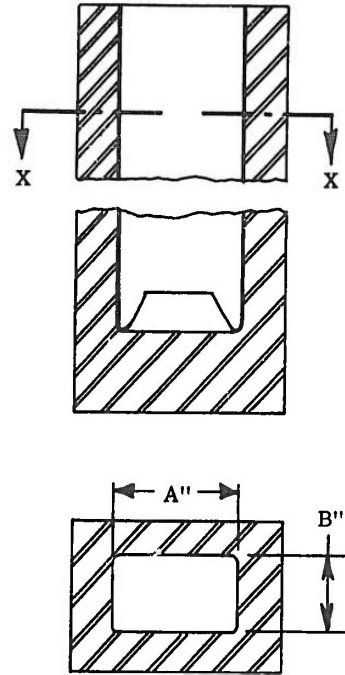


Figure 78. Exemplary Part 8
Mat'l: René 41

TABLE 17
OPERATING PARAMETERS, EXEMPLARY PART 8

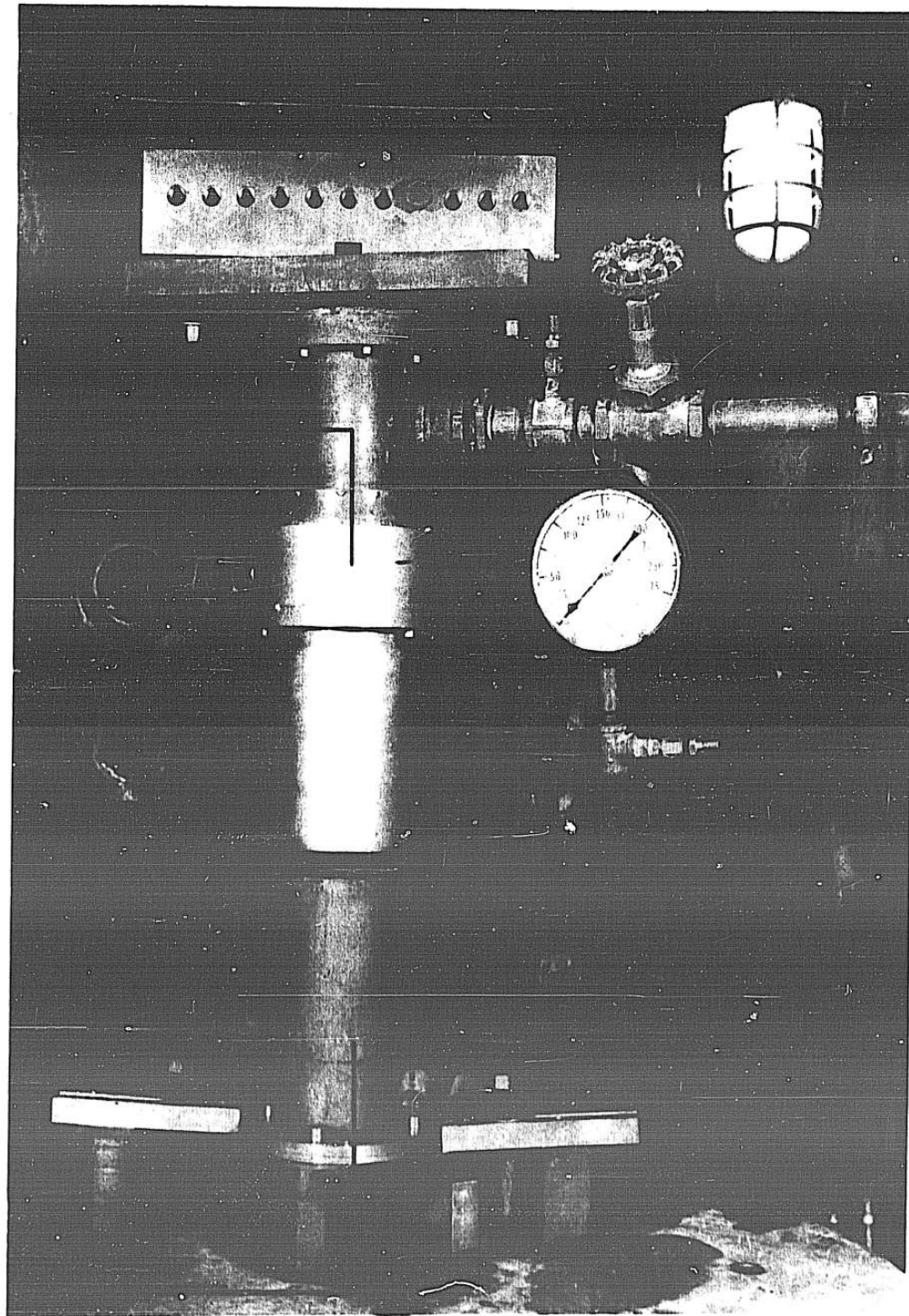
Ser. No.	1	2	3	4 thru 6
Electrolyte Composition: NaCl				
Electrolyte Concentration: 2.1 lb/gal				
Electrolyte temperature at tank: 103 °F				
Feed rate (in/min)	.150	.125	.203	.203
Applied voltage (volt)	24.0	24.0	28.0	28.0
Current, start (amp)	125	125	250	250
Current, after .25" travel (amp)	440	500	590	580
Current, end (amp)	512	605	640	635-650
Electrolyte inlet pressure (psig)	300/350	320/365	320/355	320/355
Electrolyte outlet pressure (psig)	100/23	100/16	100/27	100/20
Ram stroke (in)	4.500	4.525	4.525	4.525
Cutting gap, bottom of stroke (in)	--	--	--	.012

TABLE 18
PART DIMENSIONS, EXEMPLARY PART 8



Section X-X
Section Through Workpiece

Ser. No.	Dim. A	Dim. B	Operating Condition
1	.624	.471	1
2	.611	.458	2
3	.621	.464	3
4	.619	.465	4
5	.617	.465	4
6	.618	.464	4



For Sect A-A See Figure 80

Figure 79. Assembly of Tooling for Exemplary Part 6 in Machine #1

1. Workpiece
2. Work Holder
3. Locating Disc
4. Support Stud
5. Matrix
6. Electrode
7. Machine Ram (Feed)
8. Upper Fixture Sleeve
9. Fixture Base

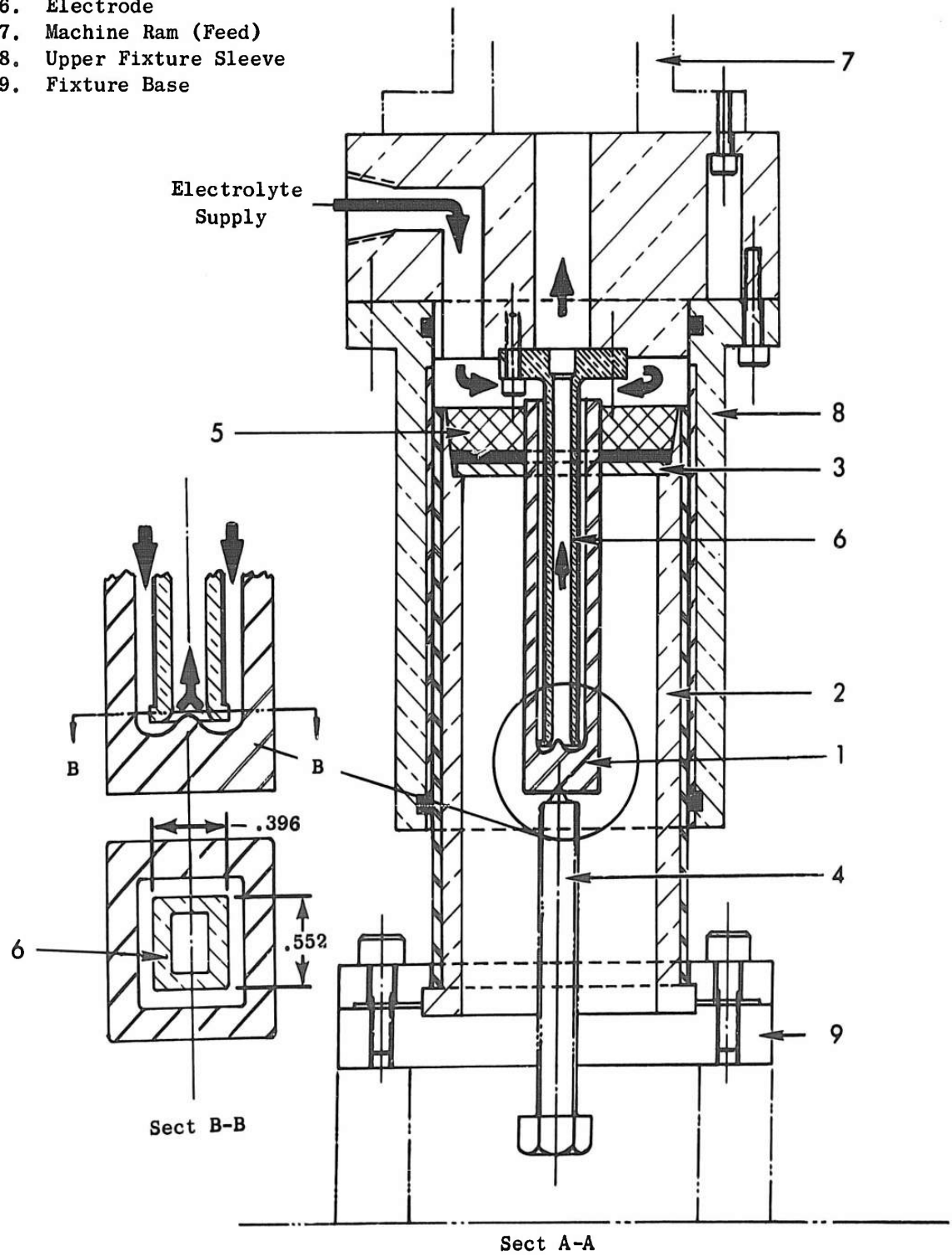
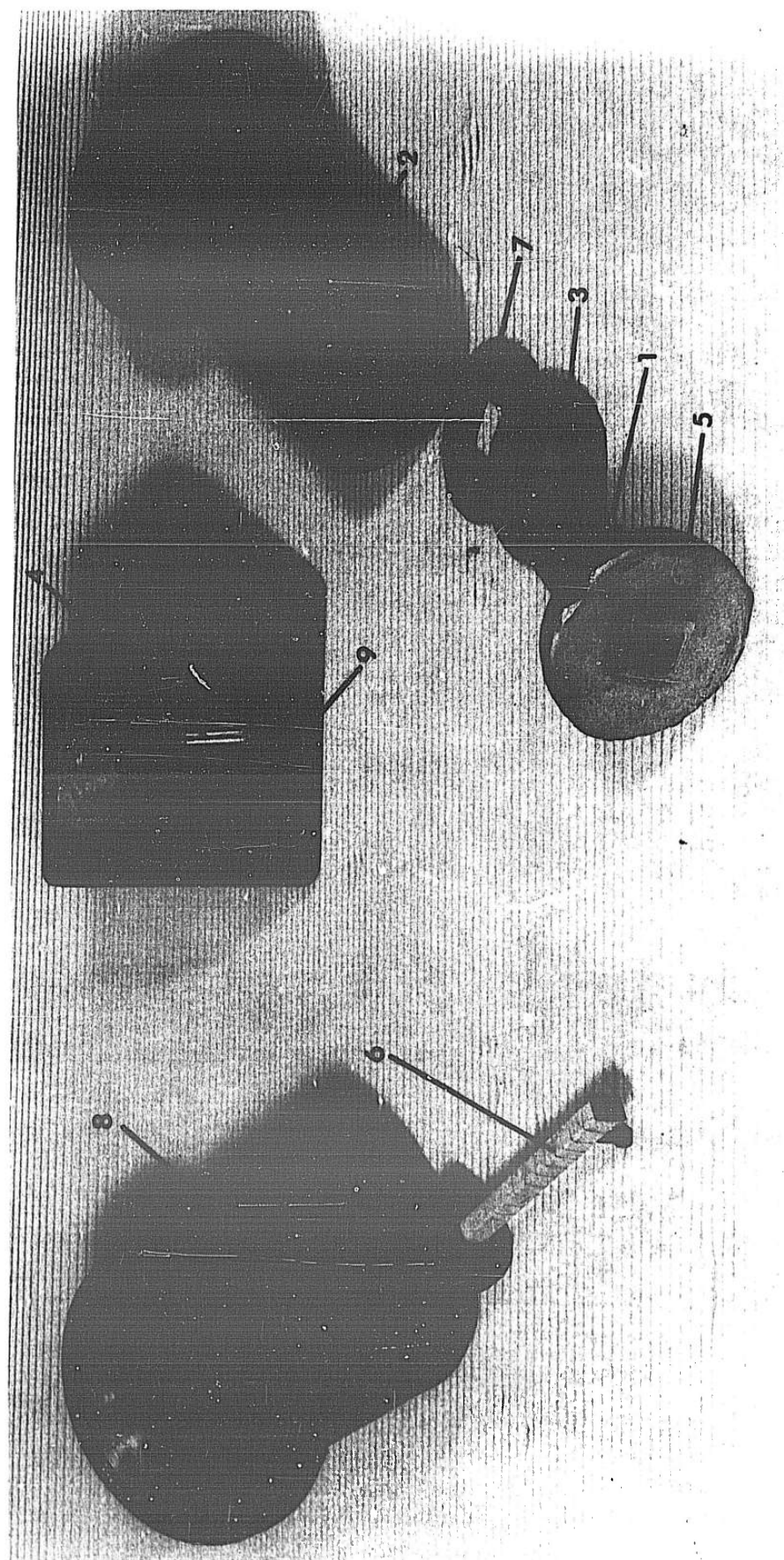


Figure 80. Schematic Sketch of Tooling for Exemplary Part 8 (Section A-A)



- | | |
|------------------|-------------------------|
| 1. Workpiece | 6. Electrode |
| 2. Work Holder | 7. Rubber Gasket |
| 3. Locating Disc | 8. Upper Fixture Sleeve |
| 4. Support Stud | 9. Fixture Base |
| 5. Matrix | |

Figure 81. Tooling for Exemplary Part 8

4. CONTOUR MACHINING — EXEMPLARY PARTS 9 AND 10

4.1 Purpose

- (a) To substantiate the mathematical analysis by generating contoured shapes in two alloy materials with varying machining parameters. See Section 4, Chapter III.
- (b) To demonstrate the ability of the electrolytic machining process to generate contoured shapes.

4.2 Areas of Advancement

For given applications and materials, this method generates complex shapes and contours more advantageously than other processes.

Compared to conventional machining, the electrolytic machining method is more advantageous in that it generates complex shapes with a linear feed motion. On hard-to-machine alloys the process accomplishes faster metal removal rates than are possible by single point cutting techniques.

Compared to electro-discharge machining, electrolytic machining is more advantageous in that it generates contours and shapes at faster metal removal rates without wearing or eroding cutting tools.

4.3 Results

- (a) Two typical examples were selected from the contour machining experiments for a comparison of results. See Figure 82.

Exemplary Part 9 was machined from the nickel-base alloy René 41; Exemplary Part 10, from the iron-base alloy A-286. Although these materials differ in hardness and composition, both parts were machined with identical penetration and metal removal rates. See Table 19.

- (b) The surface finishes ranged from 7 to 18 microinches (AA) on Exemplary Part 9, and from 10 to 36 microinches (AA) on Exemplary Part 10.
- (c) The dimensional results of these tests are discussed in Section 4, Chapter III, and in Appendix II. 6.

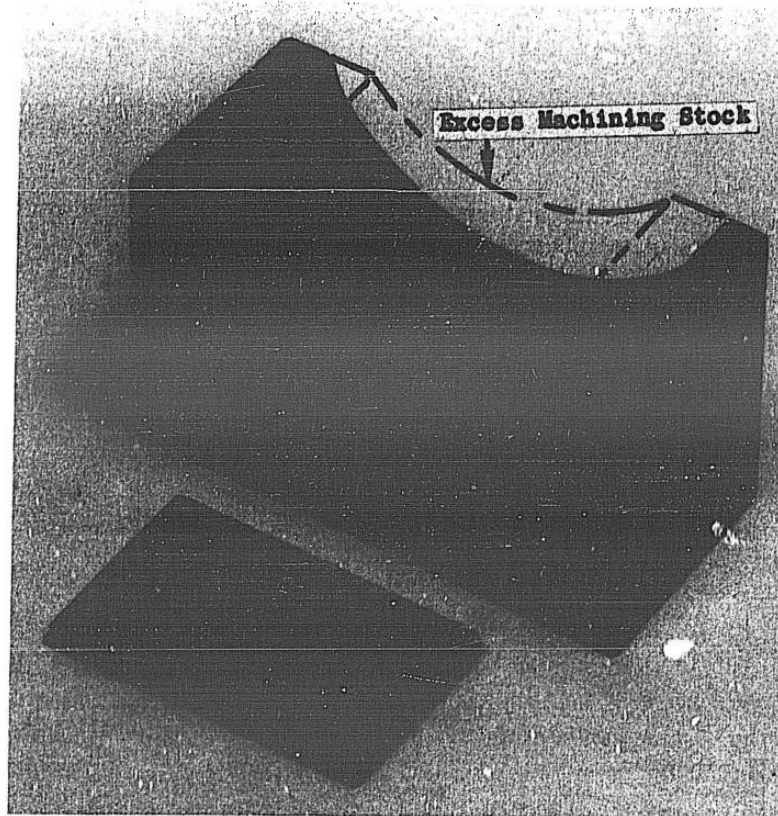
4.4 Material Hardness

- (a) Exemplary Part 9 (René 41): 34-36 Rockwell C Scale.
- (b) Exemplary Part 10 (A-286): 24-25 Rockwell C Scale.

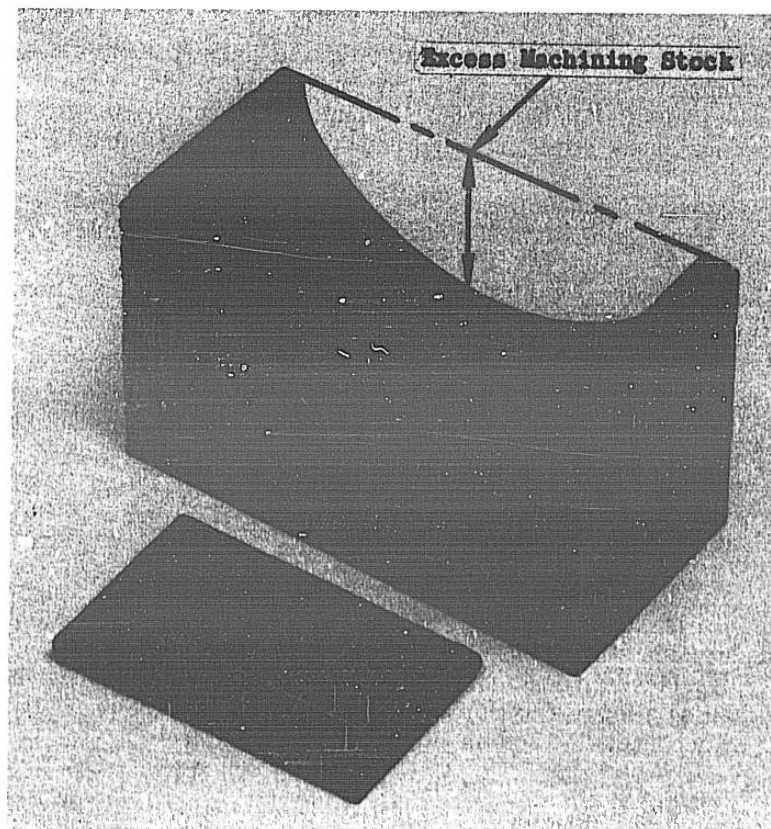
4.5 Tooling

The tooling is shown in Figures 83 and 84. The electrode (1) is actuated by the vertical feed mechanism of machine #2*, and machines a two-dimensional contour into a 1" x 1-3/4" work surface to a depth of 0.500 inch. The workpiece (2) is fixed in a holder (3) with a low-melting alloy matrix (4) of 58% Bi and 42% Sn. The anode bus (5) extends into the matrix and connects the bottom surface of the workpiece.

* See Appendix II. 5. 1



Exemplary Part 9 - René 41



Exemplary Part 10 - A286

Figure 82. Exemplary Parts 9 and 10

TABLE 19
OPERATING PARAMETERS, EXEMPLARY PARTS 9 & 10

EXEMPLARY PART

OPERATING PARAMETERS	9			10		
	Ser. No.			Ser. No.		
	C-1-9	C-1-10	C-1-11	D-3-4	D-3-5	D-3-10
Electrolyte composition	NaCl	NaCl	NaCl	NaNO ₃	NaNO ₃	NaNO ₃
Electrolyte concentration (lb/gal)	2.1	2.1	2.1	5.0	5.0	5.0
Electrolyte temperature, tank (°F)	94	94	94	100	100	100
Feed rate (in/min)	.040	.040	.040	.040	.040	.040
Applied voltage (volt)	11.0	11.0	11.0	12.0	12.0	12.0
Current* (amp)	692	650	646	729	741	737
Electrolyte pressure, inlet (psig)	240	240	240	240	240	240
Electrolyte pressure, outlet (psig)	20	20	20	20	20	20
Electrolyte flow* (gal/min)	3.8	3.9	3.9	3.6	3.9	3.2
Ram travel (in)	.197	.195	.195	.509	.511	.501

*Listed values are for end of machining cycle.

The electrolyte is channeled through passages from the inlet to the upstream side of the electrode, across the cutting gap, and to the exit port of the tool.

A gap measurement device is incorporated in the electrode. A measuring pin (6), which is normally flush with the electrode cutting surface, is extended to the anode surface, and a dial indicator (7) measures the gap dimension. The gap measurements were made while the electrolyte was flowing through the tooling.

4.6 Operating Parameters

See Table 19.

4.7 Comments

The Rene 41 workpieces, Exemplary Part 9, were premachined by conventional methods to a contoured shape, leaving approximately uniform excess machining stock of 0.190" for electrolytic machining.

The A-286 workpieces, Exemplary Part 10, were electrolytically machined into a flat work surface, Figure 82.

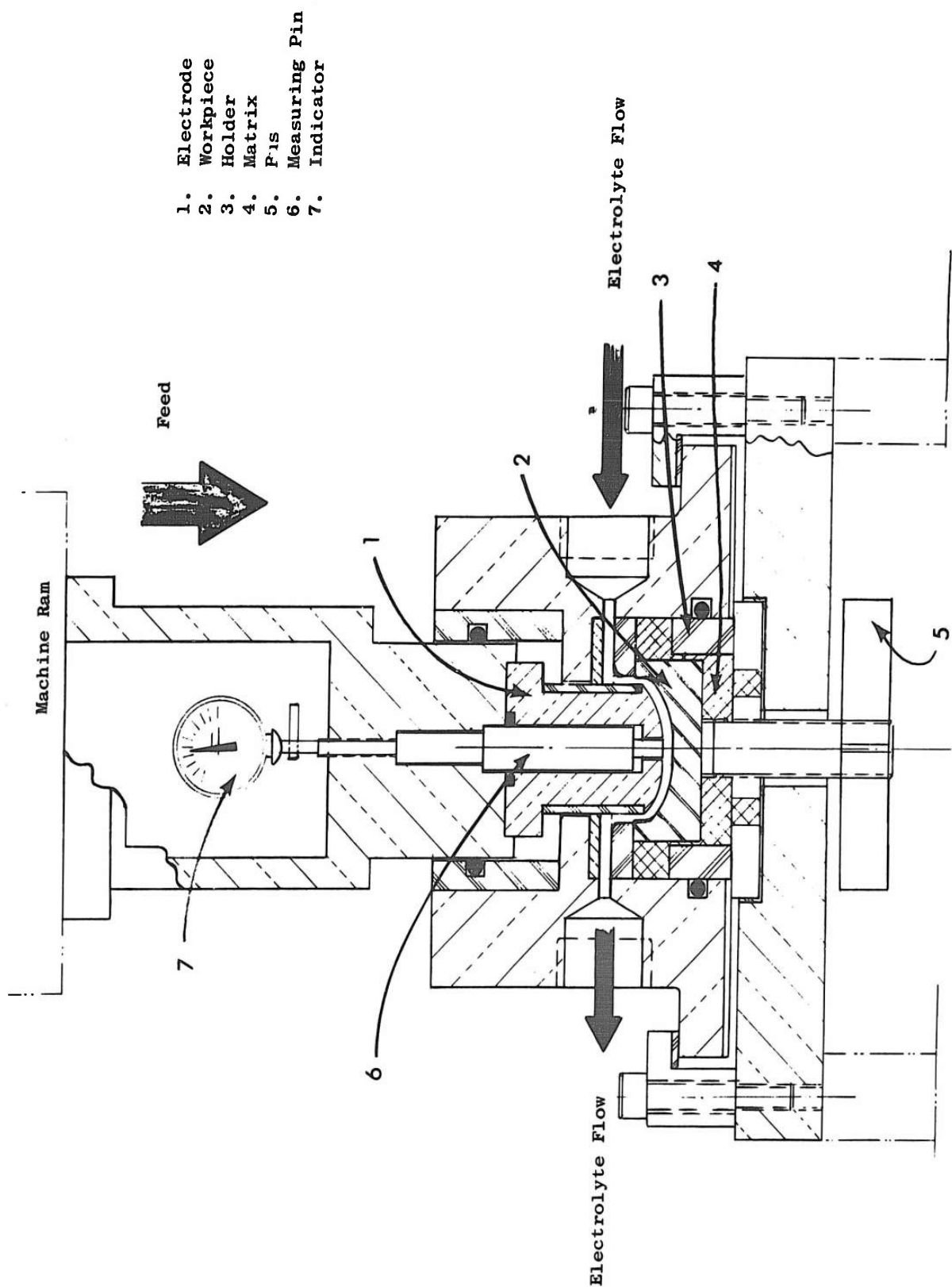
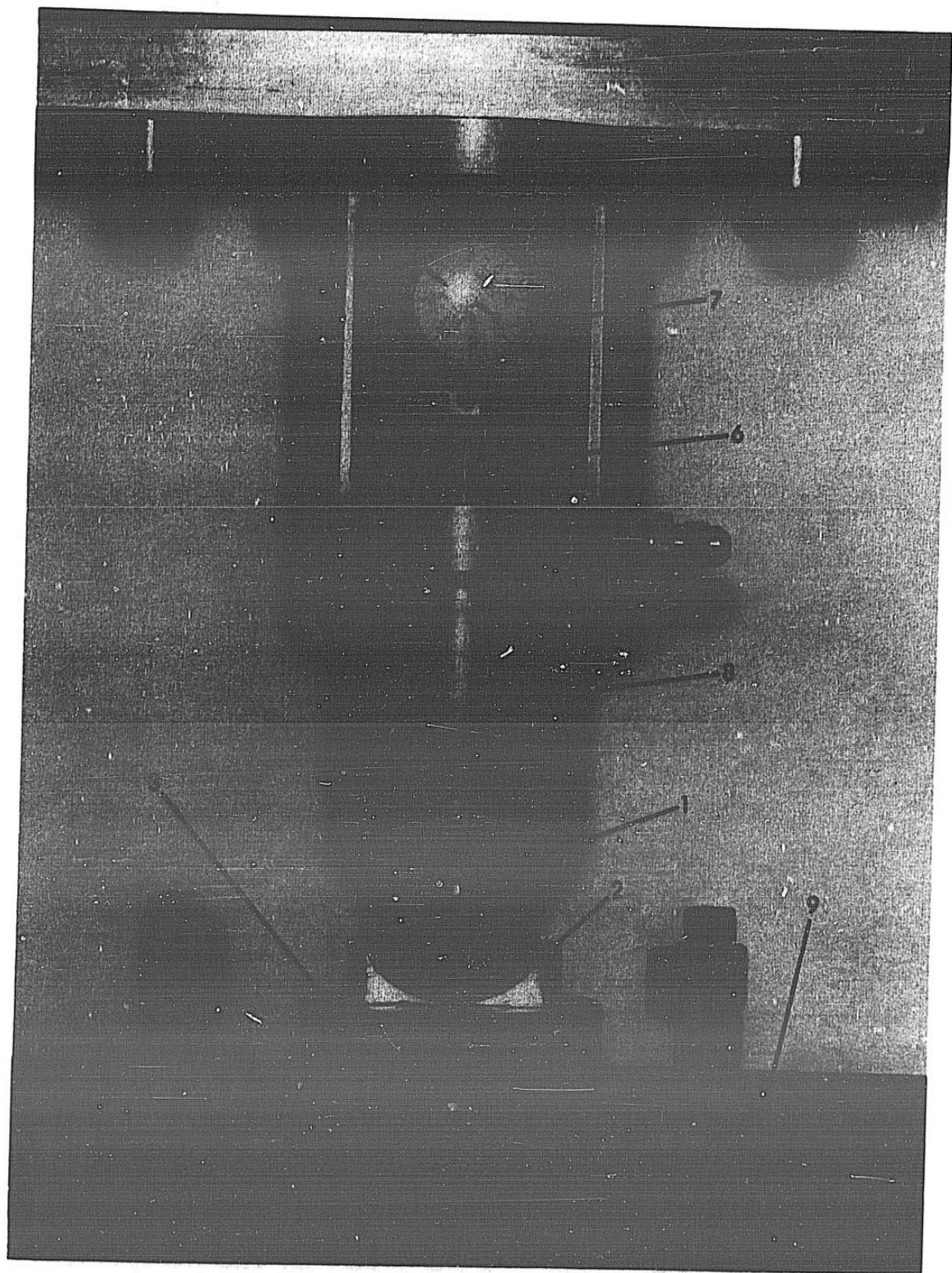


Figure 83. Schematic Sketch of Tooling for Exemplary Parts 9 and 10



- | | |
|----------------------|---------------------|
| 1. Electrode | 7. Dial Indicator |
| 2. Workpiece | 8. Electrode Holder |
| 3. Work Holder | 9. Fixture Base |
| 6. Gap Measuring Pin | |

Figure 84. Tooling for Exemplary Parts 9 and 10
Details of Electrode Assy and Work Holder

CHAPTER V

PROCESS SPECIFICATION AND SELECTION GUIDE

This chapter covers guidelines for the preparation of electrolytic machining process specifications and for the selection of process operating parameters.

1. PROCESS SPECIFICATION GUIDE

Separate process specifications shall be prepared for different work materials and different machining operations.

The specification for a selected application of the electrolytic machining process shall conform to military specification MIL-S-6644A (USAF) except that the contents of the following specification sections shall conform to this guide:

- (a) Scope.
- (b) Applicable documents.
- (c) Requirements.
- (d) Quality assurance provisions

1.1 Scope

The scope of the specification shall cover the machining operation, and the work material, including the material's metallurgical structure, and heat treat conditions.

When more than one metallurgical structure or heat treat condition is covered, they shall be listed as material classes and identified in this section.

1.2 Applicable Documents

This section of the specification shall list all documents referred to in the text.

The listing shall include applicable workpiece drawings and specifications, work material specifications, subsidiary electrolytic machining process specification, electrolytic facility specifications, and documents covering applicable safety requirements.

1.3 Requirements

The specification for the application of a machining operation to a specific material shall cover the following requirements for each material class:

- (a) The tooling and workpiece fixtures.
- (b) Process operating parameters.
- (c) Process control.
- (d) Excess machining stock.
- (e) Treatment after machining.

1.3.1 Tooling

The tooling consists of one or more electrode tools and the workpiece fixtures. The tooling shall conform to the requirements listed in Section 5, Chapter VI.

This section of the specification shall describe the tooling for the intended machining operation and it shall identify the electrolytic machining facility on which the tooling is to be used by reference to applicable facility specification.

The description of the tooling shall include scaled drawings of the electrode tools and workpiece fixtures showing plan view, front elevation, end elevation, necessary sectional views, and all points at which designated operating parameters are to be gaged.

1.3.2 Process Operating Parameters

This section of the specification shall list the nominal values of the operating parameters to be used for the selected application. The following operating parameters shall be included:

- (a) Electrolyte composition, the purity of the chemicals used, and either chemical concentration or chemical conductivity, related to a standard temperature and to a designated location in the facility, usually at the electrolyte storage tank.
- (b) Electrolyte temperature, related to a designated location in the tooling or in the facility, usually at the electrolyte storage tank or at the tool entrance.
- (c) The pH content, where applicable, related to a standard temperature and to a designated location, usually at the electrolyte storage tank.
- (d) Electrolyte inlet and outlet fluid pressures, related to designated locations, usually at the tooling entrance and exit.
- (e) The applied electropotential between designated gage points, usually between the electrode tool and workpiece.
- (f) The feed rate of electrode tool, or workpiece, or both by magnitude and direction.
- (g) The minimum distance between the electrode-tool and a designated point of the workpiece at the beginning of the machining cycle.
- (h) The duration of the machining cycle, or the length of cutting stroke in the case of rectilinear feed motions.

If one or more operating parameters vary during a single machining cycle, their values shall be related to respective cycle elements of other parameters, such as cutting time, feed motions, or feed strokes.

More than one combination of operating parameters may be specified if different combinations accomplish the same machining results.

1.3.3 Process Control

This section of the process specification shall describe the tolerances within which the specified operating parameter values are to be maintained to accomplish the intended workpiece shape.

A tolerance shall be specified for each process operating parameter required for a given machining operation and material. In addition, a tolerance shall be specified for a permissible range of precipitate, or sludge content in the electrolyte where applicable. The sludge content shall be related to a standard temperature and to a designated location in the facility, usually at the electrolyte storage tank. The method of sludge measurement shall be specified.

1.3.4 Excess Machining Stock

This section shall describe the excess machining stock and the machining stock tolerances which will permit the accomplishment of the final workpiece shape with the specified operating parameters.

The description shall include scale drawings of the workpiece before electrolytic machining showing plan view, front elevation, end elevation, and, if necessary, sectional views.

More than one combination of excess machining stock and stock tolerance may be specified. When the same workpiece shape can be accomplished with different amounts of excess stock or different stock tolerances, or by using different combinations of operating parameters, each raw material condition shall be related to the specific combination of operating parameters which will accomplish the desired final workpiece shape.

1.3.5 Treatment After Machining

This section shall describe the method for rinsing, drying, and otherwise protecting an electrolytically machined workpiece against corrosion after machining.

1.4 Quality Assurance

This section of the specification shall include inspection of specified tooling and raw material procedures and the acceptance of the process procedure.

Procedures shall be specified which will establish that the final workpiece shape is achieved within the tolerances and permissible surface finish and subsurface defect ranges specified in the applicable part drawing when the specified operational requirements are implemented.

Acceptance tests may be specified which cover a minimum number of workpieces produced over a minimum time period, and sampling procedures may be included which assure that established quality levels are maintained over extended production periods.

2. PROCESS SELECTION GUIDE

The information in this section may be used as guidelines in selecting operating parameters for a given material and application.

2.1 Electrolyte Selection*

For a given material, an electrolyte must be chosen which does not form adherent, nonporous, dielectric films at the anode during electrolytic machining. The chosen electrolyte must result in a uniform removal rate of all metal elements in multiconstituent alloys.

In addition, it is desirable that the electrolyte meet these criteria:

- (a) It should precipitate the reaction products from the electrolyte.
- (b) It should be noncorrosive.
- (c) It should be inexpensive, nontoxic, and reusable.

* See Section 5, Chapter III

For materials with substantial amounts of intermetallic compounds, highly acidic electrolytes may be required to achieve uniform metal removal.

2.2 Electrolyte Conductivity

The electrical conductivity of an electrolyte is dependent upon its concentration and temperature. If other considerations permit, the concentration and temperature of the electrolyte should be selected so that for relatively large changes in concentration and temperature, small changes in conductivity result.

Electrolyte conductivity is one of the determining factors for the size of the cutting gap. For a given voltage range of the power supply, the higher the electrolyte conductivity, the larger the choice of cutting gap sizes. When the chemical concentration in an electrolyte solution is near saturation, detrimental crystallization may occur in the electrolyte conduits and control elements.

2.3 Electrolyte Temperature

The temperature of the electrolyte in the cutting gap depends on the electrolyte supply temperature, on its velocity, on metal removal rate, and on inherent thermal properties of the workpiece and the tooling. The temperature of the electrolyte supply must be chosen so that the electrolyte does not boil during electrolytic machining. The choice of electrolyte supply temperature may be restricted by the capacity of the heat exchanger in the electrolyte supply system.

2.4 Electrolyte Pressures

The difference between the electrolyte pressure at the tool inlet and outlet is one of the determining factors for electrolyte velocity and for static pressure head in the cutting gap.

A minimum electrolyte velocity is determined by the metal removal rate.* The fluid pressure of the electrolyte in the cutting gap can contribute to deflection of the workpiece, the fixtures, and the machine tool.

2.5 Feed Rate

The rate of relative electrode to workpiece feed is one of the determining factors for metal removal rate and current density. The current density related to cutting area determines the total current flow.

The total current flow for a given application may be estimated by the formula:

$$I = \frac{A_c \times F}{K} \quad (51)$$

where I is total current flow in amp

A_c is surface area of electrode cutting tool in in²

F is rate of relative electrode to workpiece feed in in/min

K is a metal removal factor in in³/amp-min. **

* See Section 7, Chapter III

** See Section 2, Chapter III

For a given application, the maximum permissible feed rate may depend on:

- (a) The electrical conductivity and size of the workpiece.
- (b) The capacity of the power supply.
- (c) The maximum electrolyte supply pressure.

The minimum feed rate may depend on a permissible minimum current density.

2.6 Applied Voltage

When all other operating parameters have been selected, the applied voltage determines the size of the cutting gap. The optimum size of the cutting gap varies between applications. Generally, it is desirable to cut with the smallest practical gap. As the cutting gap becomes smaller, profile details are reproduced more accurately and the dimensional repeatability improves. The smallest practical cutting gap depends upon the capacity of the filtration system in the electrolyte supply, the size of nonconductive inclusions in the work material, and the rigidity of the machine and fixture.

The maximum voltage may be determined by the capacity of the power supply or by safety considerations. A minimum voltage is determined by the value of the over-potential ΔE for a given work material and electrolyte.*

* See Sections 2 and 3, Chapter III

CHAPTER VI
EQUIPMENT SPECIFICATION GUIDE

1. INTRODUCTION

This chapter covers functional criteria for the design of physical components which implement the electrolytic machining process. The information is intended for use as a guide line in preparing specifications for electrolytic machining facilities.

The following documents shall be used in the preparation of specification for electrolytic machining facilities:

(a) Specifications

Military

MIL-S-6644A(USAF)

Specifications, Equipment Contractor-prepared, Instructions for the preparation of.

(b) Standards

National Machine Tool
Builders Association (NMTBA)

Machine Tool Electrical Standards
(MTES)

Joint Industrial Committee (JIC)

Hydraulic Standards for Industrial
Equipment

U.S. Department of Labor

Safety & Health Standards for Federal
Supply Contracts (Walsh-Healey Act)

The physical components which implement the electrolytic machining process consists of four interrelated subsystems*:

- (a) The machine tool.
- (b) The electrical power supply.
- (c) The electrolyte supply system.
- (d) The electrode tool and workpiece fixture.

The assembly of these subsystems constitutes the electrolytic machining facility. Each facility shall be classified by its intended machining functions and its rated machining capacity.

The machining functions shall be described by the mode of relative electrode motion to the work surface and by the electrolyte type which accomplishes the machining application.**

Machining capacity shall be expressed in permissible metal removal rate, in in³/hr.

2. THE MACHINE TOOL

It shall be the function of the machine tool to:

* See Section 1, Chapter III

** See Section 1, Chapter V

- (a) Position the electrode tool and the workpiece fixture.
- (b) Maintain the alignment of the electrode tool and workpiece fixture during electrolytic machining.
- (c) Supply feed motions to the electrode tool, or the workpiece, or both.
- (d) Link the electrical power conduits with the electrode tool and the workpiece.
- (e) Link the electrolyte supply and return conduits to the electrode tool, or the workpiece fixture, or both.

2.1 Positioning Requirements

The machine tool shall provide for the attachment of the electrode tool and the workpiece fixture at the positions determined by the intended machining function.

The positioning components shall provide for establishing positioning alignment between electrode tool and the workpiece fixture. When positioning components are adjustable, provisions shall be included which assure the maintenance of a selected position during continuous electrolytic machining.

2.2 Support Structures

The electrolytic machine tool shall consist of support structures which provide for the maintenance of alignment between the electrode tool and workpiece fixture within a selected tolerance during continuous electrolytic machining. In the design of the support structure, the following forces shall be considered:

- (a) Weight Forces - which may consist of the workpiece, electrode tool and fixture, the electrolyte and power supply conduits, and control and metering devices.
- (b) Hydrostatic Forces - which may consist of the static electrolyte pressure in the cutting gap and of forces exerted in the electrolyte supply and return conduits.
- (c) Vibration Forces - which may consist of pulsating electrolyte pressures and of forces caused by unbalanced rotating parts in the machine tool mechanism.

2.3 Feed Mechanism

The feed mechanism may supply rectilinear or rotating feed motions to the components supporting the workpiece fixture, or to components supporting the electrode tool, or to both. The direction of feed motions, the range of motions and feed rates, and the strokes of components supplying rectilinear motions shall be determined by the intended machining function.

The feed mechanism may provide for rapid advance and withdrawal feeds, and for continuously variable cutting feeds within the selected range.

Provisions shall be included in the design of the feed mechanism which assure the maintenance of a feed rate within a selected tolerance during continuous machining under constant or changing loads resulting from forces listed in Section 2.2, Chapter VI.

The machine mechanism shall facilitate intermittent stops and starts of cutting and rapid feed motions within selected response tolerances.

2.4 Electrical Power Connections

Electrical power conduits shall be included in the machine tool to link the power supply lines with anode and cathode terminals in the tooling. The size of the conduits shall be determined by the rated capacity of the machining facility. They shall be electrically insulated from the structure of the machine to prevent leakage of electrical current from the power conduits to the machine structure during continuous electrolytic machining.

2.5 Electrolyte Supply Connections and Enclosures

Electrolyte conduits, storage or catch tanks, and splash guards shall be included in the machine tool to link the electrolyte supply and storage system with the electrode tool and workpiece fixture, and to confine the electrolyte to the work station.

Electrolyte conduits and tanks which are a part of the machine tool shall either be made from dielectric materials or they shall be electrically insulated from the machine structure and electrically connected to the negative pole of the power supply to prevent leakage of electrical current into the machine tool structure during continuous electrolytic machining.

When work enclosures are included in the machine tool, provisions shall be made for forced ventilation of the enclosed area. In addition, the work mounting area shall be readily accessible to the operator.

The size of the electrolyte conduit, of the work enclosure, and of the ventilation system shall be determined by the rated capacity of the facility.

3. THE ELECTRICAL POWER SUPPLY

It shall be the function of the electrical power supply to provide DC current for the machining operation.

The supply voltages range shall be determined by the intended machining functions. The power supply may provide for continuously variable supply voltage within a selected range.

The power supply shall provide for the maintenance of a voltage within a selected tolerance during continuous electrolytic machining over the full range of the current supply capacity.

When the primary power source is an alternating current, the variations of the supply voltage, or ripple, shall be maintained within a selected tolerance during continuous electrolytic machining.

When provisions are included in the electrical power supply for intermittent reversal of the current polarity, they shall assure the maintenance of reversal frequency and time at reversed polarity within selected tolerance limits.

The range of the supply current shall be determined by the rated capacity of the facility.

Provisions may be included in the power supply system which facilitate the maintenance of current flow rate within a selected tolerance.

Automatic control circuits may be included in the power supply which disengage the power supply when a selected maximum current level is exceeded, or when the current flow

deviates from selected flow rates. A tolerance may be selected for the response time of the disengage system.

The size and capacity of connecting leads between the power supply and the machine tool shall be determined by the rated capacity of the power supply.

4. THE ELECTROLYTE SUPPLY SYSTEM

It shall be the function of the electrolyte supply system to:

- (a) Store the electrolyte.
- (b) Maintain selected electrolyte properties.
- (c) Pump the electrolytes through the gap between the electrode tool and the workpiece.
- (d) Prevent foreign particles from entering the cutting gap.

4.1 Electrolyte Storage

The storage space for the electrolyte shall be determined by the rated capacity of the electrolytic machining facility and by anticipated production rates.

4.2 Regulation of Electrolyte Properties

The electrolyte system shall provide for the maintenance of electrolyte properties including the electrolyte temperature within selected tolerance limits.

Provisions shall be included in the electrolyte supply system to implement procedures by which the electrolyte conductivity can be regulated within selected tolerance limits. The procedures may consist of continuous or intermittent sampling or metering of the electrolyte conductivity, or of adjustment of the electrolyte conductivity by automatic regulating devices. When the intended machining functions require using electrolytes which precipitate machining products in the form of sludge, provisions shall be included to implement procedures by which the sludge content of the electrolyte can be regulated within selected tolerance limits. The procedures may consist of continuous or periodic clarification of the electrolyte by anyone or a combination of the following methods:

- (a) Filtration.
- (b) Centrifugal separation.
- (c) Sedimentation.
- (d) Flotation.

4.3 Pumping Facilities

The electrolyte supply system shall include pumping facilities to supply the electrolyte to the gap between the electrode tool and the workpiece at the velocities and flow rates required by the intended machining function.

The range of flow rates and supply pressures shall be determined by the rated capacity of the electrolytic machining facility.

Provisions shall be made for the maintenance of required flow rates and for continuous, nonpulsating supply pressures within selected tolerance limits.

4.4 Filtration

The electrolyte supply system shall include devices in the supply conduits to the electrode tool and workpiece fixture which limit the particle size of foreign or undissolved objects in the electrolyte. The maximum permissible particle size shall be determined by the intended machining function. The devices shall be of a capacity which is compatible with the rated capacity of the pumping facility, and they shall permit the maintenance of selected flow rates and supply pressures within a selected tolerance during continuous electrolytic machining.

5. ELECTRODE TOOL AND WORKPIECE FIXTURE

It shall be the function of the electrode tool to generate the work surface, and to conduct electrical current to the machining zone.

The material for the electrode tool may be selected on the basis of electrical conductivity, corrosion resistance, machinability, abrasion resistance, spark resistance, and material cost.*

It shall be the function of the workpiece fixture to:

- (a) Position the workpiece in the machine tool.
- (b) Maintain the workpiece alignment with the electrode tool.
- (c) Link the electrical power conduits with the workpiece.

The workpiece fixture shall consist of support structures which provide for the maintenance of alignment between electrode tool and the workpiece within a selected tolerance during continuous electrolytic machining. In the design of the workpiece fixture, the forces listed in Section 2.2, Chapter VI, shall be considered.

Electrical power conduits shall be included in the workpiece fixture to link the power supply with the workpiece. The size of the conduit shall be determined by the intended machining function, and by the maximum continuous current flow required by the intended machining function.

Electrical power conduits shall be electrically insulated from the structure of the fixtures, and the fixture may be electrically connected to the negative pole of the power supply to prevent electrolytic erosion.

It shall be the function of the tool assembly to link the electrolyte supply and return conduits with the cutting gap between the electrode tool and the workpiece. Provisions may be included in the tool assembly to confine the electrolyte flow to the work surface.

6. GENERAL FACILITY REQUIREMENTS

6.1 Control and Metering Devices

The electrolytic machine facility shall include control and metering devices for all operating parameters** which implement the electrolytic machining process for the intended machining function. These devices may include, but are not restricted to, the following:

* See Section 9, Chapter III

** See Section 1, Chapter V

- (a) Electrode position indicators.
- (b) Feed rate indicators.
- (c) Voltage and ammeters.
- (d) Electrolyte temperature gages.
- (e) Electrolyte pressure gages.
- (f) Electrolyte flow meters.

6.2 Corrosion Protection

All facility components which are normally in contact with the electrolyte shall be corrosion-proof to the electrolyte types required for the intended machining functions, except that electrical connections and terminals may be of the expendable type or they may be protected by coatings which are resistant to the electrolyte types required.

All components which are not normally in contact with the electrolyte and which are from noncorrosion resistant materials, except those surfaces which are part of mechanisms, shall be protected by coatings which are resistant to the electrolyte types required for the intended machining functions.

All mechanisms shall be enclosed and sealed against the electrolyte. Electro-mechanical moisture detection systems may be used to indicate the leakage of electrolyte into internal machine components or mechanisms.

6.3 Hydraulic Equipment

When hydraulic equipment is included in the facility, it shall be provided with switches to indicate over-temperature conditions, and to shut off electric motors in the event that the hydraulic fluid temperatures exceed permissible limits. Heat exchangers may be installed in the hydraulic system to reduce the possibility of overheating.

6.4 Electrical Equipment

Where dielectric materials are used as electrical insulators they shall maintain their dielectric properties when exposed to the electrolyte type required by the machining function.

All motors shall be totally enclosed and may be of nonventilated or fan-cooled construction.

All electrical equipment and wiring shall be in accordance with the National Machine Builders Association, "Machine Tool Electrical Standards," (MTES). All electrical cabinet doors shall be equipped with suitable locks. Individual start-stop buttons shall be provided for each motor.

A single disconnecting means shall be provided to open all power sources to the facility simultaneously.

6.5 Lubrication and Maintenance Provisions

All sliding, and rotating parts and all points of adjustment, excepting those parts with pack seal bearings shall have provisions for lubrication. The lubrication system may be equipped with low level and system failure alarms.

Provisions shall be made for the use of lubrication oils of the rust and oxidation inhibiting types.

The facilities, including all auxiliaries, interconnecting wiring, piping, and ducts shall be arranged so that filters, access panels, doors, lubrication points and fittings, and adjustment points are accessible for ease of maintenance.

All expendable parts shall be permanently marked with the manufacturer's part number or their part number and description shall be listed in manual diagrams and section drawings to facilitate ordering of replacement parts.

6.6 Safety Provisions

All moving parts shall be shielded or guarded in accordance with applicable requirements of the respective state codes and U.S. Department of Labor "Safety and Health Standards for Federal Supply Contracts".

When toxic electrolytes are used, the electrolyte storage facility shall be totally enclosed and ventilated with forced air ventilating systems.

The design of the electrolytic machining facility shall provide for protection against electrical shock.

6.7 Quality Assurance

All facility functions for which performances and safety provisions have been specified shall be checked or tested for conformance under conditions which simulate or duplicate the intended machining function.

CHAPTER VII

REFERENCES

- (1) BAYER, J., "Interim Report - Electrolytic Machining Process, #R62FPD320", Cincinnati, Ohio 45215: General Electric Company (1962).
- (2) BOCKRIS, J. O'M., "Electrochemical Aspects of the Deposition and Dissolution of Metals", Trans. of Symposium of Electrode Processes, page 161, New York: John Wiley & Sons (1961).
- (3) BOMBERGER, H.B., BECK, F.H.; FONTANA, M.G.; J. Electrochem. Soc. 102, page 53 (1955).
- (4) CHRISTOPHER, P.M. and KING, C.V., J. Electrochem. Soc. 107, page 493 (1960).
- (5) DANIEL, CUTHBERT, "Use of Half-Normal Plots in Interpreting Factorial Two-Level Experiments", Technometrics, Volume 1, Number 4 (November 1959).
- (6) DAVIES, OWEN L., (ed), "The Design and Analysis of Industrial Experiments", (Second Edition), New York: Hafner Publishing Company (1956).
- (7) EDWARDS, J., J. Electrochem. Soc. 100, page 189C through 194C (1953).
- (8) ELMORE, W.C., "Electrolytic Polishing", J. App. Physics 10, page 724 through 727 (1939).
- (9) FRANKLIN, T.C. and GOODWYN, J., "The Effects of Additives upon Electro-deposition and Electro-dissolution of Metals", ASD-TDR-63-212, page 28.
- (10) FRANKLIN, T.C. and PARSONS, C.R., J. Electrochem, Soc. 109, page 641 (1962).
- (11) GLASSTONE, S., "Physical Chemistry", (Second Edition), page 30, New York: Van Nostrand Company (1946).
- (12) GLASSTONE, *ibid*, page 927.
- (13) GLASSTONE, *ibid*, page 1014.
- (14) GLASSTONE, *ibid*, page 1018.
- (15) HOAR, J.P. and MOVAT, J.A.S., "Mechanism of Electropolishing", Nature 165, page 64 (1950).
- (16) PAHLITZSCH, A., "Stossläpp-Elysieren", International Institute for Production Engineers, Summary of Articles and Papers from CIRP, page 71, Berlin-Germany: Springer Verlag (May 1963).
- (17) WALTON, H.F., J. Electrochem. Soc. 97, page 219 through 226 (1950).

CHAPTER VIII

APPENDIXES

APPENDIX I

DEVELOPMENT APPROACHES

The development approaches reported in this appendix were abandoned because they did not yield anticipated results; however, they are related here in order to include the pertinent information previously published in two interim progress reports.

I.1 Study of Operating Parameters by Curve Fitting Method

From work done prior to this project and from statistical analyses of data, we formulated a model equation

$$\hat{E} = A_0 + A_1 \frac{F}{N} + A_2 FT + A_3 FP^{-.047} + A_4 \ln F + A_5 \frac{FT}{N} + A_6 \frac{F^3}{N} + A_7 F^3 T + A_8 \frac{FT}{\sqrt{P}} \quad (52)$$

where

\hat{E} is applied voltage

A_0 through A_8 are constants

F, N, T, P are operating parameters.

Our attempts to fit data from this investigation into this model were unsuccessful.

I.2 The \bar{r} Approach

In the beginning of the project we tested a mathematical model for a single electrolytic cell of the form

$$E - \Delta E = \frac{F dA_1}{K} \cdot \frac{\bar{r} L}{dA_2} \quad (53)$$

where

E is applied voltage

ΔE is overvoltage

F is the feed rate in the direction of the shortest gap distance

dA_1 is the anode area on which metal removal occurs

dA_2 is the cross-sectional area of the cell

K is a metal removal factor

\bar{r} is the weighted average specific resistance

L is the gap distance.

For our test tooling, described in Appendix II-1, we assumed that $dA_1 = dA_2$, we reduced our model, Equation (53), to the form

$$E - \Delta E = \frac{F \bar{r} L}{K} \quad (54)$$

and we proceeded to calculate \bar{r} values from our test data.

The results of our studies showed that the calculated \bar{r} values reflected specific environmental conditions and the model, Equation (54), did not represent the general case of electrolytic machining.

We then proceeded to develop mathematical models described in Section 3, Chapter III.

Comparing one of these models, which we verified by tests,

$$\frac{A_{i1}}{L_{i1}} = \frac{F_i A_{ci}}{\frac{E - \Delta E}{\beta_i \rho} K} \quad (6c)$$

with Equation (54), we found that \bar{r} reflects the value of the specific resistance (ρ), the overcut index (β_i), and the area relationship in our test tooling (dA_1 and dA_2) which we failed to consider.

In one of our early test series (JB-4), we investigated the effects of operating parameters and response variables on the ratio ($\frac{\bar{r}}{\rho}$). See Appendix II. 1.4.

I.3 Analysis of Electrolytic Cell Forces

In the beginning of the project, we made an attempt to define a model to cover electrolytic processes by examining the forces at work in a general electrolytic cell. Then our plan was to separate those forces which were at work in an electrolytic machining process. Solving the resulting differential equation would not only have given information on the effect of process variables, such as electrolyte velocity, gap, and concentration of electrolyte on the over-all process, but it would have enabled us to define analytically a ΔE for any given system. The equations obtained from developing this approach are stated below for reference, although this approach was not followed to any conclusion.

Let an ion of charge e_j in an electric field intensity X enter an electrolyte of velocity v_o . The mass of the ion multiplied by its acceleration must be equal to the sum of all the forces acting on the ion. The major forces are:

- (a) The electrical force.
- (b) The relaxation force.
- (c) The frictional force.
- (d) The electrophoretic force.
- (e) The diffusion force.
- (f) The pressure gradient force.
- (g) The electrostrictive pressure gradient force.

Adding the mathematical equivalent of these forces on the righthand side, we obtain the differential equation:

$$m_j \frac{dv_j}{dt} = e_j X - e_j^2 X \left[\frac{|Z + Z_-|}{3DkT} \cdot \frac{q}{1+q} \cdot \frac{K}{1+Ka} \right] - z_j (V_j - V_o) - \frac{e_j \kappa X z_j}{6\pi \mu_o} \quad (55)$$

$$- \frac{k T}{N_j} \frac{\partial N_j}{\partial x} + V_j \rho_o \frac{dv_o}{dt} - \frac{2P}{X}$$

where

$$q = \frac{|Z_+ Z_-| (\lambda_+ + \lambda_-)}{|Z_+ + Z_-| (Z_+ \lambda_- + Z_- \lambda_+)} \quad (56)$$

$$N_j = N_i \exp \left(- \frac{Z_i e_i \psi}{k T} \right) \quad (57)$$

$$\kappa^2 = \frac{4\pi e_j^2 \sum N_i Z_i^2}{D k T} \quad (58)$$

$$P = \frac{\bar{\epsilon} X^2}{8\pi} \quad (59)$$

$$\bar{\epsilon} = \frac{1}{X} \int_0^X \epsilon dn \quad (60)$$

$$\epsilon = \epsilon_\infty - (\epsilon_0 - \epsilon_\infty) (1 + 2bX^2)^{-1/2} \quad (61)$$

and

m_j = mass of the ion

v_j = velocity of the ion

e_i, e_j = charge on the ion

X = electric field intensity

Z_+, Z_- = valences plus or minus

D = dielectric constant

k = Boltzmann's constant

T = absolute temperature

q = function of the valances and the equivalent conductance of the ions

κ = effective radius of the ionic atmosphere

a = radius of the ion

z_j = frictional coefficient

v_0 = velocity of the electrolyte

μ_0 = viscosity of the electrolyte

N_i = concentration at any point in space and time

N_j = bulk concentration of the ion

x = distance across gap in the direction of diffusion

V_j = volume of the electrolyte

ρ_o = density of the electrolyte

t = time

P = electrostrictive pressure perpendicular to the metallic surface

λ_+, λ_- = equivalent conductance of the ions

Z_i = positive numeral value of the valence

ψ = field potential

ϵ_o = dielectric constant at 0 field strength

ϵ_∞ = limiting dielectric constant at very high field strength

$\bar{\epsilon}$ = integral dielectric constant

b = parameter for specific relationship

I.4 Temperature Effects on Cutting Gap

In Test Series JB-6 and JB-7*, we determined electrolyte and tool face temperature changes in the work area for a variety of operating conditions. We concurrently determined the gaps along the cutting face. We were unable to relate our observations to other electrolytic machining situations. We have reported our conclusions in Section 2, Chapter III.

I.5 Electrolyte Flow Observations

When we investigated the electrolyte fluid flow we noted that below an apparent minimum velocity the process became unstable, whereas above the minimum, the process stabilized and changes in fluid flow did not appreciably affect the relationship among the operating parameters. On the other hand, the surface roughness appeared to be affected by the electrolyte flow.

We attempted to observe the electrolyte flow behavior during machining so that we might determine the stabilizing phenomenon, and the effect of flow on surface finish but we did not succeed in developing a satisfactory observation technique. Our approaches are reported in Appendix II-8.

* See Appendix II-2.

APPENDIX II

DEVELOPMENT TESTS

All development tests are described in this appendix with sufficient information to enable other installations to duplicate these tests.

In addition, results are included in this appendix that have not appeared in the main body of the report.

II.1 Operating Parameters Studies

II.1.1 Test Series JB-1

We completed test series JB-1 prior to this contract.⁽¹⁾ We used the data for conclusions in this investigation which we report in Section 2, Chapter III.

II.1.2 Test Series JB-2

We conducted our tests on annealed René 41, and NaCl electrolyte.

II.1.2.1 Purpose

- (a) To identify significant operating parameters and response variables for this combination.
- (b) To estimate the metal removal factor K (in^3 metal removed/amp-min).

II.1.2.2 Design of Experiment

We used a four-variable Box design test.

II.1.2.3 Test Facilities and Tooling

The test facility components are identified by (A) through (Y), Figures 85 and 86, and the tooling components by (1) through (13), Figure 87.

A flat anode (1) and a flat cathode (2) both 0.250" x 0.125", are aligned by plastic block (3) which has an inlet chamber (4). Plastic block (5) with exit chamber (6) is attached to block (3). The assembly of these blocks is clamped between two plates (7) and (8). Plate (7) is attached to tooling base (9). The work area is sealed with "O" rings (10) and rubber grommets (11). A hand-operated valve (W) controls the outlet pressure. The pressure and inlet temperature are sensed at (12) and (13).

The anode (1) is clamped in a holder (Y), and it advances toward the cathode (2) when the feed mechanism is actuated. The feed mechanism consists of a Bodine constant speed motor (B_1), change gears (B_2), and lead screw (B_3). The lead screw (B_3) drives the head (B_4) and the anode holder (Y). The head (B_4) is aligned with the fixture base by guide posts (B_5). The electrolyte inlet pressure is regulated by the pump speed which is controlled by an air-operated remote control station (X). The current leads from the power supply are connected to the anode holder (Y) and to the cathode (2).

II.1.2.4 Test Procedure

We adjusted feed rate, gap, inlet temperature, and NaCl concentration for each test point, and held the electrolyte pressure constant at 166-167 psig. We adjusted the gap between anode and cathode while the electrolyte was flowing. We lowered the anode until it touched the cathode (determined by an ohmmeter). We then set the desired gap dimensions and checked it on a Ames 0.0001" dial indicator.

The test was controlled by a GraLab 15-minute timer which simultaneously actuated the power supply and the feed mechanism. During pre-trials, we varied the voltage until the starting current and the operating current for a given gap were equal. The current signals were plotted on a Sanborn recording device. When the currents were equal, metal was removed from the anode at the same rate the anode advanced toward the cathode.

(1) See References.

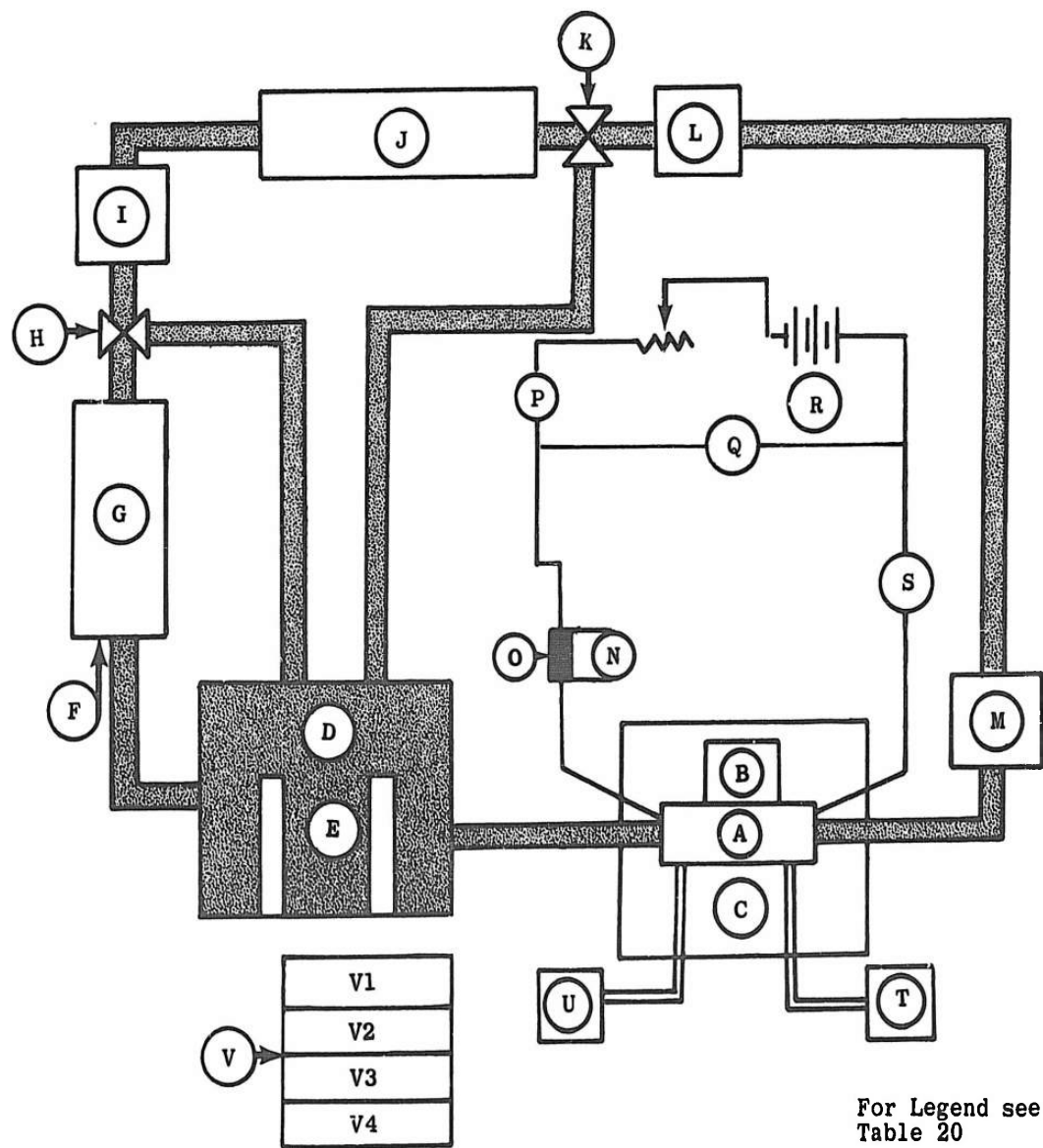


Figure 85. Facility Layout - Operating Parameter Studies

TABLE 20
LEGEND FOR FACILITY INPUT
OPERATING PARAMETER STUDIES
FIGURES 85 & 86

A. Test Tooling	K. Manual By-pass Valve	U. Outlet Pressure Gage
B. ⁽¹⁾ Feed System	L. G. P. M. Recorder	V. Sanborn Recorder
C. Splash Tank	M. Line Pressure Gage	V. A. C. -D. C. Preamp
D. Supply Tank	N. Millivolt Overload Relay	V ₂ . Carrier Preamp
E. Submersible Heaters	O. Shunt	V ₃ . Low Level Preamp
F. Electrolyte Flow	P. Ammeter	V ₄ . Low Level Preamp
G. Pump (Moyno Screw Type)	Q. Voltmeter	W. ⁽³⁾ Hand Operated Valve
H. Overload By-pass Valve	R. Power Supply ⁽²⁾	X. ⁽³⁾ Remote Pump Control
I. Cartridge Filter	S. Digital Voltmeter	Y. ⁽³⁾ Station Anode Hold
J. Heat Exchanger - Cooling	T. Inlet Pressure Gage	

NOTES:

- (1) See Figure 86 for B₁, B₂, B₃, B₄ and B₅.
- (2) Power supply - Warner Brothers 23 V, 1000 amp output or Perkins 50 V, 50 amp output.
- (3) See Figure 86.

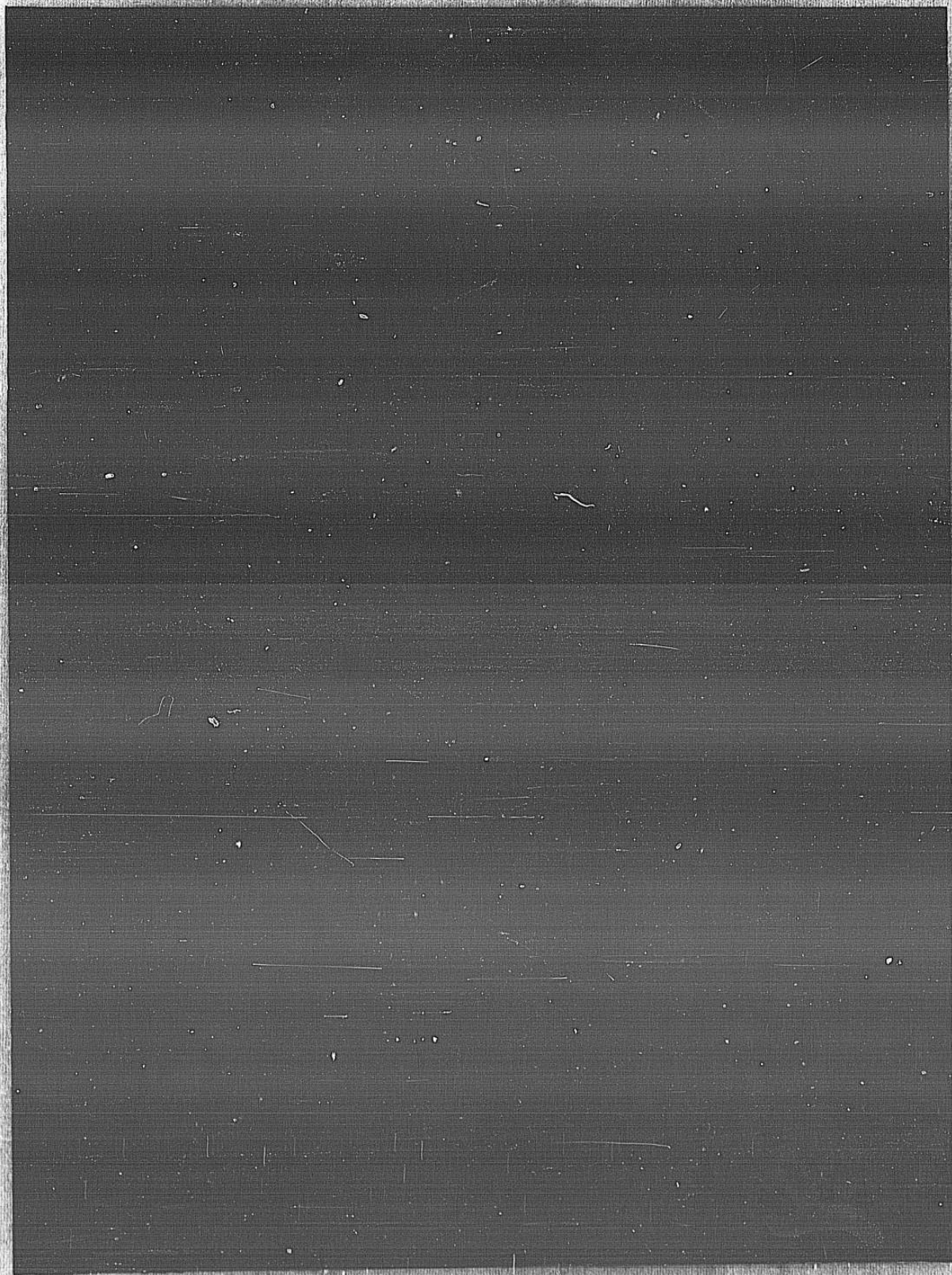


Figure 86. Test Facility - Operating Parameter Studies

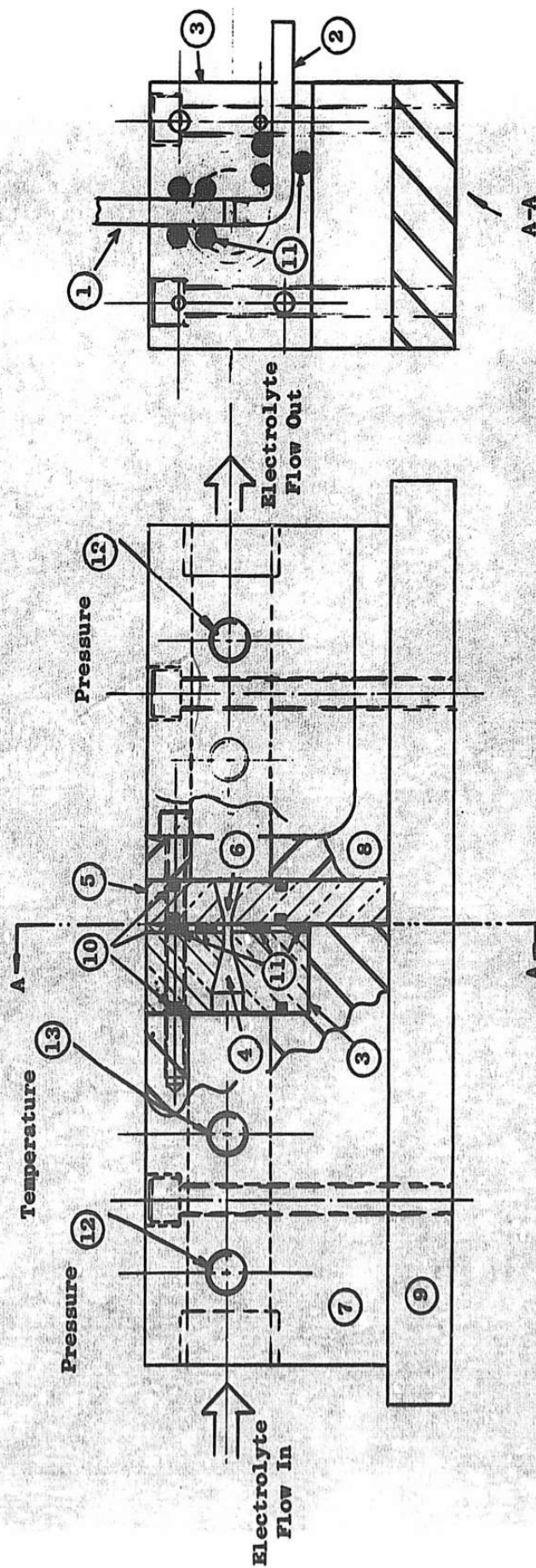


Figure 87. Schematic Sketch of Tooling for Test Series JB-2 and JB-3

II.1.2.5 Test Analysis and Results

We used analysis of variance.

The test results are summarized in Section 3, Chapter III.

II.1.3. Test Series JB-3

We conducted our tests on annealed SAE1025 tool steel with 26.4 gm/l NaNO_2 and 120 gm/l NaHCO_2 electrolyte.

II.1.3.1 Purpose

- (a) To identify significant operating parameters and response variables.
- (b) To estimate the metal removal factor (K).

II.1.3.2 Design of Experiment

We used a four-variable 1/2 replicated Box design test.

II.1.3.3 Test Facilities and Tooling

We conducted our tests in the facility and tooling described under Test Series JB-2.

II.1.3.4 Test Procedure

Same as for Test Series JB-2 except we held the electrolyte concentration constant and varied the pressure.

II.1.3.5 Test Analysis and Results

We used analysis of variance.

The analysis of the factors which affect current and applied voltage is summarized in Section 2, Chapter III.

We estimated K to be $0.76 \times 10^{-4} \text{ in}^3/\text{amp-min}$ for the SAE1025- $\text{NaNO}_2/\text{NaHCO}_2$ combination.

II.1.4 Test Series JB-4

We conducted our tests on annealed René 41 with 280 gm/l NaCl electrolyte at 85 °F.

II.1.4.1 Purpose

- (a) To determine the effect of tested factors on ratio of $\frac{\bar{r}}{\rho}$.
- (b) To determine the factors which affect surface roughness. See Appendix II.5.6.
- (c) To inspect test samples for subsurface defects. See Appendix II.5.7.

II.1.4.2 Design of Experiment

We did not use a statistical design of experiment in this test series. We varied the following factors so as to achieve a variety of operating conditions:

- (a) Gap - set and maintained by voltage - 0.006" to 0.030".
- (b) Feed rate - 0.035 to 0.070 in/min
- (c) Fluid pressure in the gap - 19 to 225 psig.
- (d) Pressure drop from inlet to outlet of work area - 4 to 200 psi.

We held these factors constant during the tests:

- (a) Electrolyte concentration - 280 gm/l of NaCl.
- (b) Electrolyte temperature - 85°F.
- (c) Sludge content at the tool inlet - less than 0.2 cc/10 cc.
- (d) Cutting time - 60 sec.

II.1.4.3 Test Facilities and Tooling

Test tooling shown in Figure 88 was used in the facility described for Test Series JB-2.

A flat 0.115" x 0.187" Elkonite cathode (1) mounted on the face of a brass cylinder (2) is encased in plastic block (3). A movable Elkonite-tipped measuring pin (4) is installed in the center of the cathode (1). The pin (4) actuates a 0.0001" dial indicator (5). A flat anode (6), 0.115" x 0.187", is mounted in a cylindrical brass tool holder (7). Interchangeable disc (8) control the size of the electrolyte inlet and outlet passages. The discs are installed in the tool body (9) and aligned with the cathode (1) by dowel pin (10). A rectangular hole (11) in the disc (8) aligns the anode (6) with the cathode (1). The anode (6) and cathode (1) are also aligned by concentric holes in the tool body (9). The inlet pressure is sensed at (12), the outlet pressure at (13), the inlet temperature at (14), and the outlet temperature at (15). A hand-operated valve (W-Figure 86) controls the outlet pressure.

II.1.4.4 Test Procedure

We used the same test procedure as Test Series JB-2, except that we incorporated refinements. With the tooling assembled and the anode in position at approximately the test gap, the pump was turned on and the gap pressure regulated to approximately test pressure. The gap measuring pin was then advanced from a flush position with the cathode until contact was made with the anode (checked with an ohmmeter), and the gap distance read from a 0.0001" indicator. The pin was then retracted and the gap adjusted to within ± 0.0001 " of the test dimension. At this time, the test flow and pressure were set. A final gap check was made before the test point was attempted. The system was then energized with the "GraLab" timer which simultaneously actuated the feed system and the power supply.

Prior to actuating the system, a voltage was selected and set which would be near the test requirement. Several pretrials were then made with voltage adjustment until the current remained within ± 0.1 ampere of the starting current as recorded on the Sanborn device, and until the final gap measured within ± 0.0002 " of the test

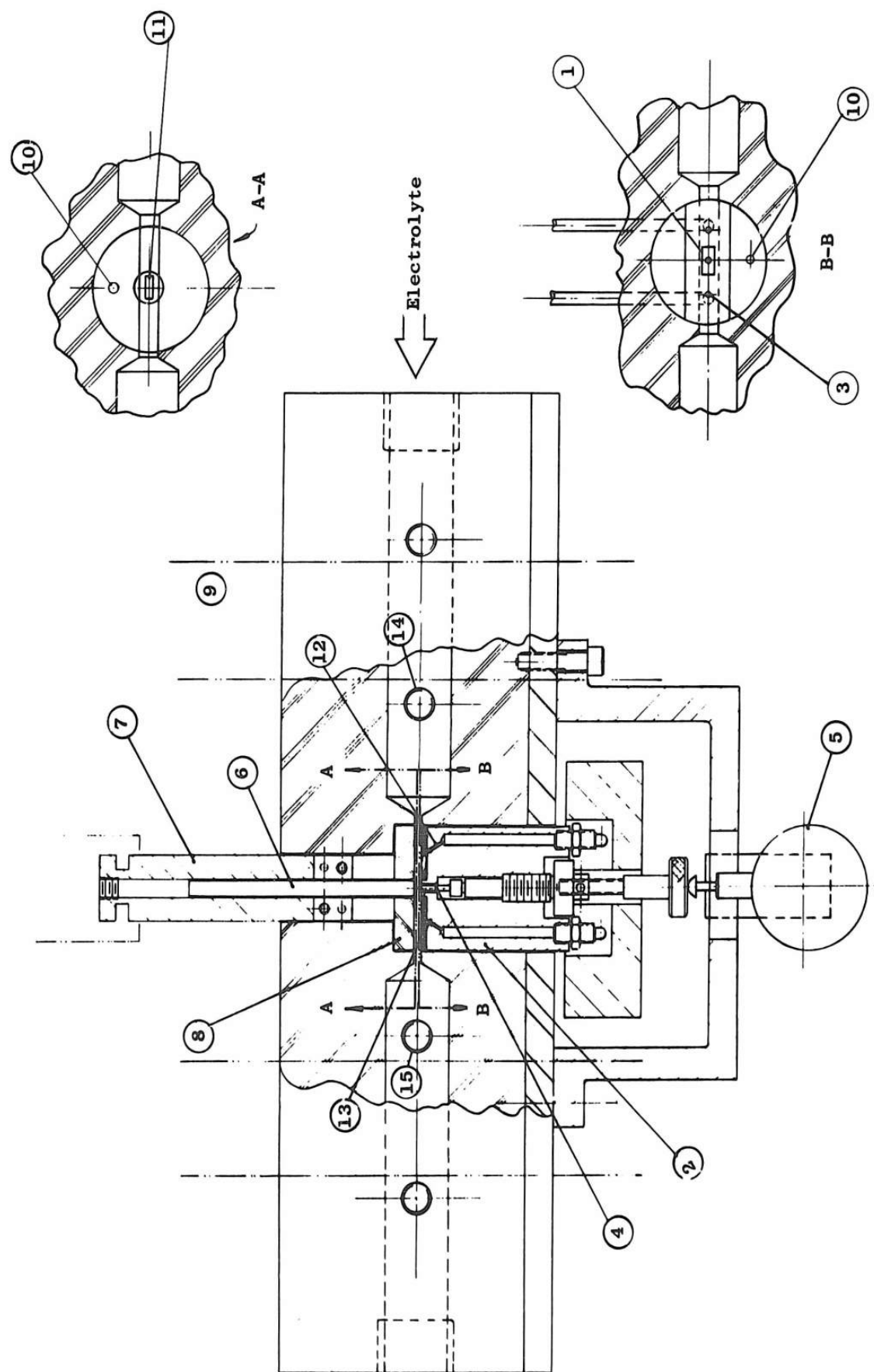


Figure 88. Schematic Sketch of Tooling for Test Series JB-4-5-8-9

requirements. A final gap measurement was always made with the electrolyte flowing at test levels. When these conditions were met, metal was removed from the anode at the same rate as the anode was being fed toward the cathode.

II.1.4.5 Test Results

The cutting gap affected the value of ratio $\frac{\bar{r}}{\rho}$ significantly, Figure 89.

Average static pressure, pressure drop, and feed rate did not significantly affect the $\frac{\bar{r}}{\rho}$ ratio.

II.1.5 Test Series JB-5 and JB-5A

We conducted our tests on annealed René 41 with 275 gm/l NaCl electrolyte at 85°F.

II.1.5.1 Purpose

To estimate $\Delta \hat{E}$ for a variety of gap and feed rates.

II.1.5.2 Design of Experiment

We ran two-factor experiments with replications at the following levels:

<u>Factors</u>	<u>Levels</u>
Feed rate (in/min)	.02-.04-.06-.08
Gap (in)	.006-.010-.012-.015-.020-.025-.030
Inlet & Outlet pressures (psig)	Varied randomly
Inlet temperature (°F)	85°F constant
Concentration NaCl (gm/l)	275 constant

At 0.004", the only feed rate levels tested were at 0.04 and 0.06 in/min.

We conducted our experiments in the facility and tooling described for Test Series JB-4, and we used the same procedure.

II.1.5.3 Test Analysis and Results

- The estimate of $\Delta \hat{E}$ is described in Section 2, Chapter III.
- The $\Delta \hat{E}$ was not significantly affected by the factors tested, Table 21.

II.1.6 Test Series JB-8

We conducted our tests on annealed A-286 with 600 gm/l NaNO₃ electrolyte.

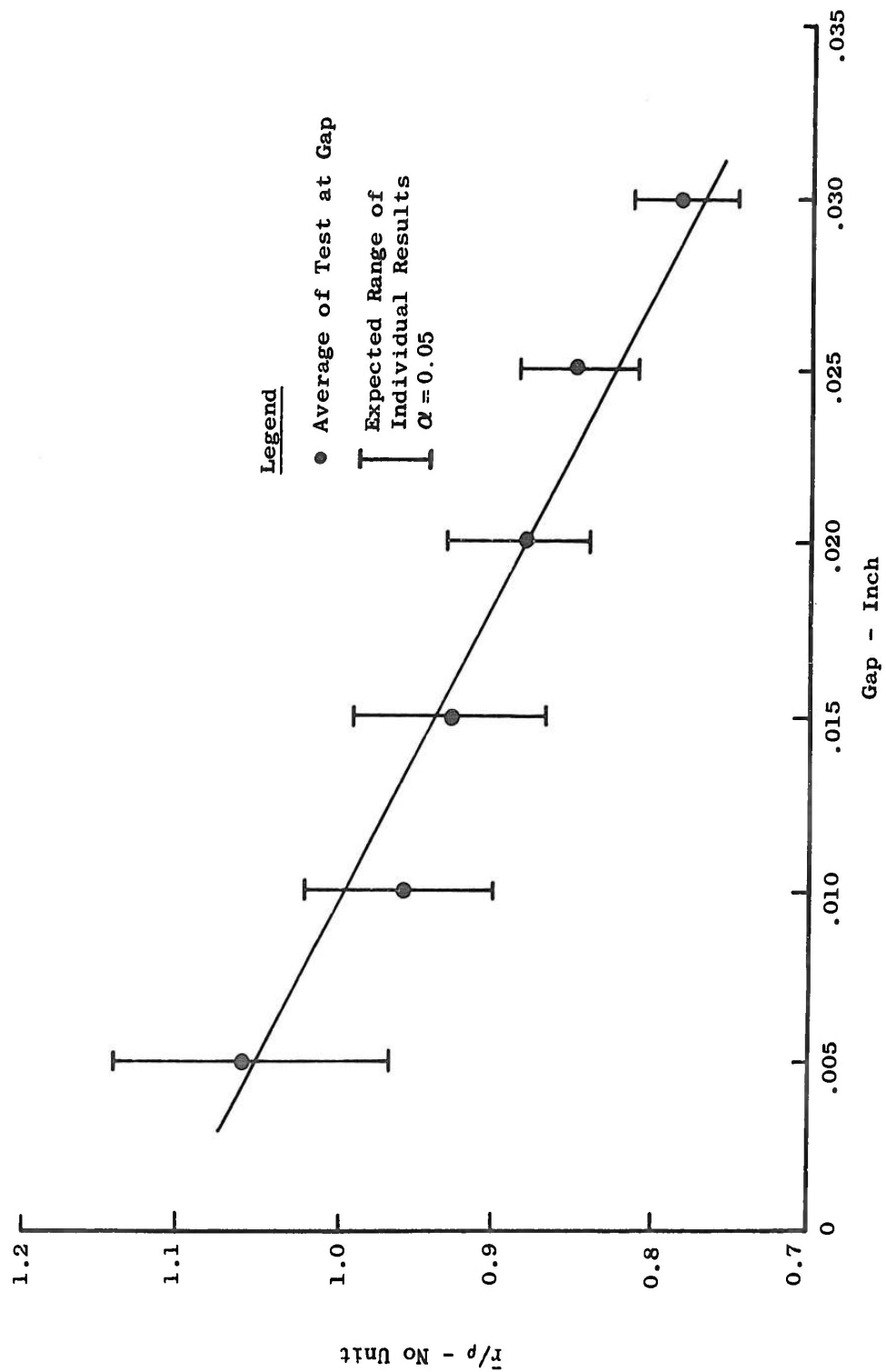


Figure 89. \bar{r}/ρ - vs Gap-Test Series JB-4

TABLE 21
ESTIMATES OF $\hat{\Delta E}$
TEST SERIES JB-5 AND JB-5A

From Test Series	Gap Inch	Number of Tests n	Intersect a	Slope b
JB-5	.006	8	2.70	0.535
JB-5	.010	8	2.62	0.760
JB-5A	.012	8	3.23	0.800
JB-5	.015	8	3.19	0.928
JB-5A	.015	5	2.84	0.989
JB-5	.020	8	3.27	1.314
JB-5	.025	8	2.42	1.704
JB-5A	.030	4	3.57	1.812
JB-5A	.004	3	2.33	0.447

From $E = a + bI$

a is estimate $\hat{\Delta E}$

b is slope of the linear curve

F ratio for $\frac{\left(\hat{S^2_{\Delta E}}\right)_2}{\left(\hat{S^2_{\Delta E}}\right)_1} = 0.057$, where $\left(\hat{S^2_{\Delta E}}\right)_2$ is for the residual from the curve fit, and $\left(\hat{S^2_{\Delta E}}\right)_1$ is for the expected variation in $\hat{\Delta E}$ from the intercept at $I = 0$.

Therefore, the estimate of $\hat{\Delta E}$'s from the intercept are likely to be random estimates of a common $\hat{\Delta E}$.

II.1.6.1 Purpose

- (a) To identify significant operating parameters and response variables when A-286 is machined with NaNO_3 electrolyte and when gap pressures and pressure drops are allowed to vary randomly.
- (b) To estimate the metal removal factor.
- (c) To determine the effect of operating parameters and response variables on the surface finish. See Appendix II.5.7.

II.1.6.2 Design of Experiment

We ran two factorial experiments with some common test points,
Figure 90.

II.1.6.3 Test Facilities and Tooling

The facilities used were the same as those described for Test Series JB-2. The test tooling used was the same as that shown in Figure 88 under Test Series JB-4, except that the discs (8) were altered to a width of 0.115", which is the width of the anode.

II.1.6.4 Test Procedure

Same as for Test Series JB-4.

II.1.6.5 Test Analysis and Results

We used analysis of variance.

The factors which affect current are reported in Section 2, Chapter

III.

The factors which determine applied voltage are shown in Figure 90.

The estimate of the metal removal factor is reported in Section 2,

Chapter III.

II.1.7 Test Series JB-9

We conducted our tests on annealed A-286 with 600 gm/l NaNO_3 electrolyte.

II.1.7.1 Purpose

- (a) To determine if, in addition to these factors identified in Test Series JB-8, pressure drop and gap pressure affect the current and applied voltage.
- (b) To estimate the metal removal factor.
- (c) To estimate the ΔE for the combination.
- (d) To determine the effect of test factors on the ratio $\frac{\bar{r}}{\rho}$.
- (e) To determine the effect of the test factors on surface roughness. See Appendix II.5.8.

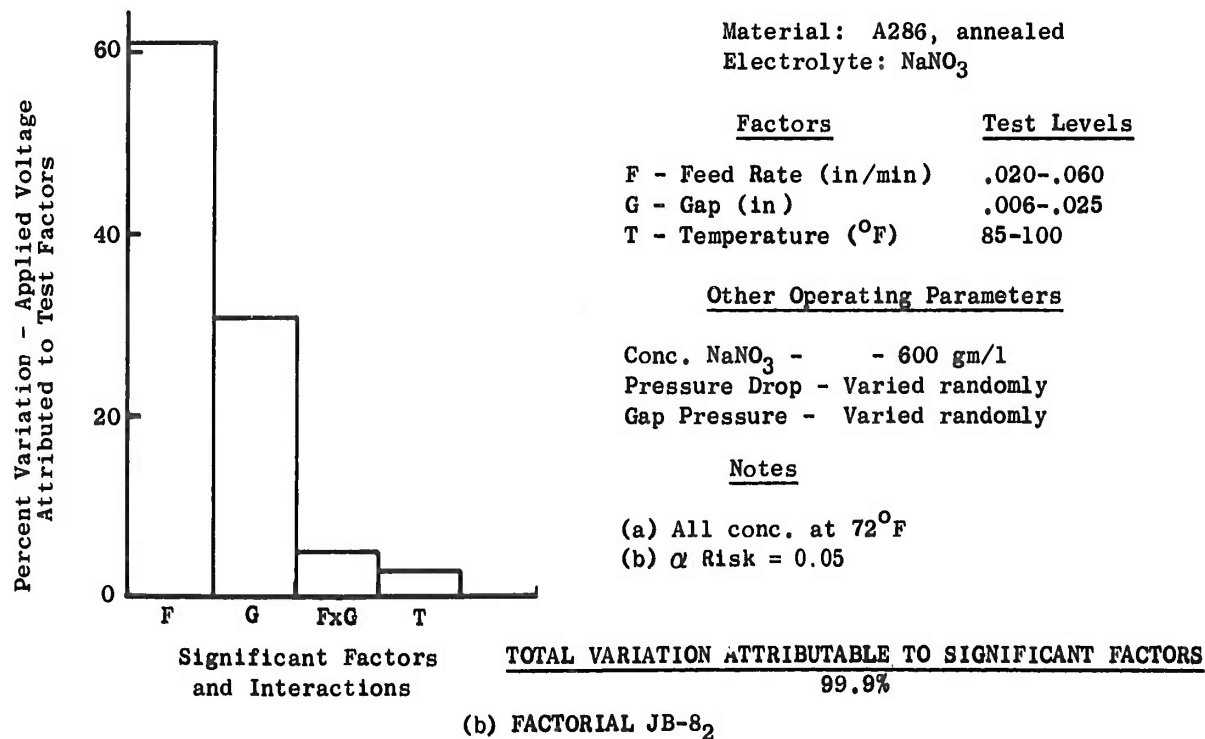
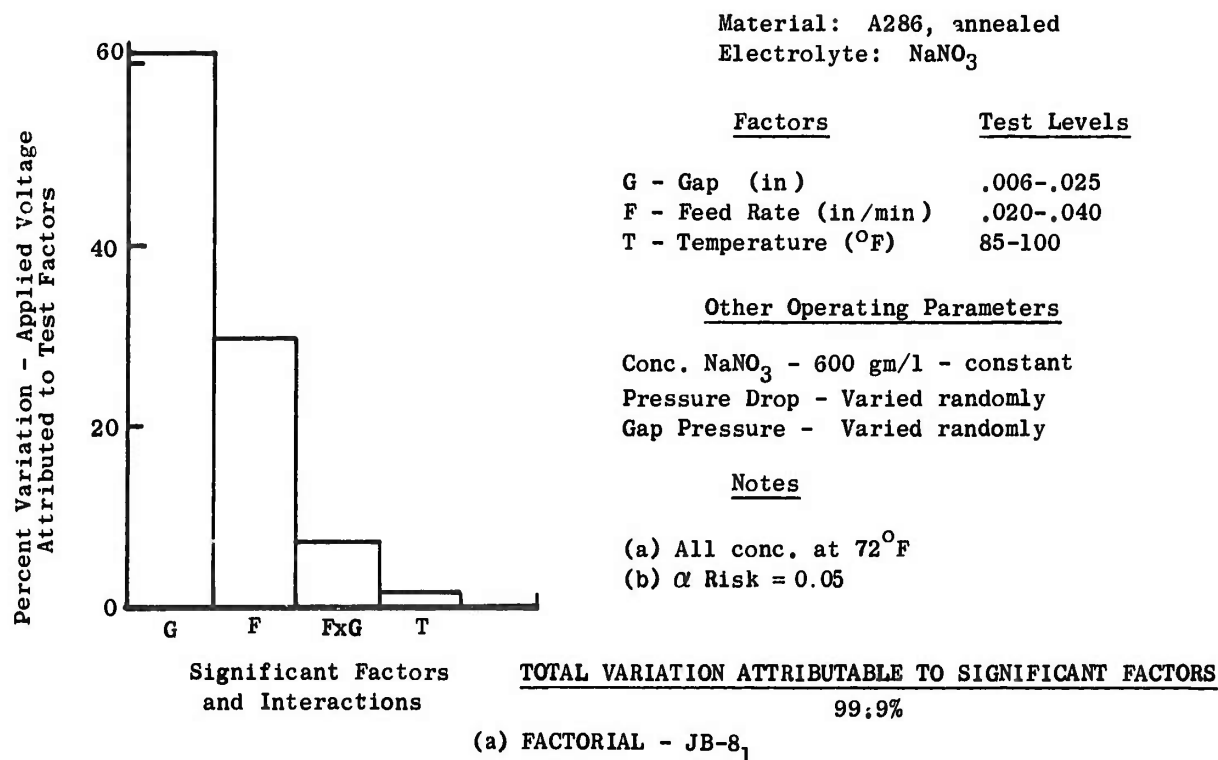


Figure 90. Significant Factors Determining Applied Voltage Test Series JB-8

II. 1. 7. 2 Design of Experiment

We used a five-factor experiment.

We conducted our experiments in the facility and tooling described for Test Series JB-8, and the test procedure used in Test Series JB-4.

II. 1. 7. 3 Test Analysis and Results

We used analysis of variance. The factors which affect current and determine applied voltage are reported in Section 2, Chapter III.

The estimate of ΔE is reported in Section 2, Chapter III. In Table 22, we show that ΔE , as determined, may be considered constant for the test conditions.

Average gap pressure, pressure drop, temperature and feed rate did not significantly affect the ratio of $\frac{\bar{r}}{\rho}$. However, the gap distance did affect $\frac{\bar{r}}{\rho}$ as follows:

<u>At Gap</u>	<u>Average value</u> <u>$\frac{\bar{r}}{\rho}$</u>	<u>Range of $\frac{\bar{r}}{\rho}$</u> <u>during test</u>
0.012"	0.924	0.87 to 0.98
0.025"	0.802	0.75 to 0.86

II. 2 Temperature Studies

II. 2. 1 Test Series JB-6

We conducted our tests on annealed René 41 with NaCl electrolyte.

II. 2. 1. 1 Purpose

- (a) To observe the temperature rise in the electrolyte and at the electrode face during electrolytic machining at steady state conditions.
- (b) To determine the gaps in the direction of the electrolyte flow after machining at steady state conditions.

II. 2. 1. 2 Design of Experiment

We chose test points to represent a range of feed rates, applied pressure drops, electrolyte inlet temperatures, and electrolyte concentrations. We selected the applied voltage to establish an approximate gap. The test range for each factor was:

<u>Factor</u>	<u>Test Range</u>
Feed rate (in/min)	0.016 to 0.062
Pressure drop (PSI)	100 to 280
Inlet temperature (°F)	79 to 103
Applied voltage	4.8 to 24
NaCl concentration (gm/l)	130 to 290

TABLE 22
ESTIMATE OF $\hat{\Delta E}$
TEST SERIES JB-9

(1) For $E = \hat{\Delta E} + bI$ at various gaps

(2) By linear curve fit technique of data in Test Series JB-9, we obtain the following:

Gap inch	Temp. °F	No of Tests	Estimated $\hat{\Delta E}$	Estimated b	Estimate of Deviation from Straight Line	F* Ratio for Goodness of Linear Fit
.012	85	8	3.402	1.189	0.38	4486
.012	100	8	3.833	0.955	1.27	913
.025	85	8	3.744	2.030	4.487	1263
.025	100	8	3.900	1.750	3.28	1338

(3) *All F ratios indicate linear fit is highly probable.

(4) The residual from the curve fits, indicate a weighted variance of error expected in $\hat{\Delta E}$.

$$\left(S^2_{\hat{\Delta E}} \right)_1 = 0.253$$

(5) However, from the four calculated $\hat{\Delta E}$, the variance is

$$\left(S^2_{\hat{\Delta E}} \right)_2 = 0.0489$$

$$\text{F ratio for } \frac{\left(S^2_{\hat{\Delta E}} \right)_2}{\left(S^2_{\hat{\Delta E}} \right)_1} = 0.193$$

is of insignificant value.

(6) Therefore, the four estimated $\hat{\Delta E}$'s are likely to be random estimates of a common $\hat{\Delta E}$.

II. 2. 1. 3 Test Facilities and Tooling

The test facility is described in Appendix II. 1, Test Series JB-2 except as noted below:

A Bristol millivolt recorder was used in the test facility to record thermocouple millivolt outputs.

The test tooling is shown schematically in Figure 91. A flat cathode (1) and a flat anode (2), both machined to .115" x .937", are aligned by inserts (3) and (4) in tool body (5). The cathode (1) contains three electrically insulated thermocouples (6) mounted within 0.010" from the surface of the cathode (1). One couple is located in the center of the cathode (1) and two are spaced .400" from the center. The inserts (3) and (4) are adjustable in a vertical direction for setting flow passage gaps. Pressure tubes (7) are mounted in inserts (3); one for inlet, the other for outlet pressure. These tubes (7) are located 3/8" from the cathode (1). The inlet and outlet temperatures are sensed at (8); the inlet and outlet pressures at (9). The work area is sealed with rubber gaskets (10) and (12), and flat rubber strips (11). The face plate (13) is locked in place with eight bolts (14).

The alignment of inserts (3), (4), and cathode (1) was checked by a Bausch and Lomb 40X microscope with a lens insert graduated in 0.0001". The microscope was mounted on a small compound table which is attached to the basic fixture. A microscope light behind the tooling was connected to the table.

II. 2. 1. 4 Test Procedure

We advanced that anode at the start of each test until a predetermined gap had been established. This was checked with the graduated microscope. We turned the pump on and set the pressure at a predetermined level. The system was energized by the use of the GraLab timer which simultaneously actuated the feed and the power supply. We observed the process through the microscope and we adjusted the voltage until the rate of metal removal matched the anode feed rate. After the steady state condition was attained and held for thirty seconds, we turned off the power supply and feed simultaneously, but we maintained the electrolyte pressure. We used the calibrated microscope to measure the gaps after the machining process.

The temperatures reported were those recorded at the steady state condition.

II. 2. 1. 5 Test Analysis and Results

The observed electrolyte and tool temperature, and the measured gaps for the test conditions are shown in Figures 92 through 95.

II. 2. 2 Test Series JB-7

We conducted our tests on annealed A-286 and 600 gm/l NaNO_3 electrolyte.

II. 2. 2. 1 Purpose

- (a) To observe the temperature rise in the electrolyte and at the tool face during electrolytic machining at steady state conditions when A-286 is machined with NaNO_3 electrolyte.
- (b) To determine the gap in the direction of the electrolyte flow after machining at steady state conditions.

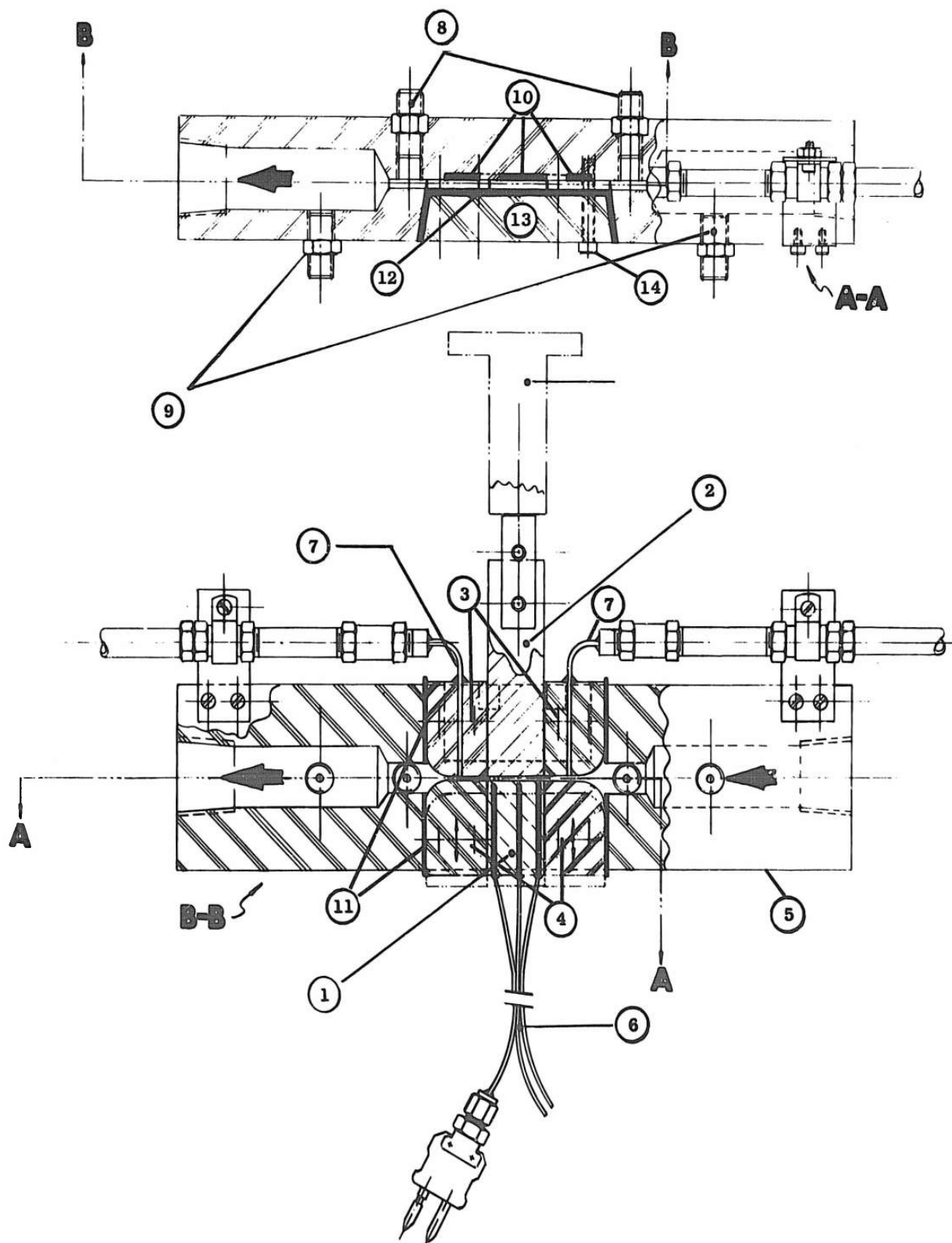
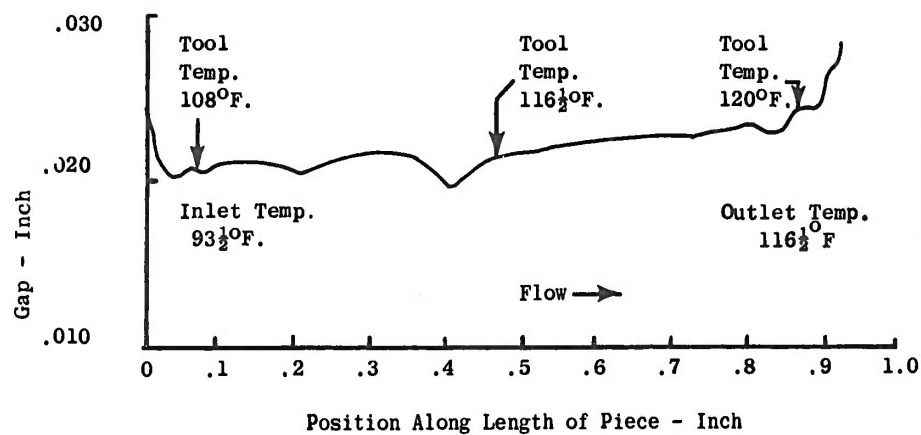
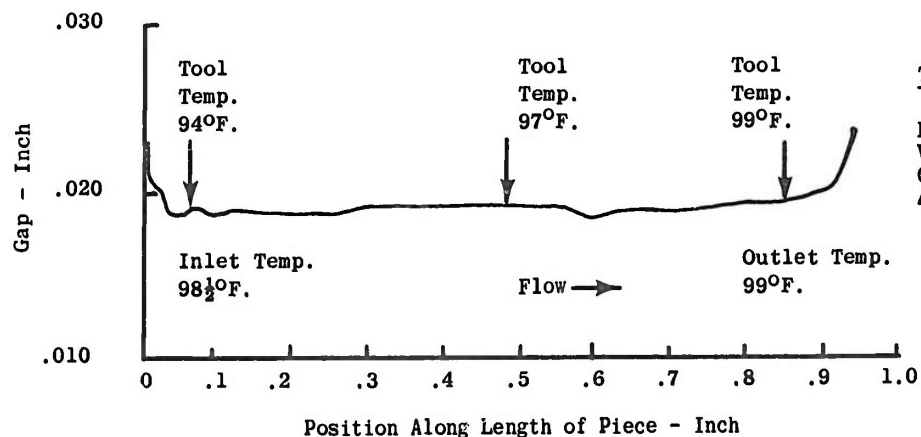


Figure 91. Schematic Sketch of Tooling for Temperature Studies



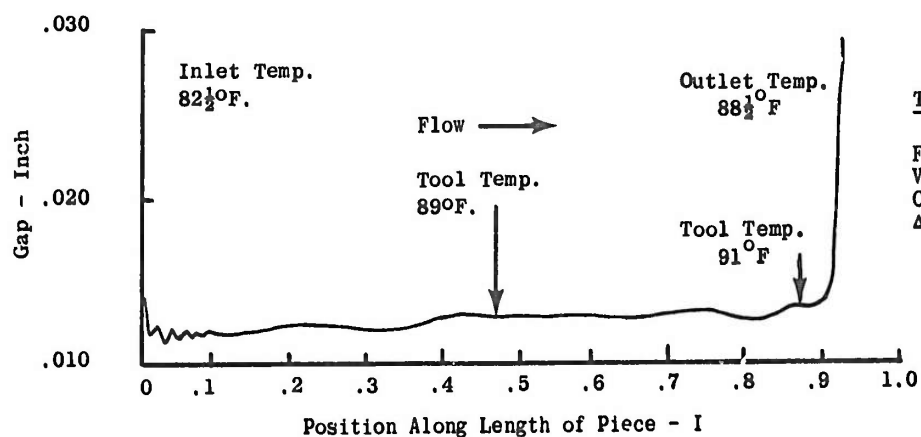
Test #2 Conditions

Feed Rate - 0.0611 in/min
Voltage - 18.6 volt
Current - 69.0 amp
Δ Pressure - 243 psi



Test #3 Conditions

Feed Rate - 0.0199 in/min
Voltage - 7.9 volt
Current - 240 amp
Δ Pressure - 168 psi

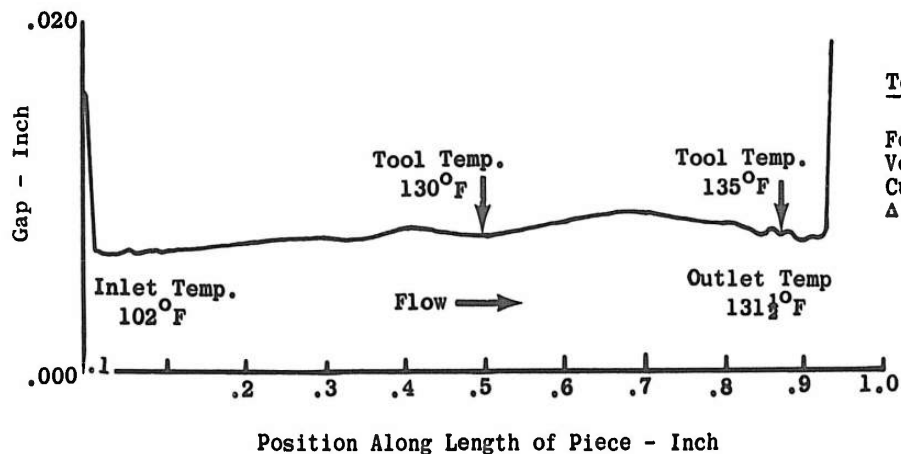
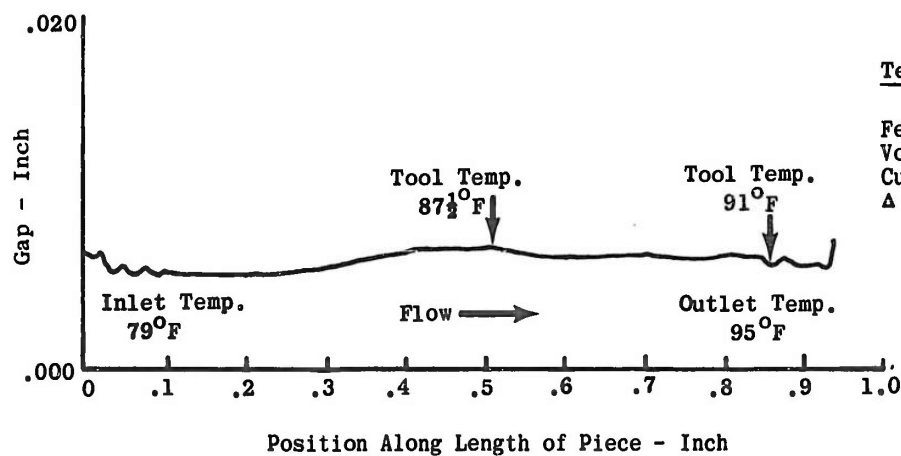
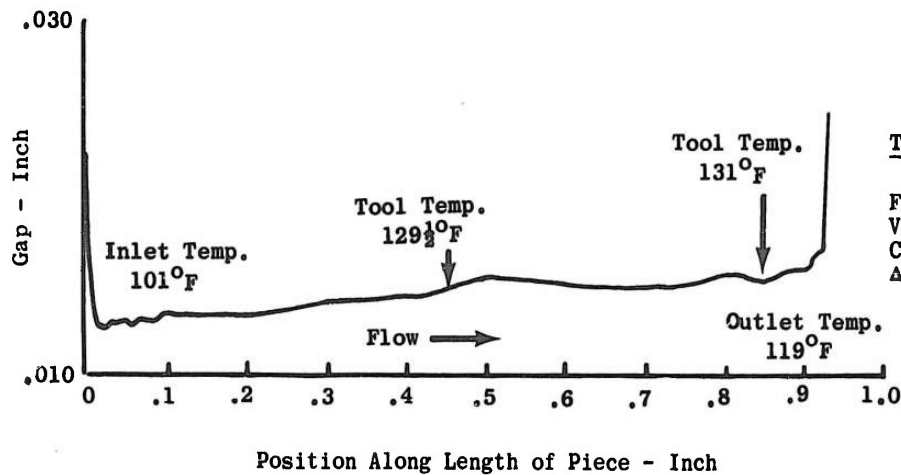


Test #4 Conditions

Feed Rate - 0.0385 in/min
Voltage - 10.6 volt
Current - 44.8 amp
Δ Pressure - 201 psi

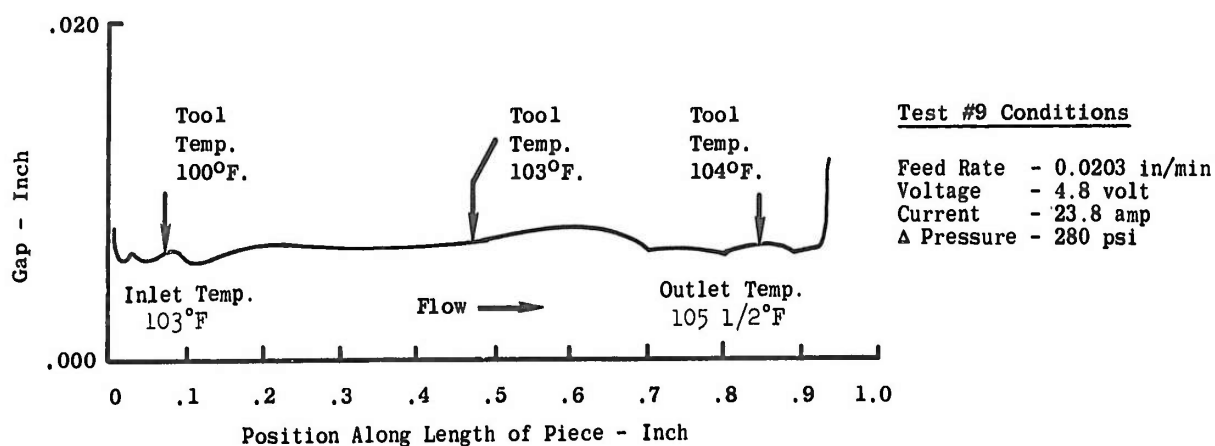
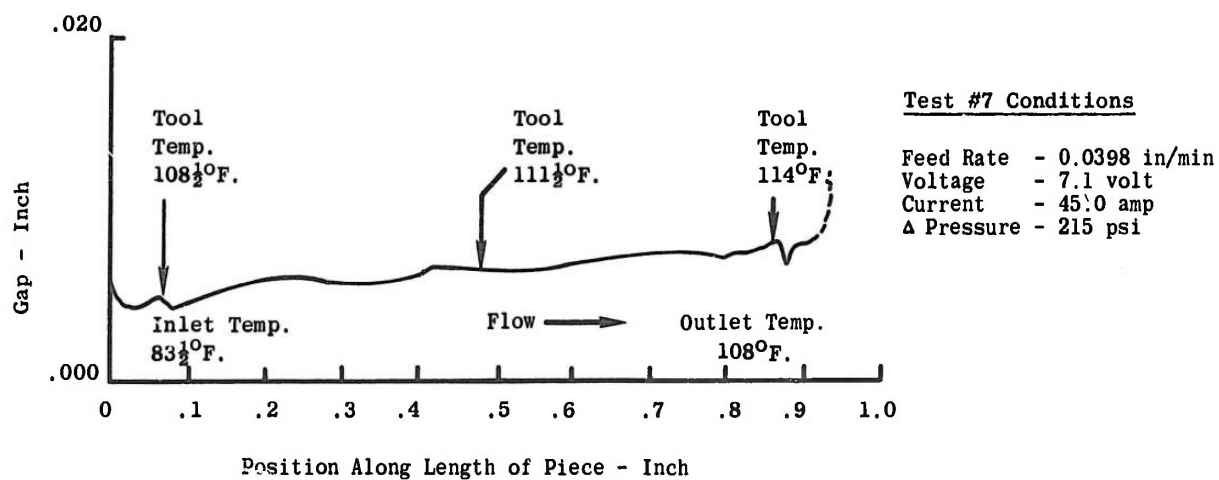
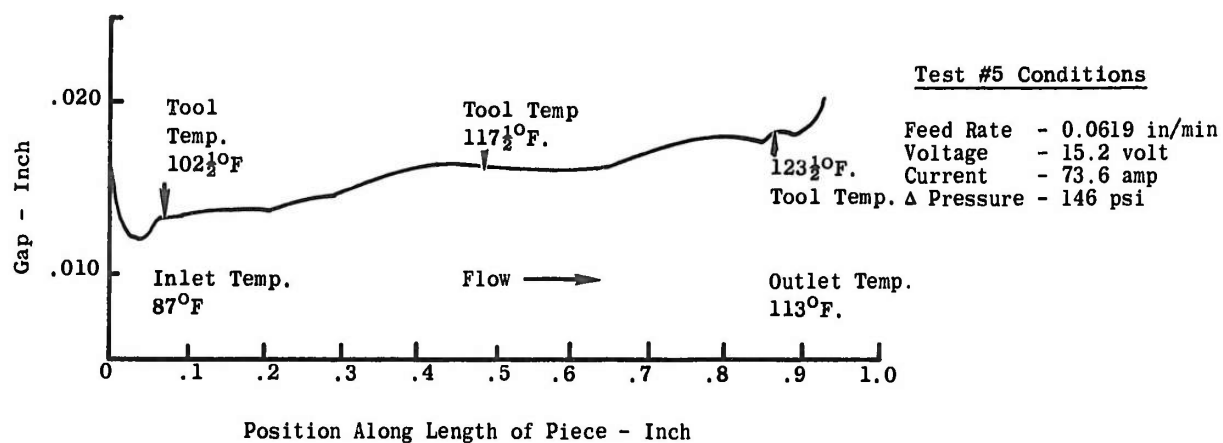
Annealed René 41 - NaCl, 290 gm/liter

Figure 92. Gap vs Temperature Profile Test Series JB-6



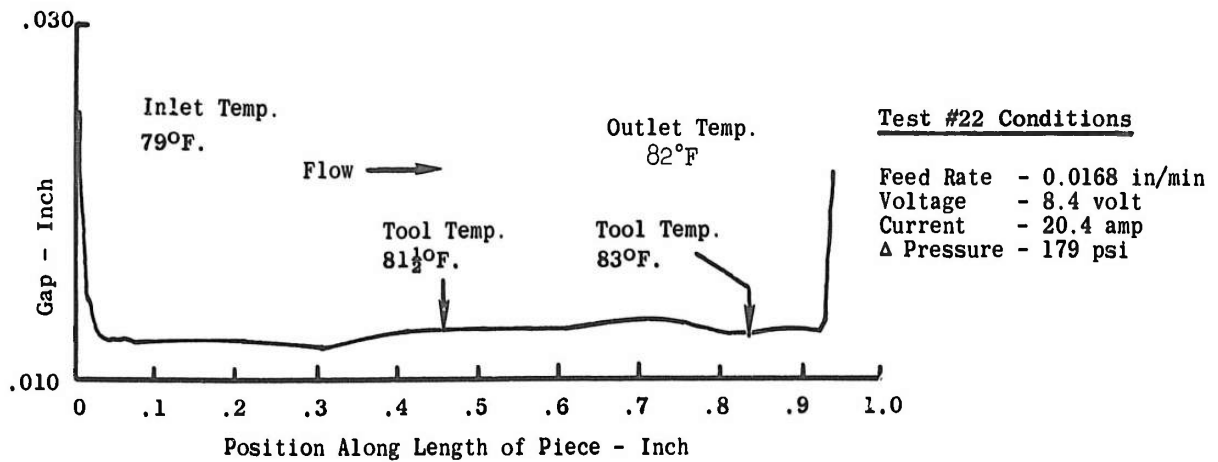
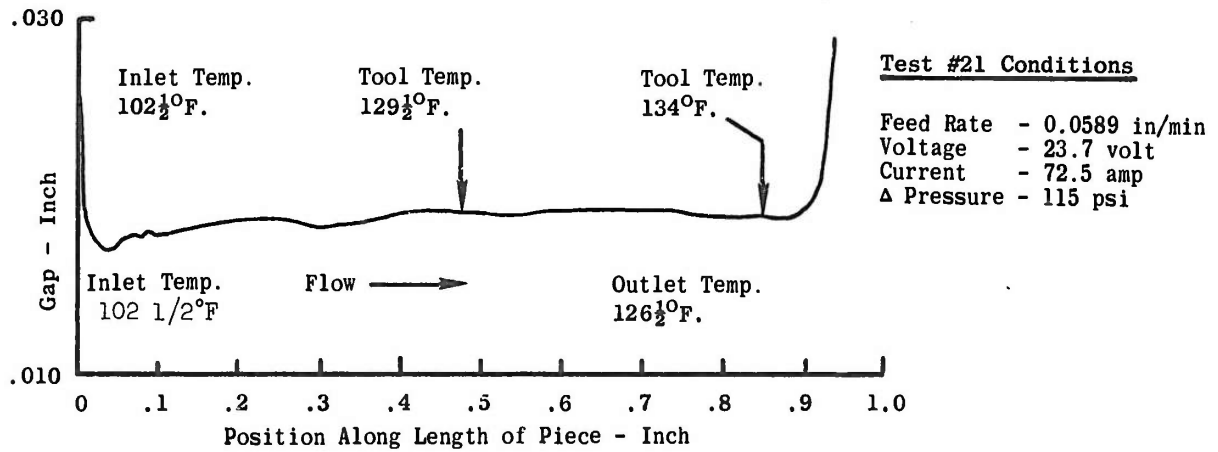
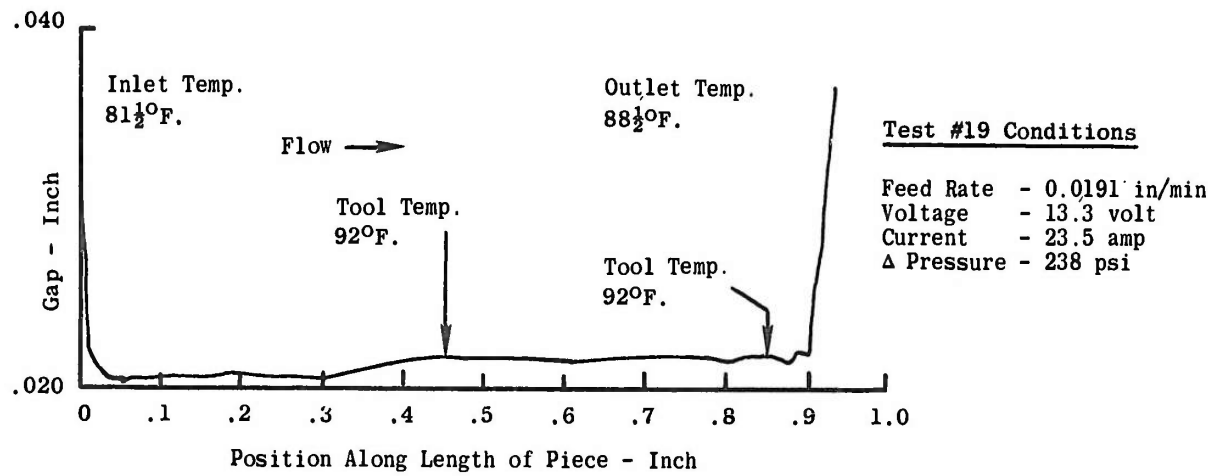
Annealed René 41 - NaCl, 130 gm/l

Figure 93. Gap vs Temperature Profile Test Series JB-6



Annealed René 41 - NaCl, 290 gm/l

Figure 94. Gap vs Temperature Profile Test Series JB-6



Annealed René 41 - NaCl, 130 gm/l

Figure 95. Gap vs Temperature Profile Test Series JB-6

II. 2. 2. 2 Design of Experiment

We tested at an approximate gap of 0.007". We varied the feed rate and the pressure drops. We selected the applied voltage to establish the approximate gap.

The test range for each factor was:

<u>Factors</u>	<u>Test Ranges</u>
Feed rate (in/min)	0.020 to 0.061
Applied volts	5.4 to 10.2
Pressure drop (psi)	100 to 245

We conducted our tests in the facility and tooling described for Test Series JB-6, and we used the same procedure.

II. 2. 2. 3 Test Analysis and Results

The observed tool and electrolyte temperatures and the measured gaps are shown in Figure 96.

II. 3 Ripple Study

We conducted our tests on annealed René 41 with NaCl electrolyte.

II. 3. 1 Purpose

To determine if the amount of ripple in a DC power supply affects the metal removal rate or the voltage/current relationship.

II. 3. 2 Experimental Data

We compared data from Test Series JB-2, JB-4 and JB-5. The operating conditions selected for these tests were the same, except that the ripple in the power supply varied.

II. 3. 3 Test Facilities and Tooling

The facility and tooling are described in previous discussions of these test series. We used the following power packs:

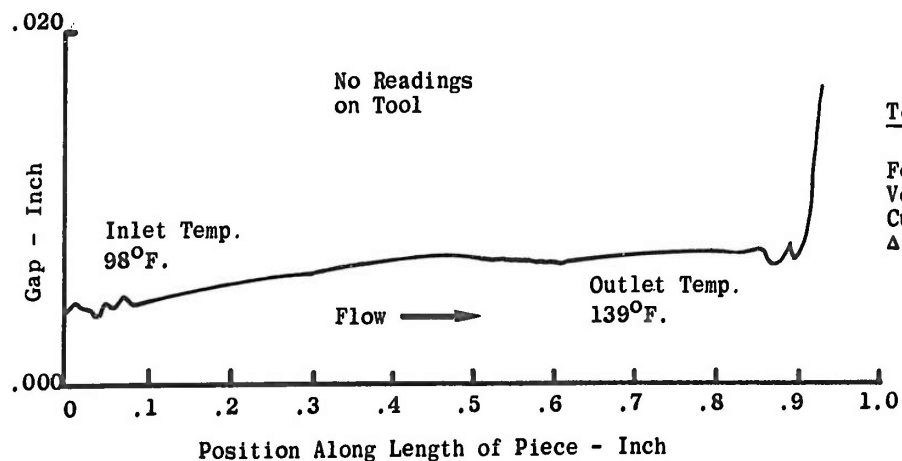
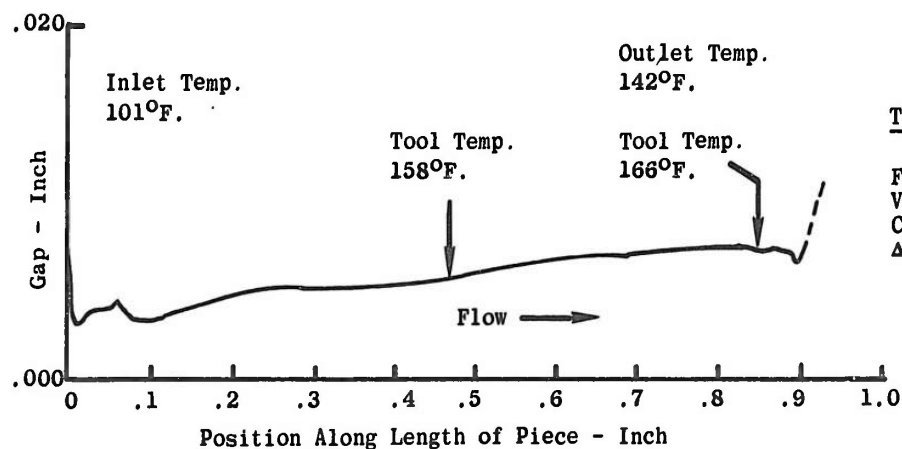
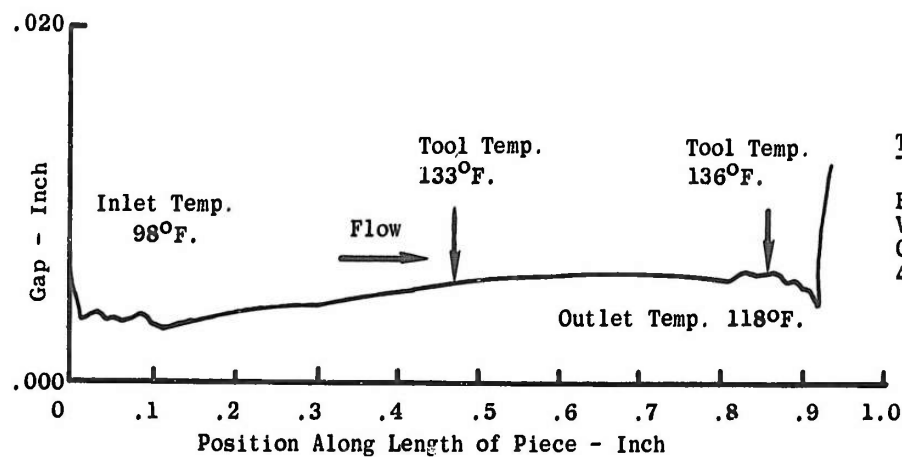
- (a) Pack #1 - Wagner - Model A18101R for Test Series JB-4
AC input - 220/440V, 3 phase, 60 cycle, amperage rating not shown.
DC outlet - 18V/1000A, rated ripple - 5% at 26 KVA.
- (b) Pack #2 - Perkins - Model M1193 for Test Series JB-2 and JB-5
AC input - 420-460V, 11 amp, single phase, 60 cycle
DC output - 50V/60A, rated ripple - 1% at 2.5 KVA.

II. 3. 4 Test Procedures

We determined the ripple with a Dumont type 304H cathode ray oscillograph.

II. 3. 5 Test Analysis and Results

Figure 97 reports the ripple in the DC voltage for the two power packs.



Annealed A-286 - NaNO_3 , 600 gm/l

Figure 96. Gap vs Temperature Profile Test Series JB-7

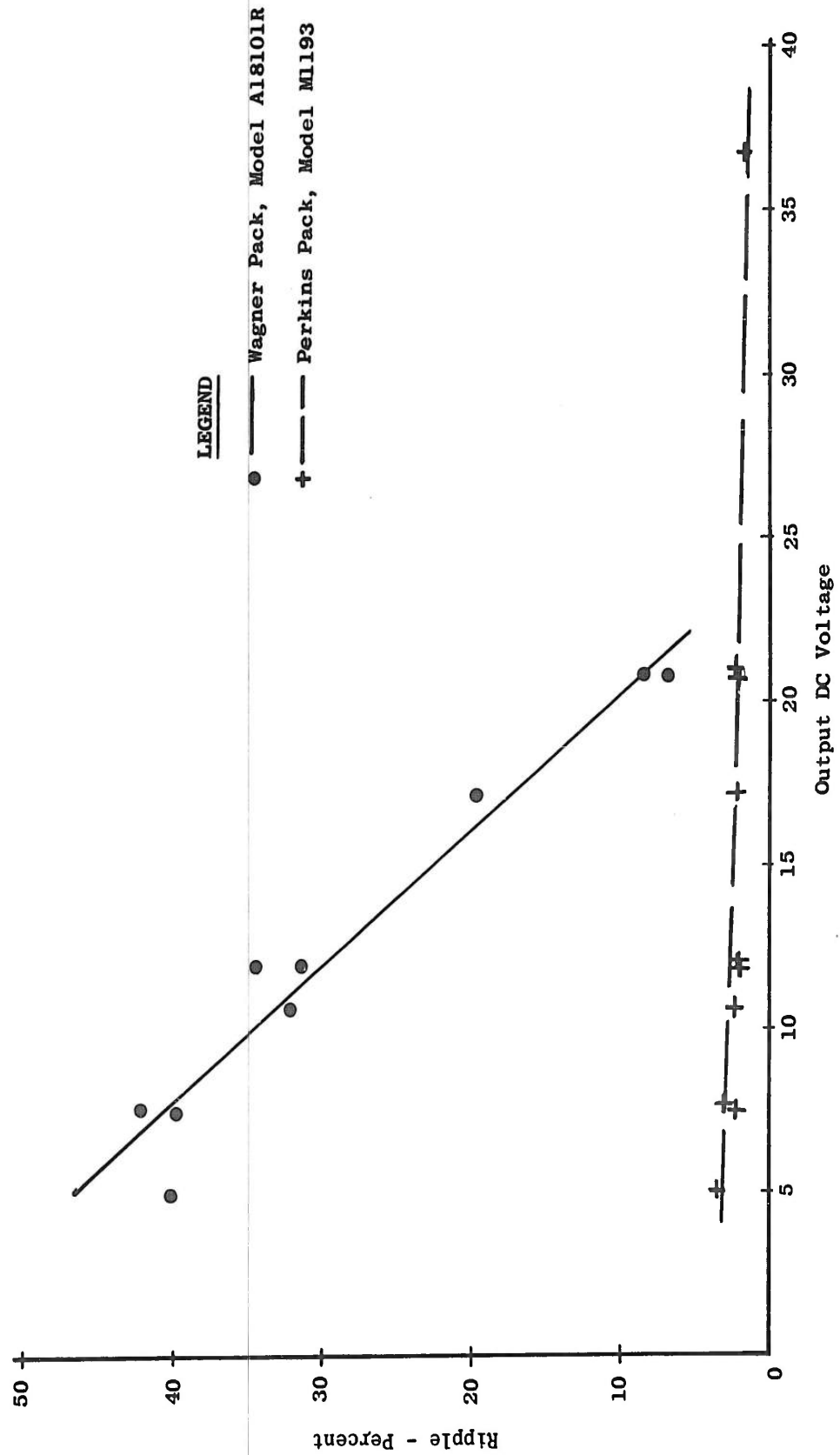


Figure 97. Percent Ripple vs DC Voltage

The wave form of the DC voltage in the Perkins power pack is sinusoidal. The wave form of the DC voltage in the Wagner power is illustrated in Figure 98.

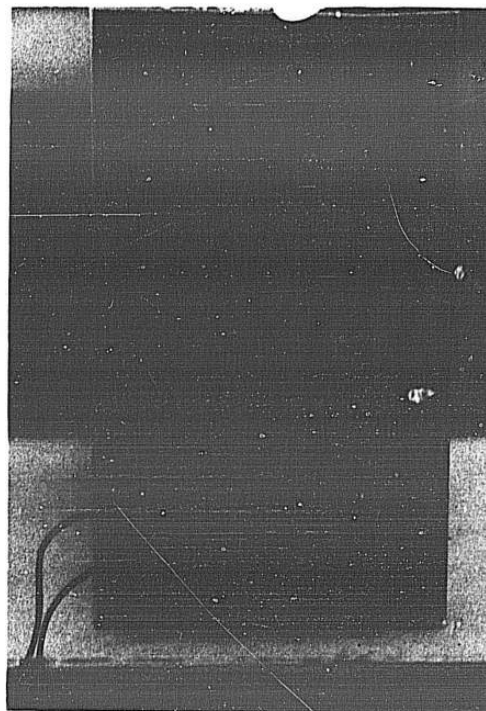


Figure 98. Wave Form of DC Voltage "WAGNER" Power Pack

Our data analysis, Table 23, shows:

- (a) There is no significant effect on the metal removal rate attributable to the ripple.
- (b) There is no significant effect on the voltage/current relationship attributable to ripple.

II.4 Sludge Study

We conducted our tests on NaCl electrolyte which had been aged by machining René 41.

II.4.1 Purpose

- (a) To determine the effect of sludge on:
 - (1) The electrolyte specific resistance.
 - (2) The electrolyte specific gravity.
 - (3) The electrolyte viscosity.
- (b) To determine the effect of temperature on sludge content.

TABLE 23
ANALYSIS OF RIPPLE EFFECT

I Ripple Effect on Metal Removal Rate

<u>At 0.0355 in/min feed rate</u>	<u>Ripple Range %</u>	<u>Test Series</u>	<u>No. of Tests</u>	<u>Average Metal Removal Rate-in³/kiloamp-hr</u>	<u>Estimated Standard Deviation</u>
Perkins Pack	1.7-3.5	JB-2	11	5.340	± 0.203
Wagner Pack	6.7-42	JB-4	8	5.344	± 0.199
<u>At 0.062 in/min feed rate</u>					
Perkins Pack	1.7-3.5	JB-5	10	5.546	± 0.101
Perkins Pack	1.7-3.5	JB-5a	4	5.618	± 0.098
Wagner Pack	6.7-42	JB-4	10	5.519	± 0.090

II Ripple Effect on E/I Relationship

Ripple Range - 1.7 to 3.5% - test series JB-5 - Perkins Power Pack

E vs I plot

$\Delta E = 2.6$ volt

slope for 0.020" gap - 1.31

slope for 0.006" gap - 0.53

Ripple Range - 6.7 to 42% - test series JB-4 - Wagner Power Pack

E vs I plot

$\Delta E = 2.8$ volts

slope for 0.020" gap - 1.31

slope for 0.006" gap - 0.49

II.4.2 Design of Experiments

We conducted a three-level, full-factorial experiment for sludge, temperature and NaCl concentration, Figure 99. We measured the viscosity of a 280 gm/l NaCl electrolyte at 75 °F over a range of sludge contents.

II.4.3 Test Facilities and Tooling

- (a) Brookfield Synchro-lectric Viscometer, Model LVF to determine viscosity.
- (b) International Clinical Centrifuge, Model CL941068-1 to determine sludge content.
- (c) Resistant bridge, Industrial Instrument Company, Model RC16B1 with a platonized conductivity cell with a factor of 0.83 to measure specific resistance.
- (d) A hydrometer, range 1.000 to 1.2000, which meets National Bureau of Standards requirements to measure specific gravity. Our tests showed that the specific gravity determined by the hydrometer did not differ within the experimental error from specific gravity determined by weight methods.

II.4.4 Test Procedures

We mixed aged electrolyte, high in sludge content, with aged clarified electrolyte to make an electrolyte of the desired sludge content. We determined the sludge content by centrifuging four 10 cc samples at test temperature. The centrifuge was on full power for 60 seconds, then allowed to coast to a stop after the power was turned off. The sludge content was measured as the ratio of the averaged cc's of settled (sludge) layer, after centrifuging, to that of the original volume.

We measured the viscosity, specific gravity, and specific resistance at the test temperature.

II.4.5 Test Analysis and Results

The effects of sludge content, temperature, and concentration of NaCl on specific gravity, viscosity, and specific resistance, based on an analysis of variance, is shown in Figure 99.

The change in viscosity over a range of sludge contents and the effect of temperature on the sludge content is reported in Section 2, Chapter III.

II.5 Surface Finish Studies

II.5.1 Test Series AJ-B

We conducted our tests on René 41 with NaCl electrolyte at 2.2 lb/gal and 96 °F.

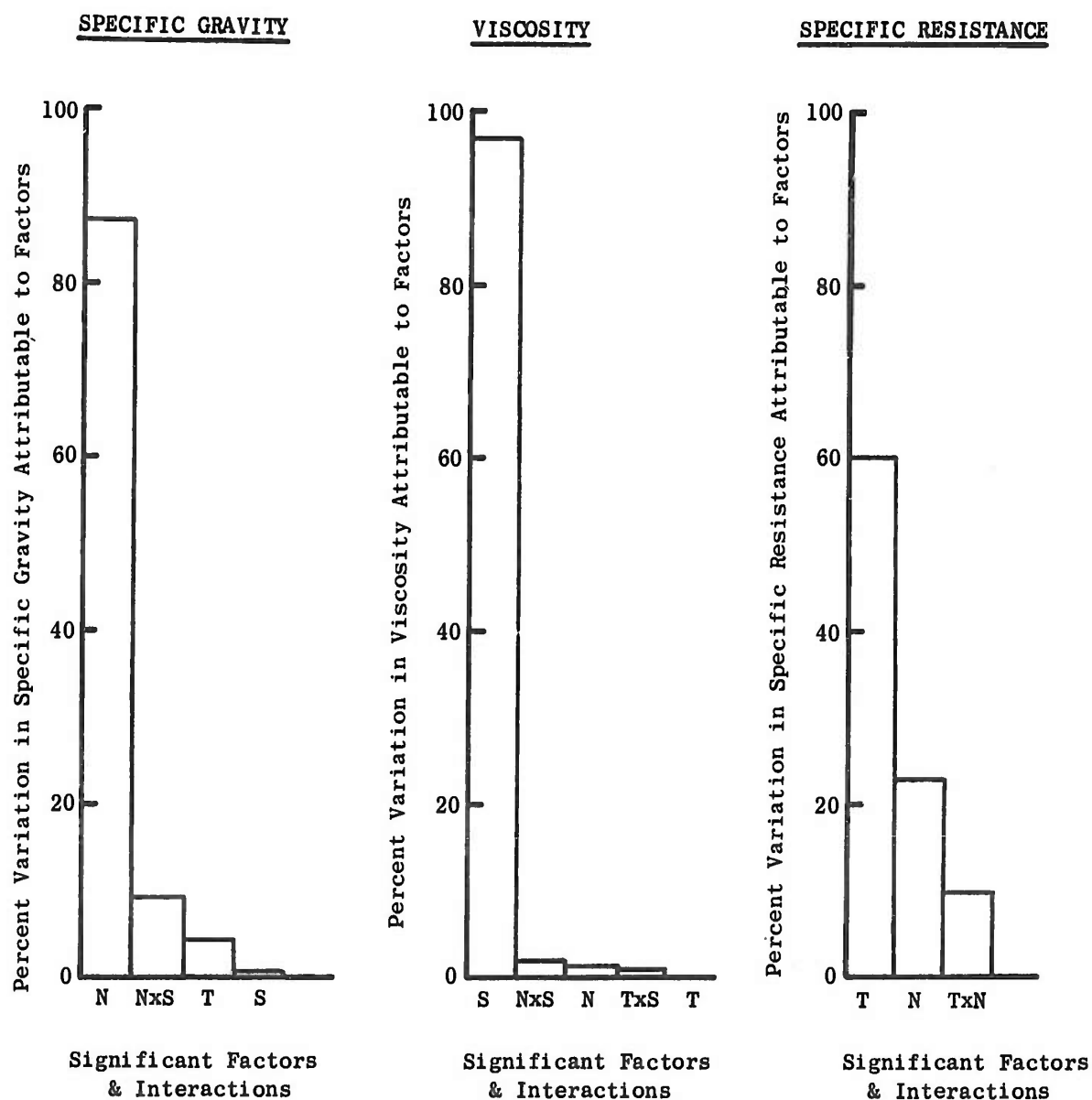
II.5.1.1 Purposes

To determine the operating parameters which significantly affect surface finish roughness.

II.5.1.2 Design of Experiment

We did not use a statistical design of experiments. Instead, we varied the process operating parameters as follows:

ELECTROLYTE PROPERTIES



<u>Factors</u>	<u>Test Levels</u>
S - Sludge Content (cc/10 cc)	6.2-2.4-1.2
T - Temperature (°F)	80-95-110
N - Concentration (gm/l)	166-196-223

Notes

- (1) Aged NaCl electrolyte from production tank. Diluted with tap water.
- (2) Concentration at 72°F.
- (3) Analysis of variance of full factorial. α risk = 0.05

Figure 99. Significant Factors Contributing to Variations of Electrolyte Properties

Feed Rate (F) (in/min)	Applied Voltage (E) (volt)	Average Pressure (P) (psig)	Pressure Drop (ΔP) (psi)	No. of Tests
.020	6 - 10	20 - 90	20 - 220	3
.040	8 - 10	50 - 130	60 - 220	4
.060	8 - 14	60 - 144	80 - 278	7
.080	10 - 12	100 - 130	160 - 220	3
.100	18	130	330	1

We measured response variables within these ranges:

- (a) G - cutting gaps in inch -0.005 - 0.0235
- (b) V - velocities in ft/sec - 31 - 178
- (c) Surface roughness in microinch RMS - 9 - 150

II.5.1.3 Test Facilities and Tooling

The arrangement of the test facility is shown in Figure 100 and Table 24. The ECM Machine #2 (P) has a vertical feed ram which is actuated by a pneumatic cylinder. The feed rate is controlled by a variable speed driven cam and a ram-mounted cam follower.

Settling tanks, not shown on the schematic facility layout, separated the sludge from the electrolyte.

We used two instruments to measure surface finish:

- (a) Profilometer manufactured by Micrometrical Manufacturing Corp.
- (b) Talisurf manufactured by Taylor, Taylor-Hobson Ltd.

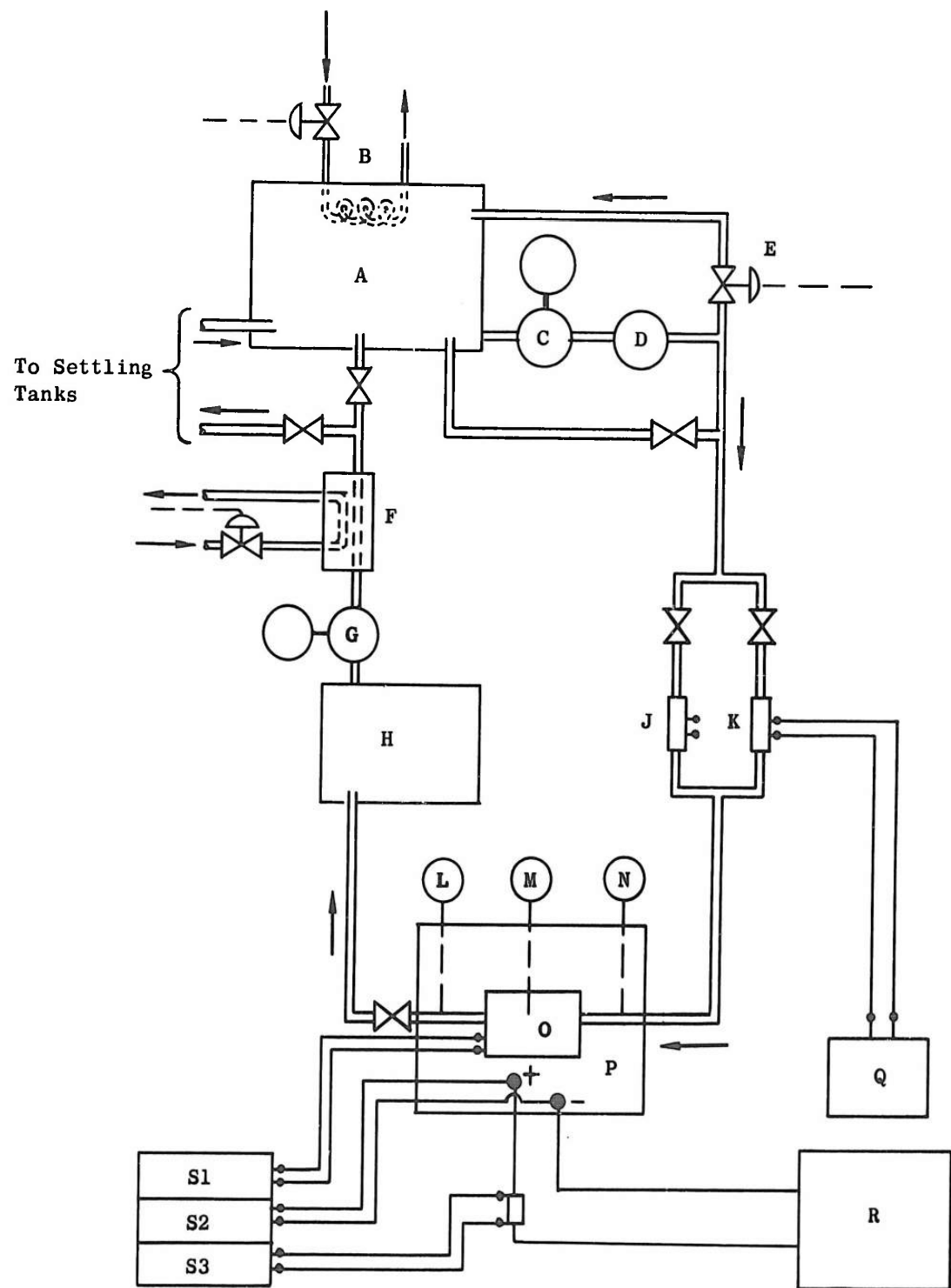
The tooling, Figures 101 and 102, consists of an electrode (1) mounted in a support (2). The electrode is actuated by the vertical ram (3) of ECM Machine #2, which machines a 1" x 1" flat into workpiece (4) to a depth of 0.375". The workpiece is fixed in a holder (5) with a low-melting alloy matrix (6) of 58% Bi and 42% Sn. The anode bus (7) extends into the matrix and connects the bottom surface of the workpiece.

The electrolyte is channeled through the fixture sleeve (8), from the inlet to the upstream side of the electrode, across the cutting gap, and to the exit part of the tool.

A gap measurement device is incorporated in the electrode. A measuring pin (9), which is normally flush with the electrode cutting surface, is extended to the anode surface, and a dial indicator (10) measures the gap dimension. The gap is measured while the electrolyte is flowing through the tooling.

II.5.1.4 Test Procedure

We conducted our experiments as follows:



For Legend see Table 24

Figure 100. Facility Layout; ECM Machine #2

TABLE 24
LEGEND FOR FACILITY LAYOUT
MACHINE #2, FIGURE 100

- A Main Supply Tank
- B Heat Exchanger - Heating
- C Main Supply Pump
Wheatley Piston Pump and Accumulator
735 psi Max, 39 gal/min
- D Cartridge Filter, Fulflo, 75 Micron
- E Jordon Sliding Gate Back Pressure Regulator, 3/4, Model S4
- F Heat Exchanger - Cooler
- G Centrifugal Pump, 50 gal/min, 50 psi
- H Scavenge Tank
- J 3/8" Potter Flow Sensor
- K 5/8" Potter Flow Sensor
- L Precision Pressure Gage, Tool Exit
- M Precision Pressure Gage, Gap
- N Precision Pressure Gage, Tool Inlet
- O Test Tooling
- P ECM Machine #2
- Q Beckman E-put Meter - Model 71S1BEK
- R Rapid 5,000 Amp Power Supply
- S Sanborn Recorder
 - 1. Temperature Channel
 - 2. Voltage Channel
 - 3. Current Channel

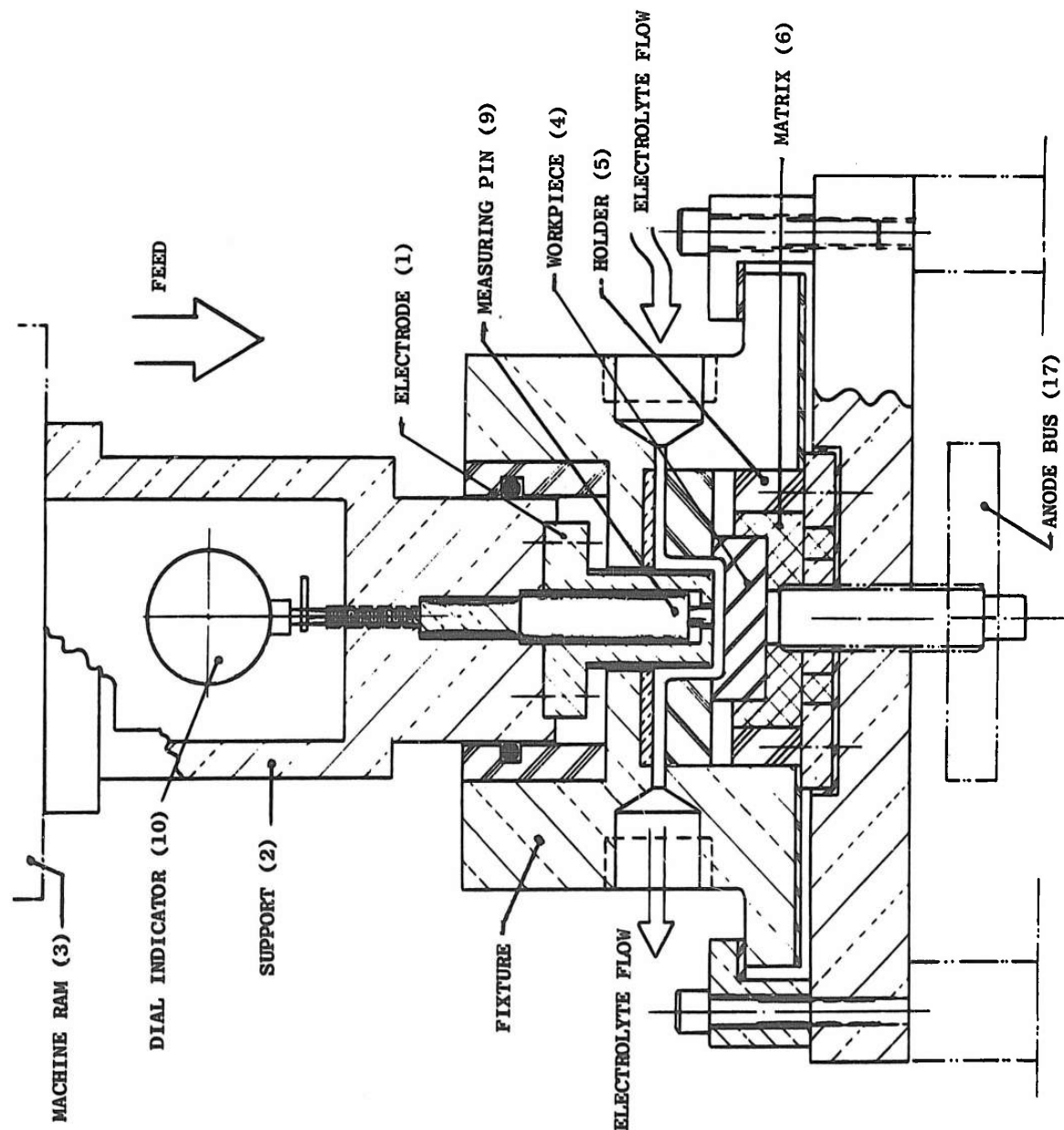


Figure 101. Schematic Sketch of Tooling for AJ Series Surface Finish Tests

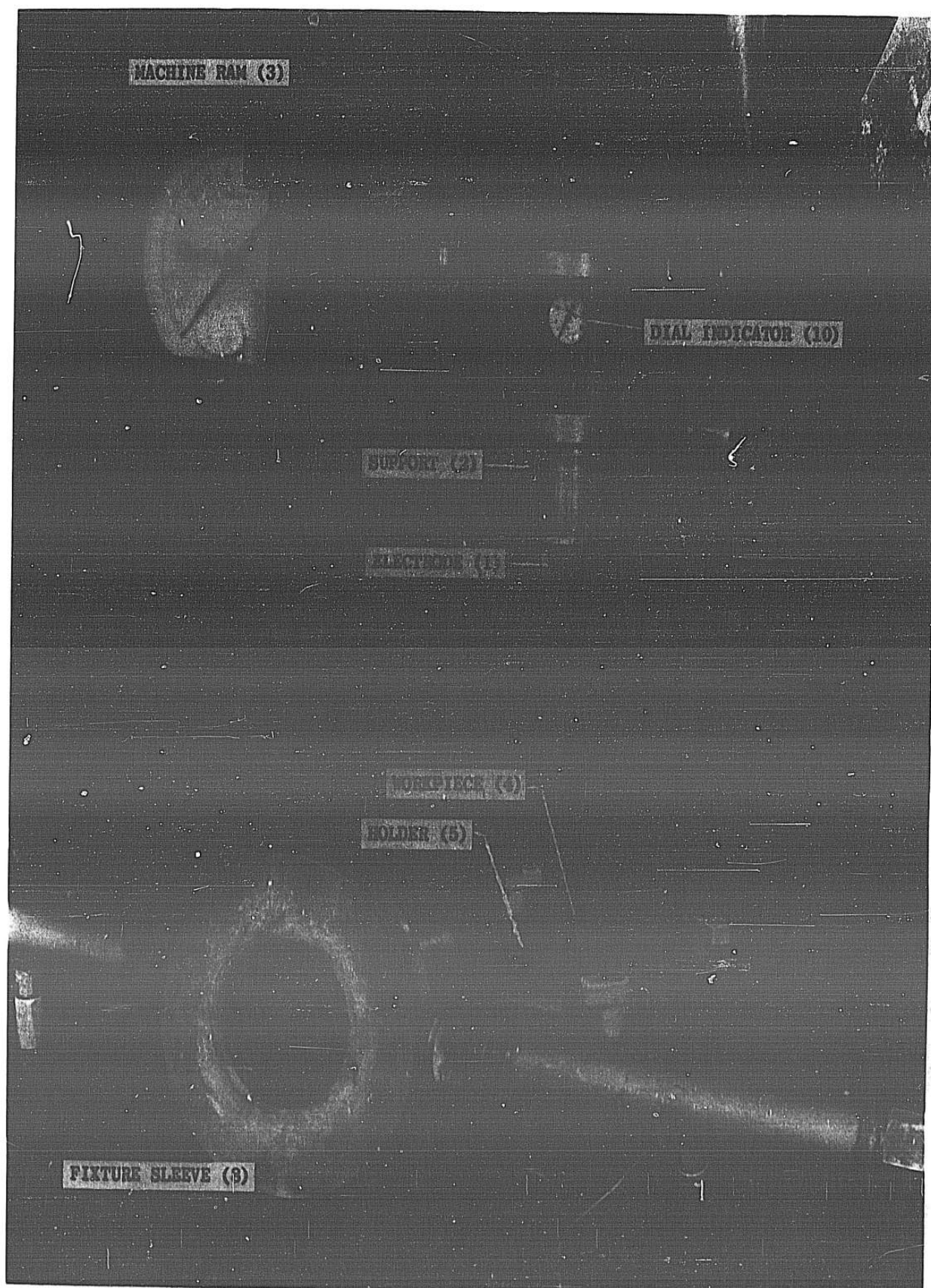


Figure 102. Tooling for AJ Series Surface Finish Tests

- (a) Turn on Sanborn recorder and flow meter. Allow 45 minutes warm-up time. Set electrolyte control thermostat and circulate electrolyte through by-pass. Check and adjust electrolyte concentration.

Set machine feed and cutting stroke.

Calibrate Sanborn recorder and pressure gages.

- (b) Load workpiece in holder and install holder in tooling. Lower electrode to start position and set starting gap at $0.020'' \pm 0.002''$.

Close electrolyte bypass and circulate electrolyte through tooling.

Check and record electrolyte supply temperatures.

Take electrolyte sample from tooling exit line; check concentration and sludge content (at control temperature) and record.

- (c) Start machining cycle.

During machining, adjust voltage and electrolyte pressures.

During last 0.025" of stroke, read and record mass flow and pressures.

- (d) After completion of cycle, with ram at end of stroke and while electrolyte is flowing through the tooling, measure cutting gap.

Turn pumps off and unload workpiece.

Calibrate Sanborn current and temperature channels, record maximum cutting current and tool exit temperature at start and end of cycle.

- (e) Measure and record surface finish in three places, Figure 55.

We held the concentration of the electrolyte and the electrolyte supply temperature within 5% and 1% respectively of their nominal values. We limited the sludge to a maximum level of 0.5 cc/15 cc. We measured the sludge content of electrolyte samples as the ratio of the settled sludge after centrifuging for 60 seconds to the original volume of the electrolyte sludge mixture.

We held the operating parameter at the selected levels throughout the machining cycle, and we measured the response variables after steady state conditions had been approximated, i.e., after current and electrolyte temperature at tool exit had leveled off.

II.5.1.5 Test Analysis and Results

We evaluated our data by regression analysis.

From the analysis we concluded that these factors contributed significantly to the variation of surface finish at measuring line L3:

- (a) M - Mass Flow - in gal/min
- (b) F - Feed rate - in in/min
- (c) G - Cutting gap - in inch.

The average electrolyte pressure was not a significant factor.

The relationship of significant factors was calculated to be:

$$\ln \text{RMS} = 10.23 - 1.316 \ln M + .918 \ln F + .646 \ln G \quad (62)$$

When we continued our analysis by testing nine additional models, we found that the equation

$$\ln \text{RMS} = 4.936 - 1.323 \ln V + .7082 \ln F \quad (63)$$

where

V is velocity in ft/sec

yielded a better fit than Equation (62). The F ratios for the velocity (V) and feed rate (F) in our model, Equation (63), were calculated to be 38.4 and 4.63 respectively.

II.5.2 Test Series AJ-F

We conducted this test series on René 41 with NaCl electrolyte at 2.2 lb/gal.

II.5.2.1 Purpose

To determine the effect of electrolyte temperature in addition to previously tested factors on surface finish roughness.

II.5.2.2 Design of Experiments

We selected a $1/2 \times 2^4$ fractional analysis of variance experiment for the following factors and levels:

- (a) T - electrolyte temperature ($^{\circ}\text{F}$) - 95 and 108
- (b) G - cutting gap (in) - 0.008 and 0.015
- (c) M - electrolyte flow (gal/min) - 3.7 and 2.2
- (d) F - feed rate (in/min) - 0.040 and 0.060

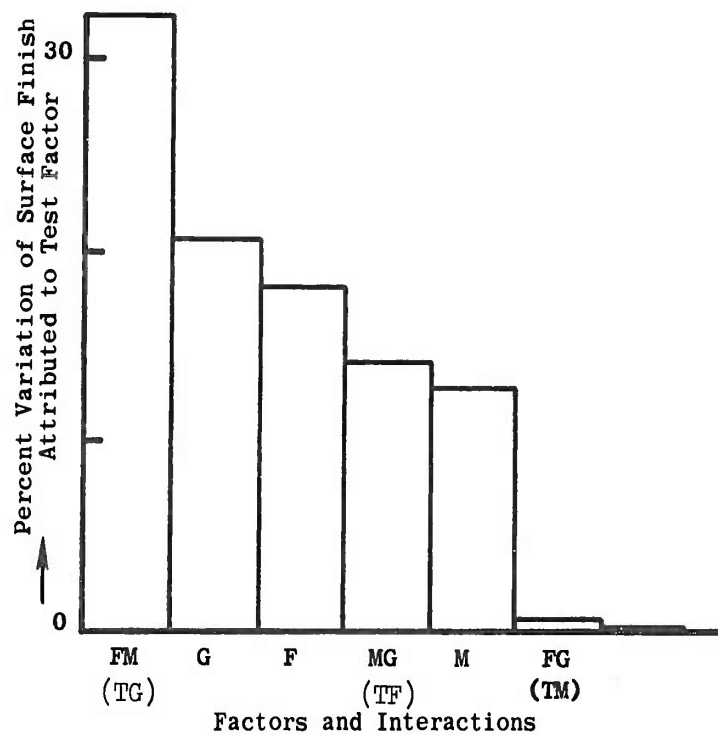
We conducted our tests in the facility and tooling described for Test Series AJ-B, and we used the same procedures.

II.5.2.3 Test Analysis and Results

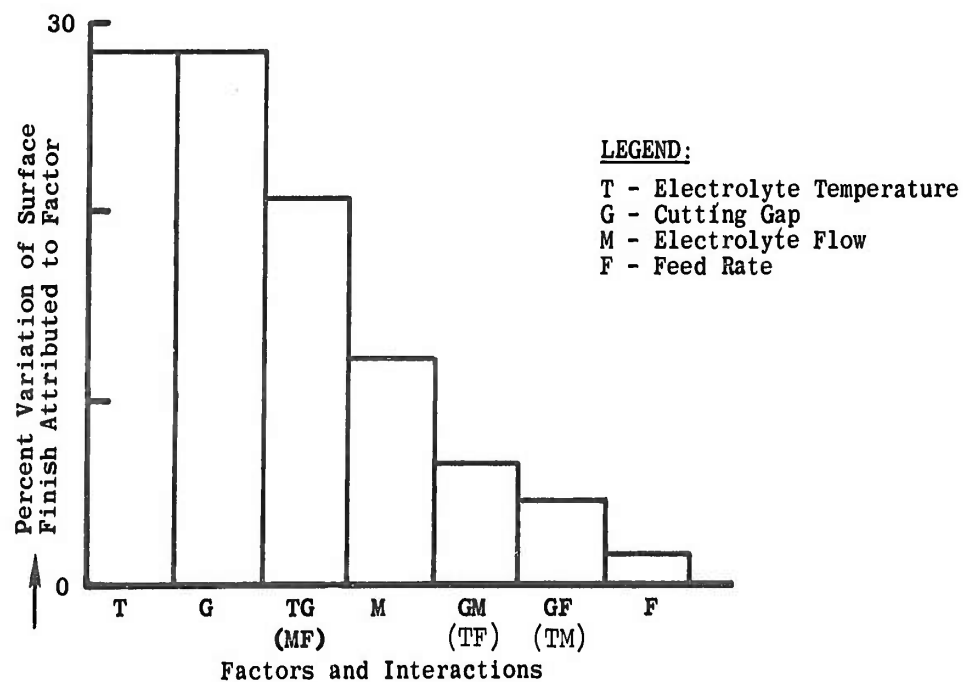
From our analysis of conditions at the flow exit (measuring line L3), we concluded that factors T, G, and TG taken together are significant at the 90% level only, Figure 103, and, therefore, are not firmly proven to be significant. We believe this is due, in part, to the size of the experiment (8 tests).

We confounded the TG interaction deliberately with the MF interaction under the assumption that a logarithmic model would remove the significance of the interactions. This was not the case, however, and we calculated a linear relationship.

Considering T, G, and TG as the predominant factors for this test series, we calculated the best-fit equation to be



(a) FLOW ENTRANCE



(b) FLOW EXIT

Figure 103. Factors Contributing To Variations Of Surface Roughness
Test Series AJ-F

$$\text{RMS} = \frac{269}{8} - \frac{167}{8} \left(\frac{T-101.5}{6.5} \right) + \frac{167}{8} \left(\frac{G-.0115}{.0035} \right) - \frac{141}{8} \left(\frac{T-101.5}{6.5} \right) \left(\frac{G-.0115}{.0035} \right) \quad (64)$$

II. 5.3 Test Series AJ-G

We conducted this test series on René 41 with NaCl electrolyte at 2.2 lb/gal.

II. 5.3.1 Purpose

- (a) To determine the effects of previously tested operating parameters on surface finish for extended test ranges.
- (b) To check the effect of a feed rate to mass flow ratio (dilution ratio) on surface finish.

II. 5.3.2 Design of Experiment

The design experiment is discussed in Section 7, Chapter III, Figure 49.

We conducted our tests in the facility and tooling described for Test Series AJ-B, and we used the same procedure.

II. 5.3.3 Test Analysis and Results

The analysis of these tests is summarized in Section 7, Chapter III. We interpreted the results as follows:

- (a) Factor A - the F/M ratio and primarily feed rate - appears to affect L1 finish but not L3. This is apparently because the feed rate effects the transition point.
- (b) Factor B - the mass flow effect - appears and disappears. This indicates that it is an effect which is not strong and is easily hidden by experimental error.
- (c) Factor C - the gap effect - appears and disappears as a main effect, but it is involved in all the interaction effects, primarily with temperature (CD); however, it also appears with mass flow (BC), and once with (BCD). This indicates that it is a strong effect, but its effect differs depending on mass flow and temperature. Multiple regression strongly suggests that BC effect may actually be a velocity effect.
- (d) Factor D - the temperature effect - appears and disappears as a main effect, but it is not significant in all the analysis either as a main effect or as an interaction, influencing the gap or flow effect. Nevertheless, temperature effect is always present.

II. 5.4 Test Series AJ-H

We conducted this test series on A-286 with NaNO₃ electrolyte at 5 lb/gal.

II. 5.4.1 Purpose

To determine the effect of previously tested operating parameters on the surface finish of A-286 machined with NaNO₃ electrolyte.

II.5.4.2 Design of Experiments

We did not use a statistical design of experiments; instead, we varied the electrolyte supply temperature between 85°F and 100°F and the other operating parameters as follows:

Feed Rate (F) (in/min)	Applied Voltage (E) (volts)	Average Pressure (P) (psig)	Pressure Drop (ΔP) (psi)	No. of Tests
.020	5 - 14	50 - 130	50 - 220	5
.040	4.5 - 23.5	50 - 135	50 - 250	8
.060	10 - 18	50 - 130	50 - 220	6
.080	10 - 18	125 - 160	90 - 200	3

We measured response variables within these ranges:

- (a) G - Cutting gaps in inch - 0.005 - 0.025.
- (b) V - Velocities in ft/sec - 56 - 267.
- (c) ΔT - Temperature rise in gap in °F - 1 - 49.
- (d) Surface roughness in microinch AA - 8 - 165.

We conducted our tests in the same facilities and tooling described for Test Series AJ-B, and we used the same procedure.

II.5.4.3 Test Analysis and Results

We evaluated our data by regression analysis.

Twelve models were tested in our multiple regression program.

In all our models:

- (a) The electrolyte temperature at the gap exit (T_2) always improved the fit, except when P, the average pressure, was included.
- (b) A better fit was obtained with G and T_2 than with G and electrolyte supply temperature (T_1); and with G, P and T_1 than with G, P and T_2 .
- (c) Including P in the model did not improve fit.
- (d) Including $\frac{F}{M}$, the ratio of feed rate to mass flow, did not improve the fit as much as including F alone.

We concluded that in this test series surface roughness at the flow entrance was significantly affected by the velocity and electrolyte temperatures, and at the flow exit only by gap size.

II.5.5 Test Series JB-4 (Surface Roughness Analysis)

The data and test specimens generated in Test Series JB-4, which we described in Appendix II-1, were also analyzed with respect to surface roughness.

II.5.5.1 Purpose

To determine if surface roughness is significantly affected by:

- (a) Fluid pressure in the gap
- (b) Mass flow.
- (c) Pressure drop across the gap.
- (d) The gap.
- (e) Feed rate.

II.5.5.2 Procedure

We measured the surface roughness with a Profilometer manufactured by the Micrometrical Manufacturing Corporation, Ann Arbor, Michigan.

II.5.5.3 Test Analysis and Results

We measured the data from 69 tests, which represented steady state conditions, by regression analysis to determine which factors significantly affected surface roughness, Figure 104.

The fluid pressure in the gap had no significant effect on surface roughness.

II.5.6 Test Series JB-4 (Surface Defect Analysis)

We inspected 116 test samples from Test Series JB-4 for subsurface defects. The test samples encompassed these ranges:

Current density:	380 - 690 amp/in ²
Average gap pressure:	19 - 232 psig
Average linear velocity:	12 - 184 ft/sec

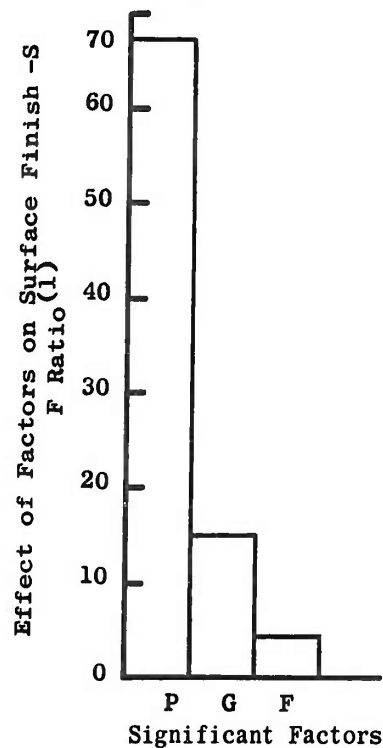
We sectioned one-half the specimens in a plane parallel to the flow; the other half, in a plane perpendicular to the flow. We examined each sample unetched at 500X for selective pitting or intergranular attack.

We did not find any subsurface defects on our test samples except that samples 66 and 122 showed superficial attack (less than 0.0002"). A microphotograph of sample 66 at 800X is reproduced in Figure 61(b), Section 7, Chapter III.

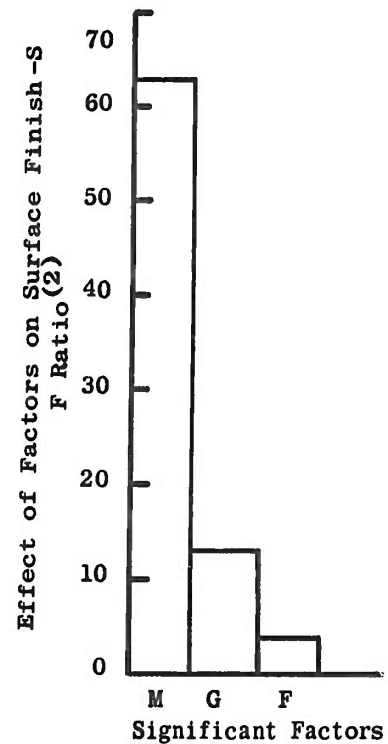
II.5.7 Test Series JB-8 (Surface Roughness Analysis)

The data and test specimens generated in Test Series JB-8, which we described in Appendix II-1, were also analyzed with respect to surface roughness.

Relationship-Note(1)



Relationship-Note(2)

FACTOR RANGES REPRESENTED IN ANALYSIS

G	F	P	P _g	M	No. of Tests in Analysis
Gap in	Feed Rate in/min	Pressure Drop psi	Average Gap Pressure psig.	Mass Flow cc/min	
.006	.0355	81-130	108-124	1210-2000	4
.006	.047	10-193	94-230	370-2600	18
.006	.070	42-170	75-112	770-1630	4
.010	.047	4-144	22-113	580-4680	20
.015	.047	9-225	19-104	1650-6520	13
.020	.0355	21-170	75-100	4940-9720	5
.020	.062	20-170	85-102	4200-9300	5

S - SYMBOL FOR SURFACE FINISH IN RMS

Notes:

- (1) Based on relationship - $\ln S = A_0 + A_1 \ln P + A_2 \ln G + A_3 \ln F + A_4 \ln P_g$
 (2) Based on relationship - $\ln S = A_0 + A_1 \ln M + A_2 \ln G + A_3 \ln F + A_4 \ln P_g$
 (3) Alloy - Electrolyte System - Rene' 41 - Aged NaCl - 280 gm/l
 (4) F ratio significant at 4.00 for $\alpha = 0.05$

Figure 104. Factors Contributing to Surface Roughness
Test Series JB-4

II.5.7.1 Purpose

To determine the effect of electrolyte viscosity on surface roughness when the effects of electrolyte temperature, electrolyte velocity, and feed rate are also considered.

II.5.7.2 Procedure

We measured the surface roughness as described in Test Series JB-4 in Appendix II.5.5.

II.5.7.3 Test Analysis and Results

The test analysis and results are reported in Section 7, Chapter III.

II.5.8 Test Series JB-9 (Surface Roughness Analysis)

The data and test specimen generated in Test Series JB-9, which we describe in Appendix II-1, were also analyzed with respect to surface roughness.

II.5.8.1 Purpose

To determine the effect of feed rate, temperature, pressure drop, gap pressure, and gap on surface roughness of A-286 machined with NaNO_3 electrolyte.

II.5.8.2 Procedure

We measured the surface roughness as described for Test Series JB-4 in Appendix II.5.5.

II.5.8.3 Test Analysis and Results

We could determine no significant factors affecting surface roughness. The relative effects of the factors on surface roughness are shown in Figure 105.

II.6 Contour Machining Tests

We conducted contour machining tests to substantiate the mathematical analysis and to demonstrate advantages of the process.

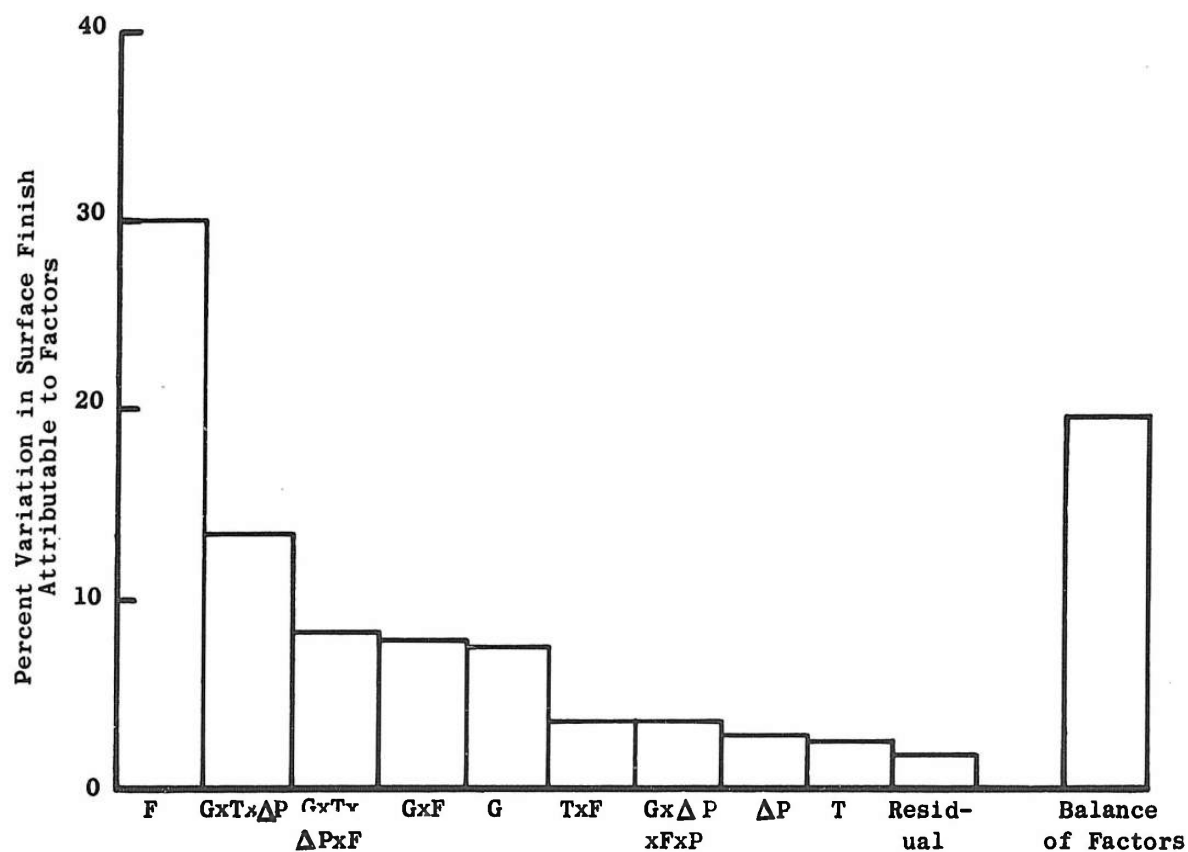
The test tooling is described in Section 4, Chapter IV.

We used the facilities described in Appendix II.5 for these tests.

II.6.1 Test Procedure

We conducted our machining tests as follows:

- (a) Turn on Sanborn recorder and flow meter. Allow 45 minutes warm-up time.
Set electrolyte control thermostat and circulate electrolyte through bypass.
Check and adjust electrolyte concentration.
Set machine feed and cutting stroke.
Calibrate Sanborn recorder and pressure gages.
- (b) Load workpiece in holder and install holder in tooling. Lower electrode to start position and set starting gap at $0.020" \pm 0.002"$.



Based on Full Fractional

FACTOR	TEST RANGE
F - Feed Rate (in/min)	0.021 - 0.062
G - Gap (in)	0.012 - 0.025
T - Temperature (F)	85 - 100
Δ P - Pressure Drop Across Tool (psi)	20 - 60
P - Average Gap Pressure (psig)	40 - 100

NOTE: None of the factors can be shown to be significant. The analysis only indicates the relative effects of the factors and interaction.

Figure 105. Factors Contributing To Surface Roughness
Test Series JB-9

Close electrolyte bypass and circulate electrolyte through tooling.
Check and record electrolyte supply temperatures.
Check concentration and sludge content (at control temperature) and record.

- (c) Start Machining cycle.
During machining, adjust voltage and electrolyte pressures.
During last 0.025" of stroke, read and record mass flow and pressures.
- (d) After completion of cycle, with ram at end of stroke and while electrolyte is flowing through the tooling, measure cutting gap.
Take sample of electrolyte and store for checks prior to subsequent test.
Turn pumps off and unload workpiece.
Calibrate Sanborn current and temperature channels, record maximum cutting current and tool exit temperature at start and end of cycle.

We held the concentration of the electrolyte and the electrolyte supply temperature within 5% and 1% respectively of their nominal values. We limited the sludge to a maximum level of 0.5 cc/15 cc. We measured the sludge content of electrolyte samples as the ratio of the settled sludge after centrifuging for 60 seconds to the original volume of the electrolyte sludge mixture.

We measured the contours of the machined workpieces on a numerically-controlled inspection and layout machine. We aligned the workpiece on the inspection machine table, and the rotating head of the machine checked the deviation of the machined contour from the nominal electrode contour. The contours were checked along predetermined section lines and at predetermined intervals according to instructions incorporated in the machine control tapes. The results were recorded by a printer.

The gap dimensions used for the plots of "actual gaps," Figures 16 through 23, were calculated from the contour measurements and by deducting from, or adding to, the recorded dimensions the difference between the assumed nominal contour of the electrode and its actual dimension which had also been measured on the inspection machine.

The deviations of the actual electrode contour, from its assumed nominal shape of 1.0000"R, did not exceed 0.0007", except that we had ground a 1/8" wide flat across the apex of the electrode and the measuring pin which deviated 0.0022" from the nominal radius at its lowest point.

II.6.2 Test Results

We have reported our test results in Section 4, Chapter III and in Section 4, Chapter IV.

The cutting gap and overcut index plots included in Section 4, Chapter III are based on computed results, Table 5 and Tables 25 through 28.

II.7 Electrode Material Investigation

We conducted spark resistance and abrasion tests on 14 candidate-electrode materials to establish selection criteria.

II.7.1 Description of Spark Resistance Tests

We turned a short length of one-inch rod of the material to be tested to a 1/8-inch diameter, and the end to a point (30 degrees). We mounted the machined rod in the electrolytic machining test rig, with the pointed end in positive contact with a block of either Gentrode or M252 material. No electrolyte was used.

TABLE 25
COMPUTED RESULTS
TESTS #C1 and C3

Mesh No	Coordinates						M Σ j=2	β
	x	y	z	ΔL	L _{ij}			
5 27	0.36800	0.68256	0.24655	1.39698-09	2.82812-02	1.66644-02	9.37512-01	
5 28	0.36800	0.74061	0.30025	2.56114-09	2.96659-02	1.81749-02	9.33735-01	
5 29	0.36800	0.79757	0.36620	1.39698-09	4.07296-02	1.87440-02	9.54547-01	
6 1	0.46000	-0.79757	0.36620	2.79397-09	4.10587-02	1.87504-02	9.54230-01	
6 2	0.46000	-0.74061	0.30025	-1.39698-09	3.01436-02	1.81775-02	9.33309-01	
6 3	0.46000	-0.68256	0.24655	-2.56114-09	2.83073-02	1.66726-02	9.37096-01	
6 4	0.46000	-0.62513	0.19948	-2.56114-09	2.71647-02	1.56901-02	9.39666-01	
6 5	0.46000	-0.56784	0.15886	-1.97906-09	2.61616-02	1.48757-02	9.41837-01	
6 6	0.46000	-0.51074	0.12385	-1.39698-09	2.53875-02	1.42438-02	9.43543-01	
6 7	0.46000	-0.45377	0.09351	-5.47152-09	2.47591-02	1.37449-02	9.44923-01	
6 8	0.46000	-0.39688	0.06762	-4.42378-09	2.42299-02	1.33359-02	9.46062-01	
6 9	0.46000	-0.34008	0.04578	-5.23869-09	2.38251-02	1.30117-02	9.46969-01	
6 10	0.46000	-0.28333	0.02769	-4.30737-09	2.34948-02	1.27559-02	9.47693-01	
6 11	0.46000	-0.22662	0.01312	-5.12227-09	2.32374-02	1.25572-02	9.48260-01	
6 12	0.46000	-0.16994	0.00195	-5.23869-09	2.30436-02	1.24084-02	9.48686-01	
6 13	0.46000	-0.11328	-0.00595	-5.23869-09	2.29090-02	1.23054-02	9.48981-01	
6 14	0.46000	-0.05664	-0.01066	-5.23869-09	2.28306-02	1.22450-02	9.49154-01	
6 15	0.46000	0.	-0.01223	-5.35510-09	2.28049-02	1.22251-02	9.49212-01	
6 16	0.46000	0.05664	-0.01066	-5.35510-09	2.28318-02	1.22450-02	9.49154-01	
6 17	0.46000	0.11328	-0.00595	-5.23869-09	2.29124-02	1.23054-02	9.48981-01	
6 18	0.46000	0.16994	0.00195	-5.12227-09	2.30486-02	1.24084-02	9.48686-01	
6 19	0.46000	0.22662	0.01312	-5.12227-09	2.32437-02	1.25572-02	9.48260-01	
6 20	0.46000	0.28333	0.02769	-4.30737-09	2.35040-02	1.27559-02	9.47693-01	
6 21	0.46000	0.34008	0.04578	-5.35510-09	2.38379-02	1.30117-02	9.46969-01	
6 22	0.46000	0.39688	0.06762	-4.42378-09	2.42466-02	1.33359-02	9.46062-01	
6 23	0.46000	0.45377	0.09351	-5.47152-09	2.47794-02	1.37449-02	9.44923-01	
6 24	0.46000	0.51074	0.12385	-4.54020-09	2.54166-02	1.42438-02	9.43543-01	
6 25	0.46000	0.56784	0.15886	-5.58794-09	2.62110-02	1.48756-02	9.41837-01	
6 26	0.46000	0.62513	0.19948	-2.56114-09	2.71977-02	1.56901-02	9.39666-01	
6 27	0.46000	0.68256	0.24655	-2.56114-09	2.84610-02	1.66726-02	9.37096-01	
6 28	0.46000	0.74061	0.30025	9.31323-10	2.98585-02	1.81775-02	9.33309-01	
6 29	0.46000	0.79757	0.36620	2.56114-09	4.10586-02	1.87504-02	9.54230-01	
7 1	0.55200	-0.79754	0.36620	9.31323-10	4.06718-02	1.87256-02	9.54586-01	
7 2	0.55200	-0.74062	0.30025	-1.62981-09	2.99477-02	1.81803-02	9.33717-01	
7 3	0.55200	-0.68256	0.24655	-1.16415-09	2.81226-02	1.66650-02	9.37510-01	
7 4	0.55200	-0.62513	0.19949	-2.79397-09	2.69920-02	1.56850-02	9.40052-01	

TEST #C1

5 26	0.36800	0.62463	0.20017	3.37604-09	2.70331-02	1.48781-02	9.42939-01	
5 27	0.36800	0.68199	0.24719	1.39698-09	2.82760-02	1.58011-02	9.40501-01	
5 28	0.36800	0.73992	0.30090	6.75209-09	2.96814-02	1.72299-02	9.36897-01	
5 29	0.36800	0.79684	0.36682	3.02680-09	4.07526-02	1.77891-02	9.56722-01	
6 1	0.46000	-0.79684	0.36682	2.09548-09	4.10443-02	1.77949-02	9.56420-01	
6 2	0.46000	-0.73992	0.30089	8.14907-09	3.01454-02	1.72320-02	9.36491-01	
6 3	0.46000	-0.68199	0.24719	1.62981-09	2.83248-02	1.58085-02	9.40105-01	
6 4	0.46000	-0.62463	0.20012	1.97906-09	2.71738-02	1.48790-02	9.42554-01	
6 5	0.46000	-0.56741	0.15749	4.65661-10	2.61715-02	1.41083-02	9.44623-01	
6 6	0.46000	-0.51037	0.12448	1.86265-09	2.53941-02	1.35103-02	9.46249-01	
6 7	0.46000	-0.45346	0.09414	-9.31323-10	2.47677-02	1.30380-02	9.47564-01	
6 8	0.46000	-0.39662	0.06825	-1.74623-09	2.42355-02	1.26507-02	9.48649-01	
6 9	0.46000	-0.33985	0.04640	-1.16415-09	2.38304-02	1.23438-02	9.49514-01	
6 10	0.46000	-0.28314	0.02831	-1.16415-09	2.34998-02	1.21016-02	9.50203-01	
6 11	0.46000	-0.22647	0.01375	-1.86265-09	2.32422-02	1.19135-02	9.50743-01	
6 12	0.46000	-0.16983	0.00757	-1.74623-09	2.30483-02	1.17725-02	9.51148-01	
6 13	0.46000	-0.11321	-0.00432	-1.74623-09	2.29137-02	1.16750-02	9.51429-01	
6 14	0.46000	-0.05660	-0.01003	-2.09548-09	2.28357-02	1.16179-02	9.51594-01	
6 15	0.46000	0.	-0.01160	-1.97906-09	2.28095-02	1.15989-02	9.51650-01	
6 16	0.46000	0.05660	-0.01003	-2.09548-09	2.28364-02	1.16179-02	9.51594-01	
6 17	0.46000	0.11321	-0.00757	-1.86265-09	2.29169-02	1.16750-02	9.51429-01	
6 18	0.46000	0.16983	0.00757	-1.74623-09	2.30360-02	1.17725-02	9.51148-01	
6 19	0.46000	0.22647	0.01375	-1.97906-09	2.32481-02	1.19135-02	9.50743-01	
6 20	0.46000	0.28314	0.02831	-1.16415-09	2.35083-02	1.21016-02	9.50203-01	
6 21	0.46000	0.33985	0.04640	-1.16415-09	2.38431-02	1.23438-02	9.49514-01	
6 22	0.46000	0.39662	0.06825	-1.74623-09	2.42522-02	1.26507-02	9.48649-01	
6 23	0.46000	0.45346	0.09414	-8.14907-10	2.47812-02	1.30380-02	9.47564-01	
6 24	0.46000	0.51037	0.12448	1.86265-09	2.54703-02	1.35103-02	9.46249-01	
6 25	0.46000	0.56741	0.15949	1.51340-09	2.62158-02	1.41283-02	9.44623-01	
6 26	0.46000	0.62463	0.20017	1.97906-09	2.71466-02	1.48790-02	9.42554-01	
6 27	0.46000	0.68199	0.24719	1.62981-09	2.84402-02	1.58085-02	9.40105-01	
6 28	0.46000	0.73992	0.30089	7.91624-09	2.98780-02	1.72320-02	9.36491-01	
6 29	0.46000	0.79684	0.36682	2.09548-09	4.10443-02	1.77949-02	9.56420-01	
7 1	0.55200	-0.79682	0.36682	5.87077-09	4.06687-02	1.77717-02	9.56759-01	
7 2	0.55200	-0.73993	0.30090	6.05360-09	2.99606-02	1.72351-02	9.36880-01	
7 3	0.55200	-0.68198	0.24719	5.38794-09	2.81286-02	1.58017-02	9.40499-01	

TEST #C3

TABLE 26
COMPUTED RESULTS
TESTS #C4 and C5

Mesh No		Coordinates				$\sum_{j=2}^M$		
x	y	x	y	z	ΔL	L_{ij}	β	
5	27	0.36800	0.67998	0.24941	5.82077-10	2.82636-02	1.28215-02	9.51028-01
5	28	0.36800	0.73754	0.30313	6.63567-09	2.97474-02	1.39712-02	9.48042-01
5	29	0.36800	0.79432	0.36897	-2.32831-10	4.08066-02	1.44802-02	9.64383-01
6	1	0.46000	-0.79432	0.36897	4.65661-10	4.10781-02	1.44801-02	9.64135-01
6	2	0.46000	-0.73754	0.30312	5.23869-09	3.01508-02	1.39717-02	9.47709-01
6	3	0.46000	-0.67999	0.24940	1.74623-09	2.83254-02	1.28265-02	9.50703-01
6	4	0.46000	-0.62290	0.20232	4.42378-09	2.71855-02	1.20781-02	9.52724-01
6	5	0.46000	-0.56592	0.16169	1.04774-09	2.61811-02	1.14571-02	9.54432-01
6	6	0.46000	-0.50909	0.12667	2.09548-09	2.54011-02	1.09749-02	9.55774-01
6	7	0.46000	-0.45236	0.09637	-3.49246-10	2.47767-02	1.05939-02	9.56858-01
6	8	0.46000	-0.39569	0.07043	1.16415-10	2.42461-02	1.02814-02	9.57752-01
6	9	0.46000	-0.33907	0.04858	6.98492-10	2.38394-02	1.00337-02	9.58465-01
6	10	0.46000	-0.28251	0.03049	5.82077-10	2.35093-02	9.83811-03	9.59033-01
6	11	0.46000	-0.22597	0.01592	3.49246-10	2.32519-02	9.68615-03	9.59478-01
6	12	0.46000	-0.16946	0.00474	0.	2.30580-02	9.57232-03	9.59813-01
6	13	0.46000	-0.11296	-0.00315	1.16415-10	2.29235-02	9.49356-03	9.60044-01
6	14	0.46000	-0.05648	-0.00786	-1.16415-10	2.28450-02	9.44736-03	9.60180-01
6	15	0.46000	0.	-0.00943	2.28231-02	2.28191-02	9.43207-03	9.60226-01
6	16	0.46000	0.05648	-0.00786	0.	2.28459-02	9.44736-03	9.60180-01
6	17	0.46000	0.11296	-0.00315	-1.16415-10	2.29260-02	9.49356-03	9.60044-01
6	18	0.46000	0.16946	0.00474	2.32831-10	2.30618-02	9.57232-03	9.59813-01
6	19	0.46000	0.22597	0.01592	3.49246-10	2.32567-02	9.68615-03	9.59478-01
6	20	0.46000	0.28251	0.03049	5.82077-10	2.35161-02	9.83811-03	9.59033-01
6	21	0.46000	0.33907	0.04858	6.98492-10	2.38492-02	1.00337-02	9.58465-01
6	22	0.46000	0.39569	0.07043	0.	2.42594-02	1.02814-02	9.57752-01
6	23	0.46000	0.45236	0.09632	-4.65661-10	2.47870-02	1.05939-02	9.56858-01
6	24	0.46000	0.50909	0.12667	2.56114-09	2.54262-02	1.09749-02	9.55774-01
6	25	0.46000	0.56592	0.16169	4.65661-10	2.62132-02	1.14571-02	9.54432-01
6	26	0.46000	0.62290	0.20232	4.30737-09	2.72135-02	1.20781-02	9.52724-01
6	27	0.46000	0.67999	0.24940	1.51340-09	2.84538-02	1.28265-02	9.50703-01
6	28	0.46000	0.73754	0.30312	5.23869-09	2.98579-02	1.39717-02	9.47709-01
6	29	0.46000	0.79432	0.36897	4.65661-10	4.10781-02	1.44801-02	9.64135-01
7	1	0.55200	-0.79432	0.36897	1.16415-09	4.08066-02	1.44802-02	9.64114-01
7	2	0.55200	-0.73755	0.30313	2.91038-09	2.99445-02	1.39753-02	9.48028-01
7	3	0.55200	-0.67999	0.24941	4.54020-09	2.81417-02	1.28220-02	9.51027-01
7	4	0.55200	-0.62290	0.20233	3.14321-09	2.70042-02	1.20753-02	9.53026-01

TEST #C4

5	25	0.36800	0.56467	0.16354	3.37604-09	2.40416-02	9.22327-03	9.63142-01
5	26	0.36800	0.62145	0.20418	3.60887-09	2.70257-02	9.72451-03	9.61743-01
5	27	0.36800	0.67831	0.25127	1.04774-09	2.82394-02	1.03188-02	9.60123-01
5	28	0.36800	0.73555	0.30500	1.16415-10	2.97826-02	1.12374-02	9.57679-01
5	29	0.36800	0.79219	0.37078	3.25963-09	4.08260-02	1.16850-02	9.71001-01
6	1	0.46000	-0.79220	0.37078	2.91038-09	4.11329-02	1.16876-02	9.70799-01
6	2	0.46000	-0.73555	0.30499	4.19095-09	3.01527-02	1.12370-02	9.57408-01
6	3	0.46000	-0.67831	0.25126	2.32831-10	2.83235-02	1.03221-02	9.59859-01
6	4	0.46000	-0.62145	0.20418	1.97906-09	2.71730-02	9.72384-03	9.61507-01
6	5	0.46000	-0.56467	0.16354	2.56114-09	2.61821-02	9.22700-03	9.62900-01
6	6	0.46000	-0.50801	0.12852	2.44472-09	2.54003-02	8.84104-03	9.63995-01
6	7	0.46000	-0.45143	0.09816	1.16415-10	2.47733-02	8.53601-03	9.64879-01
6	8	0.46000	-0.39490	0.07227	4.65661-10	2.42471-02	8.28370-03	9.65808-01
6	9	0.46000	-0.33842	0.05041	4.65661-10	2.38395-02	8.08717-03	9.66190-01
6	10	0.46000	-0.28197	0.03332	3.49246-10	2.35092-02	7.93046-03	9.66653-01
6	11	0.46000	-0.22595	0.01775	1.74623-10	2.32516-02	7.80866-03	9.67015-01
6	12	0.46000	-0.16915	0.00657	3.49246-10	2.30581-02	7.71740-03	9.67288-01
6	13	0.46000	-0.11276	-0.00133	1.16415-10	2.29238-02	7.65426-03	9.67476-01
6	14	0.46000	-0.05638	-0.00504	5.82077-11	2.28452-02	7.61722-03	9.67587-01
6	15	0.46000	0.	-0.00760	0.	2.28193-02	7.60496-03	9.67624-01
6	16	0.46000	0.05638	-0.00804	5.82077-11	2.28460-02	7.61722-03	9.67587-01
6	17	0.46000	0.11276	-0.00133	0.	2.29258-02	7.65426-03	9.67476-01
6	18	0.46000	0.16915	0.00657	3.49246-10	2.30611-02	7.71740-03	9.67288-01
6	19	0.46000	0.22595	0.01775	1.16415-10	2.32555-02	7.80866-03	9.67015-01
6	20	0.46000	0.28197	0.03332	3.49246-10	2.35146-02	7.93046-03	9.66653-01
6	21	0.46000	0.33842	0.05041	5.82077-10	2.38472-02	8.08717-03	9.66190-01
6	22	0.46000	0.39490	0.07227	-4.65661-10	2.42584-02	8.28370-03	9.65808-01
6	23	0.46000	0.45143	0.09816	1.16415-10	2.47853-02	8.53601-03	9.64879-01
6	24	0.46000	0.50801	0.12852	3.02680-09	2.54189-02	8.84103-03	9.63995-01
6	25	0.46000	0.56467	0.16354	2.79397-09	2.62099-02	9.22699-03	9.62900-01
6	26	0.46000	0.62145	0.20418	3.49246-09	2.72005-02	9.72384-03	9.61507-01
6	27	0.46000	0.67831	0.25126	3.49246-10	2.84295-02	1.03221-02	9.59859-01
6	28	0.46000	0.73555	0.30499	4.30737-09	2.99953-02	1.12370-02	9.57408-01
6	29	0.46000	0.79220	0.37078	2.91038-09	4.11329-02	1.16876-02	9.70799-01
7	1	0.55200	-0.79218	0.37078	1.16415-09	4.07852-02	1.16876-02	9.71028-01
7	2	0.55200	-0.73555	0.30500	2.91038-09	2.99336-02	1.12407-02	9.57668-01
7	3	0.55200	-0.67831	0.25127	1.16415-09	2.81494-02	1.03192-02	9.60122-01
7	4	0.55200	-0.62145	0.20418	2.21189-09	2.70044-02	9.72218-03	9.61752-01

TEST #C5

TABLE 27
COMPUTED RESULTS
TEST #C6

Mesh No		Coordinates			M			
x	y	x	y	z	ΔL	L_{ij}	$\Sigma_{j=2}$	β
8	27	0.36800	0.67868	0.25086	1.16415-10	2.62444-02	1.08709-02	9.58097-01
8	28	0.36800	0.72599	0.30458	4.65661-10	2.97763-02	1.10402-02	9.55532-01
8	29	0.36800	0.79267	0.37038	0.	4.08112-02	1.23029-02	9.69526-01
6	1	0.46000	-0.79267	0.37038	1.86265-09	4.11145-02	1.23057-02	9.69315-01
6	2	0.46000	-0.73599	0.30458	6.98492-10	3.01440-02	1.18400-02	9.55247-01
6	3	0.46000	-0.67868	0.25086	1.28057-09	2.83318-02	1.08746-02	9.57819-01
6	4	0.46000	-0.62177	0.20377	1.16415-09	2.71777-02	1.02433-02	9.59550-01
6	5	0.46000	-0.56495	0.16313	3.02680-09	2.61804-02	9.71921-03	9.61014-01
6	6	0.46000	-0.50825	0.12811	1.28057-09	2.54008-02	9.31212-03	9.62164-01
6	7	0.46000	-0.45164	0.09776	4.65661-10	2.47737-02	8.99040-03	9.63093-01
6	8	0.46000	-0.39508	0.07186	-6.98492-10	2.42474-02	8.72642-03	9.63859-01
6	9	0.46000	-0.33856	0.05001	-1.16415-10	2.38399-02	8.51706-03	9.64469-01
6	10	0.46000	-0.28209	0.03191	1.04774-09	2.35098-02	8.35181-03	9.64956-01
6	11	0.46000	-0.22564	0.01735	1.16415-10	2.32524-02	8.22337-03	9.65337-01
6	12	0.46000	-0.16922	0.00617	0.	2.30588-02	8.12715-03	9.65623-01
6	13	0.46000	-0.11280	-0.00173	1.16415-10	2.29243-02	8.06058-03	9.65821-01
6	14	0.46000	-0.05640	-0.00644	1.16415-10	2.28458-02	8.02152-03	9.65938-01
6	15	0.46000	0.	-0.00801	1.16415-10	2.28199-02	8.00859-03	9.65977-01
6	16	0.46000	0.05640	-0.00644	1.16415-10	2.28466-02	8.02152-03	9.65938-01
6	17	0.46000	0.11280	-0.00173	0.	2.29265-02	8.06058-03	9.65821-01
6	18	0.46000	0.16922	0.00617	2.32831-10	2.30619-02	8.12715-03	9.65623-01
6	19	0.46000	0.22564	0.01735	1.16415-10	2.32563-02	8.22337-03	9.65337-01
6	20	0.46000	0.28209	0.03191	9.31323-10	2.35155-02	8.35181-03	9.64956-01
6	21	0.46000	0.33856	0.05001	-1.16415-10	2.38481-02	8.51706-03	9.64469-01
6	22	0.46000	0.39508	0.07186	-6.98492-10	2.42586-02	8.72642-03	9.63859-01
6	23	0.46000	0.45164	0.09776	3.49246-10	2.47860-02	8.99040-03	9.63093-01
6	24	0.46000	0.50825	0.12811	1.16415-09	2.54209-02	9.31211-03	9.62164-01
6	25	0.46000	0.56495	0.16313	1.86265-09	2.62102-02	9.71921-03	9.61014-01
6	26	0.46000	0.62177	0.20377	1.16415-09	2.71983-02	1.02433-02	9.59550-01
6	27	0.46000	0.67868	0.25086	1.16415-09	2.84279-02	1.08746-02	9.57819-01
6	28	0.46000	0.73599	0.30458	9.31323-10	2.99739-02	1.18400-02	9.55247-01
6	29	0.46000	0.79267	0.37038	1.86265-09	4.11145-02	1.23057-02	9.69315-01
7	1	0.55200	-0.79265	0.37038	-1.16415-10	4.08140-02	1.22910-02	9.69553-01
7	2	0.55200	-0.73599	0.30458	3.72529-09	2.99209-02	1.18437-02	9.55191-01
7	3	0.55200	-0.67868	0.25086	4.07454-09	2.81472-02	1.08713-02	9.58096-01
7	4	0.55200	-0.62177	0.20377	2.91038-09	2.70057-02	1.02415-02	9.59808-01

TABLE 28
COMPUTED RESULTS
TEST #D2 and D3

Mesh No		Coordinates			M			
x	y	x	y	z	ΔL	L_{ij}	$j=2$	β
5	26	0.36800	0.62318	0.20198	1.16415-10	2.70304-02	1.25195-02	9.51402-01
5	27	0.36800	0.68030	0.24906	4.54020-09	2.82668-02	1.32909-02	9.49348-01
5	28	0.36800	0.73792	0.30278	3.37604-09	2.97420-02	1.44843-02	9.46263-01
5	29	0.36800	0.79472	0.36863	3.60887-09	4.08030-02	1.50029-02	9.63160-01
6	1	0.46000	-0.79472	0.36863	-1.04774-09	4.10889-02	1.50070-02	9.62904-01
6	2	0.46000	-0.73792	0.30277	5.47152-09	3.01500-02	1.44851-02	9.45918-01
6	3	0.46000	-0.68030	0.24905	6.98492-10	2.83240-02	1.32963-02	9.49012-01
6	4	0.46000	-0.62317	0.20198	-1.16415-10	2.71797-02	1.25195-02	9.51101-01
6	5	0.46000	-0.56615	0.16134	3.14321-09	2.61795-02	1.18750-02	9.52867-01
6	6	0.46000	-0.50929	0.12633	4.65661-10	2.54023-02	1.13747-02	9.54254-01
6	7	0.46000	-0.45253	0.09598	6.98492-10	2.47746-02	1.09794-02	9.55375-01
6	8	0.46000	-0.39583	0.07009	2.32831-10	2.42455-02	1.06552-02	9.56300-01
6	9	0.46000	-0.33920	0.04824	-1.16415-10	2.38391-02	1.03981-02	9.57037-01
6	10	0.46000	-0.28261	0.03014	8.14907-10	2.35086-02	1.01953-02	9.57625-01
6	11	0.46000	-0.22605	0.01558	4.65661-10	2.32509-02	1.00376-02	9.58085-01
6	12	0.46000	-0.16952	0.00440	2.32831-10	2.30572-02	9.91952-03	9.58431-01
6	13	0.46000	-0.11300	-0.00350	-1.16415-10	2.29226-02	9.83783-03	9.58670-01
6	14	0.46000	-0.05650	-0.00820	1.16415-10	2.28441-02	9.78990-03	9.58811-01
6	15	0.46000	0.	-0.00977	0.	2.28183-02	9.77404-03	9.58858-01
6	16	0.46000	0.05650	-0.00820	1.16415-10	2.28451-02	9.78990-03	9.58811-01
6	17	0.46000	0.11300	-0.00350	0.	2.29253-02	9.83783-03	9.58670-01
6	18	0.46000	0.16952	0.00440	1.16415-10	2.30611-02	9.91952-03	9.58431-01
6	19	0.46000	0.22605	0.01558	3.49246-10	2.32599-02	1.00376-02	9.58085-01
6	20	0.46000	0.28261	0.03014	8.14907-10	2.35158-02	1.01953-02	9.57625-01
6	21	0.46000	0.33920	0.04824	0.	2.38487-02	1.03981-02	9.57037-01
6	22	0.46000	0.39583	0.07009	-6.98492-10	2.42587-02	1.06552-02	9.56300-01
6	23	0.46000	0.45253	0.09598	5.82077-10	2.47892-02	1.09794-02	9.55375-01
6	24	0.46000	0.50929	0.12633	4.65661-10	2.54271-02	1.13747-02	9.54254-01
6	25	0.46000	0.56615	0.16134	2.32831-09	2.62129-02	1.18750-02	9.52867-01
6	26	0.46000	0.62317	0.20198	0.	2.71980-02	1.25195-02	9.51101-01
6	27	0.46000	0.68030	0.24905	5.82077-10	2.84466-02	1.32963-02	9.49012-01
6	28	0.46000	0.73792	0.30277	5.70435-09	2.99341-02	1.44851-02	9.45918-01
6	29	0.46000	0.79472	0.36863	-1.04774-09	4.10889-02	1.50070-02	9.62904-01
7	1	0.55200	-0.79470	0.36863	2.91038-09	4.07509-02	1.49883-02	9.63192-01
7	2	0.55200	-0.73792	0.30278	4.30737-09	2.99391-02	1.44866-02	9.62248-01
7	3	0.55200	-0.68030	0.24906	1.28057-09	2.81412-02	1.32914-02	9.49348-01
7	4	0.55200	-0.62317	0.20198	2.79487-09	2.70004-02	1.25165-02	9.51411-01

TEST #D2

5	26	0.36800	0.62302	0.20218	1.04774-09	2.70264-02	1.22619-02	9.52343-01
5	27	0.36800	0.68012	0.24926	1.51340-09	2.82682-02	1.30169-02	9.50328-01
5	28	0.36800	0.73770	0.30298	3.60887-09	2.97349-02	1.41847-02	9.47501-01
5	29	0.36800	0.79449	0.36883	5.58794-09	4.07931-02	1.46978-02	9.63873-01
6	1	0.46000	-0.79449	0.36883	1.28057-09	4.10796-02	1.50708-02	9.63022-01
6	2	0.46000	-0.73770	0.30298	1.97906-09	3.01471-02	1.41864-02	9.46962-01
6	3	0.46000	-0.68012	0.24926	5.12227-09	2.83247-02	1.30220-02	9.49998-01
6	4	0.46000	-0.62301	0.20218	2.44472-09	2.71812-02	1.22619-02	9.52048-01
6	5	0.46000	-0.56602	0.16135	2.79397-09	2.61779-02	1.16310-02	9.53779-01
6	6	0.46000	-0.50917	0.12633	2.09548-09	2.54015-02	1.11413-02	9.55140-01
6	7	0.46000	-0.45243	0.09618	6.98492-10	2.47742-02	1.07544-02	9.56240-01
6	8	0.46000	-0.39575	0.07029	4.65661-10	2.42453-02	1.04370-02	9.57147-01
6	9	0.46000	-0.33912	0.04844	1.16415-10	2.38400-02	1.01854-02	9.57870-01
6	10	0.46000	-0.28255	0.03034	5.82077-10	2.35089-02	9.98678-03	9.58446-01
6	11	0.46000	-0.22601	0.01578	-2.32831-10	2.32516-02	9.83245-03	9.58898-01
6	12	0.46000	-0.16948	0.00460	1.16415-10	2.30577-02	9.71685-03	9.59237-01
6	13	0.46000	-0.11298	-0.00330	0.	2.29231-02	9.83688-03	9.59471-01
6	14	0.46000	-0.05649	-0.00800	0.	2.28446-02	9.78995-03	9.59610-01
6	15	0.46000	0.	-0.00957	-1.16415-10	2.28188-02	9.77457-03	9.59658-01
6	16	0.46000	0.05649	-0.00800	-1.16415-10	2.28456-02	9.78995-03	9.59610-01
6	17	0.46000	0.11298	-0.00330	0.	2.29250-02	9.83688-03	9.59471-01
6	18	0.46000	0.16948	0.00460	1.16415-10	2.30615-02	9.91685-03	9.59237-01
6	19	0.46000	0.22601	0.01578	-1.16415-10	2.32563-02	9.83245-03	9.58898-01
6	20	0.46000	0.28255	0.03034	4.65661-10	2.35159-02	9.98678-03	9.58446-01
6	21	0.46000	0.33912	0.04844	-3.49246-10	2.38499-02	1.01854-02	9.57870-01
6	22	0.46000	0.39575	0.07029	5.82077-10	2.42588-02	1.04370-02	9.57147-01
6	23	0.46000	0.45243	0.09618	8.14907-10	2.47891-02	1.07544-02	9.56240-01
6	24	0.46000	0.50917	0.12633	2.32831-09	2.54257-02	1.11413-02	9.55140-01
6	25	0.46000	0.56602	0.16135	2.09548-09	2.62177-02	1.16310-02	9.53779-01
6	26	0.46000	0.62301	0.20218	2.32831-09	2.72029-02	1.22619-02	9.52048-01
6	27	0.46000	0.68012	0.24926	5.23869-09	2.84429-02	1.30220-02	9.49998-01
6	28	0.46000	0.73770	0.30298	1.97906-09	2.99238-02	1.41854-02	9.46962-01
6	29	0.46000	0.79449	0.36883	1.28057-09	4.07931-02	1.46978-02	9.63873-01
7	1	0.55200	-0.79447	0.36883	3.25943-09	4.07401-02	1.44839-02	9.63905-01
7	2	0.55200	-0.73771	0.30298	1.16415-09	2.99344-02	1.41889-02	9.47888-01
7	3	0.55200	-0.68012	0.24926	2.44472-09	2.81508-02	1.30174-02	9.50328-01
7	4	0.55200	-0.62301	0.20218	1.88265-09	2.70019-02	1.22989-02	9.52354-01

TEST #D3

We imposed a DC current at a preset voltage across the electrodes for 0.25 second. The polarity used in this test was the opposite of that used in the electrolytic machining process; that is, the pointed tip under test was the anode.

First we attempted to determine the extent of damage by measuring weight loss, but we found no correlation between weight loss and arc damage; therefore, we based our evaluation on observed results and used the following comparative scale:

- 0 - no visible tip damage
- 1 - very slight visible tip damage
- 2 - slight tip damage
- 3 - moderate tip damage
- 4 - extensive tip damage
- 5 - severe tip damage

We performed two series of tests: the first series was conducted with a Gentrode cathode and we imposed 15.3 volts on the circuit; in the second series, we tested only those materials that withstood the first test reasonably well. The second test series consisted of six tests on each material using a cathode of M252 material, and increasing the voltage to 24.2. The results of these tests are shown in Table 10.

II.7.2 Description of Abrasion Resistance Test

We used a "Taber" abraser, Model 174, for our tests.

We made a special holder to test 10 material specimens simultaneously, and we used a "Taber" H-10 abrading wheel.

Our following three test conditions were:

Cycles (rpm)	Test Time (hrs)	Temp. (°F)	Load (gm)	Suction (%)
1000	20	77	500	60
1000	24	79	500	60
1000	48	81	500	60

We evaluated our tests by the "Volume Loss Method" described in the Taber instruction manual and related the results to this rating index:

<u>Index</u>	<u>Taber Wear Factor with respect to Volume Loss</u>	<u>Abrasion Resistance</u>
1	Below 1.0 to 1.0	Excellent
2	Above 1.0 to 1.5	Good
3	" 1.5 to 2.0	Fair
4	" 2.0 to 3.0	Poor
5	" 3.0	Very poor

This rating index is included in Table 28.

II. 8 Electrolyte Flow Studies

We conducted our test with an annealed René 41 with NaCl electrolyte and NaNO_3 electrolyte.

II. 8.1 Purpose

To observe and photograph the electrolyte flow pattern in the cutting gap.

II. 8.2 Design of Experiment

We observed and photographed the electrolyte in cutting area at feed rates, electrolyte pressures, and applied voltages which simulate steady state machining conditions.

II. 8.3 Facilities

The test facilities were the same as described in Appendix II.1 for Test Series JB-2. The test tooling was similar to that described in Appendix II.2 for Test Series JB-6.

II. 8.4 Procedures

II. 8.4.1 Tests Using Regular Microscope Viewer

We made several attempts to observe and photograph the electrolytic action through a microscope described in Appendix II.2. We used a 1/3000 second duration stroboscopic light in conjunction with a Speed Graphic camera (70mm ASA speed 32 film) and a Polaroid Land camera (ASA speed 3000 film). Our electrolyte was 275 gm/l of NaCl.

Take #1

In this "take", our camera was the Speed Graphic without a shutter or lens, with the microscope 20X eyepiece and 5X objective lens acting as the camera lens. Although we made 15 exposures at gaps ranging from 0.008" - 0.012", not one was useful.

Take #2

In this take, we used a Polaroid Land camera with a 1/40 sec shutter speed and, as in Take #1, with the same microscopic setup and electrolyte. Not one of our nine photographs was useful.

Take #3

We cut the solution to 138 gm/l of NaCl and added colloidal alumina hoping the light would refract off the particles and illuminate the gap. We obtained blurred photos.

II. 8.4.2 Tests Using the Micro-Schlieren System

Discussions with photographic consultants indicated that greater success might be obtained using a Schlieren system to determine whether refraction of parallel beams of light, caused by heat strata (density layers) in an electrolytic solution, could be photographed. We decided to try the method with the expectation that the refraction pattern would suggest the velocity gradient within the gap.

Therefore, we set up a micro-Schlieren optical arrangement, cameras, and modifications of the electrolytic machining test rig, each of which consisted of the following components:

1. Micro-Schlieren apparatus:

- (a) 15X achromatic eyepiece
- (b) 6X achromatic objective
- (c) Bausch & Lomb microscope body, equipped with coarse and fine adjustments.
- (d) Adjustable knife edge (2 adjustable blades, 90 degrees apart, for cutoff of x or y parallel beams).
- (e) 0.040" pinhole disc.
- (f) Condensing lens - 6X objective
- (g) High intensity light sources
 - (1) 50-watt Bausch & Lomb microscope light
 - (2) 300-watt General Electric high-intensity continuous arc light.

2. Photographic apparatus:

Milliken high-speed, 16mm motion picture camera. (Shutter speeds of 1/640, 1/2000, 1/10,000, and 1/20,000-sec available).

3. Electrolytic machine test rig:

Modification of the electrolytic machine test rig consisted of substituting two plates of Schlieren-quality fused silica for the plexiglass walls at the cutting area.

We bench-tested the micro-Schlieren apparatus for sensitivity, focal length, and adjustment of the knife edges by introducing a high velocity jet of air from a 0.30" ID tube into the inspection area. The apparatus clearly showed the shock wave created by the air jet which we successfully photographed.

We made three takes with the 16mm Milliken high-speed motion picture camera using DuPont Superior film - speed 250 ASA. These takes were made on the following electrolytic machining setup:

Potential:	8.2 volt
Current:	5 amp
Feed:	None
Electrolyte:	NaNO_3 -300 gm/l

Take #4

We set the Milliken camera at a distance of 5-6 inches from the eyepiece of the microscope, and operated at 200 frames per second with a 7-1/2 degree shutter opening to obtain a 1/10,000 second exposure. All outside light was shielded from the camera. The micro-Schlieren cell was trans-illuminated with the 300-watt, high intensity arc light. We photographed four seconds (800 frames) of the electrolytic machining process in action. No image could be seen. We reason that the sludge created by the process reduced the light passing through the solution.

Take #5

We reset the Milliken camera to a 72-degree shutter opening, and 400 frames per second speed using the same lighting and positioning of elements as in Take #1. This adjustment resulted in an exposure of 1/2000 second. No image could be seen.

Take #6

We reset the Milliken camera to 128 frames per second using all other settings established in Take #2. This adjustment resulted in an exposure of 1/640 second. The exposure was somewhat improved; however, the image was too blurred to be readable.

II.9 Servocontrol Study

We conducted our servo study on tooling which was attached to the power and electrolyte supplies, Figure 100 and Table 24.

The tooling, Figure 106, consists of a feed and guidance fixture (1) which is actuated by a variable-speed, fractional-H.P. "Bodine" motor (2). The electrode (3) is attached to the fixture head (3) which is driven by a lead screw (4).

In the ECM tooling (5), the workpiece (6) is fixed in a holder (7) which is supported by a fixture base (8) and a manual jack (not shown). We used the jack to change the cutting gap at predetermined intervals to check the response of the servo system.

The servo control unit (9) supplies the power to motor (2).

Our tests were done on the nickel-base alloy U-500 with NaCl electrolyte and with operating parameters shown in Figures 62 through 64.

II.9.1 Description of Servo Circuit

Refer to a schematic diagram, Figure 107, a Block diagram, Figure 108, and armature voltage signals, Figure 109.

The control unit supplies the power to drive the motor which actuates the feed mechanism of the described test tooling; it supplies a constant voltage to the motor field, and a variable voltage to the motor armature. For a constant load on the motor, the speed varies linearly with the armature voltage. Maximum torque is obtained at any speed, because the field current is fixed at maximum rated level.

The armature voltage is a function of the input signal. The unit accepts either of two input signals, as selected by switch SW-1, Figure 107. A voltage differential in the negative supply line of the electrolytic machine tool is connected to the jack J-1.

Switch SW-1 has 3 positions, which select the following functions:

- Position 1: Control Unit OFF.
- " 2: Selects an internal input reference voltage.
- " 3: Selects point J-1 (gap current signal).

The reference numbers are the numbered blocks in Figure 108, unless otherwise noted.

The motor armature voltage, hence the speed of the motor, is controlled by a pair of silicon controlled rectifiers (SCR). The SCR's (7) are diodes which conduct current in one direction, and then only after a triggering pulse is applied to them. The triggering pulse is supplied by a unijunction transistor, sawtooth generator (6), which is synchronized with the 60-cps power current. Once the SCR's conduct a current, they can be turned off only by reversing the voltage across them.

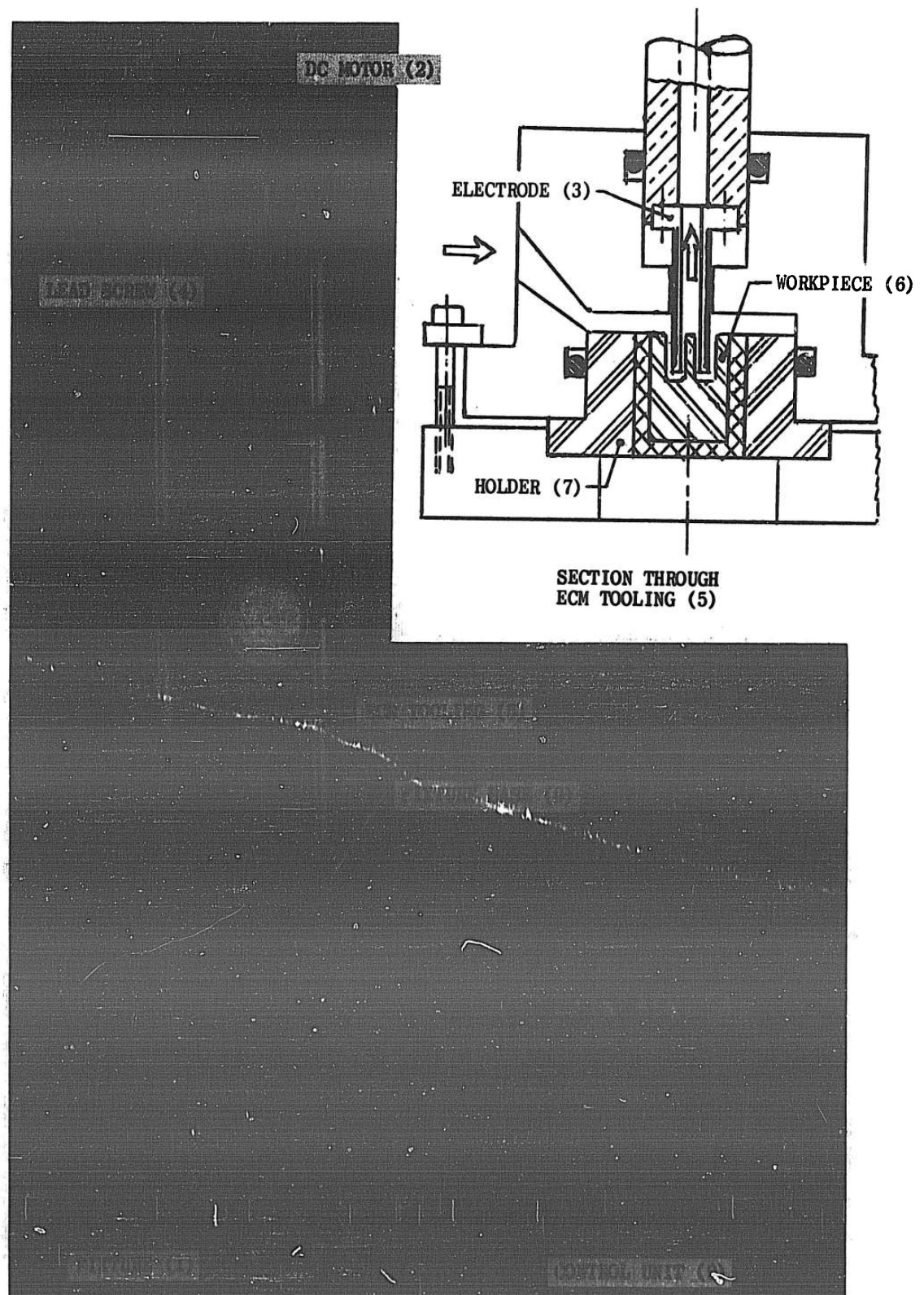


Figure 106. Tooling for Servo Study

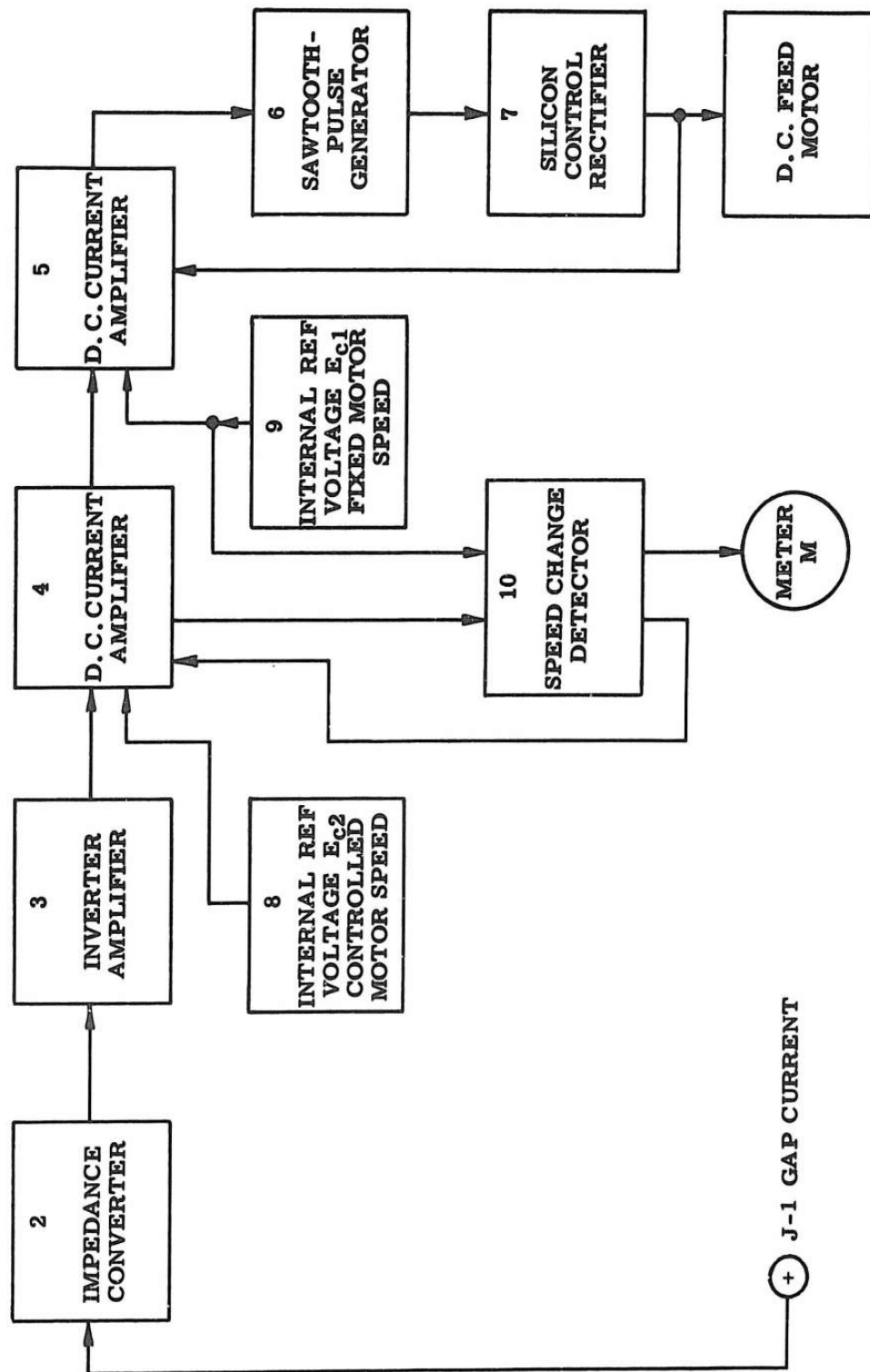
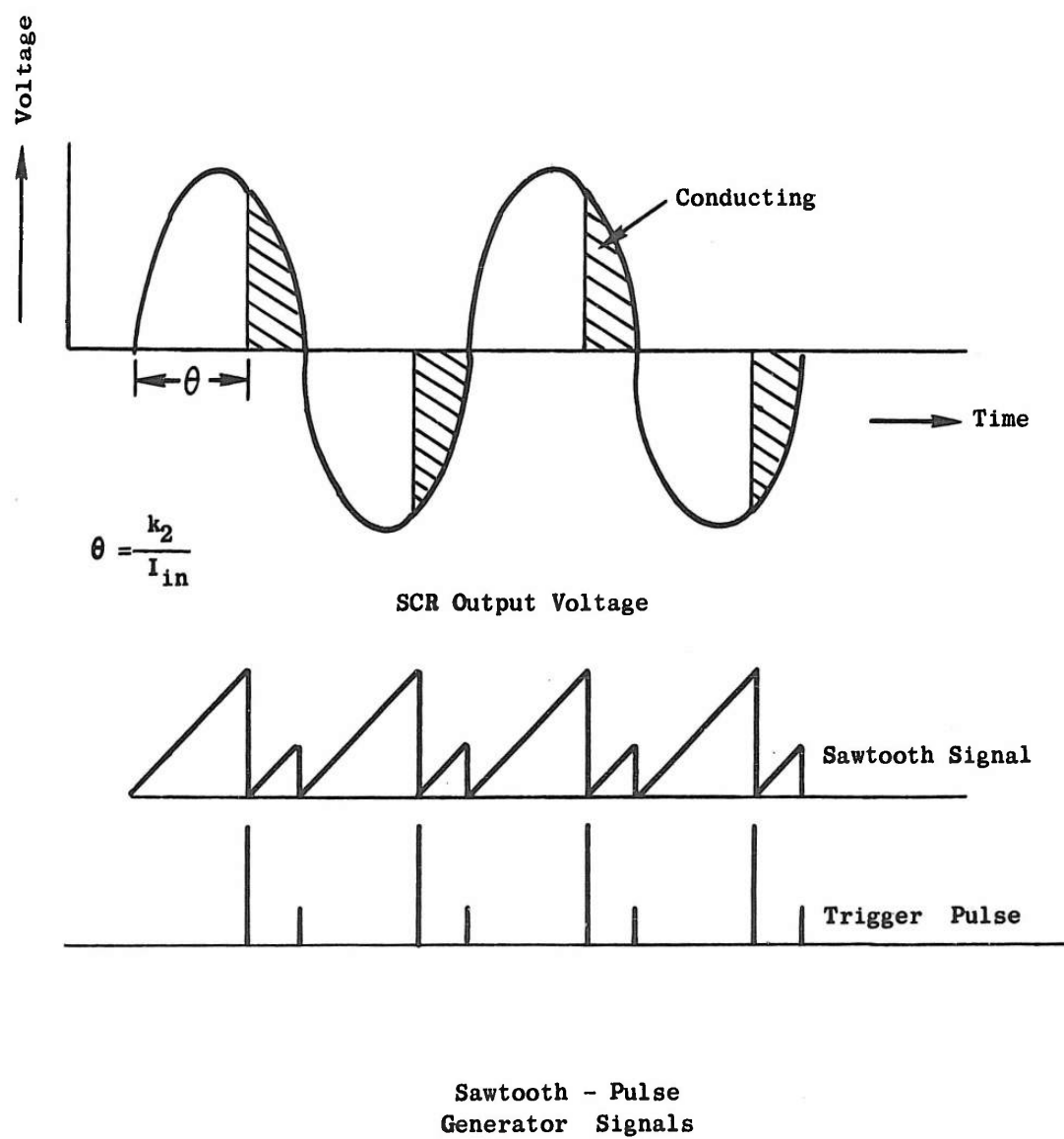


Figure 108. Block Diagram Gap Control Circuit



* where I_{in} is current through R13 into C5

$$\text{i.e. } I_{in} = I_{const} + k_1 (E_{c2} - kI_{gap})$$

$$I_{const} = k_2/\pi$$

$$\text{and } \theta = \frac{k_2}{k_2/\pi + k_1 (E_{c2} - kI_{gap})}$$

$$\text{or } \theta = \frac{\pi}{1 + k_1/k_2 (E_{c2} - kI_{gap})}$$

Figure 109. Armature Voltage Signals Gap Control Unit

The interval between pulses that trigger the SCR's depends upon the input current supplied to the unijunction transistor, Figure 109. This input current is supplied by a two-stage DC amplifier (4) and (5). There is a negative feedback loop from the output voltage to the second DC amplifier stage.

With switch SW-1 in position 2, an adjustable DC voltage (9) is supplied to the second DC amplifier. Potentiometer P-2 controls this voltage (E_{c1}). The armature voltage is constant for any given setting of P-2. With switch SW-1 in position 3, the input to (5) comes from (4), the first DC amplifier. The first DC amplifier has two inputs: one, an adjustable DC voltage, (8); the other, a voltage depending upon the selected input signal.

With switch SW-1 in position 3, the voltage at point J-1 is routed through a high-to-low impedance converter (2) and a DC inverter amplifier (3) to DC current amplifier (4). The armature output voltage is proportional to $E_{c2} - kI_{gap}$

where

E_{c2} is selected reference voltage in volt

k is transfer impedance in volt/amp

I_{gap} is gap current in amp.

The motor speed varies in such a way as to reduce any fluctuations in the controlling input signal (I_{gap}).

A detector (10) in the circuit detects any difference in speed between that set on potentiometer P-2, and that from the feedback signal. Meter (M) indicates this difference. If it exceeds a preset magnitude, the control circuit automatically switches the motor to the speed set by potentiometer P-2.

II. 10 Electrolytic Cell Investigation

II. 10. 1 Pulse Generator and Interrupter

The pulse generator and current interrupter used in the electrolytic cell investigation are described below. Diagrams of the power supply, drive and control logic circuits are given in Figures 110 and 111 respectively.

II. 10. 1. 1 Current Sources and Regulation

The electronic circuit provides a current pulse of short duration to the electrodes in the form of a square wave. The pulse repetition rate is 20 pulses/second (1 every 50 milliseconds). The pulse width is variable from 40-microseconds to 1 millisecond and the current amplitude can be set at any value from 0 to 10 amperes. The pulse rise time is 1 microsecond and the fall time is 2 microseconds. The supply voltage is adjustable from 0 to 40 volts.

In operation, the pulse current is derived from the charge on a capacitor which is renewed by a power pack when the pulse is off. The current output is measured by a Tetronix 535 oscilloscope.

The voltage between the electrodes is measured from four to seven microseconds after the electrolyzing current is turned off.

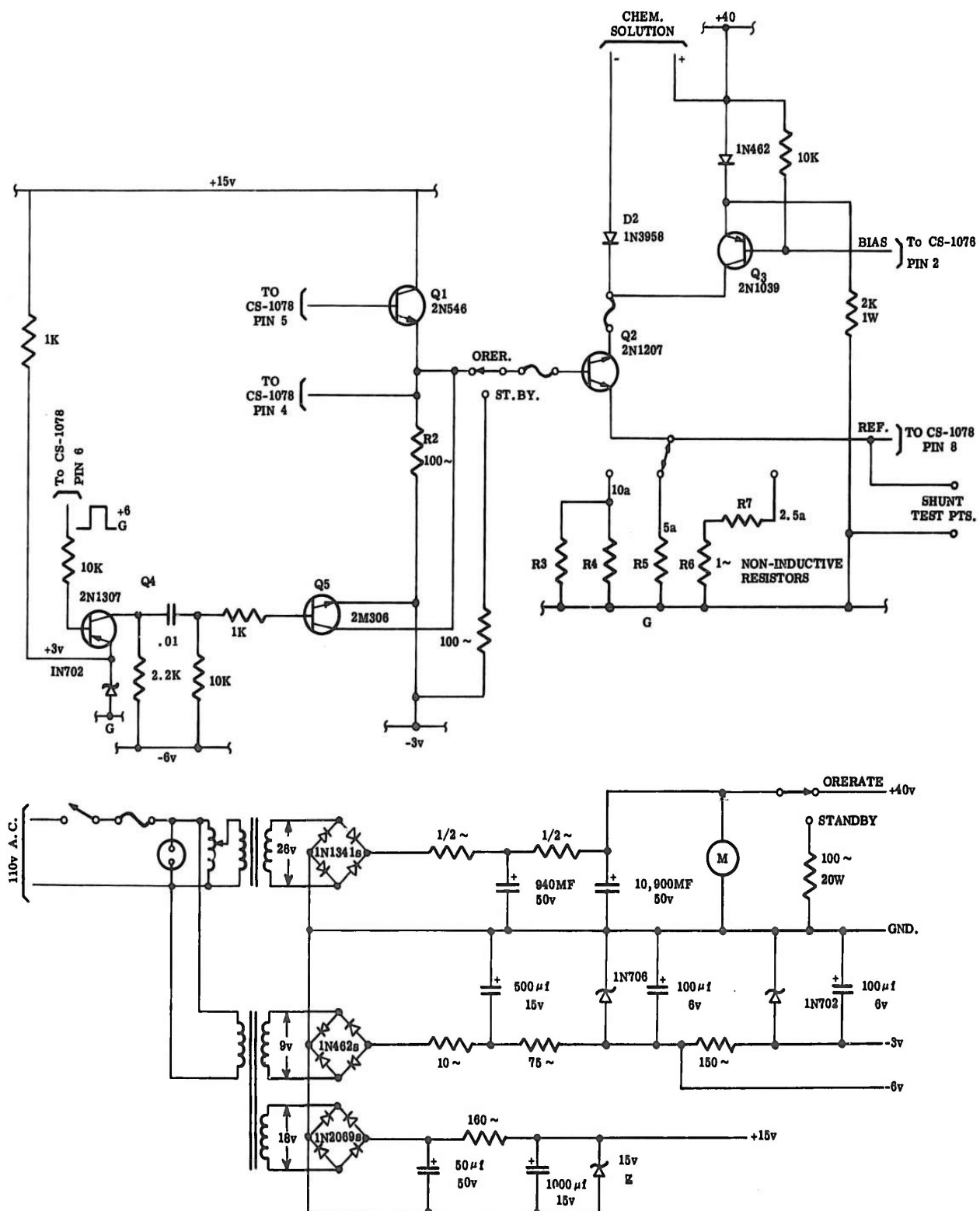


Figure 110. Schematic Diagram of Power Supply and Drive Circuit

II. 10. 1. 2 Calibration of the Pulse Generator and Interrupter

The capacity of the pulse generator to deliver 10 amperes at 40 volts, the length of pulse permissible for the voltage range and the capability of triggering the scope within seconds of current termination were ascertained for a simple resistance, a combined resistance and capacitance, and for an electrochemical cell.

The ability to produce the true decay curve was tested in two experiments; one in which the current was passed through an electrolytic capacitor; and a second in which the current was passed through nickel anodes immersed in a solution of sodium chloride. The mechanism which produces capacitance in an electrolytic capacitor, i.e., the chemical reaction, is well established. Consequently, the decay characteristics provided the proper guide in verifying the triggering mechanism. An improvised electrolytic cell of nickel electrodes and sodium chloride electrolyte was used to determine the capacity of the pulse generator and interrupter.

II. 10. 2 Electrolytic Cells

II. 10. 2. 1 Static Cell

The static cell, Figure 112 and 113, consists of an inner box, which is the electrolytic cell, and an exterior container, which is the thermostat. The thermostat controls the electrolyte temperature within 1°C using a thermal regulator, heating and cooling coils, and a stirrer. The inner box and exterior container are connected by plexiglass members 1-1/2" x 1-1/2" in cross section. A 0.875" hole in the assembly contains ball bushings which align an electrode support shaft. The bushings permit free axial motion without requiring clearance and thereby maintain alignment. The electrode support shafts are ground flat at the micrometer ends and they have a #0 Morse taper which fits the tapered adaptors. Collars on each end of the shaft contain a compression spring which holds the shaft against the stem of the micrometer. The micrometer fits into an aluminum bracket which also serves as a housing for the spring and collar assembly. Each electrode is provided with a plexiglass bracket to position the Luggin capillary.

The electrolytic cell incorporates features which prevent corrosion of the bearing assembly and prevent contamination of the electrolyte by corrosion products. Rubber bellows are cemented at one end to the cell wall and to the extremity of the drive shaft at the other end. The bellows permit the electrodes to move approximately one inch. The electrodes are aligned with the shaft by removable adaptors fitted with an #0 Morse taper. The adaptors permit complete machining of the electrodes to size and subsequent encapsulation outside the cell and assure correct positioning. The electrode connections are made directly to the adaptors to avoid errors through junction potential.

II. 10. 2. 2 Anodic Reaction Dynamic Cell

The anodic reaction cell, Figures 114 and 115, was designed to provide a smooth passage for the flow of electrolyte across the electrodes. The cell was constructed as follows: The flow passage, Figure 115, is rectangular in cross section, and it is formed by flat plates and rubber "O" seals. The width of the passage is 10 times greater than the specimen size. The length of the rectangular passage upstream of the electrodes was 30 times the electrode surface area, and the downstream length 20 times as great.

The electrodes were inserted in the flat plates forming the electrolyte passage. The lower plate converted a circular electrolyte inlet to the rectangular passage. Slots in the lower plate, along the electrolyte passage, accommodate "O" gaskets. The upper plate is bolted to the lower plate and aligned by dowel pins. The electrodes are mounted in the upper and lower plates and are aligned by bushings. Banana jacks provide the necessary electrical connections.

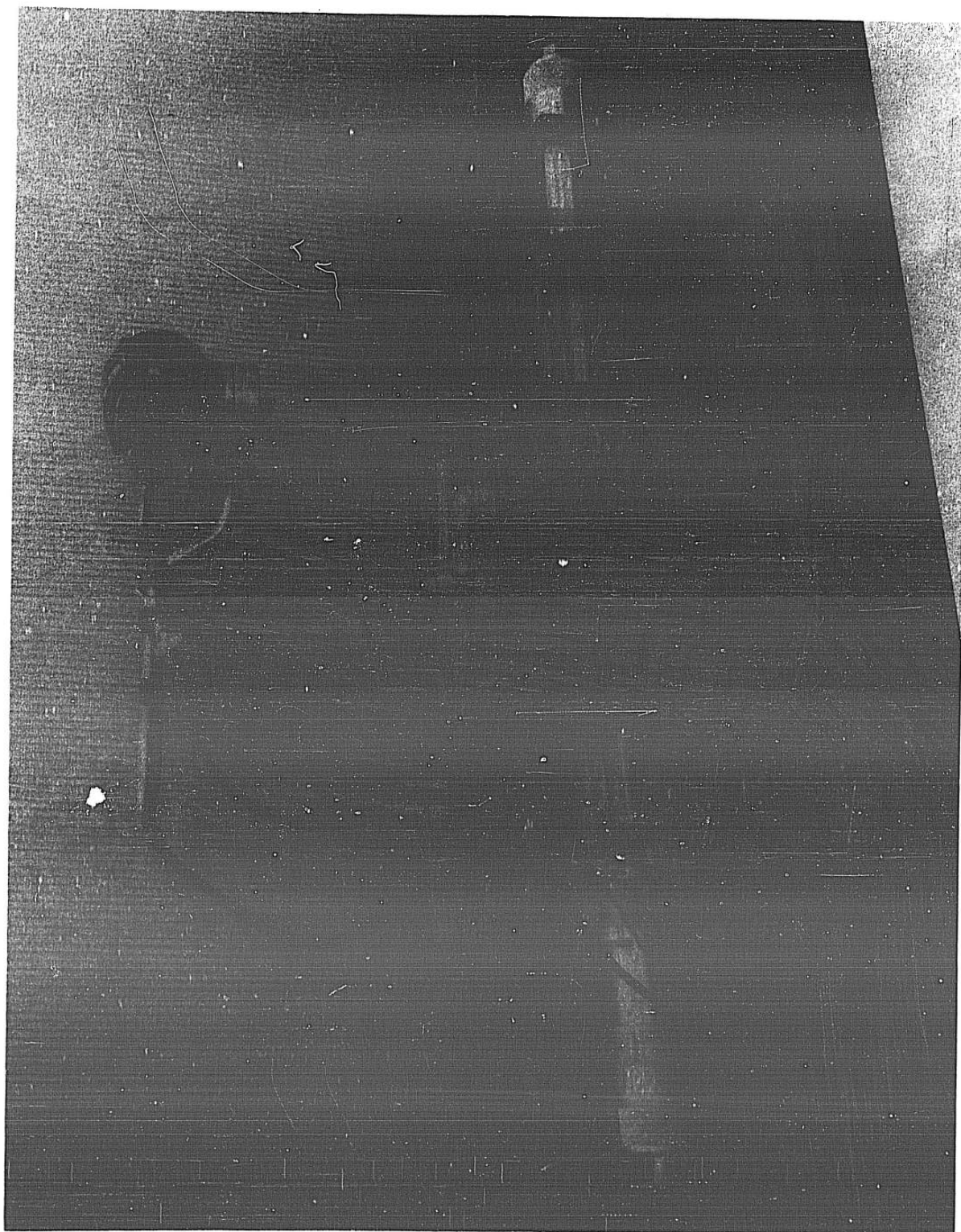


Figure 112. Static Electrolytic Cell

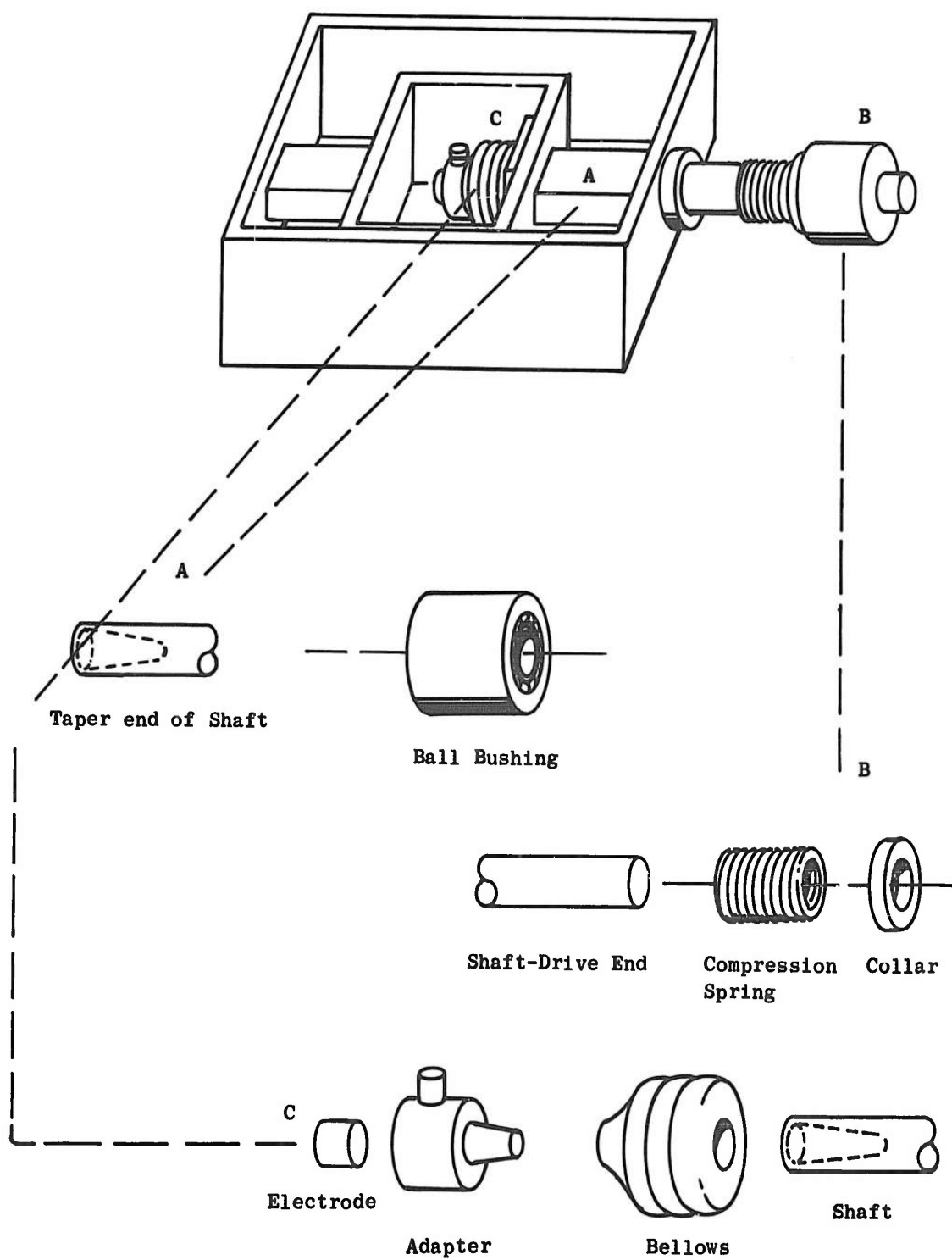


Figure 113. Schematic Sketch of Static Electrolytic Cell

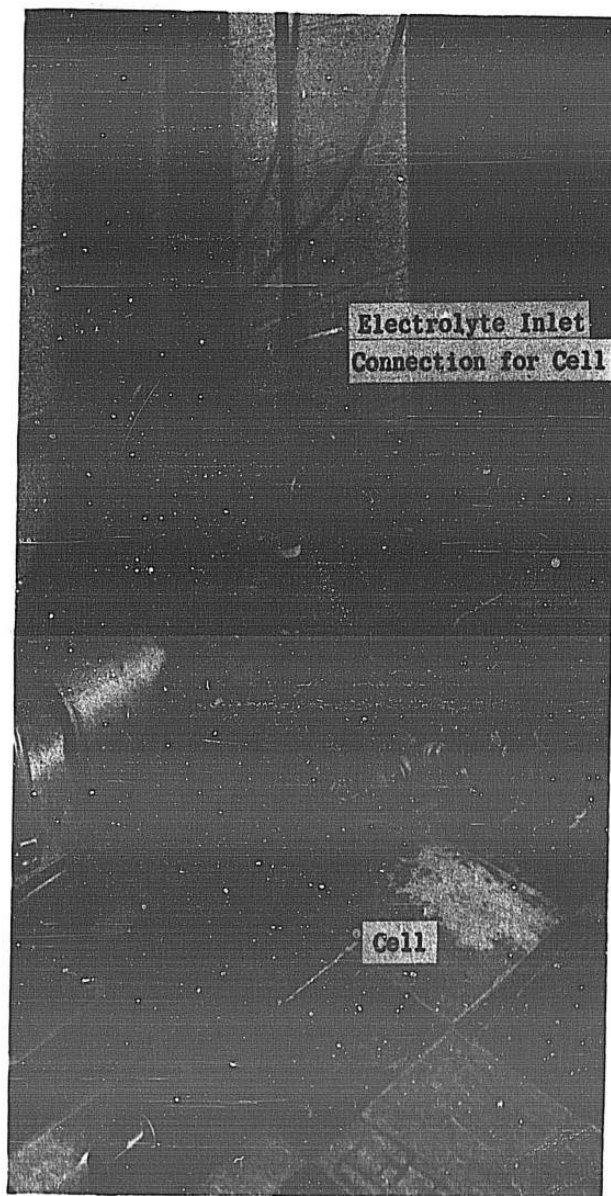


Figure 114. Anodic Reaction Dynamic Cell and Electrolyte Supply Facility

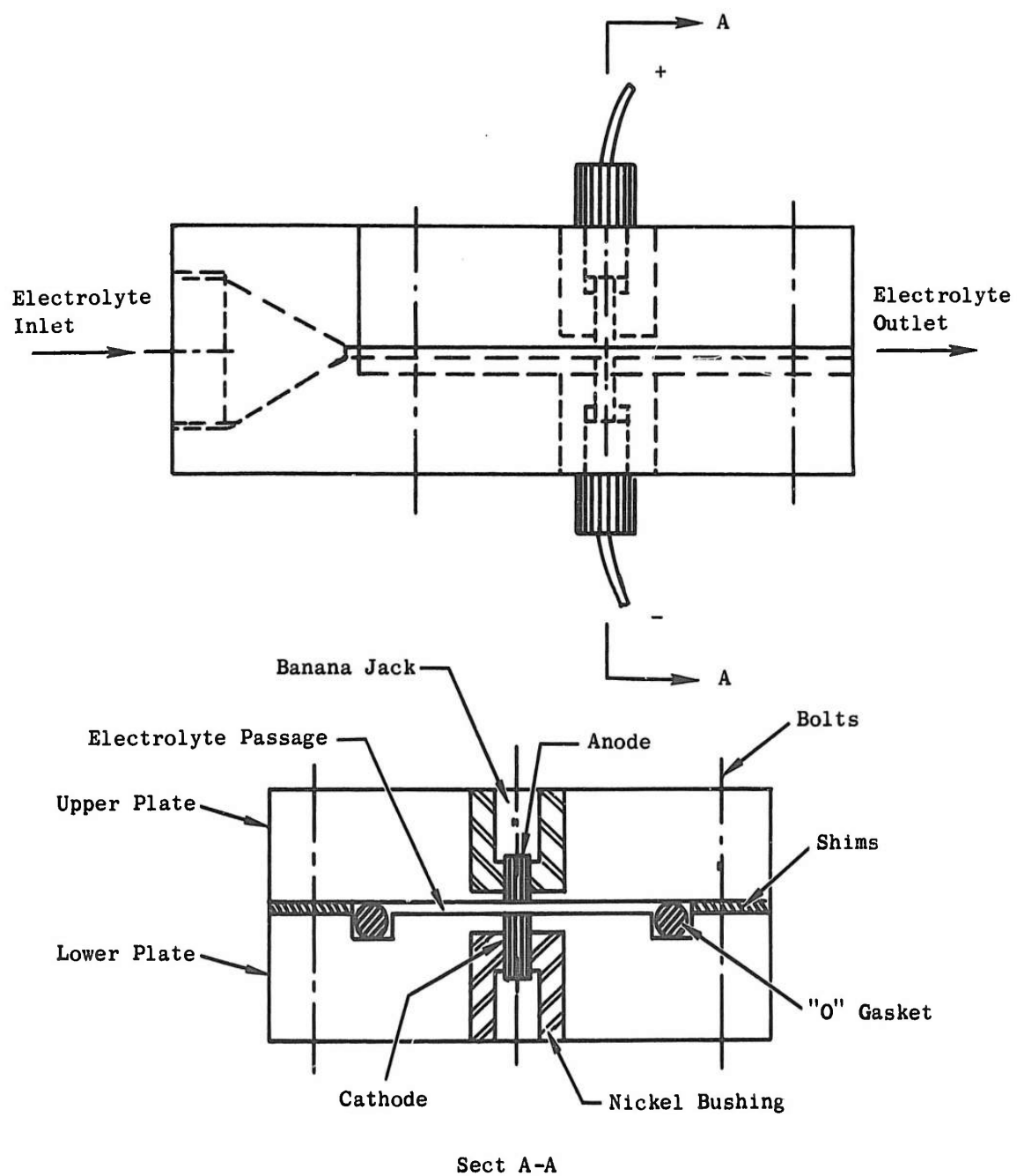


Figure 115. Schematic Sketch of Anodic Reaction Dynamic Cell

The electronic equipment for the generation of the pulse and determination of the voltage drops were those used in the static runs. The electrolyte was fed to the cell by a 5 gpm, 100 psi gear pump.

II. 10. 2. 3 Electrodes

The nickel electrodes were prepared from high purity nickel wire drawn to 0.365" and 0.114" diameter by the Techalloy Corporation, Rahn, Pennsylvania. Pure iron wire was procured from the Bram Metallurgical Company, Philadelphia, Pennsylvania, in two sizes: 0.375" and 0.125" diameter, respectively. A 0.125" diameter rod fabricated from iodide chromium was used for the chromium electrode specimens.

Electrode specimens were prepared as follows: short cylindrical pieces were ground to diameters of either 0.150" or 0.114" for most overvoltage determinations. In every case only the plane circular face was polished for electrochemical measurements. The annular surface of the specimen exposed to the solution was covered with sealing wax. For the special case of the 2000 amp/in² measurement, electrodes 0.078" in diameter were used.

II. 10. 2. 4 Electrolytes

The sodium chloride solutions were made of AR grade sodium chloride dissolved in distilled water. The sulfuric acid electrolyte was made from AR grade concentrated sulfuric acid diluted with distilled water. Commercial sodium nitrate purified in the laboratory was used for the sodium nitrate electrolyte solutions. Occasionally solutions were prepared from AR grade sodium nitrate without further purification.

II. 10. 3 Experimental Procedure

II. 10. 3. 1 Static Cell Tests

The electrodes were polished on #4 Crocus cloth using an adaptor to keep the face of the cylindrical specimen flat and perpendicular. After washing and inspecting the polished face, the anode specimen was weighed to the nearest tenth of a milligram. The electrodes were inserted firmly into adaptors and their conductivity checked with a Simpson meter. The adaptors were placed in the anode and cathode spindles and insulated with wax to prevent electrolysis on surfaces other than at the electrode faces. The electrodes were brought into contact and then retracted to the desired gap by the micrometer feed.

The electrolyte was placed in the cell and brought to the required temperature.

The selected level of current was set on the pulse generator and measured on the calibration scale of the Tetrax oscilloscope. The pulse generator, a galvanostatic type, produced a constant current regardless of resistance in the cell, except that the required EMF could not exceed the generator potential of 40 volts. The pulse width was set at a level so that the product of current and pulse width did not exceed the heat-dissipating capacity of the transistors. Electrolysis was begun and continued for 30 minutes. The maximum voltage between the electrodes and the IR drop were measured at the onset of electrolysis and at five-minute intervals thereafter. At selected electrode separations, the Luggin capillary was placed so that its tip was at the anode surface and the anode voltage was measured against the potential of the saturated calomel electrode. At the completion of electrolysis, the electrodes were washed with water and alcohol and weighed again to determine weight loss. The surfaces of the specimens were then examined and selected samples were submitted for X-ray diffraction studies and electron microscopy.

II. 10. 3. 2 Anodic Reaction Dynamic Cell Tests

After preliminary polishing, the electrodes were inserted into each section of the dynamic cell so that the electrode surfaces were flush. The entire surface of the section was first polished on medium grit paper, then on #4 Crocus cloth until the electrode and cell wall were flush with the electrolyte passage. The "O" ring seal was inserted in the slots, the spacers set in place and the two sections of the dynamic cell were bolted together after the cells were washed with water and naptha.

The cell was connected to the electrolyte supply system and the pulse generator. A predetermined current density was set and the overvoltage was measured at various flow rates.

II. 10. 3. 3 ECM Dynamic Cell Tests

The tests in the ECM dynamic cell were conducted in an apparatus described in Appendix II. 1. 4. 3.

Specimens were machined from René 41 and pure nickel to 0.187" x 0.114" x 4" dimensions and inserted into the respective anode and cathode holders. No motion was imparted to either of the electrodes. The starting gaps were set at 0.010".

The pulse generator previously used was the source of electricity. The electrode potentials were measured on the Tetronix oscilloscope.

The electrolyte flow through the ECM cell was controlled at the predetermined levels by the same procedures described in Appendix II. 1. 4. 4.

II. 10. 4 Test Data

The results of the electrolytic cell investigations not previously reported are included in this section.

Tables 29 through 35 include the results of the Static Cell tests; Tables 36 through 38 of the Anodic Reaction Dynamic Cell tests; and Tables 39 and 40 of the ECM Dynamic Cell tests.

TABLE 29.
TOTAL ΔE MEASUREMENTS
TEST SERIES Fe/ NaNO_3
STATIC CELL

Test Number	Current Density amp/ in^2	Temperature $^\circ\text{F}$	Concentration lb/gal	Gap (mil)	0-1	5	10	15	20	25	30	n Factor
1	868	139	5.47	27.5	2	7.5	0	0	0	0	0	5.57
2	868	139	5.47	6.5	5	3.5	6	5.5	0.5	0	0	3.22
3	868	139	3.71	27.5	6	5	4	12	12	13	11	5.57
4	868	139	3.71	6.5	6.5	7	7	5	5	5.5	5	4.93
5	868	83	5.47	27.5	16	16	15	15	15	15	15	0.18
6	868	83	5.47	6.5	16	15	3.5	4.5	4.5	5.5	3.5	10.3
7	868	83	3.71	27.5	6	9	4	6	8	8	8	3.0
8	868	83	3.71	6.5	35	7	7.5	8	8	7.5	5	6.59
9	232	139	5.47	27.5	7	9.5	9.8	9.8	9.8	9.8	9.8	35.7
10	232	139	5.47	6.5	2.25	6	8.5	9.5	10.25	8.1	8	3.11
11	232	139	3.71	27.5	9	8.5	8.9	9.3	8.8	8.8	8.8	66.8
12	232	139	3.71	6.5	10	7.5	7.5	7.5	7.5	8.0	8	17.1
13	232	83	5.47	27.5	5	4.5	4.5	5	5	5	5	0.42
14	232	83	5.47	6.5	3	4	4	3	3	3	3	14.3
15	232	83	3.71	27.5	3	4	4	6	6	6	5	16.4
16	232	83	3.71	6.5	4.5	4.5	5	4	4	4	4	22.2
17	1000	111	4.59	17	0	0	0	0	0	0	0	23.9
18	100	111	4.59	17	17	8.5	8	8	9	10	10	1.09
19	550	150	4.59	17	7.5	7.5	9	9	9	8	10	6.22
20	550	72	4.59	17	21	10	10	10	10	11	15	9.59
21	550	111	5.84	17	6	6	5	5	5	4.5	4.5	4.79
22	550	111	3.34	17	5	6	8	10	11	12	14	3.65
23	550	111	4.59	32	6	4	4.5	4	5	4.5	5	16.3
24	550	111	4.59	2	1.5	13	15.5	19	15	13	11	26.9
25	550	111	4.59	17	13	10	10	10	10	10	10	2.31
26	2000	111	4.59	17	16	17.5*						

*Run continued through 2 minutes only

TABLE 30
ANODE ΔE MEASUREMENTS
TEST SERIES Fe/ NaNO_3
STATIC CELL

Test Number	Current Density amp/ in^2	Temperature $^{\circ}\text{F}$	Concentration lb/gal	Gap (mil)	0-1	5	10	15	20	25	30
1	232	83	5.47	27.5	2.5	2	2.5	2	2	2.5	2
2	868	83	5.47	27.5	1	<1	<1	4	.1	.1	.1
3	232	83	3.71	27.5	1	0	0	0	0	0	3
4	868	83	3.71	32	5	5	0	1	3	2	2
5	550	111	4.59	27.5	0	0	.1	0	.1	.1	0
6	232	139	5.47	27.5	2.0	2.0	2.0	2.0	2.0	2.0	2.0
7	232	139	3.71	27.5	0	0	0.5	1.0	0.7	0.7	0.7
8	868	139	3.71	27.5	0.0	0	0	0	0	0.1	0.0

TABLE 31.
CALCULATED CATHODE ΔE 's
TEST SERIES Fe/ NaNO_3
STATIC CELL

Test Number	Current Density amp/in ²	Temperature °F	Concentration lb/gal	Gap (mil)	Cathode ΔE (volt)						
					Time in Min						
					0-1	5	10	15	20	25	30
1	232	83	5.47	27	2.5	2.5	2.0	3.0	3	3	2.5
2	868	83	5.47	27	15	15	15	11	15	15	15
3	232	83	3.71	27	3	4	4	6	6	6	2
4	868	83	3.71	27	1	4	4	5	5	6	6
5	550	111	4.59	32	6	4	4.5	4	5	4.5	5
6	232	139	5.47	27	5	7.5	7.8	7.8	7.8	7.8	7.8
7	232	139	3.71	27	9	8.5	7.4	8.3	8.1	8.1	8.1
8	868	139	3.71	27	6	5	4	12	12	13	11

TABLE 32.
TOTAL ΔE MEASUREMENTS
TEST SERIES Cr/NaCl
STATIC CELL

Test Number	Current Density amp/in ²	Temperature °F	Concentration lb/gal	Gap (mil)	0-1	5	10	15	20	25	30	n Factor
1	868	139	2.71	27.5	5	5	3.5	3.5	3.5	5	5.5	6.99
2	868	139	2.71	6.5	3.5	3.5	3.0	3.5	4.0	4.0	3.0	6.96
3	868	139	1.29	27.5	7.5	7.5	7.0	7.5	7.5	7.5	8.5	9.05
4	868	139	1.29	6.5	10	0	2.5	2.0	2.5	2.0	2.0	8.66
5	868	83	2.71	27.5	9.0	5.0	5.0	5.0	5.0	7.0	6.0	8.85
6	868	83	2.71	6.5	4.0	5.0	5.0	4.0	5.0	6.0	6.0	7.52
7	868	83	1.29	27.5	24.8	24.5	21.7	21.5	22.5	21.8	21.1	10.5
8	868	83	1.29	6.5	21.3	19.6	3.0	4.0	5.0	6.0	5.0	7.52
9	232	139	2.71	27.5	16.2	9.5	8.8	10	10.2	10.3	10.5	4.54
10	232	139	2.71	6.5	10.0	10.0	10.5	10.5	10	9.5	7.5	5.90
11	232	139	1.29	27.5	11.4	8.0	8.2	7.7	7.7	8.2	8.5	4.28
12	232	139	1.29	6.5	5.8	5.6	6.2	6.8	6.7	6.7	7.1	4.91
13	232	83	2.71	27.5	20	18	11	12	12	11	12.8	4.69
14	232	83	2.71	6.5	8.9	9.7	11.3	14	14	14.3	14.5	4.74
15	232	83	1.29	27.5	12.8	12.8	13.5	13.5	13.5	13.5	13.5	4.84
16	232	83	1.29	6.5	11	8	9	10	12.5	13.8	15	3.73
17	1000	111	2.0	17	4.0	4.5	5.0	5.3	6.0	6.0	6.0	6.95
18	100	111	2.0	17	5.0	4.0	4.0	3.8	3.4	3.4	3.8	4.07
19	550	150	2.0	17	7.5	6.5	6.5	6.5	6.5	6.5	6.9	6.29
20	550	72	2.0	17	10.0	6.0	6.0	7.0	6.0	5.5	4.5	7.32
21	550	111	3.0	17	12.5	12	12	13	11	10	11	7.20
22	550	111	1.0	17	7.0	7.5	8.0	6.0	6.5	8.0	8.0	7.0
23	550	111	2.0	32	14	10	10	10	10	11	10.0	5.72
24	550	111	2.0	2	7.5	7.0	13	16	12	13.5	13.5	5.34
25	550	111	2.0	17	11	11	10	12	8.0	7.0	9.0	5.63
26	2000	111	2.0	17	7.5	9.5*						

*Run continued through 2 minutes only

TABLE 33.
ANODE ΔE MEASUREMENTS
TEST SERIES Cr/NaCl
STATIC CELL

Test Number	Current Density amp/in ²	Temperature °F	Concentration lb/gal	Gap (mil)	Anode ΔE (volt vs SCE Time in Min						
					0-1	5	10	15	20	25	30
1	232	139	2.71	27.5	3.0	2.0	2	2	2	2.3	2.3
2	868	83	2.71	27.5	.1	.1	.1	.1	.1	.1	.1
3	868	83	1.29	27.5	.1	.1	.1	.1	.1	.1	.1
4	232	83	2.71	27.5	4.5	3	3	3	3	3	4
5	232	83	1.29	27.5	3.0	3	3	3	3.8	3.8	4
6	550	111	2.0	32	1.5	1	1	2	1	1	1

TABLE 34.
CALCULATED CATHODE ΔE 's
TEST SERIES Cr/NaCl
STATIC CELL

Test Number	Current Density amp/in ²	Temperature °F	Concentration lb/gal	Gap (mil)	0-1	5	10	15	20	25	30
1	232	139	2.71	27.5	13	7.5	6.8	8	8.2	8	8.2
2	868	83	2.71	27.5	9.0	5.0	5.0	5.0	5.0	7.0	6.0
3	868	83	1.29	27.5	7.5	7.5	7.0	7.5	7.5	7.5	8.5
4	232	83	2.71	27.5	15.5	15	8	9	9	8	8.8
5	232	83	1.29	27.5	9.8	9.8	10.5	10.5	9.8	9.8	9.5
6	550	111	2.0	32	13	9	9	8	9	10	9

TABLE 35.
TOTAL ΔE MEASUREMENTS
TEST SERIES Fe/H₂SO₄
STATIC CELL

Test Number	Current Density amp/in ²	Temperature °F	Concentration % by weight	Gap (mil)	Total ΔE (volt)		
					Time in Min		
					0	1	2
1	100	90	5	17	3.7	3.7	4.0
2	232	90	5	17	5	7	10.2
3	550	90	5	17	12	13	14
4	868	90	5	17	12	15	15
5	1000	90	5	17	16	15	15
6	2000	90	5	17	7	7	7
*7	232	90	5	17	7.2	7.2	7.2
8	550	90	5	17	16.5	16.5	-
9	868	90	5	17	13	13	-

* Replicate of 2

TABLE 36.
TOTAL ΔE MEASUREMENTS
ANODIC REACTION CELL
TEST SERIES Ni/NaCl

Test No.	Current Density amp/in ²	Flow cc/min	Velocity cm/sec	ΔE volt
1	232	2750	66	4.3
2	232	700	17	3.1
3	232	1500	36	3.6
4	232	2500	59	4.0
5	232	3000	72	4.0
6	232	4000	96	4.0
7	550	4000	96	6.5
8	550	2675	65	6.0
9	550	475	11	6.0
10	550	2100	50	6.0
11	550	3000	72	6.0
12	550	3300	78	6.25
13	868	3590	84	8
14	868	4100	97	8
15	868	4750	114	8
16	868	3000	72	8.3
17	868	1600	38	8.6
18	868	400	9	8.6

Test Conditions:

Electrolyte Concentration: 2.0 lb/gal
Electrolyte Temperature: 83°F
Starting Gap between Electrodes: 0.008"

TABLE 37.
TOTAL ΔE MEASUREMENTS
ANODIC REACTION CELL
TEST SERIES Fe/NaNO₃

Test No.	Current Density amp/in ²	Flow cc/min	Velocity cm/sec	ΔE volt
1	100	3500	440	6.0
2	100	2500	320	6.8
3	100	730	90	5.8
4	232	750	90	7
5	232	2250	290	5
6	232	2800	360	6
7	232	3750	480	4
8	550	3500	440	7
9	550	2500	320	7
10	550	1600	200	7
* 11	550	2500	440	7
12	868	2500	440	3
13	868	3600	460	3
14	868	900	170	5
15	868	2150	270	4

* Repeat (check on #9)

Test Conditions:

Electrolyte Concentration: 4.59 lb/gal
Electrolyte Temperature: 83° F
Starting Gap between Electrodes: 0.015"

TABLE 38.
TOTAL ΔE MEASUREMENTS
ANODIC REACTION CELL
TEST SERIES Cr/NaCl

Test No.	Current Density amp/in ²	Flow cc/min	Velocity cm/sec	ΔE volt
1	100	4500	3.1	580
2	100	3450	3.0	440
3	100	1000	3.0	120
4	100	2450	2.6	3.0
5	100	400	2.2	50
6	232	900	5.0	110
7	232	1700	4.5	210
8	232	2750	4.5	350
9	232	3750	4.5	480
10	232	4700	5.0	590
11	550	1200	6	150
12	550	3100	6	270
13	550	3370	5.5	420
14	550	4700	6	590
15	868	4200	6	490
16	868	3150	7	400
17	868	2000	7	250
18	868	1050	7	130
19	868	400	7	50

Test Conditions:

Electrolyte Concentration: 2.0 lb/gal
 Electrolyte Temperature: 86° F
 Starting Gap between Electrodes: 0.015"
 (Chromium Anode, Nickel Cathode)

TABLE 39.
TOTAL ΔE MEASUREMENTS
E.C.M. CELL
TEST SERIES R41/NaCl

Test Number	Current Density amp/in ²	Flow cc/min	Pressure psig	Total ΔE (volt) Time in Min				Gap change during electrolysis in $\times 10^{-4}$
				0	1	2	3	4
1	458	2778	276	3.4	3.4	3.4	3.4	3.4
2	458	2778	54	3.5	3.8	3.4	3.6	3.7
3	458	722	276	3.5	3.5	3.5	3.5	3.5
4	458	722	54	3.5	3.5	4.0	3.5	3.5
5	67	2778	276	1.3	1.3	1.4	1.4	1.3
6	67	2778	54	1.2	1.2	1.2	1.2	1.2
7	67	722	276	1.2	1.2	1.2	1.2	1.2
8	67	722	54	1.2	1.2	1.2	1.3	1.4
9	500	1750	165	2.1	2.0	2.0	2.0	2.0
10	25	1750	165	0.6	0.8	0.8	0.8	0.8
11	263	3000	165	2.8	3.0	3.0	2.9	3.1
12	263	500	165	3.0	2.7	2.7	3.0	3.0
13	263	1750	300	2.9	3.2	3.2	3.2	3.3
14	263	1750	30	2.0	3.0	3.0	3.0	3.0
15	263	1750	165	3.0	3.0	3.0	3.1	3.1

Test Conditions:

Electrolyte Concentration: 2.35 lb/gal
Electrolyte Temperature: 90° F

TABLE 40.
TOTAL ΔE MEASUREMENTS
E.C.M. CELL
TEST SERIES Ni/NaCl

Test Number	Current Density amp/in ²	Flow cc/min	Pressure psig	Total ΔE (volt) Time in Min				Gap change during electrolysis in $\times 10^{-4}$
				0	1	2	3	4
1	458	2778	276	4.5	4.5	4.5	4.6	4.7
2	458	2778	54	3.5	3.5	3.2	3.5	3.5
3	458	722	276	3.0	3.0	3.1	3.1	3.1
4	458	722	54	3.5	3.5	3.7	3.7	3.7
5	67	2778	276	2.5	2.6	2.6	2.6	2.6
6	67	2778	54	1.6	1.7	1.8	1.8	1.8
7	67	722	276	1.2	1.2	1.2	1.2	1.3
8	67	722	54	1.2	1.4	1.4	1.4	1.4
9	500	1750	165	3.2	3.2	3.2	3.5	3.5
10	25	1750	165	0.7	0.8	0.8	1.0	1.0
11	263	3000	165	2.5	2.5	3.0	3.2	3.2
12	263	500	165	3.1	3.3	3.3	3.3	3.3
13	263	1750	300	2.4	2.7	2.7	2.7	2.8
14	263	1750	30	3.0	3.1	3.3	3.3	3.3
15	263	1750	165	3.8	3.8	3.8	3.9	3.9

Test Conditions:

Electrolyte Concentration: 2.35 lb/gal
Electrolyte Temperature: 90°F

APPENDIX III

FORTRAN INSTRUCTIONS

The following instructions apply to the mathematical model, with Equation (6d) representing the steady state electrolytic machining.

```

*ELECTRO00
C... MAIN PROGRAM TO CHECK CATHOD
COMMON AX,AY,AZ,CX,CY,CZ,NZ,MZ,N,M,GAP,
1GAMMA,XP,YP,ZP,OPTION,DUMMY,NIT,ALPHA,AIMAX,F0,GK
2,TAFFY,FGK
COMMON RBART,GAPT,EE,DEE,NGAP
DIMENSION RBART(30),GAPT(30)
DIMENSION AD(30,30),BD(30,30),CD(30,30)
DIMENSION AX(30),AY(30),AZ(30,30),CX(900),CY(900),
1CZ(900),GAMMA(30,30),OPTION(10),IDENT(10),GK(20)
100 READ DIP AX,AY,AZ,NZ,MZ,GAP,GAMMA,OPTION,
1N,M,NIT,XP,YP,ZP,DUMMY,IDENT,ALPHA,AIMAX,F0,GK
2,TAFFY,FGK,EE,DEE,RBART,GAPT,NGAP
IF(NZ+MZ)101,101,102
101 NZ=1
MZ=1
102 CONTINUE
WRITE OUTPUT TAPE 3,1000,(IDENT(I),I=1,10)
N=N
M=M
WRITE OUTPUT TAPE 3,1100,N,M,NZ,MZ,GAP,XP,YP,ZP,AIMAX,F0,GK(1)
WRITE OUTPUT TAPE 3,1200,(AX(I),I=1,N)
WRITE OUTPUT TAPE 3,1300,(AY(I),I=1,M)
WRITE OUTPUT TAPE 3,1400
DO 140 I=1,N
JST =-3
DO 130 J=1,M,4
JST = JST+4
JSP=XMINOF((JST+3),M)
WRITE OUTPUT TAPE 3,1500,I,(AZ(I,K),K=JST,JSP)
130 CONTINUE
140 CONTINUE
IF(NGAP)2,7,2
*ITERATE FOR VALUE OF GAP BASED ON INPUT TABLES
2 DO 50 I=1,N
DO 50 J=1,M
CALL NORMAL(AX,AY,AZ,I,J,N,M,A,B,C)
AD(I,J)=A
BD(I,J)=B
CD(I,J)=C
50 CONTINUE
KTR=0
LIMIT=40
LIM=0
INDA=0
INDB=0
CHECK = COSF(DUMMY*.01745329)
CALL LINIT(GAP,RBAR,GAPT,RBART,NGAP,FN)
7 BETA=F0/((GK/RBAR)*(EE-DEE))
DO 10 I=1,N
DO 10 J=1,M
GAMMA(I,J)=BETA*CD(I,J)
10 CONTINUE
150 CALL CATHOD
GO TO 100
1000 FORMAT
RESTORE
-X
END OF FORMAT
1100 FORMAT
SPACE 1

```

-A

```

      N = -I  M = -I  NZ = -I  NZ = -I  GAP =      -0PF4
      XP =      -0PF4  YP =      -0PF4  ZP =      -0PF4
IMAX=      -1PE5  F0 =      -1PE5  K =      -1PE5
SPACE 1
      INPUT ANODE
SPACE 2
END OF FORMAT
1200 FORMAT
      X VALUES
SPACE 1
-0PF4  -0PF4  -0PF4  -0PF4  -0PF4  -0PF4  -0PF4  -0PF4
REPEAT 1
END OF FORMAT
1300 FORMAT
SPACE 2
      Y VALUES
SPACE 1
-0PF4  -0PF4  -0PF4  -0PF4  -0PF4  -0PF4  -0PF4  -0PF4
REPEAT 1
END OF FORMAT
1400 FORMAT
SPACE 2
      Z VALUES
      I      Z      Z      Z      Z
END OF FORMAT
1500 FORMAT
      -I      -0PF4      -0PF4      -0PF4      -0PF4
END OF FORMAT
END

```

*CATHOD00

C... SUBROUTINE TO COMPUTE CATHODE AS A SERIES OF POINTS

C... C(X,Y,Z) NECESSARY TO PRODUCE GIVEN ANODE WHICH

C... IS KNOWN AS A MESH OF POINT A(X,Y,Z).

C... CALLING SEQUENCE

C... CALL CATHOD

SUBROUTINE CATHOD

COMMON AX,AY,AZ,CX,CY,CZ,NZ,MZ,N,M,GAP,

1 GAMMA,XP,YP,ZP,OPTION,DUMMY,NIT,ALPHA,AIMAX,F0,GK

2,TAFFY,FGK

COMMON RBART,GAPT,EE,DEE,NGAP

DIMENSION RBART(30),GAPT(30)

DIMENSION OPTION(10),AREA(900),GK(20)

DIMENSION AX(30),AY(30),AZ(30,30),CX(900),CY(900),

1 CZ(900),GAMMA(30,30),XL(900),EP(900),DXL(900)

DIMENSION S(900),DS(900),AD(30,30),BD(30,30),CD(30,30),RATIO(900)

DIMENSION ARPP(900)

NZ=NZ

MZ=MZ

N=N

M=M

FIRST=0.0

TESTA=ABSF(.00001*GAP)

CHECK=COSF(DUMMY*.01745329)

ALPHR=ALPHA*.01745329

RC=GAP*SINF(ALPHR)/COSF(ALPHR)

AS = 3.1415927*RC**2

DO 990 I=1,N

DX1=ABSF(AX(I)-AX(1))

DX2=ABSF(AX(N)-AX(I))

IF(RC-DX1)810,810,830

810 IF(RC-DX2)820,820,850

820 A1=0.0

H1=RC+1.0

GO TO 860

830 DX=DX1

840 H=RC-DX

H1=RC-H

HK2=SQRTF(2.0*RC*H-H**2)

IF(ABSF(H1/RC)-1.0E-3)841,841,842

841 A1=AS/2.0

GO TO 860

842 A1=RC**2*ATANF(SQRTF(RC**2-H1**2)/H1)-H1*HK2

GO TO 860

850 DX=DX2

GO TO 840

860 CONTINUE

DO 980 J=1,M

IJ=(J-1)*N+1

DY1=ABSF(AY(J)-AY(1))

DY2=ABSF(AY(M)-AY(J))

IF(RC-DY1)870,870,890

870 IF(RC-DY2)880,880,910

880 A2=0.0

GO TO 940

890 DY=DY1

900 HK=RC-DY

HK1=RC-HK

H2=SQRTF(2.0*RC*HK-HK**2)

IF(ABSF(HK1/RC)-1.0E-3)901,901,902

```

901 A2=AS/2.0
    GO TO 920
902 A2=RC**2*ATANF(SQRTF(RC**2-HK1**2)/HK1)-HK1*H2
    GO TO 920
910 DY=DY2
    GO TO 900
920 IF(H1**2+HK1**2-RC**2)930,940,940
930 AP=HK1*(H1-H2)+(H2/2.0)*SQRTF(RC**2-H2**2)
    AP=AP-(H1/2.0)*SQRTF(RC**2-H1**2)
    DENOM=SQRTF(RC**2-H2**2)
    IF(DENOM)400,401,400
401 DENOM=H2*.001
400 DENOM1=SQRTF(RC**2-H1**2)
    IF(DENOM1)403,402,403
402 DENOM1=H1*.001
403 AP=AP+(RC**2/2.0)*(ATANF(H2/DENOM)-ATANF(H1/DENOM1))
    GO TO 945
940 AP=0.0
945 RATIO(IJ)=(AS-A1-A2 +AP)/AS
980 CONTINUE
990 CONTINUE
    Q=SQRTF((AX(NZ)-XP)**2+(AY(MZ)-YP)**2
    1+(AZ(NZ,MZ)-ZP)**2)
    AA=(AX(NZ)-XP)/Q
    BB=(AY(MZ)-YP)/Q
    CC=(AZ(NZ,MZ)-ZP)/Q
C... CHECK OPTION TO SEE HOW FIRST GUESS IS COMPUTED
10 IF(OPTION)20,20,50
C... CONSTRUCT SURFACE AS POINTS ON NORMALS
20 DO 40 I=1,N
    DO 30 J=1,M
    CALL NORMAL(AX,AY,AZ,I,J,N,M,A,B,C)
    AD(I,J)=A
    BD(I,J)=B
    CD(I,J)=C
    IJ=N*(J-1)+I
    CX(IJ)=AX(I)+A*GAP
    CY(IJ)=AY(J)+B*GAP
30 CZ(IJ)=AZ(I,J)+C*GAP
40 CONTINUE
    GO TO 100
C... CONSTRUCT FIRST GUESS FROM COSINE LAW
50 DO 90 I=1,N
    DO 80 J=1,M
    D=SQRTF((AX(I)-XP)**2+(AY(J)-YP)**2
    1+(AZ(I,J)-ZP)**2)
    E=(AX(I)-AX(NZ))**2+(AY(J)-AY(MZ))**2
    1+(AZ(I,J)-AZ(NZ,MZ))**2
    IF(A-1.0E-6)60,60,70
60 NMZ=N*(MZ-1)+NZ
    CX(NMZ)=AX(NZ)+AA*GAP
    CY(NMZ)=AY(MZ)+BB*GAP
    CZ(NMZ)=AZ(NZ,MZ)+CC*GAP
    GO TO 80
70 E=SQRTF(E)
    CSI=(Q**2+D**2-E**2)/(2.0*Q*D)
    IJ=N*(J-1)+I
    CX(IJ)=AX(I)+AA*GAP/CSI
    CY(IJ)=AY(J)+BB*GAP/CSI
    CZ(IJ)=AZ(I,J)+CC*GAP/CSI
80 CONTINUE

```

```

90 CONTINUE
C... CHECK FOR FIRST GUESS PRINT
100 IF(OPTION(3))110,110,130
110 WRITE OUTPUT TAPE 3,1000
1000 FORMAT
RESTORE
FIRST GUESS AT CATHODE
SPACE 2
I J X Y Z
SPACE 1
END OF FORMAT
DO 120 I=1,N
DO 120 J=1,M
K=N*(J-1)+I
WRITE OUTPUT TAPE 3,1100,I,J,CX(K),CY(K),CZ(K)
120 CONTINUE
1100 FORMAT
-I -I -OPF5 -OPF5 -OPF5
END OF FORMAT
130 IT=0
IF (OPTION(6))131,133,131
131 CONTINUE
DO 132 I=1,N
DO 132 J=1,M
IJ=N*(J-1)+I
S(IJ)=0.0
132 DS(IJ)=1.0
133 CONTINUE
NMZ=(MZ-1)*N+NZ
NM=N*M
140 IT=IT+1
IF(FIRST)141,143,141
141 DO 142 I=1,N
DO 142 J=1,M
IJ=(J-1)*N+I
GP=SQRTF((AX(I)-CX(IJ))**2+(AY(J)-CY(IJ))**2+(AZ(I,J)-CZ(IJ))**2)
CALL LINIT(GP,RBAR,GAPT,RBART,NGAP,FN)
GAMMA(I,J)=FO*CD(I,J)/((GK/RBAR)*(EE-DEE))
142 GAMMA(I,J)=-GAMMA(I,J)
143 CONTINUE
XLMAX = 0.0
IF(IT-NIT)150,300,300
150 DO 151 I=1,N
DO 151 J=1,M
CALL CAREA(CX,CY,CZ,I,J,N,M,AR)
IJ=(J-1)*N+I
151 AREA(IJ)=AR/RATIO(IJ)
470 DO 190 IC=1,N
DO 190 JC=1,M
K=N*(JC-1)+IC
ARPP(K)=0.0
XL(K)=0.0
160 DO 180 I=1,N
DO 170 J=1,M
IF(OPTION(5))165,162,165
162 IF(K-((J-1)*N+I))165,1672,165
165 CONTINUE
SQ=(CX(K)-AX(I))**2+(CY(K)-AY(J))**2+(CZ(K)-
1AZ(I,J))**2
SQ=1.0/SQRTF(SQ)
IF (OPTION(9))167,166,167

```

```

166 AREAP=AREA(K)*(AD(IC,JC)*AD(I,J)+BD(IC,JC)*BD(I,J)
1+ CD(IC,JC)*CD(I,J))
VALUE=AREAP/AREA(K)
IF (VALUE-CHECK)1671,1661,1661
1661 CONTINUE
SQ=SQ*AREAP
167 CONTINUE
XL(K)=XL(K)+SQ
1672 L= N*(J-1)+I
ARPP(K)=ARPP(K)+AREA(L)
1671 CONTINUE
170 CONTINUE
180 CONTINUE
XL(K)=XL(K)*TAFY
190 CONTINUE
EPMAX=0
EPCMAX=0
DXLMAX=0.0
TOLA=0.0
DO 196 I=1,N
DO 196 J=1,M
IJ=N*(J-1)+I
EP(IJ)=GAMMA(I,J)*AREA(IJ)-XL(IJ)
ER = GAMMA(I,J)-XL(IJ)
EPMAX=MAX1F(ER,EPMAX)
192 XLZ=SQRTF((CX(IJ)-AX(I))**2+(CY(IJ)-AY(J))**2
1+(CZ(IJ)-AZ(I,J))**2)
DXL(IJ)=AREA(IJ)/EP(IJ)-XLZ
196 TOLA=TOLA+AREA(IJ)
C... CHECK VARIABLE GAP OPTION(2)
481 DO 270 I=1,N
DO 260 J=1,M
IJ=N*(J-1)+I
235 DXLS=DXL(IJ)
236 CX(IJ)=CX(IJ)+DXLS*AD(I,J)
CY(IJ)=CY(IJ)+DXLS*BD(I,J)
CZ(IJ)=CZ(IJ)+DXLS*CD(I,J)
250 DXLMAX=MAX1F(ABSF(DXL(IJ)),DXLMAX)
260 CONTINUE
270 CONTINUE
C... CHECK OPTION(4)-PRINT ITERATION
IF(OPTION(4))280,280,140
280 WRITE OUTPUT TAPE 3,1200,IT,EPMAX,DXLMAX,TOLA
1200 FORMAT
RESTORE
CATHODE AFTER -I ITERATIONS
SPACE 1
MAX.ERR. = -1PE5 MAX. DL = -1PE5 TOLA = -1PE5
SPACE 2
I J X Y Z DL XL
X XLZ KAPPA
SPACE 1
END OF FORMAT
DO 290 I=1,N
DO 290 J=1,M
IJ=N*(J-1)+I
282 XLZ=SQRTF((CX(IJ)-AX(I))**2+(CY(IJ)-AY(J))**2
1+(CZ(IJ)-AZ(I,J))**2)
CUMNS=1.0-XL(IJ)/(GAMMA(I,J)*AREA(IJ))
WRITE OUTPUT TAPE 3,1201,I,J,CX(IJ),CY(IJ),CZ(IJ),DXL(IJ),XL(IJ),
1XLZ,CUMNS

```

```

290 CONTINUE
  IF(ABSF(DXLMAX)-TESTA)1213,1213,140
1213 IT=1
  FIRST=FIRST+1.0
  IF(FIRST)140,300,300
300 RETURN
1201 FORMAT
  -I    -I    -OPF5    -F5    -F5    -1PE5    -1PE5
X      -1PE5    -1PE5
  END OF FORMAT
  END

```

```

*NORMAL000
C... SUBROUTINE TO COMPUTE DIRECTION COSINES OF NORMAL TO
C... A SURFACE AT A POINT. THESE COSINES WILL BE SUCH
C... THAT NORMAL IS POINTING AWAY FROM THE ORIGIN
C... SURFACE IS ASSUMED TO BE DEFINED AS A MESH
C... CALLING SEQUENCE
C... CALL NORMAL(X,Y,Z,I,J,N,M,ALPHA,BETA,GAMMA)
C... X,Y,Z ARE THE ARRAYS OF COORDINATES
C... I,J INDICES OF POINT
C... N,M SIZE OF ARRAYS
C... ALPHA,BETA,GAMMA COMPUTED DIRECTION COSINES
SUBROUTINE NORMAL(X,Y,Z,I,J,N,M,ALPHA,BETA,GAMMA)
DIMENSION X(30),Y(30),Z(30,30)
  10 I1=I
    JJ=J
    NN=N
    MM=M
C... CHECK FOR SPECIAL POINT
    IF(I1-1)20,20,70
  20 IF(JJ-1)30,30,40
C... CORNER POINT
  30 I1=1
    J1=1
    I2=2
    J2=2
    GO TO 120
  40 IF(MM-JJ)50,50,60
C... CORNER POINT
  50 I1=1
    I2=2
    J2=MM-1
    J1=MM
    GO TO 120
C... EDGE POINT
  60 I2=1
    I1=2
    J1=JJ-1
    J2=JJ
    J3=JJ+1
    GO TO 140
  70 IF(NN-I1)80,80,150
  80 IF(JJ-1)90,90,100
C... CORNER POINT
  90 I2=NN-1
    I1=NN
    J1=1
    J2=2
    GO TO 120
 100 IF(MM-JJ)110,110,130
C... CORNER POINT
 110 I2=NN-1
    I1=NN
    J2=MM-1
    J1=MM
C... COMPUTE NORMAL AT CORNER AS NORMAL TO PLANE
C... THRU THREE POINTS
 120 X1=X(I1)
    X2=X(I2)
    Y1=Y(J1)
    Y2=Y(J2)

```

```

      Z11=Z(I1,J1)
      Z12=Z(I1,J2)
      Z21=Z(I2,J1)
      DEL=(X1-X2)*(Y1-Y2)
      A=(Z11-Z21)*(Y1-Y2)/DEL
      B=(Z11-Z12)*(X1-X2)/DEL
      C=Z11*(X2*Y2-X1*Y1)+Z12*(X1*Y1-X2*Y1)
      1+Z21*(X1*Y1-X1*Y2)
      C=C/DEL
1201 GO TO 220
C... EDGE POINT
130 I1=NN-1
      I2=NN
      J1=JJ-1
      J2=JJ
      J3=JJ+1
140 X1=X(I1)
      X2=Y(I2)
      Y1=Y(J1)
      Y2=Y(J2)
      Y3=Y(J3)
      Z21=Z(I2,J1)
      Z12=Z(I1,J2)
      Z22=Z(I2,J2)
      Z23=Z(I2,J3)
      GO TO 195
150 IF(JJ-1)160,160,170
C... EDGE POINT
160 I1=II-1
      I2=II
      I3=II+1
      J2=1
      J1=2
      GO TO 190
170 IF(MM-JJ)180,180,210
C... EDGE POINT
180 I1=II-1
      I2=II
      I3=II+1
      J1=JJ-1
      J2=JJ
190 X1=X(I1)
      X2=X(I2)
      X3=X(I3)
      Y1=Y(J1)
      Y2=Y(J2)
      Z12= Z(I1,J2)
      Z21= Z(I2,J1)
      Z22= Z(I2,J2)
      Z32= Z(I3,J2)
      A1= X1**2 + 2.0*X2**2 + X3**2
      A2= X1*Y2 + X2*Y1 + X2*Y2 + X3*Y2
      A3= X1 + 2.0*X2 + X3
      D1= X1*Z12 + X2*Z21 + X2*Z22 + X3*Z32
      B2= Y1**2 + 3.0*Y2**2
      B3 = Y1 + 3.0*Y2
      D2 = Y2*(Z12 + Z22 + Z32) + Y1*Z21
      C3= 4.0
      D3 = Z12 + Z21 + Z22 + Z32
      GO TO 200
195 A1=X1**2+3.0*X2**2

```

```

      B2=2.0*Y2**2+Y1**2+Y3**2
      C3=4.0
      A2 = X1*Y2 + X2*(Y2 + Y3 + Y1)
      B3=2.0*Y2+Y1+Y3
      A3=X1+3.0*X2
      D1=X1*Z12+X2*(Z21+Z22+Z23)
      D2=Y2*(Z12+Z22)+Y1*Z21+Y3*Z23
      D3=Z12+Z21+Z22+Z23
200  DEL=A1*B2*C3+A2*B3*A3+A3*B3*A2
      1-(B2*A3**2+A1*B3**2+C3*A2**2)
      A=D1*(B2*C3-B3**2)+D2*(A3*B3-A2*C3)
      1+D3*(A2*B3-B2*A3)
      A=A/DEL
      B=D1*(A3*B3-A2*C3)+D2*(A1*C3-A3**2)
      1+D3*(A2*A3-A1*B3)
      B=B/DEL
      C=D1*(A2*B3-A3*B2)+D2*(A2*A3-A1*B3)
      1+D3*(A1*B2-A2**2)
      C=C/DEL
      GO TO 220
C...  INTERNAL POINT FIT LEAST SQUARE PLANE THRU
C...  POINT AND FOUR ADJACENT POINTS
210  J1=JJ-1
      J2=JJ
      J3=JJ+1
      I1=II-1
      I2=II
      I3=II+1
      X1=X(I1)
      X2=X(I2)
      X3=X(I3)
      Y1=Y(J1)
      Y2=Y(J2)
      Y3=Y(J3)
      Z12=Z(I1,J2)
      Z21=Z(I2,J1)
      Z22=Z(I2,J2)
      Z23=Z(I2,J3)
      Z32=Z(I3,J2)
      A1=X1**2+3.0*X2**2+X3**2
      A2=X2*(Y2+Y3+Y1)+X1*Y2+X3*Y2
      A3=X1+3.0*X2+X3
      D1=X2*(Z21+Z22+Z23) + X3*Z32 + X1*Z12
      B2=Y1**2+3.0*Y2**2+Y3**2
      B3=Y1+3.0*Y2+Y3
      C3= 5.0
      D2=Y2*(Z12+Z22+Z32)+Y1*Z21+Y3*Z23
      D3=Z12+Z21+Z22+Z32+Z23
      GO TO 200
C...  COMPUTE NORMAL DIRECTION COSINES
220  IF(C-1.0E-6)240,230,230
230  A=-A
      B=-B
      D=1.0
      GO TO 250
240  D=-1.0
      C=-C
250  SQ=SQRTF(A**2+B**2+D**2)
      ALPHA=A/SQ
      BETA=B/SQ
      GAMMA=D/SQ
      RETURN
      END

```

```

* CAREA00
C... SUBROUTINE TO COMPUTE EFFECTIVE AREA
C... OF POINT ON CATHODE CORRESPONDING TO
C... POINT A(I,J) ON ANODE
C... AREA OF CATHODE AT THE POINT IS TAKEN
C... AS AREA ON PLANE THRU POINT AND ADJACENT POINTS
C... CALLING SEQUENCE
C... CALL CAREA (CX,CY,CZ,I,J,N,M,AREA)
C... WHERE-CX,CY,CZ ARRAYS CONTAINING CATHODE COORDS.
C... I,J-INDICES OF POINT ON ANODE
C... N,M-DIMENSIONS OF ANODE
C... AREA-EFFECTIVE AREA OF CATHODE
SUBROUTINE CAREA
  1(CX,CY,CZ,I,J,N,M,AREA)
  DIMENSION CX(900),CY(900),CZ(900)
100  II=I
      JJ=J
      NN=N
      MM=M
C... CHECK FOR SPECIAL POINT
      IF(II-1)200,200,360
200  IF(JJ-1)300,300,320
C... CORNER POINT 1,1
300  K1=1
      K2=2
      K3=NN+1
310  NGO =1
      X1=CX(K1)
      X2=CX(K2)
      X3=CX(K3)
      Y1=CY(K1)
      Y2=CY(K2)
      Y3=CY(K3)
      Z1=CZ(K1)
      Z2=CZ(K2)
      Z3=CZ(K3)
      DEL=X2*Y3-X3*Y2+X3*Y1-X1*Y3+X1*Y2-X2*Y1
      A=Z1*(Y2-Y3)+Z2*(Y3-Y1)+Z3*(Y1-Y2)
      A=A/DEL
      B=Z1*(X3-X2)+Z2*(X1-X3)+Z3*(X2-X1)
      B=B/DEL
      C=Z1*(X2*Y3-X3*Y2)+Z2*(X3*Y1-X1*Y3)+
1Z3*(X1*Y2-X2*Y1)
      C=C/DEL
      GO TO 490
320  IF(MM-JJ)330,330,340
C... CORNER POINT 1,M
330  K1=(MM-1)*NN+1
      K2=K1-NN
      K3=K1+1
      GO TO 310
C... EDGE POINT 1,J
340  K2=(JJ-1)*NN+1
      K1=K2-NN
      K3=K2+NN
      K4=K2+1
350  NGO=2
      X1=CX(K1)
      X2=CX(K2)
      X3=CX(K3)

```

```

X4=CX(K4)
Y1=CY(K1)
Y2=CY(K2)
Y3=CY(K3)
Y4=CY(K4)
Z1=CZ(K1)
Z2=CZ(K2)
Z3=CZ(K3)
Z4=CZ(K4)
355 A1=X1**2+X2**2+X3**2+X4**2
A2=X1*Y1+X2*Y2+X3*Y3+X4*Y4
A3=X1+X2+X3+X4
D1=X1*Z1+X2*Z2+X3*Z3+X4*Z4
B2=Y1**2+Y2**2+Y3**2+Y4**2
B3=Y1+Y2+Y3+Y4
D2=Y1*Z1+Y2*Z2+Y3*Z3+Y4*Z4
C3=4.0
D3=Z1+Z2+Z3+Z4
GO TO 480
360 IF(NN-11)370,370,420
370 IF(JJ-1)380,380,390
C... CORNER POINT N,1
380 K1=NN
K2=NN-1
K3=K1+NN
GO TO 310
390 IF(MM-JJ)400,400,410
C... CORNER POINT N,M
400 K1=NN*MM
K2=K1-1
K3=K1-NN
GO TO 310
C... EDGE POINT N,J
410 K2=(JJ-1)NN+NN
K1=K2-NN
K3=K2+NN
K4=K2-1
GO TO 350
420 IF(JJ-1)430,430,450
C... EDGE POINT I,1
430 K2=II
K1=II-1
K3=II+1
K4=II+NN
GO TO 350
450 IF(MM-JJ)460,460,470
C... EDGE POINT I,M
460 K2=(MM-1)*NN+II
K1=K2-1
K3=K2+1
K4=K2-NN
GO TO 350
C... INTERIOR POINT
470 K1=(JJ-1)*NN+II
K2=K1-1
K3=K1+1
K4=K1-NN
K5=K1+NN
X1=CX(K1)
X2=CX(K2)
X3=CX(K3)

```

```

X4=CX(K4)
X5=CX(K5)
Y1=CY(K1)
Y2=CY(K2)
Y3=CY(K3)
Y4=CY(K4)
Y5=CY(K5)
Z1=CZ(K1)
Z2=CZ(K2)
Z3=CZ(K3)
Z4=CZ(K4)
Z5=CZ(K5)
NGO=3
A1=X1**2+X2**2+X3**2+X4**2+X5**2
A2=X1*Y1+X2*Y2+X3*Y3+X4*Y4+X5*Y5
A3=X1+X2+X3+X4+X5
B2=Y1**2+Y2**2+Y3**2+Y4**2+Y5**2
B3=Y1+Y2+Y3+Y4+Y5
C3=5.0
D1=X1*Z1+X2*Z2+X3*Z3+X4*Z4+X5*Z5
D2=Y1*Z1+Y2*Z2+Y3*Z3+Y4*Z4+Y5*Z5
D3=Z1+Z2+Z3+Z4+Z5
480 DEL=A1*B2*C3+A2*B3*A3+A2*B3*A3
1-(B2*A3**2+A1*B3**2+C3*A2**2)
A=D1*(B2*C3-B3**2)+D2*(A3*B3-A2*C3)
1+D3*(A2*B3-B2*A3)
A=A/DEL
B=D1*(A3*B3-A2*C3)+D2*(A1*C3-A3**2)
1+D3*(A2*A3-A1*B3)
B=B/DEL
C=D1*(A2*B3-A3*B2)+D2*(A2*A3-A1*B3)
1+D3*(A1*B2-A2**2)
C=C/DEL
C... COMPUTE DIRECTION COSINES OF NORMAL
490 GO TO (530,560,580),NGO
530 XA=(X1+X2)/2.0
XB=(X1+X3)/2.0
YA=(Y1+Y2)/2.0
XC=X1
YC=Y1
YB=(Y1+Y3)/2.0
ZC=Z1
540 ZA=A*XA+B*YA+C
ZB=A*XB+B*YB+C
DA=SQRTF((XC-XA)**2+(YC-YA)**2+(ZC-ZA)**2)
DB=SQRTF((XC-XB)**2+(YC-YB)**2+(ZC-ZB)**2)
DC=SQRTF((XA-XB)**2+(YA-YB)**2+(ZA-ZB)**2)
S1=.5*(DA+DB+DC)
AR=2.0*SQRTF(S1*(S1-DA)*(S1-DB)*(S1-DC))
AREA = AR
AREA =4.0*AREA
GO TO 600
560 XA=(X1+X2)/2.0
XC=(X3+X2)/2.0
XD=(X4+X2)/2.0
XB=X2
YA=(Y1+Y2)/2.0
YB=Y2
YC=(Y3+Y2)/2.0
YD=(Y4+Y2)/2.0
70 ZA=A*XA+B*YA+C

```

```

ZB=A*XB+B*YB+C
ZC=A*XC+B*YC+C
ZD=A*XD+B*YD+C
DA=SQRTF((XA-XB)**2+(YA-YB)**2+(ZA-ZB)**2)
DB=SQRTF((XB-XC)**2+(YB-YC)**2+(ZB-ZC)**2)
DC=SQRTF((XC-XD)**2+(YC-YD)**2+(ZC-ZD)**2)
DD=SQRTF((XA-XD)**2+(YA-YD)**2+(ZA-ZD)**2)
D=SQRTF((XB-XD)**2+(YB-YD)**2+(ZB-ZD)**2)
S1=.5*(DA+D+DD)
S2=.5*(DB+D+DC)
AR=2.0*SQRTF(S1*(S1-DA)*(S1-DD)*(S1-D))
AR=AR+2.0*SQRTF(S2*(S2-DB)*(S2-DC)*(S2-D))
AREA = AR
AREA =2.0*AREA
GO TO 600
580 XA=(X1+X3)/2.0
YA=(Y1+Y3)/2.0
ZA=A*XA+B*YA+C
XB=(X2+X1)/2.0
YB=(Y2+Y1)/2.0
ZB=A*XB+B*YB+C
XC=(X5+X1)/2.0
YC=(Y5+Y1)/2.0
ZC=A*XC+B*YC+C
XD=(X4+X1)/2.0
YD=(Y4+Y1)/2.0
ZD=A*XD+B*YD+C
DA=SQRTF((XA-XB)**2+(YA-YB)**2+(ZA-ZB)**2)
DB=SQRTF((XB-XC)**2+(YB-YC)**2+(ZB-ZC)**2)
DC=SQRTF((XC-XD)**2+(YC-YD)**2+(ZC-ZD)**2)
DD=SQRTF((XD-XA)**2+(YD-YA)**2+(ZD-ZA)**2)
D=SQRTF((XC-XA)**2+(YC-YA)**2+(ZC-ZA)**2)
S1=.5*(DA+DB+D)
S2=.5*(DC+DD+D)
AR=2.0*SQRTF(S1*(S1-DA)*(S1-DB)*(S1-D))
AR=AR+2.0*SQRTF(S2*(S2-DC)*(S2-DD)*(S2-D))
AREA = AR
600 RETURN
END

```

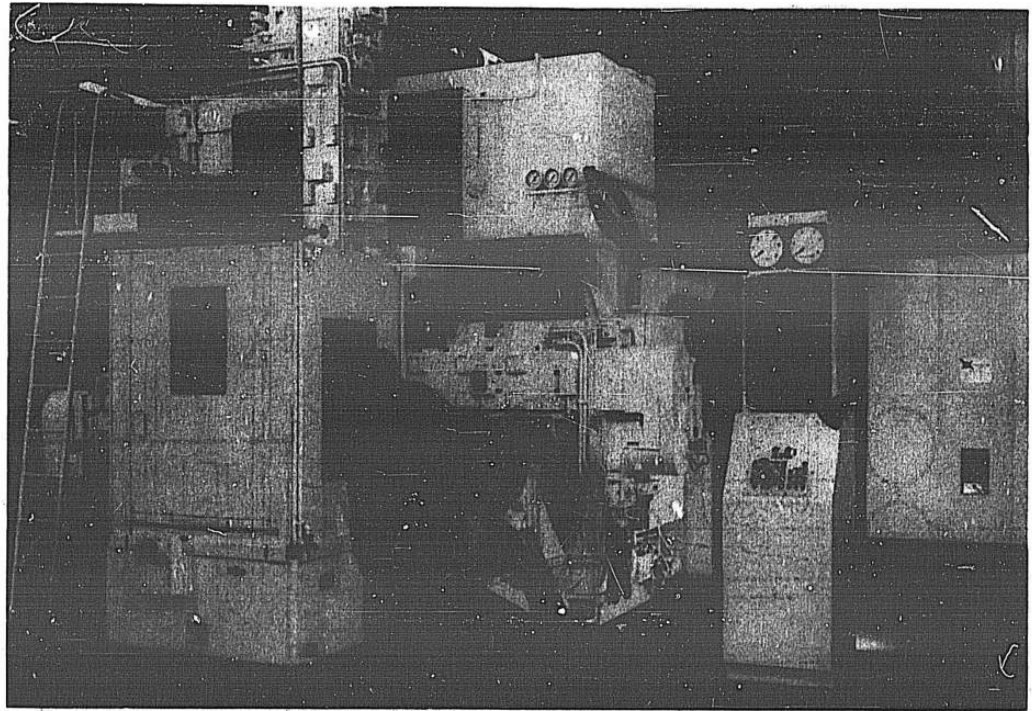
APPENDIX IV
TEST EQUIPMENT

This section includes test equipment
not further described elsewhere in
this report.

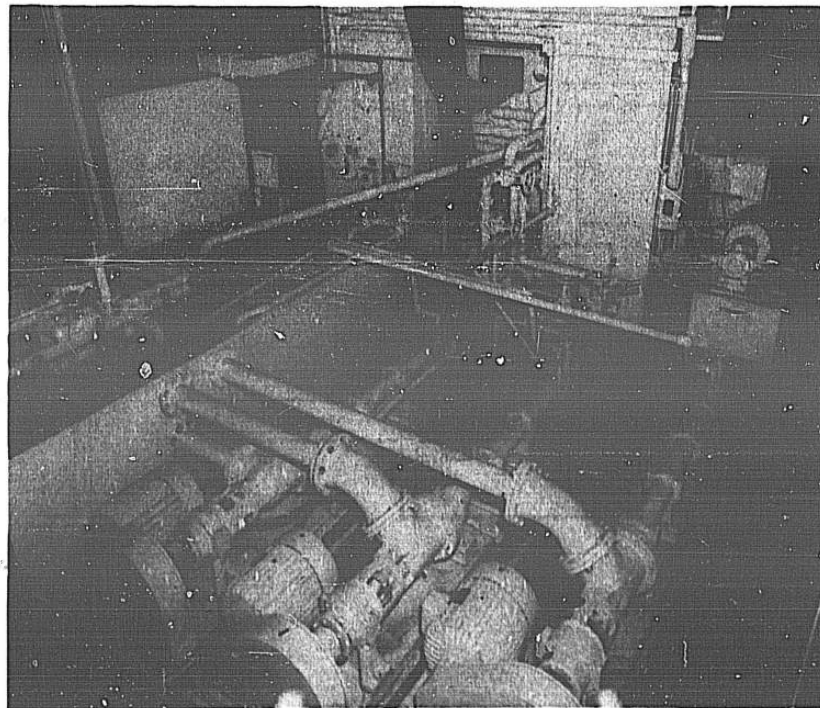
IV.1 Machine #1

Machine #1, Figure 116, is a three-spindle ECM machine. It is supplemented by equipment shown in Figure 117, Table 41.

The machine has a 44" work cube space between the three rams. Each ram has a 20" stroke and a position readout in 0.001" on the control panel. A 1000-gallon tank for the electrolyte is automatically temperature controlled by a water-steam system. Three 50 gal/min, 350 psig pumps are used individually or in parallel. Hydraulic motors drive the rams which ride in preloaded recirculating roller bearings. A rate valve for each hydraulic motor controls the feed rate of each ram. The machine has a 36" manual indexing table and a 36" diameter variable speed rotary table with a slip ring capacity of 10,000 amperes.



(a) Frontal View of Machine and Work Enclosure



(b) Pumps, Power Pack and Supporting Equipment

Figure 116. ECM Machine #1

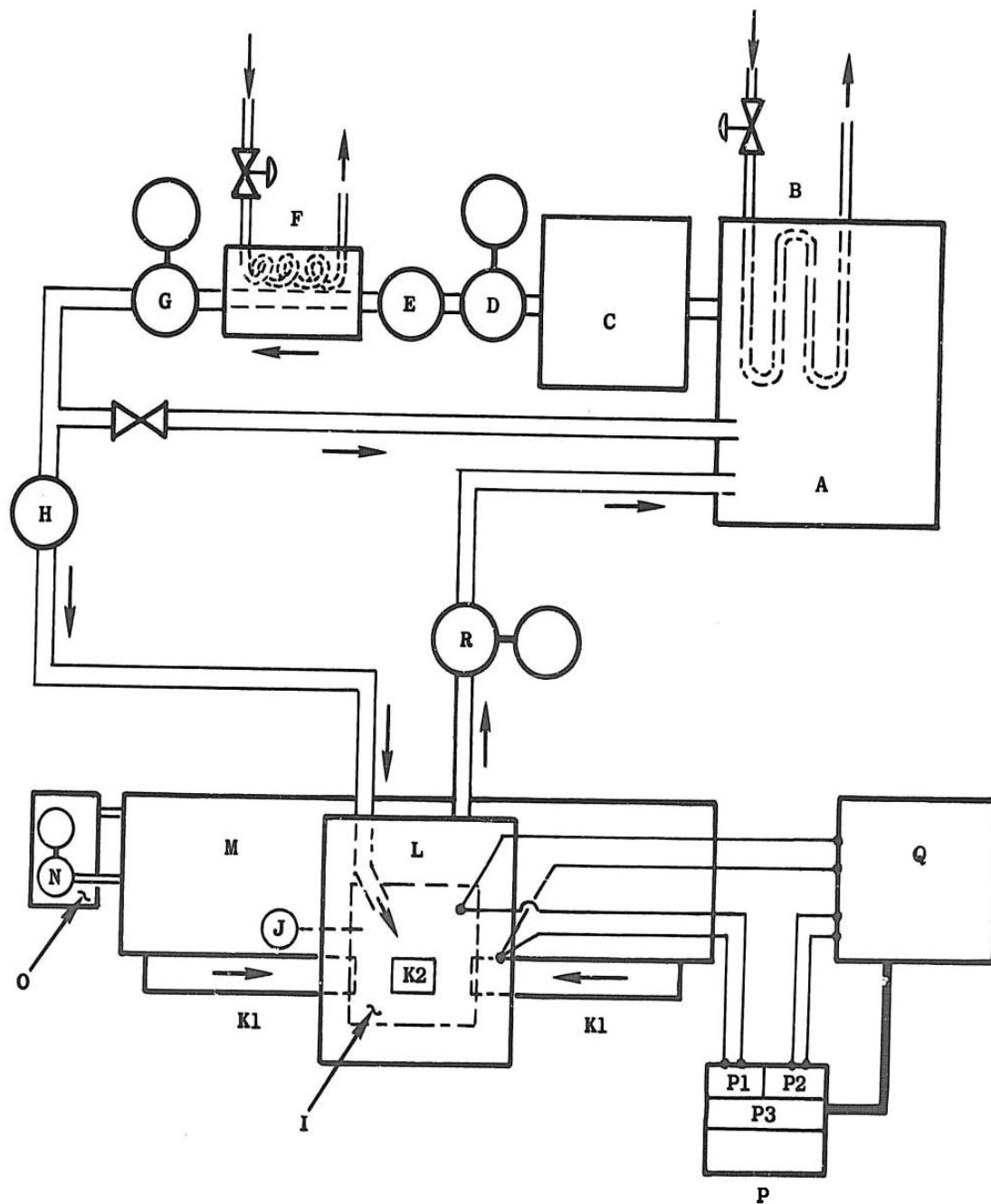


Figure 117. Facility Layout ECM Machine #1

TABLE 41
LEGEND FOR FACILITY LAYOUT
MACHINE #1, FIGURE 117

- A Main Supply Tank
- B Heating Coils
- C Auxiliary Supply Tank
- D Centrifugal Pump 150 gal/min Max.
- E Cartridge Filter
- F Heat Exchanger - Cooling
- G Three "Moyno" Screw-Type Pumps, 300 psi Max., 50 gal/min each
- H Percent Flow Indicator
- I Test Tooling
- J Test Tooling Pressure Gage
- K Feed Spindles
 - 1. Horizontal Spindles
 - 2. Vertical Spindle
- L Electrolyte Catch Tank
- M ECM Machine #1
- N Hydraulic Pump Motor
- O Hydraulic Supply Tank
- P Control Console
 - 1. Voltmeter
 - 2. Ammeter
 - 3. Spindle Feed Readout
- Q "C K M" Power Supply, 25 VDC-3000A
- R Centrifugal Pump 150 gal/min

DISTRIBUTION LIST

AFML (MAA/Mr. J. Teres)
WPAFB, Ohio 45433 (1)

AFML (MAAE)
WPAFB, Ohio 45433 (1)

AFML (MAAM/Librarian)
WPAFB, Ohio 45433 (2)

AFML (MATF/W. M. Webster)
WPAFB, Ohio 45433 (6)

AFML (MAX/Dr. Lovelace)
WPAFB, Ohio 45433 (1)

Hq USAF (AFRSTC/Colonel Hamlin)
Washington, D. C. 20013 (1)

RTD (RTTM/Colonel Hemm)
Bolling AFB, D. C. 20332 (1)

SEG (SEPIE)
WPAFB, Ohio 45433 (1)

SEG (SEPIR)
WPAFB, Ohio 45433 (1)

Defense Documentation Center
Cameron Station
Alexandria, Virginia 22314 (20)

MAAMA (MAE/Technical Library)
Olmsted AFB, Pa. 17057 (1)

MOAMA (MCAE/Technical Library)
Brookley AFB, Ala. 36615 (1)

OOAMA (OCAE/Technical Library)
Hill AFB, Utah 84401 (1)

OCAMA (OCAE/Technical Library)
Tinker AFB, Okla. 73145 (1)

ROAMA (ROAE/Technical Library)
Griffiss AFB, N. Y. 13442 (1)

SMAMA (SMAE/Technical Library)
McClellan AFB, Calif. 95652 (1)

SBAMA (SBAE/Technical Library)
Norton AFB, Calif. 92409 (1)

WRAMA (WRAE/Technical Library)
Robins AFB, Ga. 31094 (1)

SAAMA (SAAE/Technical Library)
Kelly AFB, Texas 78241 (1)

Mr. E. E. Welch, Plant 5
Allison Division
General Motors Corporation
P. O. Box 894
Indianapolis, Indiana (1)

University of Arkansas
Attn: K. W. Stalker
Industrial Engineering Dept.
Fayetteville, Arkansas (1)

Tullahoma Division
Altamil Corporation
Attn: E. G. Wolf, Jr.
William Northern Field
Tullahoma, Tennessee (1)

Mr. D. R. Smoak (AMXPE-MT)
Manufacturing Technology Division
U.S. Army Production Equipment Agency
Rock Island Arsenal
Rock Island, Illinois (1)

North American Aviation, Inc.
Space & Information Systems Division
Attn: L. E. Gatzek D/098
12214 Lakewood Blvd.
Downey, California (1)

Union Carbide Corporation
Stellite Division
Attn: Mr. B. R. Barrett
Kokomo, Indiana (1)

Nortronics
Attn: Mr. P. H. Halderman
Gen. Supv. Dept. 2883
222 Prairie Avenue
Hawthorne, California (1)

American Machine & Foundry
Attn: Mr. C. L. Morrison
1025 N. Royal St.
Alexandria, Virginia (1)

Commanding General
Frankford Arsenal
Attn: ORDBA, 5500
Philadelphia 37, Penn. (1)

Autonetics
Division of North American Aviation
Attn: Technical Library
9150 East Imperial Highway
Downey, Calif. (1)

BSD
 Norton AFB, Calif. (1)

Cmdr. R. A. Holmes, III
 PH-42
 Dept. of the Navy
 Bureau of Weapons
 Washington 25, D.C. (1)

Aerospace Corporation Library
 Technical Reports
 2400 E. El Segundo Blvd.
 El Segundo, Calif. (1)

The Brush Development Company
 Attn: Mr. W. R. Stern
 3405 Perkins Avenue
 Cleveland 14, Ohio (1)

Concord Control, Inc.
 Attn: Mr. H. P. Grossimon
 1282 Soldiers Field Road
 Boston 35, Mass. (1)

Stromberg-Carlson Company
 Attn: W. G. Steve
 Rochester 3, New York (1)

The Maico Company, Inc.
 Attn: Mr. R. A. Carlson
 Maico Bldg.
 Minneapolis, Minnesota (1)

DeVlieg Machine Company
 Attn: Mr. C. R. DeVlieg
 450 Fair Avenue
 Ferndale, Detroit 20, Michigan (1)

Ex-Cell-O Corporation
 Attn: Mr. G. D. Stewart
 1200 Oakman Blvd.
 Detroit 32, Michigan (1)

The Heald Machine Company
 Attn: Mr. C. C. Menard
 10 New Bond Street
 Worcester 6, Mass. (1)

The Fosdick Machine Tool Co.
 Attn: Mr. C. E. Linden
 Cincinnati, Ohio (1)

Jones & Lamson Machine Company
 Attn: Mr. H. H. Whitmore
 160 Clinton Street
 Springfield, Vermont (1)

Pratt & Whitney Co.
 Attn: Mr. E. S. Belden
 1100 Oakwood Avenue
 Dayton 19, Ohio (1)

Cincinnati Milling Machine Company
 Attn: Dr. M. Eugene Merchant
 4701-4801 Marburg Avenue
 Cincinnati 9, Ohio (1)

Giddings & Lewis Machine Tool Co.
 Attn: Mr. E. L. McFerren
 142 Doty Street
 Fond du Lac, Wisconsin (1)

Van Norman Machine Company
 Attn: Mr. J. E. Storm
 Springfield 7, Mass. (1)

Baker Brothers, Inc.
 Attn: Mr. Roland Lehr
 142 Sylvania Avenue
 Toledo 5, Ohio (1)

Giannini Controls Corp.
 Attn: Mr. A. C. Hummel
 2600 Far Hills Avenue
 Dayton 19, Ohio (1)

Norden
 11 W. Monument Avenue
 Dayton 2, Ohio (1)

Sperry Products, Inc.
 Attn: Mr. J. L. Lobdall
 Danbury, Conn. (1)

Kearney & Trecker Corporation
 Attn: Mr. W. C. Beverung
 6784 W. National Avenue
 Milwaukee 14, Wisc. (1)

General Electric Company
 Attn: Mr. E. F. Myerholtz
 Large Jet Engine Dept.
 Cincinnati 15, Ohio (1)

Republic Aviation Corp.
 Attn: Mr. George Davis
 Farmingdale, L.I. New York (1)

General Dynamics/San Diego
 Attn: Mgr. Mfg. Development
 & Process Specification
 San Diego 12, California (1)

The Boeing Company
Aerospace Division
Attn: Mr. B. K. Bucey,
Asst. to V-Pres. Mfg.
P. O. Box 3707
Seattle 24, Washington (1)

Douglas Aircraft Company, Inc.
Attn: O. L. Rumble, Tooling Mgr.
3855 Lakewood Blvd.
Long Beach 8, Calif. (1)

General Dynamics/Ft. Worth
Attn: Mr. R. A. Fuhrer
Ch. Mfg. Eng.
Forth Worth, Texas (1)

Bell Aircraft Corp.
Niagara Falls Airport
Attn: Mr. Ralph W. Varriall
Mgr. Production Engrg.
Buffalo 5, New York (1)

Bendix Production Division
Bendix Aviation Corp.
Attn: Mr. A. J. Walsh, Staff Asst.
401 Bendix Drive
South Bend, Indiana (1)

The Boeing Company
Airplane Division-Wichita Branch
Attn: Mfg. R. & D Manager (3070)
3801 South Oliver
Wichita, Kansas (1)

The Martin Company
Attn: Mr. N. M. Voorhies
Baltimore 3, Maryland (1)

Goodyear Aerospace Corporation
Plant G
Attn: Engineering Library
Akron 15, Ohio (1)

Grumman Aircraft Engrg. Corp.
Attn: Mr. William J. Hoffman
V-Pres., Mfg. Engrg.
Bethpage, L.I. New York (1)

Hughes Aircraft Company
Attn: Mr. J. W. Moffett
Ch. Equipment Eng.
El Segundo, Calif. (1)

Lockheed Aircraft Corp.
Georgia Division
Attn: Mr. R. A. Mackenzie Mfg. Mgr.
Haretta, Georgia (1)

Lockheed Aircraft Corp.
Attn: Mr. C. S. Wagner, Exec. V.-Pres.
Burbank, California (1)

McDonnell Aircraft Corp.
Attn: A. F. Hartwig, Ch. Indus. Eng.
P. O. Box 516
St. Louis 66, Missouri (1)

North American Aviation, Inc.
International Airport
Attn: Mr. Latham Pollack,
Genl. Supt. Mfg.
Los Angeles 45, Calif. (1)

North American Aviation, Inc.
Attn: Mr. M. E. Fisher,
Supt. Mfg. Develop.
4300 East Fifth Avenue
Columbus 16, Ohio (1)

The H. M. Harper Co.
Attn: K. G. Hookanson, Director R&D
Morton Grove, Illinois (1)

Northrop Corporation
Norair Division
Attn: Mr. R. R. Noland
V-Pres. & Division Mgr.
1001 E. Broadway
Hawthorne, California (1)

Rohr Aircraft Corporation
Attn: Mr. B. F. Raynes
Executive Vice-Pres.
P. O. Box 878
Chula Vista, Calif. (1)

Ryan Aeronautical Company
Attn: Mr. Robert L. Clark
Works Manager
P. O. Box 311
Lindbergh Field
San Diego 12, Calif. (1)

Thompson-Ramo-Wooldridge, Inc.
Attn: Mr. Carl W. Goldbeck
Assistant Staff Director
Industrial Engineering
23555 Euclid Avenue
Cleveland 17, Ohio (1)

Marquardt Aircraft Corp.
Attn: Dir. of Mfg.
16555 Saticoy Street
Van Nuys, Calif. (1)

Sundstrand Machine Tool
Attn: Mr. Richard Leber
Belvidere, Illinois (1)

Lockheed Aircraft Corp.
California Division
Attn: Robert L. Vaughn
Producibility Methods Eng.
2555 N. Hollywood Way
Burbank, California (1)

Department of the Navy
Bureau of Ships
Technical Library
Code 312, Rm. 1532, Main Navy Bldg.
Washington, 25, D.C. (1)

Anocut Engineering Co.
Attn: Mr. L. A. Williams, Pres.
631 Washington Blvd.
Chicago 6, Illinois (1)

Elox Corporation
Attn: Mr. John Larkins
Royal Oak, Michigan (1)

Aerojet General Corporation
Attn: K. F. Mundt, V-Pres. Mfg.
6352 N. Irwindale Ave.
Azusa, Calif. (1)

Allison Division
General Motors Corporation
Attn: Mr. L. E. Batchelor
P. O. Box 894
Indianapolis 6, Indiana (1)

Chance Vought Aircraft, Inc.
Attn: Chief Librarian, Engr. Library
P. O. Box 5907
Dallas, Texas (1)

Curtiss Wright Corporation
Metals Processing Division
Attn: V. T. Gorguze, Gen. Mgr.
P. O. Box 13
Buffalo 5, New York (1)

Defense Metals Information Center
Battelle Memorial Institute
Attn: F. Boulger
505 King Avenue
Columbus 1, Ohio (1)

The Garrett Corporation
Attn: H. Hollingsworth, Staff Eng.
9851 Sepulveda Blvd.
Los Angeles 45, Calif. (1)

Fairchild Aircraft & Missiles Div.
Attn: A. D. Jairett,
Mgr. Tool Engrg. & Mfg.
Hagerstown, Maryland (1)

Hughes Aircraft Company
Attn: W. W. Lampkin, Dir. Mfg.
Florence at Teale Street
Culver City, Calif. (1)

Lycoming Division
AVCO Manufacturing Corporation
Attn: W. H. Panke, Supt. Mfg. Engrg.
Stratford, Connecticut (1)

The Norton Company
Attn: Dr. L. P. Tarasov, R&D
Worcester 6, Massachusetts (1)

Republic Aviation Corporation
Attn: A. Kastelowitz, Mfg. Research
Farmingdale, L. I., New York (1)

Professor Orlan W. Boston
2021 Vinewood Blvd.
Ann Arbor, Michigan (1)

Vanadium Alloys Steel Company
Attn: Dr. G. A. Roberts
V-Pres. Technology
Latrobe, Pennsylvania (1)

The Boeing Company
Attn: L. Pickrell, Mfg. Development
P. O. Box 3707
Seattle 24, Washington (1)

Cornell Aeronautical Laboratory
Attn: P. Rosenthal
Buffalo 21, New York (1)

Steel Improvement and Forge Company
Sifco Metachemical Division
935 E. 63rd St.
Cleveland 3, Ohio (1)

Foreign Technology Division
AFSC, TD-E2B
Wright Patterson AFB, Ohio (1)

Scientific and Technical Information
Facility
Attn: NASA Representative (RQT-13850)
P. O. Box 5700
Bethesda, Maryland 20014 (1)

Hanson-Van Winkle & Munning Co.
Attn: Mr. Robert H. Fairchild
Matawan, New Jersey (1)

General Electric Company
Small Aircraft Engine Department
Thomson Engineering Laboratory
West Lynn, Massachusetts
Attn: Mr. R. E. Patsfall (1)

General Electric Company
Manufacturing Services
1 River Road
Schenectady, New York
Attn: Dr. W. W. Gilbert - Bldg. 69 (1)

Metcut Research Associates, Inc.
3980 Rosslyn Drive
Cincinnati 9, Ohio
Attn: Dr. Michael Field (1)

General Motors Corporation
G. M. Technical Center
Warren, Michigan
Attn: Mr. R. A Featherstone (1)

Midvale-Heppenstall
Nictown, Pennsylvania
Attn: Mr. Charles Gordon (1)

The Library
United Aircraft Corporation
400 Main Street
East Hartford 8, Connecticut (1)

Kollsman Instrument Corporation
Attn: Mr. J. T. Mealy
80-08 Forty Fifth Avenue
Elmhurst, New York (1)

Utica Division
Kelsey-Hays Company
Attn: Mr. Philip E. Munson
Utica 4, New York (1)

The Ingersoll Milling Machine Company
Attn: Joe H. Crawford
Rockford, Illinois (1)

Aerofjet-General Corporation
Attn: Technical Library
P. O. Box 296
Azusa, California (1)

The Bendix Corporation
Attn: Mr. Thomas S. Riordan
Utica Division
Utica 1, New York (1)

Varian Associates
Solid State Products
Attn: Mrs. Kathleen Mallison, Librarian
Beverly, Massachusetts (1)

Lockheed Missiles & Space Company
Attn: Mr. M. L. Buehler, Supervisor
Testing Laboratory
Manufacturing Research
Dept. 48-10, Bldg. 539
P. O. Box 504
Sunnyvale, California (1)

Library, (T.D.S.)
Jet Propulsion Laboratory
California Institute of Technology
Attn: N. E. Devereaux
4800 Oak Grove Drive
Pasadena 3, California (1)

Olin Mathieson Chemical Corp.
Attn: Mrs. Laura M. Kajuti
Research Library, 1-K-3
275 Winchester Avenue
New Haven Connecticut 06504 (1)

E. I. Du Pont De Nemours & Co.
Attn: Mr. R. K. Rathmell
Sales Technical Laboratory
Chestnut Run
Wilmington 98, Delaware (1)

Eaton Manufacturing Company
Eaton Technical Center
Attn: T. C. Griffiths, Control Supv.
4160 Mayfield Road
S. Euclid 21, Ohio (1)

Carl J. Weingartner
Manufacturing Engineering
Airesearch Manufacturing Company
402 South 36th Street
Phoenix, Arizona (1)

United Machine Tool Company
Attn: Robert E. Godfrey
2319 E. 8th Street
Los Angeles 21, California (1)

University of California
Attn: Reno R. Cole,
Professor of Engineering
Department of Engineering
Los Angeles 24, California (1)

Semicon Associates, Inc.
Attn: Dr. O. G. Koppius, President
Box 832
Lexington, Kentucky 40501 (1)

National Lead Company of Ohio
Attn: Florence R. Sharp, Librarian
P. O. Box 39158
Cincinnati, Ohio 45239 (1)

Douglas Aircraft Company, Inc.
Attn: Mr. W. J. Kinney, G-3
N/C Coordinator
Corporate Offices
Santa Monica, California (1)

University of Wisconsin
Attn: J. P. Collins
1513 University Avenue
Madison 6, Wisconsin (1)

Aerojet-General Corporation
Attn: Technical Library
P. O. Box 1947
Sacramento, California (1)

Ion Physics Corporation
Attn: Mr. Jason Weisman,
Mgr. of Operations
Burlington, Mass. (1)

Superior Plating, Inc.
Attn: Fred J. Kaim
University & 1st Ave., N. E.
Minneapolis 13, Minnesota (1)

J. Walter Castrow
Design Engineering
P. O. Box 156
Arlington 74, Mass. (1)

U.S. Naval Ordnance Plant
Attn: Code R (Library)
Iroquois Station
Louisville 14, Kentucky (1)

Vermont American Corp.
Attn: C. E. Eldridge
500 E. Main Street
Louisville 2, Kentucky (1)

Teleflex, Inc.
Attn: R. E. Mayers, Mgr.
Church Road
North Wales, Pa. (1)

R. R. Ruppender, D/519, Zone 17
Rocketdyne Division
North American Aviation, Inc.
6633 Canoga Ave.
Canoga Park, California (1)

Thompson Ramo Wooldridge, Inc.
Attn: J. N. McCarthy
23555 Euclid Avenue
Cleveland 17, Ohio (1)

United Technology Center
Attn: L. P. Bennett, Technical
Data Center
P. O. Box 358
Sunnyvale, California (1)

North American Aviation, Inc.
Rocketdyne Division
Attn: Mr. Robert Gellert
6633 Canoga Avenue
Canoga Park, California (1)

AFSC STLO (RTSAB)
Attn: Maj. Raymond Tondreau
Waltham Federal Center
Waltham, Mass. 02154 (1)

Xerox Corporation
Attn: Joan Johnson
P. O. Box 1540
Rochester 3, N.Y. (1)

Eaton Research Center
Attn: R. H. Buck, Jr.
26201 Northwestern Highway
Southfield, Mich. 48076 (1)

Sunstrand Aviation
Attn: Louis E. Trimmer
Group Leader, Material & Process
Engineering
2480 West 70th Street
Denver 21, Colorado (1)